– *An international journal for New Concepts in Global Tectonics* –

NCGT JOURNAL

Volume 13, Number 6
August 2025

Editor-in-Chief: Bruce LEYBOURNE (leybourneb@iascc.org)

ISSN 2202-0039

WWW.ncgtjournal.com

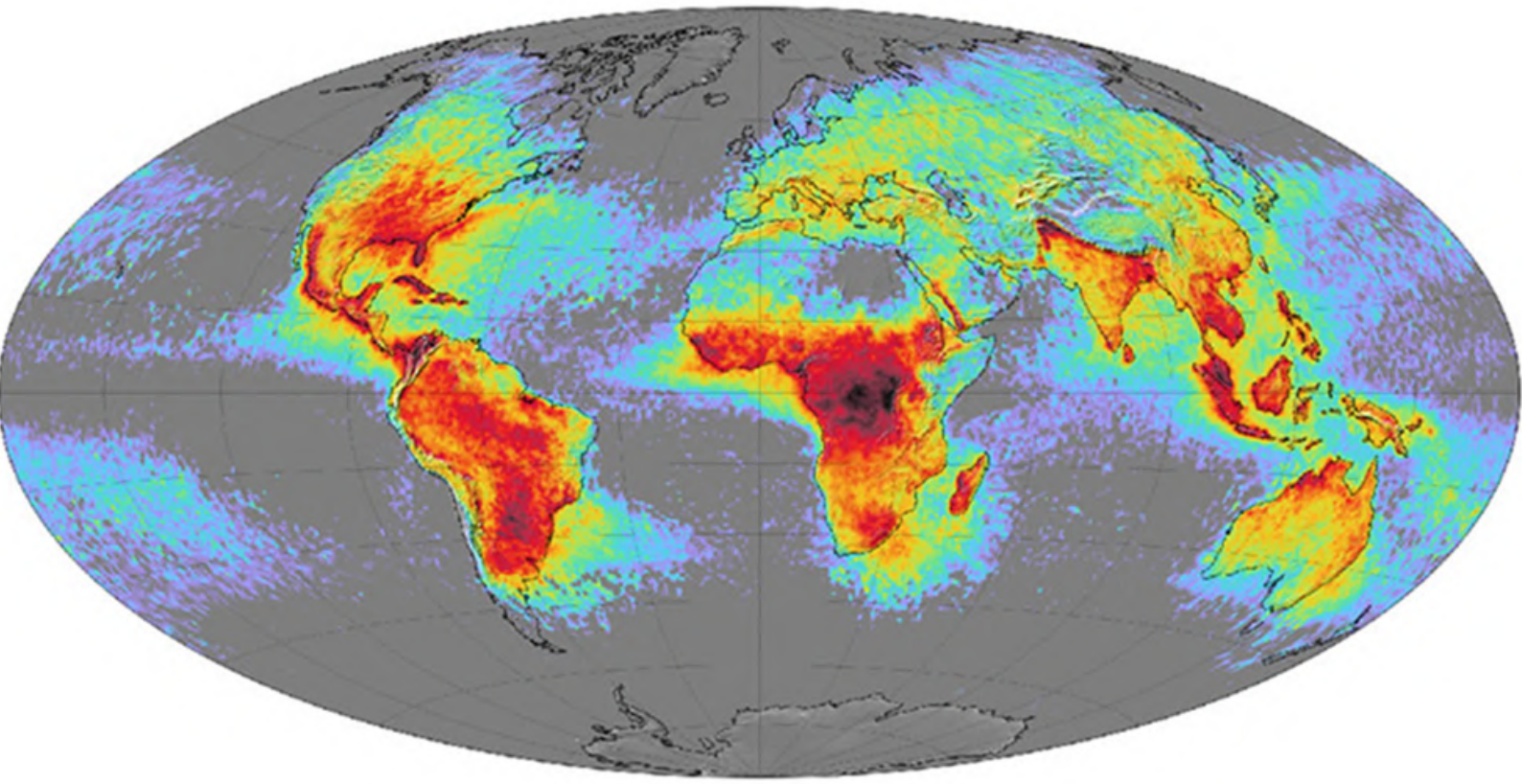

World map of the observed frequency of lightning strikes, in flashes ⟦km⟧^(-2) ⟦year⟧^(-1) (equal-area projection). Combined 1995-2003 data from the NASA OTD and 1998-2003 data from the NASA LIS. NASA image by Marit Jentoft-Nilsen, based on data provided by the Global Hydrology and Climate Center Lightning Team. Reproduced with permission.

Wildfires: a proxy of air-earth currents

Special Issue on Air-Earth Currents

NCGT Journal
New Concepts in Global Tectonics

New Concepts in Global Tectonics Journal
Volume 13, Number 6, August 2025

ISSN number; ISSN 2202-0039

– An international journal for New Concepts in Global Tectonics –

NCGT JOURNAL

Volume 13, Number 6, August 2025. ISSN 2202-0039.

CONTENTS

For donations, please feel free to contact the Research Director of the Geoplasma Research Institute, Mr. Bruce Leybourne, at leybourneb@iascc.org. For contact, correspondence, or inclusion of material in the NCGT Journal please use the following methods: *NEW CONCEPTS IN GLOBAL TECTONICS.* 1. E-mail: leybourneb@iascc.org (files in MS Word or ODT format, and figures in gif, bmp or tif format) as separate files; 3. Telephone, +61 402 509 420. *DISCLAIMER*: The opinions, observations and ideas published in this journal are the responsibility of the contributors and do not necessarily reflect those of the Editor and the Editorial Board. *NCGT Journal* is a refereed quarterly international online journal and appears in March, June, September and December. *ISSN number*; ISSN 2202-0039.

NCGT Journal
New Concepts in Global Tectonics

New Concepts in Global Tectonics Journal
Volume 13, Number 6, August 2025

ISSN number; ISSN 2202-0039

EDITOR's CORNER: - Comments by Editor in Chief - Bruce Leybourne

Announcement in this issue is we are postponing the India conference to an undetermined date in 2027 but will continue with our plans for the September 2026 in Italy. Currently we have 4 sessions that were planned for India that can now be shifted to Italy being locally organized by Valentino Straser

1.) Straser - EQ forecasting (Abstracts requested)

2.) Leybourne - Stellar Transformer - Global Space Weather interactions (6 Abstracts in Editor's Corner within New Concepts in Global Tectonics Journal - Volume 12, Number 4, December 2024)

3.) Anokhin - Lake Ladoga - Siberia (2 Abstracts in Editor's Corner within New Concepts in Global Tectonics Journal - Volume 13, Number 1, March 2025 pp. 5-8, more abstracts requested)

4.) Longhinos - Indian Tectonics (Abstracts requested)

Valentino may have more sessions in mind and if anybody is interested in chairing or organizing another session let us know.

Announcements on Upcoming Conferences - "CALL FOR PAPERS"

September 2026 – NCGT in Italy is being organized by Valentino Straser (valentino.straser@gmail .com). Please contact Valentino if you wish to become involved in any aspect of the conference . Again, we are looking for Session Topics, Abstracts, Papers, Session Chairs, Organizers, Workers, Financial Contributions etc. Let me and Valentino know how you' d like to be involved, and we may accommodate.

2027 (Date: TBD) – NCGT in Trivandrum , India is being organized by Biju Longhinos (biju .longhinos @gmail .com), where we are planning about 6 - half day sessions over 4 days with a post conference field trip. Please contact Biju if you wish to become involved in any aspect of the conference . We are looking for Session Topics , Abstracts , Papers , Session Chairs, Organizers , Workers , Financial Contributions etc . Let me and Biju know how you 'd like to be involved , and we may accommodate.

Cover Image : Wildfires are an excellent proxy of air-earth currents . A wave of crustal stress is clearly envisaged, mapped by the density of wildfires. The wave starts from the Banda Sea, and it propagates northward along the Indochina peninsula . Then it bifurcates . One branch moves along the eastern coast of China until reaching an area slightly north of Beijing where an abrupt "flash " appears of the density of wildfires . Then , the crustal stress propagation stops . The other branch moves westward , partly through Myanmar and Bangladesh , and partly , maybe , along the Himalayas , where the ice cover of soil forbids the occurrence of wildfires . However , it ends up with an abrupt "flash " similar to - but even more evident than - the " flash" of the first branch. This second "flash" occurs somewhere in some area roughly in the Karakoram region . This cycle is observed regularly and repeatedly it is not a matter of coincidence . See: **Wildfires : a proxy of air- earth currents** in Gregroi and Leybourne, 2025 in this issue **Fig. 1**.

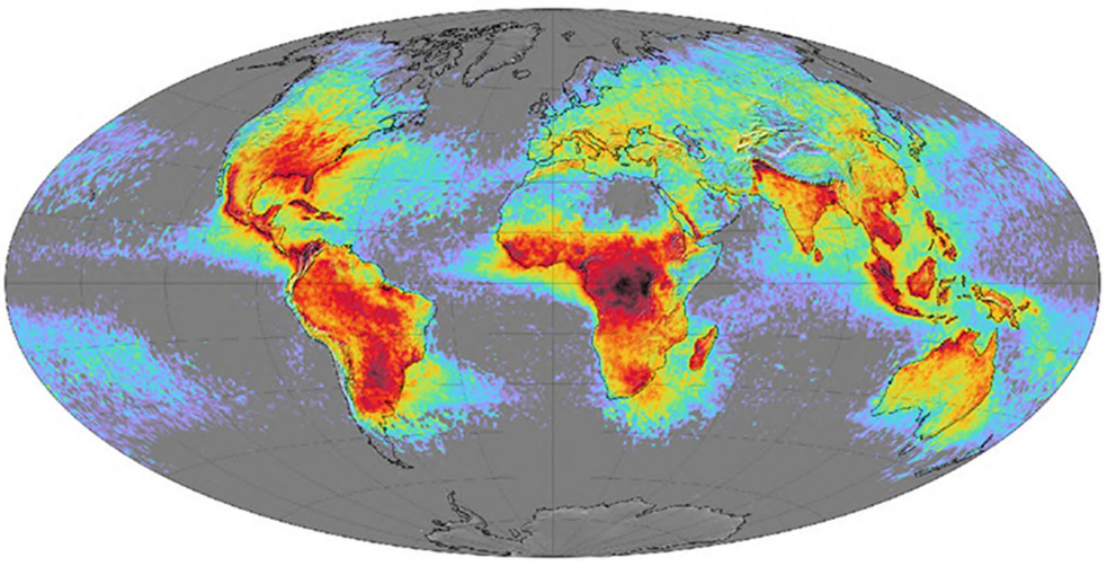

Fig . 1 - *'World map of the observed frequency of lightning strikes , in flashes ⟦km⟧^(-2) ⟦ year ⟧^(-1) (equal - area projection). Combined 1995 - 2003 data from the NASA OTD and 1998 -2003 data from the NASA LIS. NASA image by Marit Jentoft-Nilsen , based on data provided by the Global Hydrology and Climate Center Lightning Team . Reproduced with permission.*

NCGT Journal
New Concepts in Global Tectonics

New Concepts in Global Tectonics Journal
Volume 13, Number 6, August 2025

ISSN number; ISSN 2202-0039

Letters to the Editor: JWST and Hubble present new surprises that may be valuable to the community!

Hardening the Grid with Executive Order 14262: Scaling NBD Innovation for Solar and EMP Resilience

by Robert Miller[1]

The views expressed are the author's alone and do not represent any official positions.

[1] Tesla-3D in Denver, Colorado

For readers who want a rigorous, physics-first backdrop, the NCGT Journal review "Comets as probes of the solar wind; magnetospheres and cometospheres" (Vol. 13, No. 4, June 2025) lays out universal interaction rules, frozen-in field lines draped by the solar wind, pressure-balance at a magnetopause like boundary, and when a "cometosphere" behaves as a miniature magnetosphere. Plus concrete observational checks versus heliocentric distance. Those ideas are composition-agnostic, so they remain the right yardstick even if 3I/ATLAS looks chemically unusual (e.g., CO_2-dominated); the plasma physics of how any active nucleus couples to the wind still governs coma/tail structure and brightness. In short, this past NCGT Journal article provides the neutral framework we use to compare a CO_2-rich interstellar comet to canonical, H_2O-driven solar-system cases.

Checklist: What to compare explicitly in my Letter to the Editor:

- Volatile driver & mixing ratios vs. distance ($H_2O/CO_2/CO$): note where 3I/ATLAS departs from solar-system trends
- Dust vs. gas dominance and continuum color/slope (diagnoses the propulsion of grains)
- Metals: Ni I presence vs. Fe I limits; test carbonyl-linked Ni and CO correlations
- Coma/tail morphology in the solar-wind frame: field-line draping, magnetopause like boundary, neutral sheet indication
- Quantitative tail checks vs. heliocentric distance (e.g., cross-section scaling): apply the same tests across comets
- Imaging/spectroscopic anisotropies (sun ward enhancements, anti-tail) tied to out gassing physics
- Error-bar discipline & assumption audits when plotting diagnostic scaling

3I/ATLAS as a Natural Dusty-Plasma Experiment in the Heliosphere

by Robert Miller - Contributor, GeoPlasma Research Institute • Member, National EMP Task Force • Tesla3D, Inc.

During the past two weeks, interstellar object 3I/ATLAS has provided the geophysics and "geoplasma" communities with an exceptional experiment in solar-terrestrial coupling. Preliminary findings from JWST and SPHEREx indicate a coma dominated by CO_2 that is unexpectedly extensive and highly brightened in the sun ward direction. Observations from the VLT show a considerable surge in neutral nickel (Ni I) emission at greater heliocentric distances, with no matching Fe I present. These observations indicate an active process where UV photons break down nickel carbonyl complexes (e.g., $Ni(CO)_4$), thereby releasing Ni-rich nanoparticles into a coma characterized by high CO_2 and dust. To put it simply, 3I/ATLAS is introducing conductive nanograins to cometary plasma in the region where the solar wind interacts, charges, and recombines, allowing for a clean test of the "pinch-of-salt-changes-conductivity" concept that is familiar to some NCGT readers. (arXiv, SPHEREx, NASA Science)

What's new and why it matters:

JWST/NIRSpec detects a CO_2/H_2O mixing ratio of 8.0 ± 1.0 (6.1σ above the LPC/JFC trend at $r_h \approx 3.3$ au) and enhanced outgassing in the sunward direction. SPHEREx independently maps an extended CO_2 gas coma out to $\geq 3.5 \times 10^5$ km, with contemporaneous non-detections of H_2O and CO. Morphologically, Hubble resolves a **teardrop-shaped, sunward-brightened cocoon**, consistent with forward-scattered dust and a weak classical anti-tail geometry. This describes the observational anchors for an interstellar body consistent with a CO_2-rich, dust-heavy, sun ward-ejecting regime. (arXiv, SPHEREx, NASA Science, PMC)

On the metals side, VLT/X-shooter and UVES show a dramatic rise of Ni I with heliocentric distance while Fe I remains undetected; incipient CN out gassing is also observed.. This supports evidence that nickel is entering the gas phase efficiently through **low-activation channels** (photon-stimulated desorption, mild thermolysis, or **carbonyl formation plus photodissociation**), rather than by direct sublimation of refractory grains. The team specifically predicts a **Ni – CO_2 correlation** if carbonyl chemistry is in play and notes mid-IR **4.7–5.1 µm** bands where JWST could directly test for **$Ni(CO)_4$**. Ultrafast spectroscopy supports the mechanism: $Ni(CO)_4$ photo dissociates within picoseconds into NiCO, Ni, and CO under deep-UV conditions, enabling rapid conversion to Ni atoms and small clusters (with plausible nanoparticle formation) and vapor via solar UV exposure. (arXiv, PMC)

NCGT Journal
New Concepts in Global Tectonics

New Concepts in Global Tectonics Journal
Volume 13, Number 6, August 2025

ISSN number; ISSN 2202-0039

A dusty-plasma lens on 3I/ATLAS.

NCGT's audience has long emphasized **electromagnetic structure** in geophysical systems. Cometary comae are excellent dusty-plasma laboratories where **electrons, ions, and charged grains** share the current budget. Rosetta's in-situ record at 67P showed how **photoionization, electron-impact ionization, dust charging, and recombination** set the local plasma state; even modest changes in dust size distribution can **deplete electrons, shorten Debye lengths, raise effective resistivity**, and alter current closure and field draping. Injecting **vast surface area** in the form of **Ni-rich nanoparticles** into a CO_2-dominated coma should **enhance electron scavenging and recombination** , locally changing the plasma's effective electrical conductivity and current closure along draped interplanetary magnetic-field lines (i.e., how readily the plasma carries current along and across draped field lines). That is precisely the "pinch of salt" analogy: you alter the carrier population and collision landscape, and the system's **conductive response** changes measurably . (PMC, A&A , Physical Review Links)

Two additional feedbacks are worth noting:

1. **Solar-wind charge exchange (SWCX) and X-rays.** Cometary X-rays are predominantly SWCX photons. Their production and secondary photoelectrons feedback on dust charging and recombination. If 3I's Ni-nanograin injection ramps up electron losses (to grain surfaces) in the **sunward coma**, the spatial pattern of SWCX-driven secondaries and soft X-ray brightness could shift relative to a water-dominated analog. X-ray morphology can be used to diagnose these conductivity alterations through monitoring with NICER/Chandra or future SMILE-class imagers. (PMC, Astrophysics Data System, Frontiers)
2. Sunward coma and weak/classical anti-tail. A sunward-brightened coma with minimal classical dust tail is consistent with forward-scattering and anisotropic outgassing: SPHEREx shows no resolvable continuum extension at 1.0–1. 5 µm while revealing a very extended 4.3 µm CO_2 gas coma.. That is consistent with Hubble's morphology and with SPHEREx reporting no obvious tail structures at the time of its imaging. (NASA Science, arXiv, PMC)

Testable hypotheses are in order immediately.

Prediction A: Ni–CO co-evolution*:* If $Ni(CO)_4$ is a key parent, Ni I should correlate more strongly with CO than with H_2O; JWST should monitor fundamentals near 4.7–5.1 µm in tandem with VLT line monitoring.. JWST can also **search directly for Ni carbonyl features** near 4.7–5.1 µm in tandem with the VLT line monitoring. (arXiv)

Prediction B*: Dusty-plasma signatures :* As the nanoparticle surface area in the inner coma rises, Rosetta-style metrics would show **cooler electrons, lower ne, and altered spacecraft potential**—but in lieu of in-situ probes, observers can look for **enhanced dissociative emissions** (e.g., O I 6300 Å/1356 Å) that track electron-impact rates, and for **soft X-ray changes** indicative of SWCX electron production shifting with dust charging. Hybrid/PIC models calibrated to 67P can be ported rapidly to 3I's **CO_2-rich** conditions. (A&A, PMC)

Prediction C*: Morphology near orbital plane crossing:* If we catch 3I near the observer's **orbital-plane crossing**, an **anti-tail spike** may present even with minimal small-grain content; a sun ward enhancement due to forward scattering would help distinguish geometric projection from real nanoparticle-rich outflow. (PMC)

Regarding scope,

3I/ATLAS provides specific data concerning the materials within a cometary plasma, including its composition and grain size, factors that likely affect conductivity and current systems. For the **Stellar Transformer** framework and the wider **GeoPlasma** concept, this is extremely valuable: a transient, well-defined conductivity disturbance imposed on a solar-wind interaction region that can be observed in real time. (PMC)

Call to action.

I encourage a short, coordinated campaign: (i) **JWST/VLT** to test the **$Ni(CO)_4 \rightarrow Ni$** pathway and Ni–CO_2 co-evolution; (ii) **soft X-ray monitoring** for SWCX morphology; (iii) **radiative-transfer + dusty-plasma modeling** (Rosetta-vetted kernels) tuned to a **CO_2-dominated** coma with **nanoparticle-enhanced surface area**. Even in the absence of in situ probes, the combination should reveal whether "a pinch of nickel dust in a CO_2 bath" measurably **modulates electron flow and magnetic** effective conductivity and current closure along draped field lines in a cometary interaction region.

ISSN number; ISSN 2202-0039

Selected sources for readers

- Gregori and Leybourne, 2025. Comets as probes of the solar wind; magnetospheres and cometospheres NCGT Journal, June, V13N4, pp 606-674.
- JWST: Cordiner, M. A., et al. "JWST detection of a carbon dioxide dominated gas coma surrounding interstellar object 3I/ATLAS." arXiv:2508.18209 (2025). (arXiv)
- SPHEREx (preprint): Lisse, C. M., et al. "SPHEREx Discovery of Strong Water Ice Absorption and an Extended Carbon Dioxide Coma in 3I/ATLAS." arXiv:2508.15469 (2025). (arXiv)
- SPHEREx (news): "SPHEREx Discovers Extended Carbon Dioxide Coma in Interstellar Object 3I-ATLAS," Caltech/JPL SPHEREx News (Aug 21, 2025). (SPHEREx)
- Hubble/JWST mission notes: NASA Science blog posts on 3I/ATLAS (Aug 25, 2025). (NASA Science)
- VLT metals: Rahatgaonkar, R., et al. "VLT observations of interstellar comet 3I/ATLAS II: Dramatic rise of Ni I emission…" arXiv:2508.18382 (2025). (arXiv)
- Carbonyl photolysis: Cole-Filipiak, N. C., et al. "Ultrafast Production of NiCO and Ni Following 197 nm Photodissociation of Nickel Tetracarbonyl." (2024). (PMC, PubMed)
- Comet plasma environment (review): Goetz, C., et al. "The Plasma Environment of Comet 67P/Churyumov–Gerasimenko." Space Sci. Rev. (2022). (PMC)
- Ionization sources: Heritier, K. L., et al. "Plasma source and loss at comet 67P during the Rosetta mission." A& A (2018). (A&A)
- Forward scattering & dust dynamics: Marschall, R., et al. "Comae–Surface Links: Physics of Gas and Dust in Comae." Space Sci. Rev. (2020). (PMC)
- Hubble morphology: "As NASA Missions Study Interstellar Comet, Hubble Makes Size Estimate," NASA/ GSFC (Aug 7, 2025). (NASA Science)

ISSN number; ISSN 2202-0039

Company Profiles:

Tesla 3D, Inc. is an independent research and development company with a strong applied science foundation, enabling rapid and practical innovation in the energy and exploration sectors. While not a large enterprise, Tesla 3D, Inc. stays well informed about breakthroughs in electrical generation, storage, and mining technologies. When called upon, the company can comprehend complex challenges and develop strategic, real-world plans that effectively navigate regulations, funding mechanisms, and policies. Tesla 3D, Inc. actively contributes to national and industry advancement through volunteer leadership, including participation in the Homeland Security Taskforce focused on energy resilience and EMP (electromagnetic pulse) threats. The company also set a precedent by independently qualifying for federal Innovation (R&D) Tax Credits; demonstrating that small, agile innovators can leverage these incentives to streamline regulatory solutions and tackle critical infrastructure challenges. This involvement underscores Tesla 3D, Inc.'s commitment to advancing energy security and shaping the transformative role of technology in resource development. Founded: 2011 Colorado by R. Miller.

Geo-Transect LLP (www.tgeo.co.in**)** Geo-Transect LLP is a knowledge-driven geoscience consultancy, specializing in subsurface exploration and environmental intelligence across India. With core expertise in subsurface mapping, groundwater zonation, aquifer recharge quantification, coastal and shoreline analysis, landscape and topological planning, and island conservation, the firm delivers data-driven insights that empower sustainable planning and development. Representing the forefront of India's earth-science services sector, Geo-Transect blends scientific precision with advanced technologies to support governmental, industrial, and research-based initiatives across southern India and beyond. Integrating indigenous knowledge with global best practices, the firm is committed to environmental stewardship and responsible resource management. Guided by the ethos "With Wisdom in Nature," Geo-Transect envisions a future where scientific understanding harmonizes development with the natural world.

Stellar Transformer Technologies (https://stellartransformertechnologies.com/) is a private geophysical modeling company specializing in modeling the dynamic electro-magnetic Stellar Transformer interactions between Earth-Sun and planets within our solar system. Original research started in 1995 by the current owner and founder during investigations of the seafloor as a geophysicist with the Naval Oceanographic Office at Stennis Space Center. Leading to an understanding and application of new tectonic theories. Later research confirmed dynamic links to space weather affecting a myriad of environmental factors: such as everyday weather; hurricanes; tornadoes; sever weather outbreaks; earthquakes; global climate-change; and certain types of wildfire outbreaks from passing coronal mass ejections induced by internal core generated Electro-Magnetic Pulses (EMP). Current and planned services include mapping of Stellar Transformer circuits; innovative modeling of deep earth magnetics, forecasting Earth's natural hazards listed above; database development and more. Combining big data and AI to find inter-relationships. Developing algorithm inputs for forecasting, data visualization and simulations. All leading to new forecasting technologies. We are actively assisting the EMP Task Force power grid protection efforts with direct input and evaluation of EMP threats. Our company comprehends the complex challenges of geophysical modeling and development of real-world forecasting applications. Electro-magnetic or magnetic induction is the production of an electromotive force, or voltage, across an electrical conductor in a changing magnetic field. The Stellar Transformer Concept contends that simple step-down energy induction occurs between Sun and Earth, much like the transformer process that steps down your household energy from higher voltage transmission lines sourced from the power company. The Sun represents a large coil from the power company, while the Earth represents the smaller coil to your home. The larger coil element generally excites current into the smaller coil element by induction of "step down energy", although lesser feedback mechanisms occur due to the action/reaction principles. Layers within the Earth hold and release charge acting as condensers, or capacitance layers. Thus, the Earth operates somewhat like a battery where energy is either stored or released through time-change of state-of-matter. We combine new Geophysical Intelligence with AI for a winning combination of innovations that will bring new mitigation strategies for space weather to the forefront. Bringing a paradigm shift to the business community for global environmental forecasting based on solar and planetary effects. This will save lives and mitigate property damage using new science and innovative technologies. Many of these ideas were first presented at EU2015 - Electric Universe (https://www.youtube.com/watch?v=IoqgZhbxhhU). Followed up at EU2016 with discussions on geometrical modeling applications, adhering to golden ratio principles (https://www.youtube.com/watch?v=Q355Haapq-0). Founded: 2023 in Colorado by Bruce Leybourne – Owner/Operator.

NCGT Journal
New Concepts in Global Tectonics

New Concepts in Global Tectonics Journal
Volume 13, Number 6, August 2025

ISSN number; ISSN 2202-0039

Wildfires: a proxy of air-earth currents

Giovanni Pietro Gregori[1,2,3], Bruce Allen Leybourne[3]

[1] *IDASC-Istituto di Acustica e Sensoristica O. M. Corbino (CNR), Roma, now merged into IMM-Istituto per la Microelettronica e Microsistemi (CNR), Italy*
[2] *ISSO-International Seismic Safety Organization*
[3] *GeoPlasma Research Institute - (GeoPlasmaResearchInstitute.org), Aurora, CO 80014, USA*

Corresponding Author:
Giovanni Pietro Gregori
IDASC-Istituto di Acustica e Sensoristica O. M. Corbino (CNR), Roma, now merged into IMM-Istituto per la Microelettronica e Microsistemi (CNR) Italy
e-mail: giovannipgregori38@gmail.com; leybourneb@iascc.org

Abstract: Wildfires are an excellent proxy of air-earth currents. A wave of crustal stress is clearly envisaged, mapped by the density of wildfires. The wave starts from the Banda Sea, and it propagates northward along the Indochina peninsula. Then it bifurcates. One branch moves along the eastern coast of China until reaching an area slightly north of Beijing where an abrupt "flash" appears of the density of wildfires. Then, the crustal stress propagation stops. The other branch moves westward, partly through Myanmar and Bangladesh, and partly, maybe, along the Himalayas, where the ice cover of soil forbids the occurrence of wildfires. However, it ends up with an abrupt "flash" similar to - but even more evident than - the "flash" of the first branch. This second "flash" occurs somewhere in some area roughly in the Karakoram region. This cycle is observed regularly and repeatedly it is not a matter of coincidence

Keywords: wildfires trigger and fuel - planetary distribution of lightning – Banda Sea – Beijing area – Karakoram region – cyclic crustal stress and soil exhalation

Introduction

We call "climate" the "*space-time domain where the biosphere can develop and survive*". The science of "climate" must be distinguished from the statistics of environmental data - much like medical science must be distinguished from statistics compiled by *WHO*. Statistics and science are both useful but cannot be identified with each other.

Wildfires are a catastrophe that, during the last several years, is reported in several countries to occur with an increasing frequency, as extensively and regularly monitored by *NASA* satellites (*Earth Observatory*). Impressive photographs from satellite are often available. No discussion is here considered dealing with damages, with the mechanisms of development and evolution, and with the way of prevention and recovery. The focus is here on wildfires as a proxy of soil exhalation, hence of air-earth currents.

Authorities in general complain about arson being the likely primary cause of wildfires. Arson is unpredictable, whether it derives from a deliberate will or from unwanted accident. In contrast, it is hard to believe that a huge number of arson fires are simultaneously triggered within very large areas. Maybe, some conspicuous number of anthropic triggers eventually exists, but some relevant fraction of fires is certainly not arson.

In general, a mixture occurs of concurrent conditions that favor a wildfire. However, authorities - with no proof - generally claim that the fire was "probably" arson. The judiciary opens an investigation, and this represents the alibi to refrain from prevention actions for future hazard. A unique way seems available to prevent these catastrophes (e.g., Gregori, 2016; 2019), by means of fireproof corridors in order to contain fire. Every corridor must be kept permanently free of flammable dry grass, of bushes and brushes, and of dry leaves.

In any case, the largest part of wildfires is triggered by natural causes, independent of arson, even though humankind can be unconsciously responsible for wildfire trigger, because human activity is *per se* a part of the environment, i.e., this is just one aspect of anthropic "pollution". "Climate" is the result of all possible actions, and it is often difficult to separate natural and anthropic drivers. Exceptions are reported, e.g., very large wildfires occurred due to human action, in the Pantanal, a vast floodplain in South America, among the largest wetlands in the world (Voiland, 2020).

The natural exhalation of CH_4 is the primary fuel for wildfires. The exhalation of CO_2 is monitored by the *NASA* satellite *OCO-2* (see Gregori, 2020, and Gregori and Leybourne, 2021 and references therein). Conversely, the space distribution and time variation of atmospheric CH_4 concentration is not yet available. It was monitored by the *ESA* satellite *Sentinel-5 Precursor*, launched on 13 October 2017. An objective and regular monitoring of CH_4 exhalation can be provided, rather, by the planetary monthly-mean maps of wildfires, regularly provided by *NASA*'s *Earth Observatory*. In particular, an intriguing cyclic and impressively regular feature is emphasized.

The phenomenon seems to result from a combination of "domino effect" and of the sliding of the lithosphere following the uplift of a geotumor (Gregori et al., 2025a). The *NASA*'s *Earth Observatory* movie - where every single

NCGT Journal
New Concepts in Global Tectonics
New Concepts in Global Tectonics Journal
Volume 13, Number 6, August 2025
ISSN number; ISSN 2202-0039

frame is a monthly-mean of planetary distribution of wildfires – is a permanent monitoring update.

The most typical case history deals with Indochina. Wildfires are supplied by soil exhalation of CH_4. An increase of crustal fracturing favors a higher CH_4 exhalation, hence a larger number of wildfires. This cyclic feature can be repeatedly and regularly observed several times. A burst of wildfires starts from the tip of Indochina, perhaps triggered by an increased endogenous heat release in the Banda Sea. The Banda Sea region is the site of a particularly intense endogenous heat release that ought to produces a wave of crustal stress. Wildfires propagate through the whole of Indochina, until they bifurcate. One branch runs along the eastern China coast, until a "flash" of wildfire-density, which is abruptly displayed in some region slightly north of Beijing. Another branch runs through Himalaya, where no wildfires can be seen due to the ice cover, and south of it. But, after a while, a clear "flash" is observed roughly in the region of Karakoram. When these "flashes" are observed, the wildfire propagation seems to stop, and a new cycle promptly starts from Indochina etc.

In terms of physical explanation, the cyclic phenomenon ought to be the beat between the "domino effect" of crustal stress propagation, and the seasonal cycle, because wildfires require dry vegetation. On the other hand, no final and reliable interpretation is possible as long as no regular monitoring is available of crustal stress propagation (by means of acoustic emission, i.e., *AE* records; see Gregori et al., 2025a).

Other regions of the world envisage some relevant wildfire propagation, although - at present - no comparable regularity and/or repetitiveness is observed. It is therefore difficult to interpret observations with no support by *AE* monitoring of crustal stress propagation.

In addition to wildfires, other related proxies are here mentioned, such as house-fires, or beaching of deep-water fauna, or exceptional lightning strikes, or some other "unusual" phenomena that generally are not considered worthy of consideration. For instance, three recent findings agree and independently lead to an identical conclusion. These very clear hunches - although not being a "smoking gun" proof – seem to be a significant indication. One piece of evidence is, in general, the relation between solid Earth phenomena and "climate". Two additional findings are, respectively, *(i)* an astute analysis, carried out by the late John M. Quinn by means of an original inversion technique of 6 $months$ of records by the *CHAMP* magnetic satellite (see Quinn et al., 2025), and *(ii)* earthquake precursors associated with the coupling between soil and atmosphere (a large literature is available, and cannot be here quoted, but see Parrot, 2025, Straser et al., 2025, Wu, 2025, and references therein).

The planetary distribution of lightning

For future reference, the planetary mapping of lightning must be considered, including its secular variation (*SV*). In fact, air-earth currents affect the atmospheric electrical circuit, being one of the causes that contribute to the occurrence of lightning. Only a few maps are shown here, while several papers (not here listed) deal with a statistical analysis of their respective database.

Fig.1 refers to the period 1998-2003, Fig. 2 to April 1995 - February 2003, Fig. 3 to 2008-2017, Fig. 4 to 1995-2013, Fig 5 to 2010-2019, and Fig. 6 to 2010-2021. A very detailed analysis, in terms of seasonal variation and of correlation with tectonic features, was carried out by Albrecht et al. (2016) referring to the period 1998–2013. No details are reported here, as they are not pertinent to leading focus of the present paper.

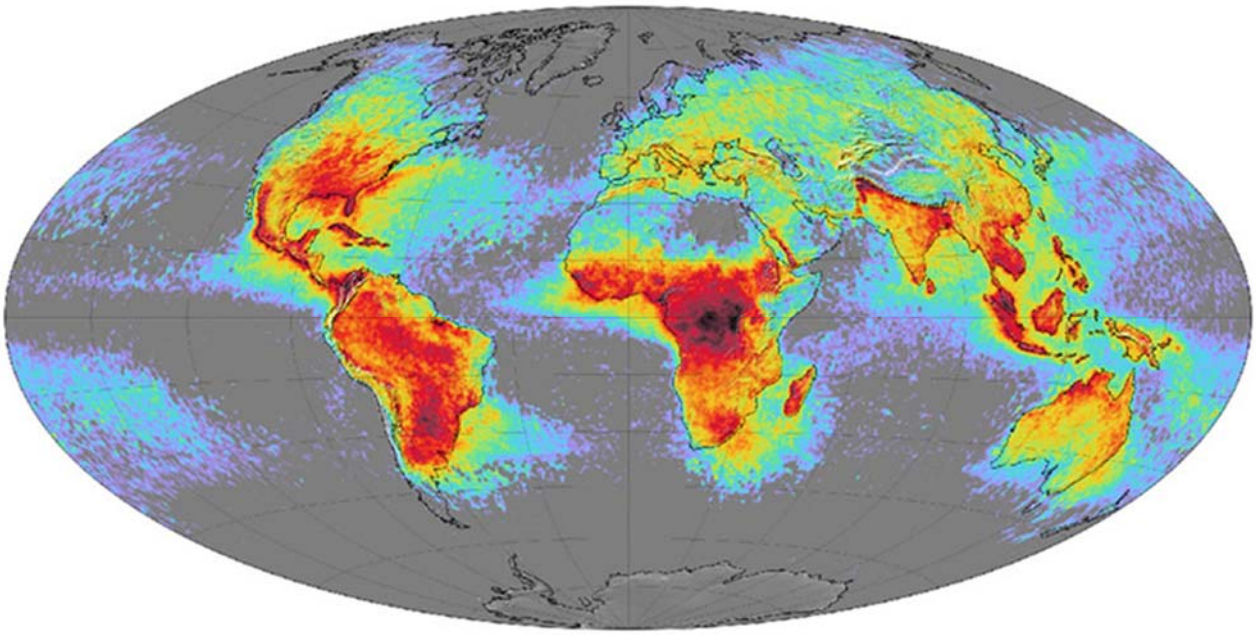

Fig. 1. World map of the observed frequency of lightning strikes, in $flashes\ km^{-2}\ year^{-1}$ (equal-area projection). Combined 1995-2003 data from the *NASA OTD* and 1998-2003 data from the *NASA LIS*. *NASA* image by Marit Jentoft-Nilsen, based on data provided by the *Global Hydrology and Climate Center Lightning Team*. Reproduced with permission.

NCGT Journal
New Concepts in Global Tectonics

New Concepts in Global Tectonics Journal
Volume 13, Number 6, August 2025

ISSN number; ISSN 2202-0039

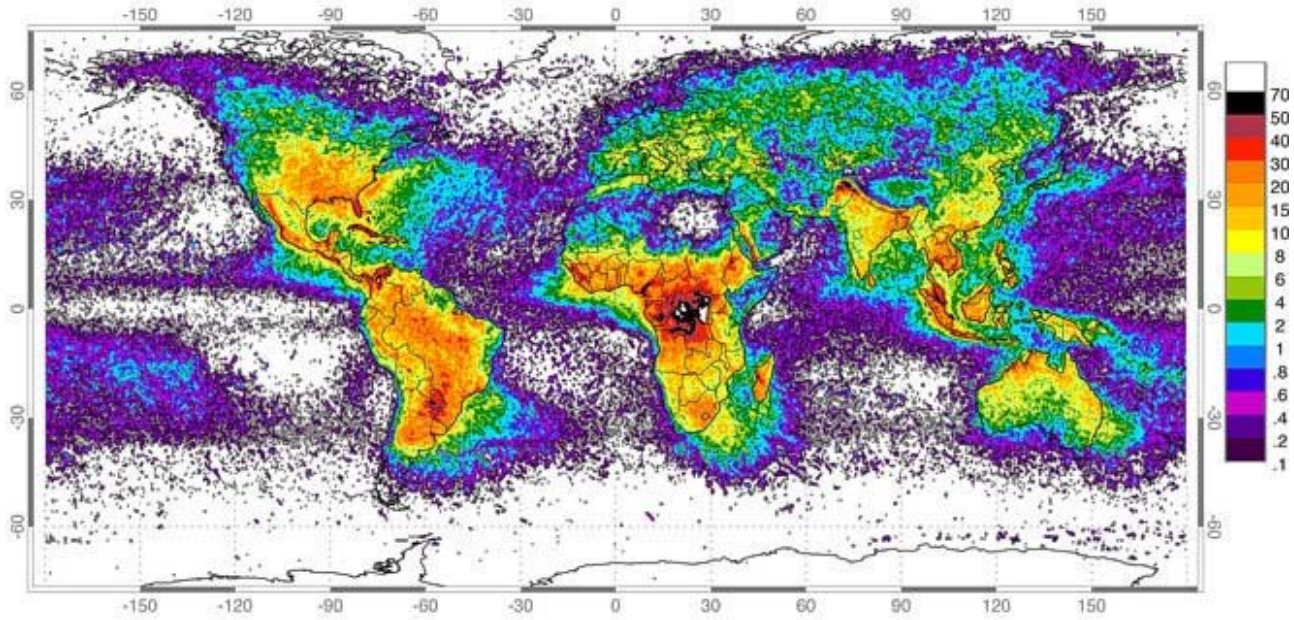

Fig. 2. High resolution global distribution of lightning yearly flash rate April 1995-February 2003 from the combined observations of the *NASA OTD* (4/95-3/00) and *LIS* (1/98-2/03) sensors. Image credit: *NSSTC Lightning Team, NASA*. After Science@ NASA Headline News, 5 December 2001. *NASA* copyright free policy.

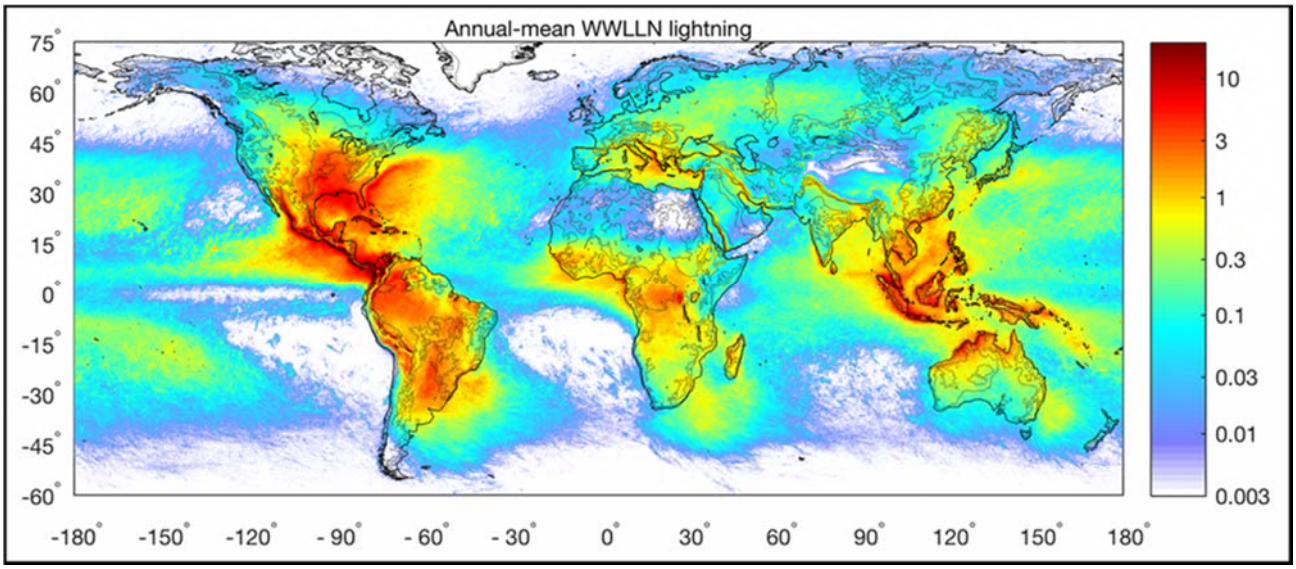

Fig. 3. "*Number of lightning strokes accumulated for the years 2008-2017, presented as strokes per year per square kilometer on a* $0.1^\circ \times 0.1^\circ$ *global grid. Data are from the* World Wide Lightning Location Network, *and the map is an upgrade of the* $0.25^\circ \times 0.25^\circ$ *global climatology published by Virts et al. (2013).*" Figure and captions after Aich et al. (2018). *AGU* copyright free policy.

NCGT Journal
New Concepts in Global Tectonics

New Concepts in Global Tectonics Journal
Volume 13, Number 6, August 2025

ISSN number; ISSN 2202-0039

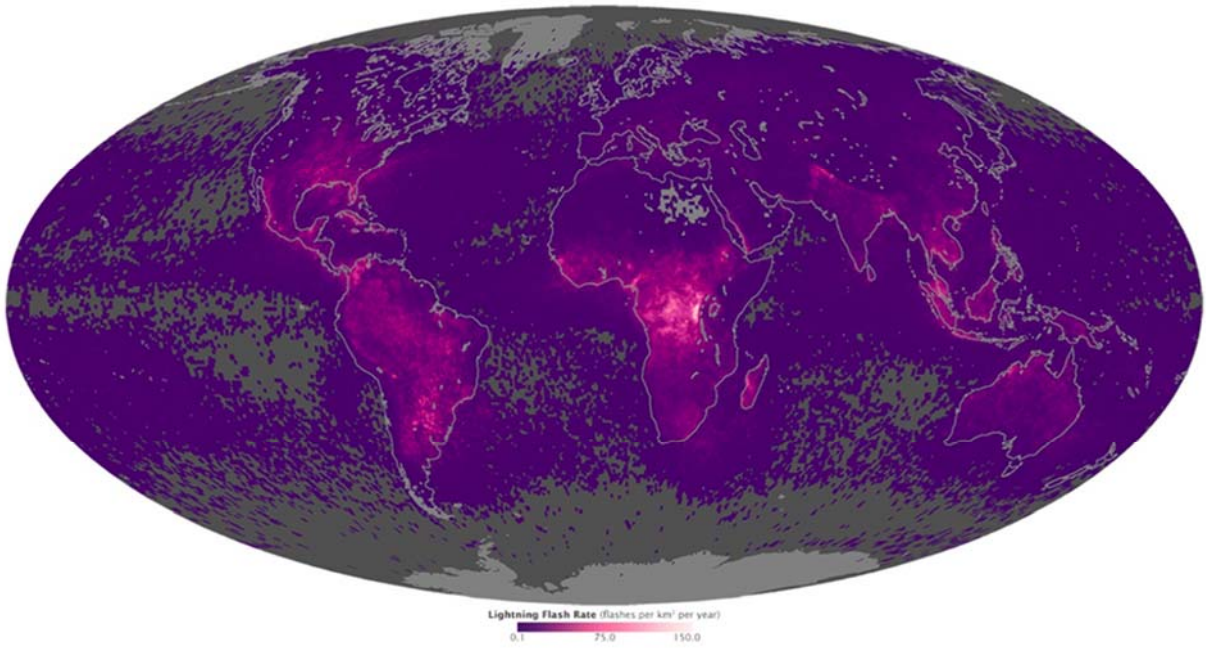

Fig. 4. "*Average yearly counts of lightning flashes per square kilometer from 1995 to 2013 … based on data collected from 1998-2013 by the* Lightning Imaging Sensor *(*LIS*) on* NASA*'s* Tropical Rainfall Measuring Mission *satellite, and from 1995-2000 by the* Optical Transient Detector *(*OTD*) on the OrbView-1/Microlab satellite. Flashes above* 38°*N were observed by* OTD *only, as the satellite flew to higher latitudes*." See text. Figure and captions after Hansen (2015). *NASA* copyright free policy.

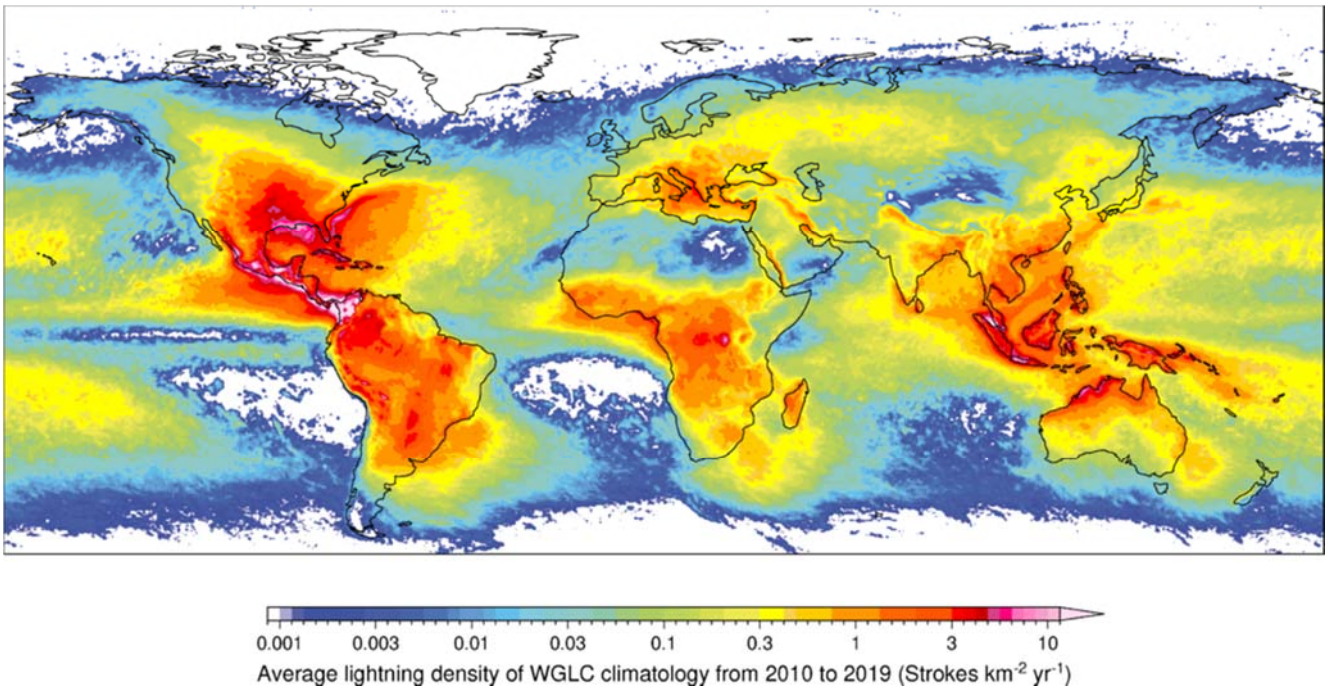

Fig. 5. "*Average lightning density of* World Wide Lightning Location Network (WGCL) *climatology from 2010 to 2019 (*$strokes\ km^{-2}\ year^{-1}$*)."* Figure and captions after Lau (2020). See also Kaplan and Lau (2021). Reproduced with CC BY 4.0 License.

NCGT Journal
New Concepts in Global Tectonics

New Concepts in Global Tectonics Journal
Volume 13, Number 6, August 2025

ISSN number; ISSN 2202-0039

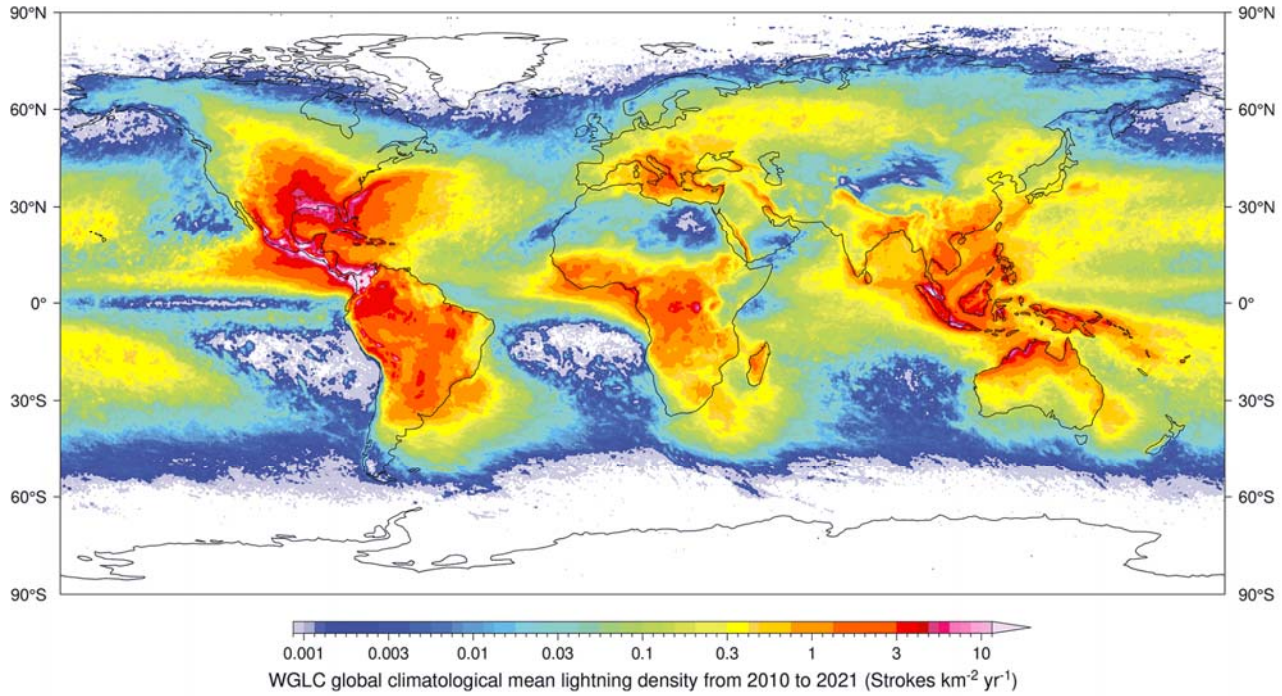

Fig. 6. Update of Fig. 5 referred to the period 2010-2021. After Kaplan and Lau (2022). Reproduced with CC BY 4.0 License.

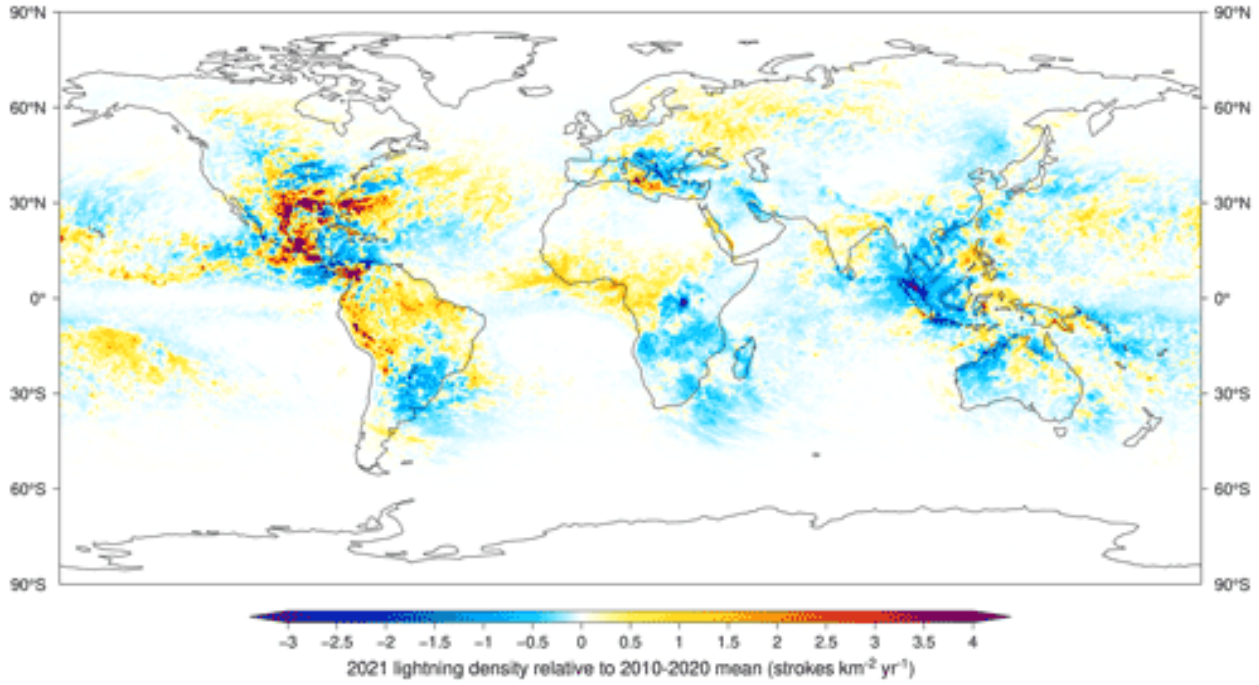

Fig. 7. "*Difference between lightning observed in 2021 and the 2010–2020 climatological mean.*" After Kaplan and Lau (2022). Reproduced with CC BY 4.0 License.

Some changes occur when comparing different years. A specific investigation was carried out by Kaplan and Lau (2022) who show Figs 6 and 7. The interannual change can be related either to atmospheric circulation – which is controlled by soil exhalation, i.e., by air-earth currents – or by a change of intensity of air-earth currents. In either case, one should monitor the planetary state of the atmospheric electrical circuit in order to understand the mechanisms responsible for the change. Note, in every figure, the enhanced lighting activity observed roughly in the Karakoram region.

The impact on atmosphere, on climate, and on soil

A few general mentions are here needed - with limited bibliographical details - while an increasing number of studies are becoming available, altogether with the ever-

ISSN number; ISSN 2202-0039

increasing number of wildfire reports. A reminder is here given about a few studies. Recent updates concerning more recent investigations ought to require a systematic review, not here carried out.

Consider the Earth like a "sensor" suited to monitor electric discharges by means of the effects associated to soil exhalation. This same phenomenon eventually affects airglow. In addition, it favors the discharge of the atmospheric condenser, e.g., in a way similar to earthquake lights (*EQL*) or to the mechanism associated with the "Andes lights", synonymous of "hot weather flashes" (see Gregori and Leybourne, 2025g). In fact, under very-extreme conditions, an electric discharge can be visible like a lightning discharge. However, even invisible discharges – which are the most frequent occurrence - can be important and sufficient to trigger a feeble diffuse light emission through some kind of almost invisible micro-sparks (see Gregori and Leybourne, 2025e, 2025f, 2025g).

Concerning the consequences of wildfires, the injection of aerosol is the first direct relevant impact, i.e., atmospheric particles with diameters $< 1 \mu m$ affect the aerosol optical thickness (*AOT*), hence the radiation balance of the atmosphere. In addition, aerosols contribute to the process of water condensation and precipitation that are an additional constraint on thermodynamics and on the water cycle - and, maybe, indirectly on atmospheric instability.

However, water condensation and precipitation require the presence of water – and convection that certainly occurs in wildfire areas. Hence, the impact of aerosols in dry areas is substantially other than in humid regions. Owing to a large amount of combustion heat, wildfires change the natural convection pattern that - through the Cowling dynamo (see Gregori et al., 2025d) - produces atmospheric precipitation, but also severely affects cloud dynamics. In fact, cloud dynamics, through the Cowling dynamo, is the primary generator that enhances the electrostatic charge of the ionosphere, i.e., of the atmospheric condenser.

Wildfires are a way by which the "sensor Earth" can detect and monitor a variation of the amount of soil exhalation. The efficiency of this "sensor" is, however, very different in different environments, depending on season, temperature, dryness, soil cover, wind, darkness, location of the observer, etc.

Unfortunately, these natural phenomena are biased by arson. Hence, their study can sometimes be poorly reliable. On the other hand, also the humans are a component of the time-varying natural environment. All this has been clearly emphasized by Tosca et al. (2015).

"*It is well established that smoke particles modify clouds, which in turn affects climate. However, no study has quantified the temporal dynamics of aerosol-cloud interactions with direct observations.*

Here for the first time, we use temporally offset satellite observations from northern Africa between 2006-2010 to quantitatively measure the effect of fire aerosols on convective cloud dynamics. We attribute a reduction in cloud fraction during periods of high aerosol optical depths to a smoke-driven inhibition of convection.

We find that higher smoke burdens limit upward vertical motion, increase surface pressure, and increase low-level divergence-meteorological indicators of convective suppression. These results are corroborated by climate simulations that show a smoke-driven increase in regionally averaged shortwave tropospheric heating and decrease in convective precipitation during the fire season.

Our results suggest that in tropical regions, anthropogenic fire initiates a positive feedback loop where increased aerosol emissions limit convection, dry the surface, and enable increased fire activity via human ignition."

A comparatively very intense event is briefly reported by Gannon (2018c), who relies on a contribution by David Peterson at the 2018 annual *EGU* meeting in Vienna.

"*Wildfires can fuel 'dirty' thunderstorms that fill the stratosphere with as much smoke as a volcanic eruption.*

That revelation comes from a study on the biggest fire-fueled thunderstorm event on record, which occurred on the night of August 12, 2017, in British Columbia, Canada …

Last year was a record breaker for wildfires in that region. And on that August evening, the heat from fires burning in relatively remote forests in British Columbia combined with the right atmospheric conditions to generate a series of four thunderstorms in a 5 hour period.

These fire storms are called pyrocumulonimbus storms, or pyroCbs. Like regular thunderstorms, they produce lightning and are very tall. [That is, in every respect, a huge ash-cloud is comparable to a volcanic plume. Hence, also electric discharge are comparable, i.e., either ash-cloud through the ionosphere by electron discharge, or ash-cloud to ground through negative ions temporarily suspended by the ionospheric electric field $\boldsymbol{E}$ that balances the weight of ash particles (see Gregori et al., 2025t).] *But pyroCbs are also filled with* [mostly electrically neutral] *smoke ...*

*The enormous smoke plume from the pyroCbs in British Columbia drifted over Europe and then eventually encircled the entire Northern Hemisphere (*NH*). Using satellite data, Peterson's team observed the signal from this smoke in the lower stratosphere for several months later.* [Note that a detectable climate impact, on the planetary scale, of a huge volcanic explosion that injects aerosols in the stratosphere lasts, say, roughly $\sim 6 - 7\ years$.]

... Normally, when you see something like this, you think volcanic eruptions ... but it's all coming from these wildfire-driven thunderstorms.

For comparison, the explosive 2008 eruption of Mount Kasatochi, an island volcano in Alaska, sent $\sim 0.7 - 0.9\ Tg$ *of aerosols ... into the stratosphere ... For months afterward, people around the* NH *documented unusually colored sunsets, thanks to the sulfate aerosols and ash the volcano injected into the atmosphere.*

Peterson's team estimated that the British Columbia pyroCb event sent ~ 0.1–0.3 Tg *of aerosols into the stratosphere - which is comparable to the amount seen with a moderate volcanic event, and more than the total stratospheric impact of the entire 2013 fire season in North America ...*

... The huge 1991 eruption of Mount Pinatubo ... lowered temperatures around the world by an average of $0.5°C$.

ISSN number; ISSN 2202-0039

... pyroCb events occur every year. But scientists have not studied these storms enough to understand their potential impact on the climate."

Another relevant impact is related to the effects on soil. Stoof et al. (2013) carried out an interdisciplinary experiment and some quantitative estimates. Wildfires burn an average of ~$3.7 \times 10^6\ km^2\ year^{-1}$ of vegetation. They leave landscapes scorched, barren, and vulnerable to erosion and flooding. This causes "*a substantial threat to life, property, and drinking water supplies in and downstream of burned areas ...* "

The general feeling based on experiments on small fields is that, for fires where smoldering combustion is absent, the more vegetative fuel the more intense the fire, the hotter the soil, and the more severe the damage to roots, seeds and microbes. However, the new experiment reported by Stoof et al. (2013), with more heterogeneous conditions, shows the opposite: the hotter the fire, the cooler the soil.

Indeed, the previous belief "*does not necessarily apply at the more relevant larger scale where soils, vegetation, and fire characteristics are heterogeneous. In a catchment-scale fire experiment, soils were surprisingly cool where fuel load was high and fire was hot and, conversely, soils were hot where expected to be cooler. This indicates that the greatest fire damage to soil can occur where fuel load and fire intensity are low rather than high, and has important implications for management of fire-prone areas prior to, during, and after fire events.*

High soil temperatures can considerably alter belowground ecosystem functioning. Effects range from seed and microbe mortality (~$60°C$*) ... and losses of nutrients (*$> 200°C$*) ... to the development of soil water repellency (*$175°C$*) ... losses of soil organic matter and water retention (*$> 200°C$*) ... and structural degradation ... These latter changes contribute to a reduction in infiltration that is frequently observed after fire ... and greatly contribute to the fire-induced increase in runoff and erosion. Information on soil temperatures reached during fire is therefore valuable for field managers ... and for the planning of hillslope rehabilitation treatments aimed at reducing environmental damage and increasing resilience of burned areas ... Because of this, fire damage to soil ('soil burn severity') is often assessed and used to map runoff and erosion risk and identify areas requiring post-fire treatments to mitigate these risks ... Unfortunately, soil burn severity cannot be mapped from satellite imagery alone; identification requires time-consuming ground-based measurements, thus making the risk mapping of post-fire land degradation tedious and complex ...* "

Several areas are interested by this kind of catastrophe, and several experiments were carried out at different locations, although always in a homogeneous environment. Stoof et al. (2013) claim that "*for an interdisciplinary study into the effects of fire on land degradation, we intentionally burned a* ~$0.1\ km^2$ *shrubland catchment in Portugal ... This gave us the opportunity to study the effect of landscape and fire heterogeneity on the relationship between fuel load, fire behavior and soil temperature in a large-scale field experiment. Before the fire, we mapped the catchment, calculated solar radiation and collected fuel data and during the fire we monitored soil surface temperatures, flame temperatures, fire intensity and fire spread*."

The most thickly vegetated areas look to burn at temperatures as high as $800°C$, while the topsoil remains below $100°C$. The reason ought to be related to an increase of upward transport of heat by convection, while dense vegetation contains most moisture. That is, also in these extreme conditions, vegetation exploits feedback for species survival.

In contrast, dry and sparsely vegetated areas burnt less intensely, but soil temperature at some places is even $> 300°C$ and it suffers the greatest damage. That is, a higher agglomerate of vegetation is a warranty for survival, much like it occurs for vegetation inside an oasis in a desert.

Conspicuous economic damages are involved, and wildfire monitoring and soil characterization are important challenges of applied science. For instance, McKenzie et al. (2012) report on a national database for calculating fuel available to wildfires. The whole difficult problem is highlighted and discussed by Kehrwald et al. (2013). The frequent wildfires in California permitted us to investigate the behavior and role of charcoal in the environment. The study was carried out by Maestrini et al. (2018) who summarize as follows their analysis.

"Pyrogenic carbon (PyC*) is hypothesized to play an important role in the carbon (*C*) cycle due to its resistance to decomposition; however, much uncertainty still exists regarding the stocks of* PyC *that persist on-site after the initial erosion in post-fire forests. Therefore, understanding how fire characteristics influence* PyC *stocks is vital, particularly in the context of California forests for which an increase of high-severity fires is predicted over the next decades.*

We measured forest C *and persistent* PyC *stocks in areas burned by low-to-moderate and high-severity fire, as well as in adjacent unburned areas in a California mixed-conifer forest,* $2-3\ years$ *after wildfire. We measured* C *and* PyC *stocks in the following compartments: standing trees, downed wood, forest floor, and mineral soil (*$0-5\ cm$*), and we identified* PyC *using the weak nitric acid digestion method.*

We found that the total stock of PyC *did not differ among fire severity classes (overall mean* $248 \pm 30\ g\ C\ m^{-2}$ *); however, fire severity influenced the distribution of* PyC *in the individual compartments. Areas burned by high-severity fire had* 2.5 *times more* PyC *stocked in the coarse woody debris (*$p < 0.05$*),* 3.3 *times more* PyC *stocked in standing trees (*$p < 0.05$*), and a lower* PyC *stock in the forest floor (*-22%, $p < 0.05$*) compared to low-to-moderate fire severity areas.*

These results have important implications for the permanence time of PyC*, which is putatively higher in standing trees and coarse woody debris compared to the forest floor, where it is susceptible to rapid losses through erosion."*

Diakakis et al. (2017) investigated the impact of wildfires on floods and landslides in the Peloponnese (Greece). They summarize their results and state what follows.

ISSN number; ISSN 2202-0039

"...Apart from the direct consequences, mega-fires induce long-term effects in the geomorphological and hydrological processes, influencing environmental factors that in turn can affect the occurrence of other natural hazards, such as floods and mass movement phenomena. This work focuses on the forest fire of 2007 in Peloponnese, Greece that to date corresponds to the largest fire in the country's record that burnt $1773\ km^2$ *, causing* 78 *fatalities and very significant damages in property and infrastructure. Specifically, this work examines the occurrence of flood and mass movement phenomena, before and after this mega-fire ...*

Observational evidence based on several data sources collected during the period 1989-2016 show that the 2007 fire has contributed to an increase of average flood and mass movement events frequency by approximately 3.3 *and* 5.6 *times respectively. Fire affected areas record a substantial increase in the occurrence of both phenomena, presenting a noticeably stronger increase compared to neighboring areas that have not been affected.*

Examination of the monthly occurrence of events showed an increase even in months of the year were rainfall intensity presented decreasing trends. Although no major land use changes has been identified and chlorophyll is shown to recover $2\ years$ *after the fire incident, differences on the type of vegetation as tall forest has been substituted with lower vegetation are considered significant drivers for the observed increase in flood and mass movement frequency in the fire affected areas."*

Kim et al. (2015) studied accelerated deforestation in the humid tropics from the 1990s to the 2000s. They summarize as follows their results.

"*Using a consistent,* $20\ year$ *series of high-(*$30\ m$*) resolution, satellite-based maps of forest cover, we estimate forest area and its changes from 1990 to 2010 in* 34 *tropical countries that account for the majority of the global area of humid tropical forests.*

Our estimates indicate a 62% *acceleration in net deforestation in the humid tropics from the 1990s to the 2000s, contradicting a* 25% *reduction reported by the* UN FAO Forest Resource Assessment. *Net loss of forest cover peaked from 2000 to 2005. Gross gains accelerated slowly and uniformly between 1990-2000, 2000-2005, and 2005-2010. However, the gains were overwhelmed by gross losses, which peaked from 2000 to 2005 and decelerated afterward. The acceleration of humid tropical deforestation we report contradicts the assertion that losses decelerated from the 1990s to the 2000s."*

Also, reforestation was considered. For instance, Yuan et al. (2014) report about a project carried out in China.

"The Chinese government started implementation of the Grain for Green Project *(*GGP*) in 1999, aiming to convert cropland to forestland to mitigate soil erosion problems in areas across the country.*

Although the project has generated substantial environmental benefits, such as erosion reduction, carbon sequestration and water quality improvements, the magnitude of these benefits has not yet been well quantified due to the lack of location specific data describing the afforestation efforts.

Remote sensing is well suited to detect afforestation locations, a prerequisite for estimating the impacts of the project. In this study, we first examined the practicability of using the MODIS *land cover product to detect afforestation locations; however, the results showed that the* MODIS *product failed to distinguish the afforestation areas of* GGP.

*Then, we used a normalized difference vegetation index (*NDVI*) time series analysis approach for detecting afforestation locations, applying statistical data to determine the* NDVI *threshold of converted croplands. The technique provided the necessary information for location of afforestation implemented under* GGP*, explaining* 85% *of conversion from cropland to forestlands across all provinces. The coefficients of determination between detected afforestation and statistical areas at the most provinces were* > 0.7 *which indicated the high performance. Moreover,* $> 60\%$ *of* GGP *locations identified in all the provinces had a slope of over* 25°*, which was consistent with the main criterion of* GGP. *These results should enable wide application of the method to evaluate the impacts of the project on regional carbon budgets, water yield and soil erosion."*

Model computation - and forecast of future evolution - are, however, difficult. For instance, refer to Kitzberger et al. (2017) who investigated the case history of North America, and conclude that "*annual wildfire area burned in coming decades is likely to be highly geographically heterogeneous, reflecting interacting regional and seasonal climate drivers of fire occurrence and spread."*

Indeed, according to the evidence, which is here reviewed, wildfires are almost entirely supplied by soil exhalation and triggered by a natural driver. The phenomenon depends therefore on the space-time distribution of endogenous heat release. Hence, it is impossible to implement any model until a suitable monitoring is eventually available of the endogenous heat release. In contrast, wildfires are to be considered as an effective and reliable natural "sensor" suited to monitor soil exhalation of CH_4, i.e., air-earth currents.

Jin et al. (2012) investigated the latitudinal dependence of wildfire effects through Canada. They "*used time series of satellite observations of surface albedo from 2000-2011 and fire perimeters since 1970 to study post-fire changes in surface net shortwave radiation along a latitudinal transect in central Canada. Fire induced surface shortwave forcing (*SSF*) integrated over an annual cycle for the first* $30\ years$ *after fire was similar (*$-4.1\ W\ m^{-2}$ *with a* 95% *confidence interval of* -4.5 *to* $-3.7\ W\ m^{-2}$*) between southern and northern boreal regions. The lack of a latitudinal difference in* SSF *was caused by counteracting latitudinal trends in seasonal contributions. Spring (March, April, and May)* SSF *increased with latitude, from* $-7.2\ W\ m^{-2}$ *in the south to* $-10.1\ W\ m^{-2}$ *in the north, primarily because of delayed snow melt, which amplified albedo differences between unburned forests and recovering stands. In contrast, winter incoming solar radiation and summer albedo change decreased from south to north, resulting in a decreasing latitudinal trend in winter and summer* SSF.

NCGT Journal
New Concepts in Global Tectonics
New Concepts in Global Tectonics Journal
Volume 13, Number 6, August 2025
ISSN number; ISSN 2202-0039

Vegetation recovery was slower in the north, leading to smaller increases in summer albedo during the first decade after fire, and a prolonged phase of elevated spring albedo during the second decade. Our results indicate that fires reduce surface net shortwave radiation considerably for many boreal forest ecosystems in North America, providing further evidence that disturbance-mediated shifts in surface energy exchange need to be considered in efforts to manage these forests for climate change mitigation."

All this shows how complicated is the relationship with - and feedback by – the biosphere, which acts both like a passive and an active agent for climate control. The phenomenon involves almost the entire planet (see below). A few regional maps are sometimes available. For instance, *NOAA* made a map of USA for wildfires during 2011 (Fig. 8).

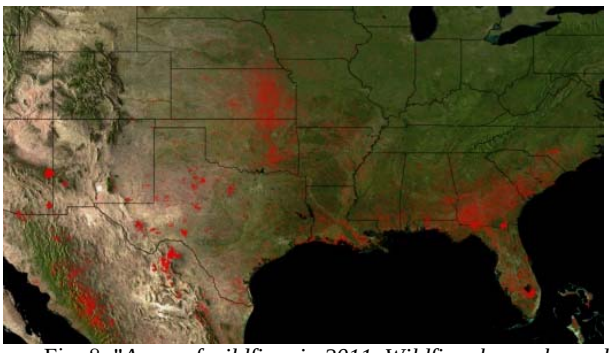

Fig. 8. "*A sea of wildfires in 2011. Wildfires have plagued much of the Southern U.S. in 2011. The data shown here plots the locations of all wildfires detected by sensors aboard the* NOAA AVHRR *and* GOES *Imager, and* NASA MODIS *satellite sensors over the entire year-to-date. Each red point is one fire - and there are thousands of them plotted here. The data shows over* 346,000 *fires - though that is an overestimate since different satellites may double-count the same fire 'target', but some may not see any at all.* NCDC *has tallied the number of U.S. wildfires at* 33,109*, but this number relies on human observations on the ground, which is probably an underestimate. The Okefenokee Swamp fire near the Florida-Georgia border, along with the Wallows fire in eastern Arizona are clearly visible as large red areas. The Okefenokee has been burning for months, and the Wallows is now the largest in Arizona history. Persistent droughts and high winds throughout much of the Southwest have created conditions ideal for wildfires during much of the winter and spring of 2011. Many of the fires in Texas, Oklahoma, and Nebraska are also drought-induced. The large fire signatures south of Lake Okefenokee in Florida are agricultural in nature*." Figure and captions after *Anonymous* (2011i). *AGU* copyright free policy.

In Fig. 8 a high density of wildfires is displayed through Oklahoma and Kansas that is just along the Dallas-Winnipeg line, which is stressed in Gregori and Leybourne (2021) and Gregori et al. (2025a). That is, this is an Earth's surface signature of the tetrahedron edge of the mid-ocean ridges (*MOR*s) planetary pattern (see Gregori and Leybourne, 2021), which is likely to be related also to the geodynamic explanation of the New Madrid seismic zone (Gregori et al., 2025x). Fig. 8 shows the precise location of soil exhalation, while the New Madrid-Wabash Valley Fault Zone shows the location of maximum crustal stress deriving from the large-scale deformation of the lithosphere – and is associated to the tetrahedron deep conductor through this area (Gregori and Leybourne, 2021; Gregori et al., 2025x).

Dennison et al. (2014) investigated the trend of large wildfires in the western United States during 1984-2011. They "*used a database capturing large wildfires* ($>$ 4.05 km^2) *in the western U.S. to document regional trends in fire occurrence, total fire area, fire size, and day of year of ignition ... Over the western U.S. and in a majority of ecoregions, we found significant, increasing trends in the number of large fires and/or total large fire area per year. Trends were most significant for southern and mountain ecoregions, coinciding with trends toward increased drought severity. For all ecoregions combined, the number of large fires increased at a rate of* 7 $fires\ year^{-1}$*, while total fire area increased at a rate of* 355 $km^2\ year^{-1}$ *...* " [That is, since the historical trend of endogenous heat release is increasing *vs.* time, also the frequency increases of soil exhalation and wildfire.]

A specific precise analysis was carried out by Lehsten et al. (2014). They used two datasets referring to the northern boreal areas, i.e., "*the* Canadian National Fire Database *(*CNFDB*) (*Canadian Committee on Forest Management*, 2012) and the boreal burned area data (*BBA*) generated by a further development of algorithm described in George et al. (2006) ... Since the* CNFDB *data before 1960 are considered to be less accurate than data for later years ... we excluded all fires before this time. Though the* CNFDB *contains very detailed fire records including small* ($<$ 1 *ha*) *fires, we excluded all fires below* 100 ha *of area since this data is of poor quality, especially in the first few decades ...*

The BBA *is a new satellite-based fire scar product ranging from 2001 to 2011, which identifies burnt areas in the boreal region on a daily basis with a* 500 *m resolution; hence, the minimum fire size considered is around* 25 *ha. It covers most areas in Canada and Alaska as well as northern Europe, Russia, and northern parts of China (Fig. 9). The* BBA *algorithm relies on the synergy of several* MODIS *products ...*

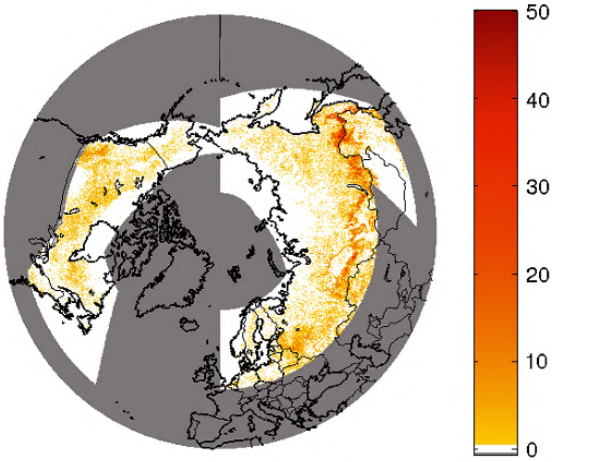

Fig. 9. "*Investigation area of the* BBA *(white) and number of fires in the combined data set per* 0.166° *pixel (mapping unit of the ecoregions map). The* CNFBD *covers the Canadian forested regions*." Figure and captions after Lehsten et al. (2014). *AGU* copyright free policy.

New Concepts in Global Tectonics Journal
Volume 13, Number 6, August 2025
ISSN number; ISSN 2202-0039

As we were only interested in 'woody' areas, we restricted our analysis to International Geosphere-Biosphere Programme *classes* 1 *to* 8 *...Any areas* $< 4\ pixels$ *in area were removed. The burnt areas are then dated using thermal anomalies ... "*

They carried out a careful statistical analysis, which is not here reported as it is not pertinent for the present discussion. They claim that they *"analyzed the contribution of fires of different fire size classes to the total burned area and suggest a novel fire characteristic, the characteristic fire size, i.e., the fire size class with the highest contribution to the burned area, its relation to bioclimatic conditions, and intra-annual and interannual variation."*

They used data from *CNFBD* (1960-2010) and the *BBA* data set (2001-2011). They correlated their data with the ecoregion divisions developed by Bailey (1995).

They "*found that the fire size distribution is best explained by a normal distribution in log space in contrast to the power law-based linear fire area relationship which has prevailed in the literature so far. We attribute the difference to previous studies in the scale invariance mainly to the large extent of the investigated ecoregion as well as to unequal binning or limiting the range at which the relationship is analyzed; in this way we also question the generality of the scale invariance for ecoregions even outside the boreal domain.*" [This means that, as it had to be expected, the probability of occurrence of a wildfire of a given surface extension is proportional to the number of wildfires of that given extension. Hence, their distribution must be lognormal (see Arley and Buch, 1950 and Paparo and Gregori, 2003).]

The characteristic fire sizes and the burned area show a weak correlation, indicating different mechanisms behind each feature. Fire sizes are found to depend markedly on the ecoregion and have increased over the last five decades for Canada in total, being most pronounced in the early season. In the late season fire size and area decreased, indicating an earlier start of the fire season." [In fact, the local biosphere is crucial for the characterization of the environment, while several degrees of freedom (*d.o.f.*s) are involved.]

As a general comment to Fig. 9, the comparatively larger fire density is likely to be closely related to permafrost, which is the ecoregion characterized by a large seasonal soil exhalation of geogas (including CH_4), consistently with the seasonal exhalation of CO_2 (see Gregori, 2020; Gregori and Leybourne, 2021 and references therein). Other local factors certainly enter into play, as a wildfire is a sensor with an efficiency that is more or less sensitive depending on the local biosphere.

Dooley (2012) refers to the pollution by isocyanic acid, which has relevant health implications (e.g., Potera, 2011; Young et al., 2012). He shows wildfires in eastern Siberia, in July 2010, during the big wave of wildfires that crossed entire Russia through whole Siberia. The patchy pattern of wildfires is evidenced in Fig. 10. In fact, some area of limited extension corresponds to a bunch of sea-urchin spikes that coalesced into one unique spike. Another possibility is that endogenous heat of frictional origin is mainly released inside a limited area. In either case, a small geotumor is generated, and cracks are formed that are located, approximately along a closed line around its topographic uplift. The crack is propagated through the "domino effect" (see Gregori, 2013a). Exhalation of CH_4, which supplies wildfires, occurs along the crack, hence the observed pattern of fires is located along closed lines.

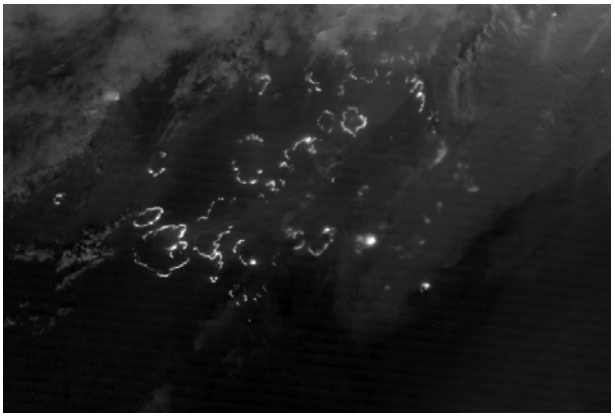

Fig. 10. "*Night fires. Rings of flame burn through eastern Siberia in this satellite image taken on August 3, 2013. Scientists have long been able to snap photos of smoke from wildfires from Earth's orbit, but this image comes from a new, extra-sensitive instrument on the* Suomi National Polar-Orbiting satellite *(*Suomi NPP*) called the* Visible Infrared Imaging Radiometer Suite *(*VIIRS*). This instrument can detect very low levels of light, making it possible to capture pictures of forest fires burning at night. Credit:* NASA Earth Observatory *image by Jesse Allen and Robert Simmon, using* VIIRS *Day Night Band data.*" Figure and captions after Pappas (2013). *NASA* copyright free policy.

The health concern is stressed by Wei et al. (2023), illustrated by *University of Iowa* (2023) that claims that "*wildfires over two decades have severely impacted air quality in the western U.S., increasing health risks and negating efforts to reduce pollution, with a conservative estimate of 670 extra premature deaths per year.*" They give a map of USA and Canada map showing areas with the highest concentrations of black carbon, a fine-particle air pollutant that has been linked with human respiratory and heart disease.

Only a few additional aspects are here discussed, focused on items related to the present discussion concerning the evidence of a possible climate impact of endogenous energy release. In any case, it is very likely that it is possible to "forecast" in space and time where and when the conditions can eventually occur that are prone for an eventual generation of natural wildfire. This can be achieved *(i)* by measuring the electric field $\boldsymbol{E}$ associated with the local electrostatic charge of the ionosphere, *(ii)* by mapping the location of the sea-urchin spikes in the hazard areas, and, maybe, *(iii)* by measuring the electrical conductivity σ of air. Monitoring the transient luminous events (*TLE*s), observed over some larger area, can, perhaps, result helpful (Gregori et al., 2025a).

When fire-prone areas are known - such as close to the top of sea-urchin spikes - it is possible to keep preventive actions in order to reduce wildfire hazard. For instance, consider that the Caronia phenomenon (see Gregori et al., 2025a) is one example of a very restricted local effect

ISSN number; ISSN 2202-0039

associated to a sharp sea-urchin spike that occurs in a typical volcanic area.

Some discussion is given by Smoot and Leybourne (2001) and Leybourne et al. (2004a, 2004b) concerning solar activity and geological trends, including eventual hydrocarbon volatile that are released either from oil fields or from coal mines, and are eventually associated with hotspot areas.

Some wildfire outbreaks in Florida were reported, and in Southern California, during the October 2003 "*Fire Siege*" that occurred simultaneously with a Coronal Mass Ejection (*CME*) (*USFS*, 2003; Lopez et al., 2004; Leybourne et al., 2004a). That is, a large increase occurred of the electric current intensity inside all sea-urchin spikes (Gregori and Leybourne, 2021, and Gregori et al., 2025a). This caused greater exhalation, while also the efficiency increased of the electromagnetic (e.m.) coupling with the ionosphere. The more efficient atmospheric electrical circuit generated better-suited conditions for the development of wildfires. The exceptional character of this *CME* is expressively highlighted by Lopez et al. (2004) as follows.

"... sunspot group 484 *came around the limb of the Sun on 18 October. By 23 October, when* 484 *was located right on the Earth-Sun line, this huge group covered* 1.7% *of the solar disk. At the far edge of the Sun, another massive sunspot group,* 486*, was just coming into the field of view. And late on the 26th, a third group,* 488*, emerged from the interior of the Sun just to the north of* 486 *(Fig. 11).*

With this sudden increase in sunspots came a series of solar flares. The most powerful, X-class, have an integrated power $(1.0-\ 80\ \text{Å}) > 0.0001 W\ m^{-2}$.

... The first of the X-class flares occurred on 19 October ...On the 23rd, another are registering between X4 and X5 was observed. This was followed by a series of smaller M- and X-class flares.

On 28 October, 486 *faced directly toward Earth, and it unleashed a huge X-17.2 solar are (Fig. 12). At the time, it was the third largest on record since 1976 ...*

The CME *was clocked leaving the Sun at* ~2000 $km\ sec^{-1}$ *... "*

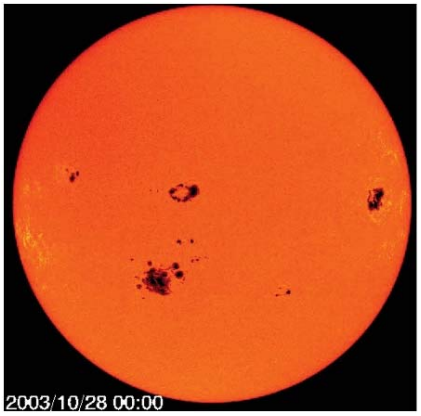

Fig. 11. "*This white light image of the Sun on 28 October shows large sunspot groups* 484 *(to the right),* 486 *(lower center), and* 488 *(center).*" Figure and captions after Lopez et al. (2004). *AGU* copyright free policy.

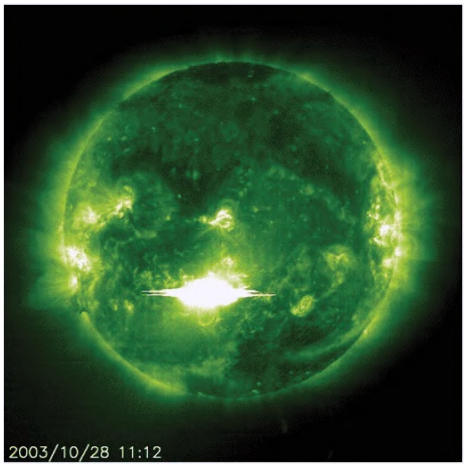

Fig. 12. Solar *CME* on 28 October 2003 (Halloween storm) that resulted to be directly correlated with the Southern California 2003 "*Fire Siege*". This is an *Extreme ultraviolet Imaging Telescope* (*EIT*) 195 Å image of the Sun. Image courtesy to Lopez et al. (2004) of the *Solar and Heliospheric Observatory* web site (*SOHO*, 2003). *AGU* copyright free policy.

Several satellites and space probes were severely affected, being overwhelmed by the blast of solar particles and radiation.

"*An X10 are exploded out of* 486 *the following day, and it also launched a* CME *at the Earth. The impact of the two* CMEs *precipitated a major geomagnetic storm beginning at 0800 UT on the 29th that was the fourth largest in the past* 40 $years$ *... The storm finally ended on Halloween, but sunspot group 486 was not yet done. As it rotated to the solar limb, it let go one last blast on 3 November. The X-rays from the flare, eventually rated an X28 ... was the largest are recorded since such measurements have been made. Earth was not directly in the path of the* CME *launched by this event, and so the geomagnetic effect was limited ... "*

This is a clear example, which shows the well-known fact that not all sunspots have the same effect on the Earth, depending on the radiation that is released, and on the location of the sunspot with respect to the Earth. Note, however, that the physical mechanism could be other than in association with solar flares. In fact, the sunspots in Fig. 11 appear to be largely concentrated inside very limited regions of the Sun's photosphere. In addition, the solar corona expansion displays large variations at different times (see Gregori and Leybourne, 2025b, 2025c; Gregori et al., 2025c). This state of the Sun is very likely to be associated to large gradients in the solar wind flow - as it is also shown by the anomalous large spots observed on the outer gaseous planets during MiniMax years (see Gregori and Leybourne, 2025c). Consider the very anomalous pattern shown during the August 2017 total solar eclipse.

Just recall that the Earth, with its whole magnetosphere, at $1\ AU$ interacts with a fraction $\sim 0.45 \times 10^{-9}$ of the spherical surface of the expanding solar corona (see Gregori and Leybourne, 2025b, 2025c; Gregori et al., 2025c). Hence, the Earth is an "almost point-like" natural probe inside the expanding solar corona suited to monitor every large spatial gradient of the solar wind flow. Therefore, in

NCGT Journal
New Concepts in Global Tectonics
New Concepts in Global Tectonics Journal
Volume 13, Number 6, August 2025
ISSN number; ISSN 2202-0039

these circumstances, the e.m. induced telluric currents are particularly intensified.

That is, the space-time gradient of the solar wind flow is relevant, more than its intensity. In addition, as a frequently occurring standard, telluric currents are channeled on the planetary scale (e.g., Lanzerotti and Gregori, 1986). Therefore, the trigger for wildfires can be associated with a temporarily planetary increased intensity of telluric currents underground, rather than with some anomalous discharge through the atmospheric electrical circuit.

Following the aforementioned 2003 "*Fire Siege*" in Florida and Southern California (Leybourne et. al., 2004, 2006, 2020), similar fire emergencies were reported in subsequent years from different parts of California. Almost every year a new record number of wildfires is reported, and no regular forecast seems possible. For instance, Jenner (2015) reports about summer 2015, when wildfires raged across the western US and Alaska. Many of those fires burned in the US Northwest. The 2015-2016 El Niño was unprecedented, exceptional, and very intense (see Gregori and Leybourne, 2025j). Hence, analogous phenomena occurred that were correlated to one another on the planetary scale.

For instance, a wildfire crisis hit southern Borneo in October 2015 due to the great drought that occurred in Indonesia (e.g., Santoso, 2018). Also 2017 was a year with huge wildfires through California (see images in Weisberger, 2017g; Wall, 2017i, 2017j; Lunsford, 2017a). Fig. 13 shows how wildfires raged contemporarily in different States, when Alaska had a particularly dramatic situation, maybe related to permafrost thawing.

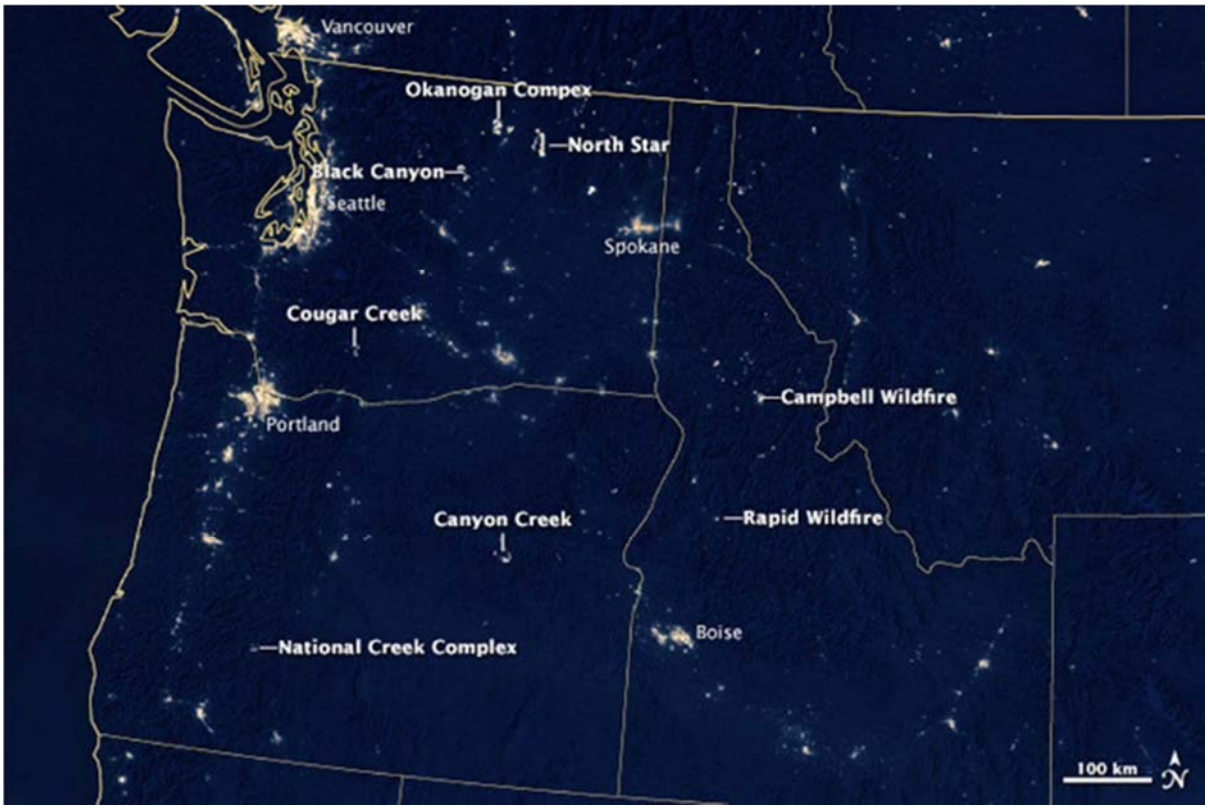

Fig. 13. Wildfires across the western US in summer 2015. "*This image was acquired in the early morning local time on August 19 with the* Visible Infrared Imaging Radiometer Suite *(*VIIRS*) sensor on the Suomi* NPP *satellite. The image was made possible by the instrument's 'day-night band', which uses filtering techniques to observe dim signals including those from wildfires. Labels point to the large, actively burning fires in the region. According to the* Northwest Interagency Coordination Center*, the Okanogan Complex Fire in Washington was among the larger active fires ... References:* NASA Earth Observatory *(2015, August 16) Fires in the Pacific Northwest.* Northwest Interagency Coordination Center *(2015, August 20)* Northwest Large Fire Information Summary. *Accessed August 21, 2015.*" Figure and captions after Jenner (2015). *NASA* copyright free policy.

In addition, several phenomena (volcanism, seismicity,[1] atmospheric dynamics, "global warming", etc.) indicate that - according to the rationale highlighted by Gregori and Leybourne (2021) - a long-term increase is in progress of the intensity of the "central fire" supplied by the *TD* (tide driven) dynamo and of geodynamic activity and seismicity, according to the rationale of warm mud tectonics (*WMT*) (Gregori, 2002; Gregori and Leybourne, 2021; Gregori et al., 2025a). Owing to this reason, soil exhalation also ought

[1] For instance, the Ring of Fire around the Pacific Ocean experienced eight $M \geq 6.5$ earthquakes during the first three weeks of August 2018 (Hickok, 2018a).

ISSN number; ISSN 2202-0039

to be correspondingly increased, hence also the mean frequency of wildfires referring to one and the same region.

Indeed, "*the trend in wildfire destruction in California and throughout the West bends toward bigger, more destructive and drought-driven blazes. On average, wildfires burn* 6 *times the acreage they did* 40 *years ago, while the annual number of wildfires over* 1,000 *acres (*4 km^2*) has doubled from* 50 *during an average year in the 1970s to more than* 100 *each year since 2002 ...* " (Magill, 2015). The trend seems to increase every year.

A temporary wildfire record in California was achieved during the 2018 season, which was increased in subsequent years. According to the *California Department of Forestry and Fire Protection* (*Cal Fire*) and the *National Interagency Fire Center* (*NIFC*), by November 30, 2018 (see article on Paradise Lost - Leybourne et. al., 2020a) this catastrophe underscored ~8,000 $wildfires$ and a ~3,000 km^2 burned area. Even the final count of fatalities (the order of magnitude was almost ~100 or maybe even more) seems to be yet unknown. A large number of dramatic satellite images are available (see, e.g., Wall, 2018n and Pappas, 2018a).

According to the general rationale that is here proposed, it is not a matter of chance that such a violent and tragic catastrophe occurred during the aforementioned MiniMax years (see Gregori and Leybourne, 2025b, 2025c; Gregori et al., 2025c), while - during some longer time lag - an anomalous high seismicity was observed worldwide, climate change seemed to have largely speeded up, atmospheric storminess seemed to have enhanced, and also violent storms were observed on the outer gaseous planets (Gregori and Leybourne, 2025c).Therefore, as far as California is concerned, a detailed investigation of the local morphology ought to be carried out, in order to understand why the ~8,000 $wildfires$ spread out at either one site rather than another. In fact, some common feature ought to be shared by the ~8,000 respective timing and location of every event. Maybe, significant statistics are available. The location of California ought to be considered, which is over the inland prolongation of the East Pacific Rise, or *EPR* (Leybourne et al., 2004a, 2006), corresponding to one edge of the tetrahedron pattern (Gregori and Leybourne, 2021).

That is, we should afford to envisage whether *(i)* some anomalous soil exhalation of CH_4 occurred, or rather *(ii)* a peculiar e.m. coupling happened of the ionosphere with the local underground sea-urchin spikes, or *(iii)* an increase of soil exhalation triggered an intense atmospheric convection that, through the Cowling dynamo, abruptly strengthened atmospheric electricity and discharges. Indeed, one should not consider only lightning discharges, which are, rather, only a spectacular manifestation of a phenomenon that - although unobserved - is certainly a steay occurrence (see Gregori and Leybourne, 2025e, 2025f, 2025g). Maybe, all three mechanisms occur simultaneously. Understanding these features are crucial in order to improve capabilities of preventing or mitigating future events.

Sometimes exceptional wildfires hit other countries (e.g., Italy, Greece, western Europe, ... in general, these phenomena are frequent occurrences in the Mediterranean area). Owing to the ongoing climate change, wildfires seem to be a frequent catastrophe that hits several countries of all continents every summer. No additional detailed case histories are here shown. Fig. 14 clearly shows that in general wildfires are independent of anthropic action. Australia is on top of a vertex of the tetrahedron pattern of deep conductors (Gregori and Leybourne, 2021). This also reminds one about the aforementioned continental size wildfires through Eurasia, occurring in summer 2010.

In general, a trigger of a natural fire occurs during periods of comparatively higher temperature and drier atmosphere, such as during a hot summer. For instance, Cai et al. (2009) searched for an explanation for "*the devastating 'Black Saturday' bushfire inferno in the southeast Australian state of Victoria in early February 2009*", which caused $>$ 170 causalities, and for the "*the 'Ash Wednesday' bushfires in February 1983*". Both these catastrophes were preceded by a *positive Indian Ocean Dipole* (*pIOD*) event. These events, which involve relevant atmospheric anomalies, are a phase in which the eastern Indian Ocean is cooler than usual, while the western Indian Ocean is warmer than usual (see Gregori et al., 2025a, and Gregori and Leybourne, 2025j). These "dipole" phenomena seem to be a regional-scale feature associated with some planetary atmospheric "oscillation". In any case, these conditions tend to lead to lower than average - rainfall and higher temperatures over southeastern Australia.

Therefore, the *pIOD*s reduce soil moisture. Hence, "*during Victoria's wet season, particularly spring, a* pIOD *contributes to lower rainfall and higher temperatures exacerbating the dry conditions and increasing the fuel load leading into summer. Consequently,* pIOD*s are effective in preconditioning Victoria for bushfires, more so than El Niño events, as seen in the impact on soil moisture on interannual time scales and in multi-decadal changes since the 1950s*."

That is, the Earth responds as a unique system (see Gregori et al., 2022a), and atmosphere, ocean, and air-earth currents contribute to every occurrence.

Cai et al. (2009) thus showed that *11* of *16 pIOD* events since 1950 were followed by major bushfires, and *11* of the past *21* major bushfires were preceded by *pIOD*. They also found that bushfires are more strongly associated with *pIOD* events than with El Niño events. Indeed, a *pIOD* is likely to be one facet of *ENSO*, although several *ENSO* events are not associated with a *pIOD*. That is, *ENSO* is a manifestation of different kinds of occurrences. Thus, the Southern Oscillation air-earth current tectonic teleconnection between Banda Sea on the Western Pacific Rim and Easter Island on the East Pacific Rise [see "El Nino tectonic modulation in the Pacific basin (revisited) by Leybourne and Adams, 2020, https://www.iiisci.org/journal/sci/FullText.asp?var=&id=IP094LL20] is likely a domino or daisy chain teleconnection to air-earth currents of the Congo-Lake Victoria lighting anomalies controlled by the Southeast Indian Ridge (*SEIR*) circuit connected to the South Pole via the Australian-Antarctic Discordance (*AAD*) south of Australia.

NCGT Journal
New Concepts in Global Tectonics

New Concepts in Global Tectonics Journal
Volume 13, Number 6, August 2025

ISSN number; ISSN 2202-0039

Fig. 14. "*Mystery lights in Western Australia.* NASA *and* NOAA *recently released a series of images from the Suomi* NPP *satellite showing Earth at night, lit by city lights. So why is nearly uninhabited western Australia so bright? It's not a lost civilization or a quirk in the data. As it turns out, wildfires were burning in western Australia in April and October 2012 when the satellite collected these images. The fires got incorporated into the composite picture created by* NASA *and* NOAA*, freezing the fires in time. Other uninhabited areas on the so-called 'Black Marble' images show lights from ships, oil drilling and mining operations. Credit:* NASA Earth Observatory/NOAA NGDC." Figure and captions after Pappas (2013). *NASA* copyright free policy.

It should be stressed, however, that several "climate" effects are triggered by an identical primary driver, i.e., by increased soil exhalation of endogenous energy, and several effects seem therefore correlated to each other, even though no direct cause-and-effect relation exists between the respective phenomena. Rather, they share a common cause.

See also the analysis by Liang (2014) by means of the "*information flow*", a statistical tool by which it is concluded that "*the causality* [between El Niño and the Indian Ocean Dipole index *IOD*] *is asymmetric: El Niño tends to stabilize* IOD*, while* IOD *functions to make El Niño more uncertain. To El Niño, the information owing from* IOD *manifests itself as a propagation of uncertainty from the Indian Ocean ...*

In other words, to El Niño, the Indian Ocean is a source of uncertainty, and the causality from IOD to El Niño is manifested as a propagation of uncertainty from the former to the latter. This assertion is also substantiated by the causality analyses between the El Niño index and the Indian Ocean SST. The resulting information flow rates, both $T_{ElNiño \to Indian}$ *and* $T_{Indian \to ElNiño}$ *, clearly show a structure reminiscent of the* IOD *and* IOBM *(*Indian Ocean Basin Mode*), which has been missing in previous observational data analyses with traditional approaches.*"

The *IOBM* is a pattern derived from dynamical models. For instance, Yang et al. (2009) claim that "*observational analysis and model experiments show that the* SST *anomaly associated with the* IOBM*, which persists from spring to summer, can generate significant circumglobal teleconnection (*CGT*) in the* NH *summer midlatitude atmosphere. A warm* IOBM *can induce a new atmospheric heating source in the south Asia through a positive feedback. An enhanced Indian summer monsoon through the increased precipitation in the south Asia induces an atmospheric heating source there. This new atmospheric heating source generates an anomalous high to its northwest over the western-central Asia, which in turn generates an eastward downstream atmospheric wave train, forming the* CGT.*"*

Owing to brevity purpose, this statistical formalism and these dynamical models cannot be here explained in detail, and the interested reader ought to refer to Liang (2014) and to the literature on the dynamic models of atmosphere and ocean.

However, sometimes wildfires are (although seldom and exceptionally) reported also during winter, such as, e.g., in the Alps valleys in northern Italy during days of foehn (in German Föhn, a specific wind called in this way in Austria, in southern Germany and in the German language parts of

ISSN number; ISSN 2202-0039

Switzerland). In fact, when the meteorological circulation is strong enough and air is forced over mountains during a relatively short period of time, it experiences adiabatic temperature changes. That is, it cools due to the lower pressure, but - if condensation temperature occurs - owing to the release of latent heat, this cooling is reduced. While flowing downward over the leeward slopes, the air - which is now much drier - is warmed due to the increasing pressures at lower altitudes. This warming is greater than the former cooling, as heat was added as a result of condensation: the air is warmer and drier than originally. A dry, warm, gusty wind eventually results, even with gale force. In winter, snowmelt can be rapid. Desiccating effects - in summer, but sometimes even in winter - can be so strong that bushfires occur, due to friction triggered by wind - but also due to micro-sparks originated by e.m. field caused by micro-Cowling dynamo. The effect sometimes rapidly spreads wildfires. Some regions are particularly fire prone.

Also, as already mentioned, the recovery time of vegetation after a wildfire ought to be investigated.[2] The phenomenon depends on the local climate.

Summarizing, according to the rationale of the present study, the trigger of wildfires can occur either *(i)* where a more intense flow occurs of channeled telluric current, or *(ii)* where electrostatic sparks occur through the atmospheric electrical circuit. In either case, electrostatic sparks are more probable to occur right on top of sea-urchin spikes, where the e.m. coupling with the ionosphere is more efficient, and e.m. induction with underground circuits is more effective. In addition, a suitably intense local electrostatic charge in the ionosphere over these areas ought to favor wildfire occurrence.

On the other hand, at present no mapping exists either of channeled currents - apart the Faynberg and Sidorov (1978) maps (Lanzerotti and Gregori, 1986) - or of sea-urchin spikes (apart, maybe, some of Quinn's figures, see Quinn et al., 2025). These maps are not suited to investigate these phenomena, which typically involve only very local features that cannot be represented on a global map. In addition, no electrostatic monitoring of the ionosphere is regularly carried out. Hence, according to the present available monitoring, these catastrophes remain a seemingly unexplained whim of nature, and we are completely incapable of forecasting or prevention. There is need for some substantially improved multidisciplinary monitoring.

The foehn hazard involves every mountain-range of the world. Alternative equivalent names for foehn are: *Halny* in the Carpathian mountains, *Fogony* in the Catalan Pyrenees, *Viento Sur* in the Cantabrian region (northern Spain), *Terral* in Màlaga, *sky sweeper* over Majorca, and the *aspre* over the Garonne plain of France, *Bergwind* in South Africa, *Chinook winds* in the Rocky Mountains, United States/Canada and in the Chugach mountains of Alaska, *Diablo winds* in the San Francisco Bay Area, *Santa Ana winds* in Southern California, *Zonda winds* in Argentina, the *Nor'wester* in Canterbury and Otago, New Zealand, ... Sometimes these winds are called *snow-eaters*, or *murder winds* due to the Föhnkrankheit (i.e., Föhn-sickness).

Fig. 15 shows a typical example of a very small spatial scale. It shows an area slightly NW of Pisa, Italy. On September 25th, 2018, at about 10 p.m. LT, a widespread wildfire occurred inside the red circle in the administrative area of Calci and Vicopisano, seemingly starting from four spots. It involved $\sim 6\ km^2$. Over 500 people were evacuated.

Fig. 15. Wildfire close to Pisa on September 25th, 2018. The red spot indicates the location of fire, and the blue arrow the wind direction. See text. Base map after *Anonymous* (2018m) (copyright © 2000-2018 - *Reti e Sistemi, Trapani*). The image is a Google map, kindly granted by *Google*.

The previous few months had been particularly hot. Soil was very dry, with dry grass, say $\sim 1.5\ m$ tall, growing among woods. The meteorological circulation abruptly changed with cold and humid, strong wind, blowing from NE (light blue arrow). The wind channeled along the valley. It rose up to the mountain ridge at the top of the valley. Then, the foehn blew down off the slope towards Pisa.

Consider that the hot soil probably triggered micro-scale convection and Cowling dynamo, originating electric field. Also consider friction heat (which is a different way to call the micro-Cowling dynamo effect), consider the strong wind, and consider the particularly dry and flammable grass. In addition, the region west of the Apennines is well-known to be characterized by geothermal phenomena that are likely to be associated to some relevant and undetected CH_4 exhalation. That is, altogether, a mixture occurred of concurrent environmental conditions that favored wildfire.

The role of *Santa Ana winds* has been investigated by Langford et al. (2015, also reported by *Anonymous*, 2015k, 2015m), who claim that the phenomenon is enhanced by stratospheric intrusions. The transport through the tropopause is a difficult topic of meteorology and is not here discussed. Note, however, that – maybe - this kind of phenomena could be better described in terms of air-earth currents related to soil exhalation. This possibility should be suitably checked by observations (see Gregori et al., 2025h).

[2] For instance, a *NASA* movie is available, concerning the Yellowstone National Park during $30\ years$ (Salazar, 2018b).

NCGT Journal
New Concepts in Global Tectonics

New Concepts in Global Tectonics Journal
Volume 13, Number 6, August 2025

ISSN number; ISSN 2202-0039

"*The Santa Ana winds of Southern California have long been associated with wildland fires that can adversely affect air quality and lead to loss of life and property. These katabatic winds are driven primarily by thermal gradients but can be exacerbated by northerly flow associated with upper level troughs passing through the western U.S. ... we show that the fire danger associated with the passage of upper level troughs can be further increased by the formation of deep tropopause folds that transport extremely dry ozone-rich air from the upper troposphere and lower stratosphere to the surface. Stratospheric intrusions can thus increase surface ozone both directly through transport and indirectly through their influence on wildland fires ...* " [On the other hand, one should consider the possibility that the stratospheric effects are a consequence of increased atmospheric convection due to wildfire.]

They study, in particular, the aforementioned case histories "*of the Springs Fire, which burned nearly* $100\ km^2$ *in Ventura County during May 2013*."

According to *Anonymous* (2015k), "*the analysis showed that in the early hours before the Springs Fire, a tongue of air characteristic of the stratosphere – extremely dry and very high in ozone from the stratosphere's ozone layer - reached to the surface in southern California and extended as far south as Baja California.*

The researchers found that ground-based monitoring stations near the fire's origin also confirmed the telltale signs of the intrusion right before the fire broke out: a large drop in relative humidity and a rise in ozone. As the day went on, a combination of factors accelerated the fire: low humidity, persistent high winds, dry condition of the grasses and other vegetation, clear skies and bright sunlight, and very warm surface temperatures. A few days later, cloudy skies, a drop in temperature, a shift in winds, and widespread rainfall helped extinguish the fire."

Stratospheric intrusions add to surface ozone pollution with implications for health, but they also "*contribute to the fire danger, particularly during La Niña years when deep intrusions are more frequent ...*

... stratospheric intrusions have previously been implicated in the explosive development of wildland fires in New Jersey and Michigan, but have not previously been connected to fires in southern California or to the Santa Ana winds. The frequent occurrence of stratospheric intrusions above the west coast during the fall, winter, and spring suggests that similar circumstances may have played a role in other major southern California fires, including the series of destructive fires that burned $> 3{,}000\ km^2$ *in October 2003, and burned ~*$4{,}000\ km^2$ *in October 2007 ...* " The October 2003 Halloween wildfire outbreak coincided with an Earth directed *CME* that elevated Total Electron Content (*TEC*) directly over Southern California likely triggering an e.m. induction driven wildfire outbreak. The 2003 Halloween San Bernardino and the November 2018 Paradise wildfire outbreaks both occurred from shorted global circuits during *CME*s and occurred at intersections of the north-south San Andreas Fault and east-west fracture zones from the Pacific, i.e., the Murray and Mendocino fracture zones, respectively, both underlain by volcanic plutons, i.e., sea urchin spikes. (see Leybourne et. al. 2020a and Leybourne and Orr, 2020; for a fuller explanation also see, *Orthogonal Megatrend Intersections "Coils of a Stellar Transformer"*;Smoot and Leybourne, 2020).

In general, every trigger, which derives from phenomena that occur in the interplanetary environment, is denoted as "Space Weather". An ever-increasing amount of literature is presently reported by scientific journals, and no attempt is here made to review it. "Space Weather" is primarily controlled by solar activity and it includes variations in the solar wind and interaction with the geomagnetic field and magnetosphere. Also, galactic cosmic rays have been considered as a secondary source of "Space Weather", being related to the Forbush decrease and to the $\sim 11\ year$ sunspot or $\sim 22\ year\ Hale$ cycle (Lui, 2001). In general, also a field reversal (*FR*) of the geomagnetic field is a peculiar effect of "Space Weather", as it is caused by a dramatic fading off of the solar wind originated by the encounter of the Solar System with a dense cloud of interstellar matter (see Gregori et al., 2025e and references therein). However, even more extreme events, maybe, occasionally occur (see Leybourne et al., 2025; Gregori et al., 2025x).

CMEs (Fig. 12) are extreme events, which can produce bursts of high energy particles and X-rays. One should not be excessively concerned about the frequency range of the signal. *CME*s are impulsive bursts being, however, an index of some very complicated phenomenon, involving large changes in the entire release of solar wind by the Sun (see Gregori and Leybourne, 2025b, 2025c; Gregori et al., 2025c), with a consequent large gradient of e.m. induction into the whole Earth system.

In fact, when their associated effects impinge on the Earth, *CME*s can cause disruptions in telecommunications, and adversely affect spacecrafts, aviation, and trigger electrical spikes in railways, power transmission grids, and oil and gas pipelines (see Lanzerotti and Gregori, 1986). That is, "Space Weather" incidents causing power outages are common during these extreme events, although this is a matter of e.m. induction into manmade technological systems, eventually causing fires.[3]

In this same respect, sometimes the concern was raised dealing with the wildfire hazard associated with power lines. On the one hand, power lines act like a Faraday cage that, in general, in some way is expected to reduce wildfire hazard. On the other hand, a power line is a channel for electric currents that are induced over some much larger area - even on the planetary or continental scale – and therefore a power line eventually results to be a conveyor for e.m. fields that sometimes can thus result to be locally enhanced, compared to the case of no power line through the same area. Differently stated, even a power-blackout is

[3] For instance, in Norway, in the early 1900s, some telegraph bureaus had spontaneous blazes; Størmer (1955) used them as an alert for planning auroral observation. Or recall the 1859 Carrington Event that melted telegraph systems in Western U.S. and Europe, simultaneously.

New Concepts in Global Tectonics Journal
Volume 13, Number 6, August 2025
ISSN number; ISSN 2202-0039

an effect of large-scale e.m. induction in the power-cable network.

Even in such a circumstance, however, a spark that triggers a wildfire can occur only on top of a sea-urchin spike. In fact, the e.m. coupling between shallow telluric currents and deeper electric currents is more likely to activate an eventual spark on top of a sea-urchin spike. In principle, in every such a case history, a simple lightning rod (instead of power lines as in the Paradise case of melted tower bases of downed power lines spreading wildfire) in the area on top of one or several sea-urchin spikes is the best practical operative prevention against wildfire hazard (consider, e.g., the Caronia phenomenon; see Gregori et al., 2025b). In any case, a lightning discharge is generally reported to be a primary frequent trigger of a wildfire. But these discharges occur right on top of some anomalous underground conducting structure, such as a typical sea-urchin spike.

Summarizing, the practical most useful information is to know the location of sea-urchin spikes (generally occurring, perhaps, at many orthogonal megatrend intersections (Smoot and Leybourne, 2020)), because a wildfire is likely to be triggered right on top of it, whether the extra current inside it is triggered by an endogenous source, or by some secondary effect associated with a power line or with any other manmade device.

An analysis of the *NASA Earth Observatory* wildfire movie

According to this whole rationale, it is interesting to consider the planetary scale space-time distribution of wildfires, monitored by satellite.

Beginning in 2000, *NASA*'s *Earth Observatory* issues a movie with fire maps that "*show the locations of actively burning fires around the world on a monthly basis, based on observations from the* Moderate Resolution Imaging Spectroradiometer *(*MODIS*) on* NASA*'s* TERRA *satellite*." [4] Large and remarkable space patterns are displayed. The accompanying comments propose the following interpretation.

"*Some of the global patterns that appear in the fire maps over time are the result of natural cycles of rainfall, dryness, and lightning*. [Note that lightning cycles are related both *(i)* to time variation of the electric potential of the ionosphere and *(ii)*, in addition, also to the ground-ionosphere e.m. coupling, which can be different at different sites, depending on local soil exhalation and sea-urchin spikes.]

For example, naturally occurring fires are common in the boreal forests of Canada in the summer [likely due to permafrost thawing]. *In other parts of the world, the patterns are the result of human activity. For example, the intense burning in the heart of South America from August-October is a result of human-triggered fires, both intentional and accidental, in the Amazon Rainforest and the Cerrado (a grassland/savanna ecosystem) to the south. Across Africa, a band of widespread agricultural burning sweeps north to south over the continent as the dry season progresses each year. Agricultural burning occurs in late winter and early spring each year across Southeast Asia*."

Several of these drivers are certainly a realistic hypothesis, and human activity is a serious bias while attempting to envisage natural causes. In addition, also other effects are likely to be associated with the peculiar local coupling between the ionospheric ***E*** and sea-urchin pattern in subsoil.

Upon a visual (i.e., only indicative, as far as the exact location is concerned) inspection of this movie, the following morphological features can be inferred, and they ought to be interpreted.

- An effect, which is suggestive of an undoubtedly meteorological driver, occurs through the latitude band of tropical forest, from Africa through Central America and Venezuela, while a comparably lesser effect occurs in the Sunda archipelago, being the likely quenching effect of ocean water and of its associated atmospheric circulation.
- An analogous effect, although triggered by dryness, is likely to occur in Australia, mainly in its northern part.
- A comparatively lesser, although well defined, feature is observed - almost regularly - in North America., where wildfires seem to be frequent, and are generally spread through the whole continent. Their distribution is not uniform, although in general they seem to display no clear regularity. There is, however, one exception, i.e., an almost straight line of greater numbers of wildfires occurs along the segment that - upon looking at the movie - roughly joins Dallas with Winnipeg (see Fig. 8 for a more precise location of the area of direct soil exhalation). According to the rationale of the present study, this feature ought to denote a possible alignment of several sea-urchin spikes, which determine a greater probability of occurrence of electric discharges, whether there are manifested like a lightning, or rather they are invisible. Note, however, that - in general - a sea-urchin spike can be a feature that is much deeper than the available geological evidence. Therefore, there is no need to expect that this pattern can be clearly recognized on a standard map (i.e., either geological, or of gravity or magnetic anomaly, or tectonic, etc.). Indeed, this evidence closely corresponds and supports the guess of a prolongation of the *MOR* along the edge of the tetrahedron (see Gregori and Leybourne, 2021; Gregori et al., 2025x) than runs from the *EPR* through the North Pole. A confirmation seems also to derive from the 10°*W* meridian "climate curtain" in USA (Fig. 16). This same feature, perhaps, may be linked to seismicity in the New Madrid area (Gregori et al., 2025x).
- A combination of meteorological effects inside a heavily forested region - combined with an ever-

[4] Retrieved on February 19th, 2014, http://eoimages.gsfc.nasa.gov/images/globalmap/data/mov/MOD14A1 M FIRE.mov.

NCGT Journal
New Concepts in Global Tectonics

New Concepts in Global Tectonics Journal
Volume 13, Number 6, August 2025

ISSN number; ISSN 2202-0039

increasing land usage - is likely to explain wildfires through the Amazon Basin.

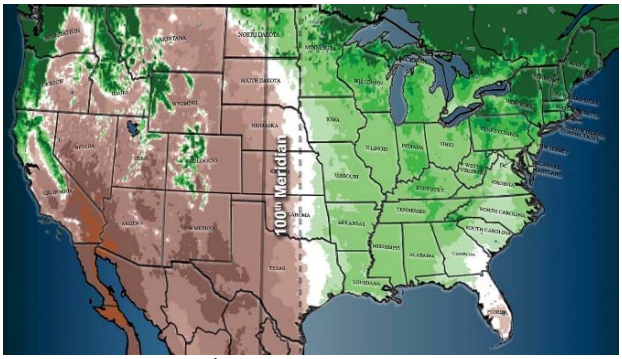

Fig. 16 -*"The 100th meridian west (solid line) has long been considered the divide between the relatively moist eastern United States and the more arid West. Climate change may already have started shifting the divide eastward (dotted line). Credit: Modified from Seager et al. (2018, 2018a)."* Figure and captions after Weisberger (2018a). *NASA* copyright free policy.

- A seemingly similar morphology is found through a half-continental-size region centered roughly around Botswana, until Madagascar (see also Fig. 20). According to the reports by mass media, this region (maybe, but this should be ascertained) is experiencing no intense change of land usage, analogous to what is reported for the Amazon Basin. However, this region is the likely location of the core of the *DUPAL* anomaly (see Gregori et al., 2025a, Supplement, for definition). That is, this is the region of an expected substantially larger geothermal release, roughly antipodal to the Hawai'i hotspot (i.e., this is the quatrefoil pattern; see Gregori et al., 2025a). A larger average release of endogenous heat is associated with a larger amount of soil exhalation and of atmospheric convection (like in the case of the "Andes lights" or "hot weather flashes", see Gregori and Leybourne, 2025g). But mostly, this is associated with some comparably more frequent and more intense impulses or bursts of heat release from the very top of the several sea-urchin spikes that certainly exist in this extended region. Indeed, they are the primary carriers of a comparatively larger local release of endogenous heat. Note that the feature of this large region around Botswana is justified by the aforementioned "quatrefoil" pattern, and it is also associated to a large region of permanent intense concentration of atmospheric CO_2 (see Gregori, 2020). In contrast, the Amazon Basin feature might be associated with the South Atlantic Anomaly (*SAA*; see Gregori et al., 2025a), although the local "pollution" must be considered, which is represented by the ever-increasing anthropic occupation of territory, and consequent great disturbance.
- Some comparatively intense and large increase of the number of wildfires is observed frequently in the southern half of eastern Europe, until Caucasus, although always depending on the appropriate season. These wildfires might be, perhaps, related to a dense number of inhabitants. However, this feature sometimes appears more or less connected with a frequently occurring wave of increased number of wildfires that spreads through northern Eurasia, i.e., forest fires through Siberia appear to be indeed quite a frequent phenomenon, and – in this area - they are definitely unlikely to be anthropic.
- But, a most impressive feature is observed, being regular and almost repetitive. It displays a reasonably steady approximate "cycle". To our knowledge, at present no interpretation was given, and this remarkable effect was never expressively noticed. A physical explanation is here proposed, which is seemingly supported also by the correlation with other relevant phenomena.

A wave of an increasing number of wildfires starts from the southern tip of the Indochina peninsula (i.e., of Laos, Cambodia, and Vietnam). Then, it moves northward until Himalaya, always keeping an approximately constant transversal cross-section. Occasionally some boundary fringes of wildfires also spread through Bangladesh and eastern India. Subsequently - almost like a "flash" in the movie - an abrupt increase of wildfire number is observed inside a comparatively narrow area, roughly around Karakoram, where the wildfire-propagation seems to stop. This Karakoram feature is also confirmed by the average yearly counts of lightning flashes per square kilometer (Figs 1 through 7).

In the meantime, a fainter wave of wildfires is frequently observed propagating northward from Indochina through a comparably large band along the eastern coast of China. In addition, eventually (although not always) it strengthens in the region around Nanjing. Moreover, frequently the sequence ends with another "flash" slightly north of Beijing, where the wildfire-propagation seems to stop. Compared to the Karakoram "flash", this "flash" looks much similar, although sometimes less intense.

This sequence is modulated by seasonal variation. The slow northward drift - which is observed either along the Indochina peninsula or along the eastern coast of China - could be a simple consequence of a regular seasonal variation of local climatic conditions. However, either one "flash" or the other can be explained by no smooth and local climatic trend. This very peculiar morphological sequence is therefore challenging, and seemingly inexplicable. An attempt of justification is discussed below, including a possible correlation with tectonics.

Summarizing, in addition to the tropical forest belt - that can be reasonably expected - a few unexpected "surprising" morphological features are observed: *(i)* the "quatrefoil" effect, *(ii)* the North American alignment[5] that surprisingly

[5] One must clearly emphasize that the drift involves only the lithosphere down to the *ALB*, not the deeper Earth's structures. In fact, the tetrahedron pattern is the result of the *rigorous* application of the interaction of sea-urchin spikes, through the requirements of the Hamilton variation principle, as extensively discussed in Gregori and Leybourne (2021). Observations on the *EPR* envisage a likely depth of the conductor at $\sim 100\ km$

NCGT Journal
New Concepts in Global Tectonics
New Concepts in Global Tectonics Journal
Volume 13, Number 6, August 2025
ISSN number; ISSN 2202-0039

very closely fits with the expectation of one edge of the tetrahedron pattern of the planetary *MOR* network, *(iii)* the extensive and frequent long pattern through Siberia and Eurasia, *(iv)* the curious feature of the southern part of eastern Europe, which is maybe connected with the long anomalous wildfire band through Siberia, and *(v)* the mysterious cyclic "sequence" ending into the two "flashes" roughly around, respectively, Karakoram and somewhere north to Beijing.

Nothing occurs by chance. Every observation should always be explained. A hypothesis is here envisaged to justify this "double flash" feature. This is, however, only *exploratory* analysis. Science also requires the *confirmatory* stage that, at present, in this case is still missing. In any case, this hypothesis can be effectively tested by observations. It is likely that no reasonably reliable explanation will be guessed of this observational evidence as long as the actual distribution is not known of sea-urchin spikes throughout the world. However, independent of it or in addition to it, crustal stress propagation can be monitored by arrays of *AE* stations (see Gregori et al., 2025a and references therein) in order to test the proposed interpretation.

A possible and realistic explanation is as follows. The phenomenon cannot be e.m., as an e.m. effect implies a higher propagation-speed, i.e., all e.m. phenomena occur almost simultaneously. A reasonable guess is to speculate about an effect derived from propagation of crustal stress. One possible hunch is the "domino effect" (Gregori, 2013a), which implies that a microcrack-process propagates through the crust; (and through the serpentosphere see Gregori and Hovland, 2025) at a typical speed of $\sim 10\ cm\ sec^{-1}$. Therefore, there is need to envisage a possible source for a trigger of the starting microcrack. Then, there is need to estimate the propagation time in order to justify the timing of different observations. In any case, this microcrack model certainly applies to the crust (and serpentosphere), i.e., to a brittle medium through some deep layers of the lithosphere.

The leading principle is that a propagating crack favors the exhalation of endogenous fluids, e.g., methane, thus enhancing the possibility of atmospheric discharges. Electric discharges certainly occur even when no lightning is observed. Lightning is an extreme occurrence, just a spectacular manifestation of a phenomenon that in general is not visible (see Gregori and Leybourne, 2025e, 2025f, 2025g).[6] An increased soil exhalation favors atmospheric convection, Cowling dynamo, and is eventually correlated to the formation of micro-sparks that trigger a wildfire.

The efficiency, however, of the "Earth sensor" for this phenomenon depends on season, because the environment must be prone to develop a fire after the trigger by the micro-spark.

The interpretation, which is here proposed - in terms of a propagation of a stress-wave through the crust - is confirmed by other evidence inferred by the Tang's school according to an analysis of their long-lasting data set of the shallow geotherms through whole China (see Gregori et al., 2025h). In particular, refer to Fig. 17 where the region with anomalous percent precipitation $> 75\%$ seems very likely to be approximately coincident with the wildfire "flash" area. Or refer to the average yearly counts of lightning flashes per square kilometer (Figs 1 through 7) that shows several features, including a relative maximum of lightning discharge activity in a region that seems to be almost coincident with the aforementioned Karakoram wildfire "flash" and lightning maximum.

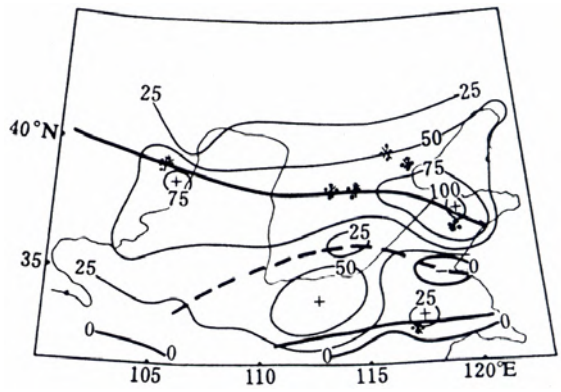

Fig. 17 - Anomalous percent rain precipitation during *April-September 1964*, and the axis of positive (solid line) and negative (dashed line; dryness). After Tang and Zhang (1990).

Or remind about *(i)* the likely correlation of the wildfire track along the eastern longitudinal belt in Fig. 18, with *(ii)* the location of the aforementioned occasional intensification of wildfires, say, roughly close to Nanjing that, in Fig. 19, seems to be located just along the axis of dry climate. In fact, dryness eventually favors the occurrence of wildfires.

The trigger can be in the Banda Sea, which is one of the regions with the highest release of endogenous heat. It is even suspected to be the trigger for *ENSO* (see Gregori and Leybourne, 2025j). More generally, the whole region around the Philippines is characterized by an intense release of endogenous heat, and (according to *WMT*; see Gregori and Leybourne, 2021 and Gregori et al., 2025a) by a consequent peculiar tectonic activity (such as, e.g., in the Moluccas Sea). This entire large region could also be the site of a plugged *MOR*.[7] The Banda Sea is not far away from the southern tip of Indochina.

(order of magnitude; see Fig. 7 of Gregori et al, 2025x). That is, the tetrahedron pattern is a fixed pattern, due to minimum energy stability, while the lithosphere can freely and independently drift over the *ALB*.

[6] Remind about the steadily increasing amount of evidence dealing with earthquake precursors associated with an effective coupling between soil and atmosphere, up to the ionosphere and magnetosphere (see Parrot et al., 2025; Wu, 2025). Until a few years ago, this correlation appeared almost unbelievable.

[7] According to a different viewpoint (Leybourne et al, 2025), the Banda Sea can be considered an upwelling mantle vortex or huge cluster of deep seated sea urchin spikes (Leybourne and Adams, 2020) associated with the octahedral configuration (quatrefoil pattern) tied to tropical lightning hotspots at 90° separation (Albrecht

NCGT Journal
New Concepts in Global Tectonics

New Concepts in Global Tectonics Journal
Volume 13, Number 6, August 2025

ISSN number; ISSN 2202-0039

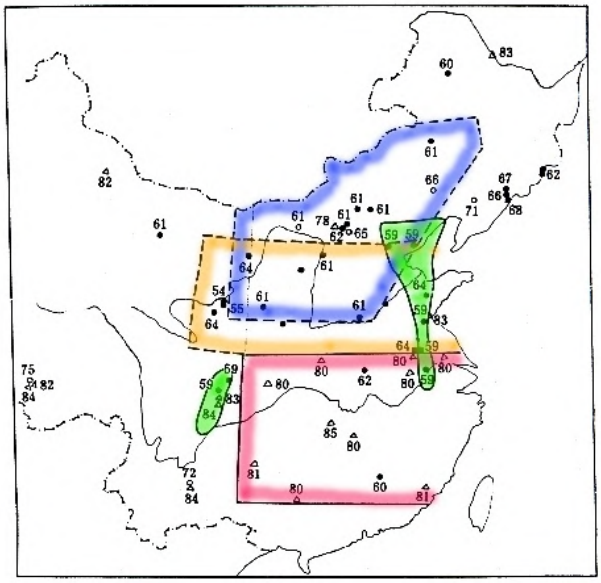

Fig. 18 – Analysis of shallow geotherm in China during 1954-1985 (see Gregori et al., 2025h). Space-time distribution and grouping of "*geothermal abnormal soil abrupt warming*" (*GA-SAW*s), evidencing *5* groups. See text. • *1954-1964*; ° *1965-1976*; Δ *1977-1985*. Different colors shows the *5* different groups. The numbers denote the years. Adapted after Tang and Zhang (1990).

Also, the average yearly counts of lightning flashes per square kilometer (Figs 1 through 7) show a comparably more intense lighting activity in this whole large region. See also the discussion related to Fig. 20 and to the relationship of wildfires with the track of typhoons and cyclones (see Gregori et al., 2025v). Fig. 20 is also consistent with the evidence that the seasonal variation of the atmospheric concentration of CO_2 seems to have a steady source of CO_2 just in the Botswana region (Gregori, 2020, and Gregori and Leybourne, 2021, and references therein).

Somewhat analogous evidence is reported by Tsunoda (2010 and 2010a) who addressed more specifically the seismic and volcanic events, respectively, in East Asia and in the Japan islands. Tsunoda (2010) proposes "*three routes (Sumatra-China,* SC*; Philippines-Japan,* PJ*; and Marianas Islands-Japan,* MJ*) for the* VE *(volcanic eruption) process movement"* and suggests that this feature *"is repeated every* 30 *to* 50 *years in Asia*". Tsunoda (2010a) challenges a problem, which is maybe even more difficult, i.e., the seismic/volcanic pattern and evolution in the very complicated tectonic scenario of Japan. These routes, and mostly the *SC* route, reminds about the evidence inferred from wildfires.

Concerning the "flash" point north of Beijing, a cluster of deep earthquake occurs north of the Korea peninsula (see Fig. 21), and of the average yearly counts of lightning flashes per square kilometer (Figs 1 through 7). After the double flash occurrence, the cycle regularly starts anew from Indochina etc.

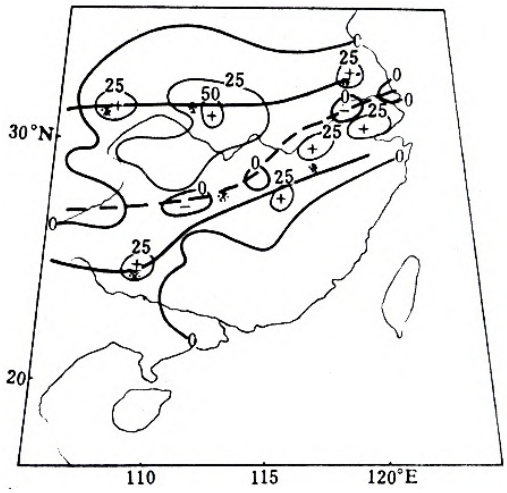

Fig. 19 - Anomalous percent rain precipitation during April-Sep 1980, and the axis of positive (solid line) and negative (dryness, dashed line) anomalies (see Gregori et al., 2025h). After Tang and Zhang (1990). Reproduced with kind permission.

The three points - i.e., the southern tip of Indochina, the Karakoram "flash", and the Beijing "flash" - are roughly located at the vertices of an equilateral triangle of size $\sim 4{,}000\ km$. A microcrack, which propagates by "domino effect" (Gregori, 2013a) at a speed of $\sim 10\ cm\ sec^{-1}$, spends $\sim 4 \times 10^8/10 = 4 \times 10^7 sec \approx 1.27\ years$ to run through the serpentosphere along a $\sim 4{,}000\ km$ distance. Hence, $\sim 1.3\ years \approx 16\ months$ is an excessively long time-delay in order to explain the observed "double flash" cyclic feature.

Consider, however, that the Earth is a "sensor" suited to monitor discharges that occur only during some given season. In fact, maybe, an overlapping occurs of two cyclic phenomena, one with $\sim 16\ months$ period, the other with $\sim 12\ months$. Hence, we should expect to monitor the beat between the two cycles, i.e., cyclic features of period $\sim 4\ months$ and $\sim 28\ months$, respectively.

The $\sim 4\ months$ cycle seems to be consistent with the "double flash" feature, while the $\sim 28\ months$ recurrence ought to require a longer observational database in order to be detectable. However, compared to the aforementioned evidence perceived while watching the *NASA*'s *Earth Observatory* wildfire movie with one frame every month, a time lag of $\sim 4\ months$ is too short, while $\sim 28\ months$ is too long. On the other hand, consider that these estimates hold only in terms of orders of magnitude. More accurate values ought to require a more specific monitoring both *(i)* of crustal stress propagation by *AE* arrays, and *(ii)* of timing of wildfire occurrence, upon also considering the local

et. al., 2016). This applies except in mid Pacific $\sim 140°W$, where there is little lightning and the N-S circuit completing the ~90° separation from *EPR* and northern extension of the *SEIR*. In addition, at $\sim 165°E$ an event blew out, stripping the Pacific lithosphere (Arc Blast hypothesis), which is hypothesized to be where the Moon was originated (Leybourne et al., 2025).

New Concepts in Global Tectonics Journal
Volume 13, Number 6, August 2025

ISSN number; ISSN 2202-0039

environment, which is eventually more or less suited to "detect" soil exhalation etc.

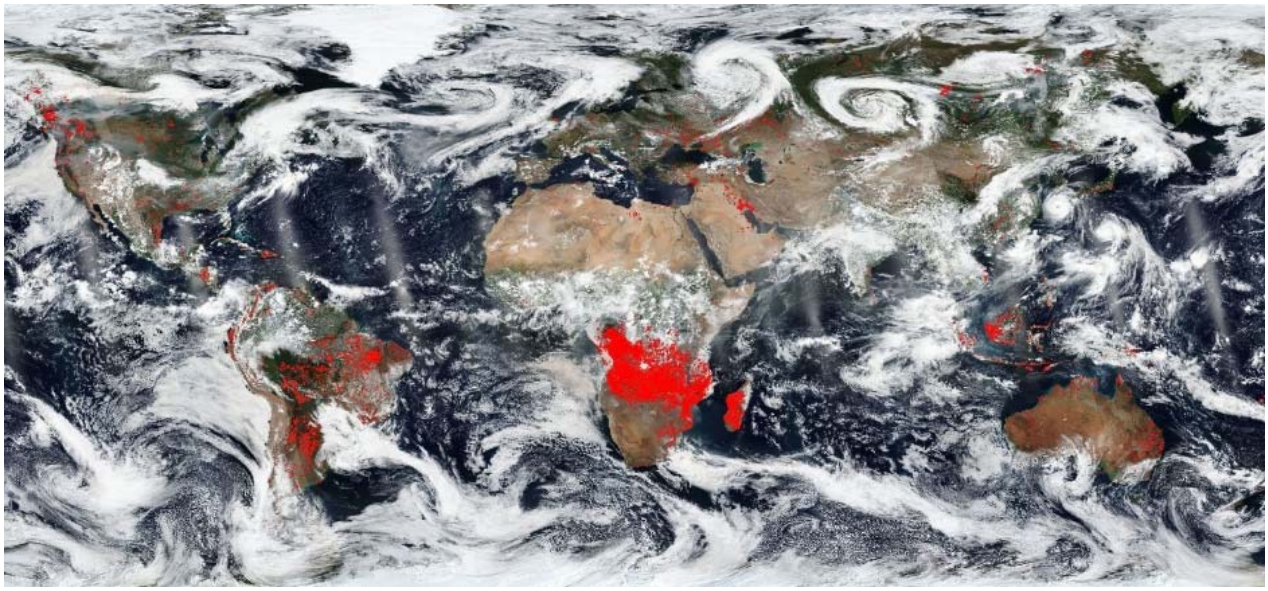

Fig. 20 - *"An image of* NASA's Worldview *highlights in red regions of the planet where satellite thermal imagers detect actively burning fires. Credit:* NASA/GSFC.*"* Figure and captions after Letzter (2018g).

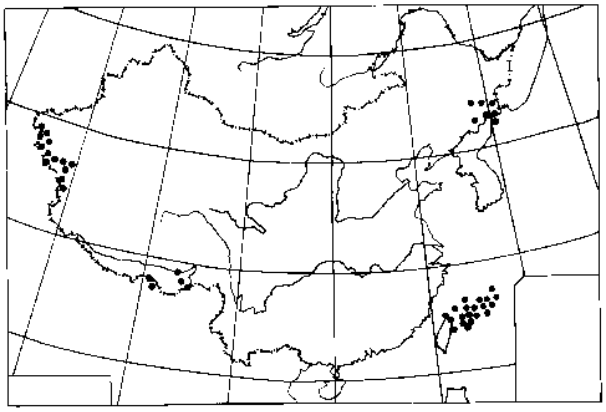

Fig. 21 - *"Distribution of earthquake focus deeper than* 80 *km in China."* Figure and captions after Tang et al. (1999).

There is a need to explain the very narrow pattern of each "flash". The lithospheric slab, which contains Indochina, slides northward on the slope of the geotumor, uplifted by the Banda Sea.[8] It seemingly experiences two hinges - or holding points - of comparatively greater strength, where a great amount of friction is released (much like Etna is tentatively speculated to be the security valve for the friction released at the "hinge" between Africa and Eurasia; see Gregori and Leybourne, 2021).

That is, each "flash" can be imagined to be associated with the presence of a holding obstacle opposing the northward drift of this Indochina lithospheric slab.

According to the evidence of the Tang Maocang school, the Tibet Plateau is a region of anomalous large heat flow (see Gregori et al., 2025h), and this fact is consistent with the present hypothesis. Karakoram is, maybe, the best-known high plateau, which is almost inaccessible except by mountaineering expeditions with very special equipment. That is, Karakoram is a topographically very elevated anomaly, which is probably permanently uplifting in order to compensate erosion by weathering. Concerning the Beijing region, it is a well-known area of particularly great seismic hazard, in terms of large-magnitude shocks (see Fig. 21), which can occur only if the tectonic structures can accumulate a great amount of potential energy, i.e., if they are composed of structures that strongly hold while experiencing a comparatively lesser deformation.

Summarizing, a confirmation of this "model", which at present is merely speculative, can derive either from the detection of the ~28 $months$ cycle, or by monitoring crustal stress propagation by means of an array of *AE* recorders, or by the knowledge of the sea-urchin spike distribution.

For the time being, this hypothesis must be considered like an *ad hoc* speculation. On the other hand, to our knowledge, no alternative hypothesis is available. In principle "all" possible hypotheses ought to be suitably considered, whenever they are eventually available, and observations should then be considered in order to discriminate between different models.

[8] Banda Sea has trenches such as the Weber Deep, not necessarily indicating uplift everywhere, all vortices have movements in opposite directions like hurricanes and tornadoes have down drafts and updrafts depending what part you are looking. According to surge tectonics, it can be analyzed as mantle and asthenosphere (counterflow) stream-flow processes, i.e., geostreams (see Leybourne and Adams, 2020).

NCGT Journal
New Concepts in Global Tectonics
New Concepts in Global Tectonics Journal
Volume 13, Number 6, August 2025
ISSN number; ISSN 2202-0039

We attempted to carry out a quantitative analysis of this cyclic phenomenon. We considered *16* large regions over the globe, and we tried to evaluate - by simple visual inspection on *NASA*'s *Earth Observatory* movie - a hierarchy of intensity of wildfire density. The *16* large regions are: (1) Venezuela, (2) Brazil, (3) Central America, (4) USA, (5) Africa (equatorial), (6) Banda Sea, (7) Indochina, (8) Thailand, (9) India, (10) China (eastern coast), (11) Beijing "flash", (12) Karakoram "flash", (13) Australia, (14) Botswana, (15) Central Europe, and (16) Siberia. We arbitrarily assigned an intensity-grade - every month (as far as possible) - expressed as a score between *0* and *3* with increments *0.5*. Then, we applied the Arp and/or $cross - Arp$ operator (see Appendix[9]) by introducing a weight as follows.

Reference must be made to two so-called "point-like processes". In the present application both "point-like processes" are identical - and identified with the time series of the months of wildfire occurrence in the time series of the monthly scores referred to each given region.

We call "pole series" the "point-like process" (of the two series) that refers to one given region and that is used to define the time origin of the stopwatch. The time origin is re-defined every time - at every month - in the "pole series", only whenever its score is not null. The other series, which can refer either to the same region in the case of Arp - or to a different region in the case of $cross - Arp$ - is used to construct the arp histogram.

In general, every different series is comparably more or less well defined, as it is based on some subjective visual evaluation of the *Earth Observatory* movie. For instance, the Banda Sea series seems comparably less clearly defined, because wildfires are seldom observed on land surrounding the sea. Similarly, no wildfire is observed through the Himalaya region, due to ice cover. In any case, *upon direct visual inspection of the movie, the wildfire propagation, which runs from Indochina through either one "flash", is objectively evident, very clear and impressively regular and repeated several times.*

As far as possible, the "pole series" was chosen when the time of occurrence of its wildfires is comparably more sharply defined (this normally occurs, e.g., for the two "flash" series).

However, sometimes the "pole series" has a month with a high score (e.g., *2*), while on other years it displays two consecutive months with smaller scores, e.g., say, *1* and *1.5*, respectively. Hence, we tried to give a greater emphasis to the case histories that are better evident inside the movie. Thus, while constructing the arp histogram, instead of adding a unit square to the histogram, we added a square with the weight given by the score of the month in the "pole series" that defines the temporary origin of time.

For instance, in the aforementioned hypothetical case history of a unique month with score 2, all squares - which added to the Arp or $cross - Arp$ histogram arp - are weighted *2*. In contrast, in the case of two subsequent months in the "pole series" with weight *1* and *1.5* respectively, the Arp or $cross - Arp$ histogram arp is step-by-step accreted by means of squares weighted once *1* and another time *1.5*, etc.

In every case, every final histogram was redrawn by taking the square root of every ordinate value, i.e., the operator $\sqrt{Arp}$ was used instead of Arp. In this way, the standard error is constant and = *±1/2* (with dimensionless units).

Note that if one computes the arp of a given series, the result always displays a 12 $month$ periodicity. Indeed, this is the obvious seasonal effect. In fact, even in the case that on some year the wildfire occurrence is eventually missing, the final arp histogram always displays the seasonal modulation. This is just due to mathematical definition, and to the physics of seasonal variation.

Consider first the case history of the Beijing "flash" series, chosen as "pole series". Compute the arp by $cross - Arp$ with, respectively, the aforementioned series of China (eastern coast), Indochina, Banda Sea, and (only for comparison purpose) Australia. Fig. 22 shows the result.

The Beijing "flash" seems to occur 9 $months$ after the Banda Sea series, and $3 - 4$ $months$ after both the Indochina and the China (eastern coast) series, as shown by the relative maxima, indicated in Fig. 22, which precede the occurrence of the Beijing "flash". They remind one about the aforementioned ~4 $months$ beat frequency. The Australia series looks unrelated to the others.

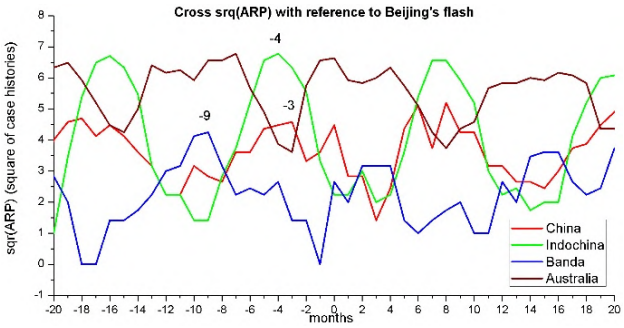

Fig. 22. Time-delayed correlation between the Beijing "flash" wildfire time series and the wildfire time series of China (eastern coast), Indochina, Banda Sea, and Australia, respectively. The error bars are = *±1/2*. See text. Unpublished figure.

Fig. 23, which is comparably less clear, is the same referring to the Karakoram "flash" series, considered like "pole series", compared – respectively - with the series of Thailand, India, Indochina, Banda Sea, and Australia. The Karakoram "flash" seems to be preceded by 3 $months$ in the Indochina series – reminding one about the aforementioned ~4 $months$ beat frequency - and by 1 $month$ in the India series. In contrast, the (poorly defined) series for the Banda Sea and for Thailand display feebler evidence with an apparent time advance of roughly ~2 $months$. The Australia series again looks unrelated to others, and shows a repetitive trend with ±6 $month$ time-

[9] Arp is an acronym for "automatic research of periodicities". See the Appendix.

NCGT Journal
New Concepts in Global Tectonics
New Concepts in Global Tectonics Journal
Volume 13, Number 6, August 2025
ISSN number; ISSN 2202-0039

lag that, maybe, can be related to the expected seasonal modulation.

Fig. 24 refers to the USA series, considered like "pole series" - compared, respectively, with the series of Central America, Venezuela, and Brazil. Note the typical seasonal modulation shown by every series, which is displayed also in every analogous other figure (not here shown). This figure is reported in order to show the peculiar absence of any apparent seasonal modulation in the Brazil series, consistently with the analysis for the Amazon Basin. In fact, compare (Williams and Sàtori, 2004) the seasonal discharge records for *(a)* the Amazon River and *(b)* the Congo River. The clear semiannual signal in the Congo record is in contrast with the Amazon record dominated by the annual cycle.

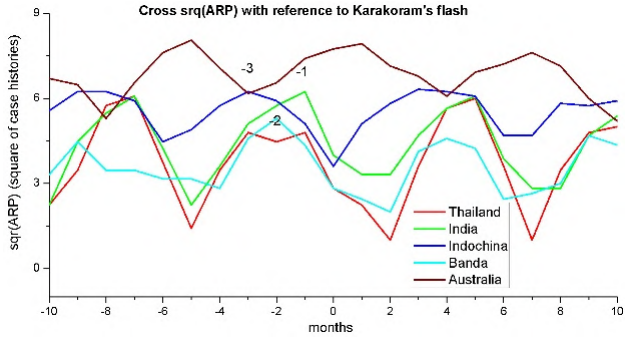

Fig. 23. Time-delayed correlation between the Karakoram "flash" wildfire time series and the wildfire time series of Thailand, India, Indochina, Banda Sea, and Australia. The error bars are = *±1/2*. See text. Unpublished figure.

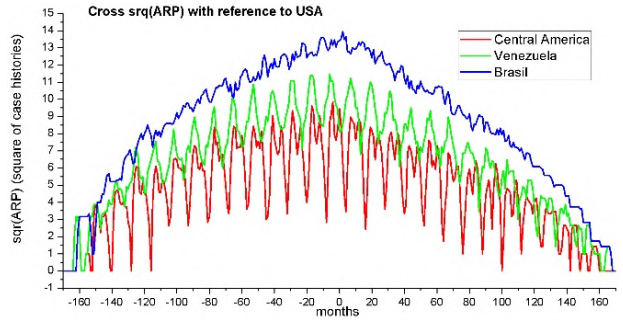

Fig. 24. Time-delayed correlation between the USA wildfire time series and the wildfire time series of Central America, Venezuela, and Brazil. The error bars are = *±1/2*. See text. Unpublished figure.

A suitable detail (horizontal axis between -20 and $+20\ months$) is shown in Fig. 25, for comparison with Figs 22 and 23. One can envisage two different interpretations in terms of propagation along the aforementioned meridional alignment that seems to be identified with the "plugged" *MOR* from the *EPR* through the North Pole (see Gregori and Leybourne, 2021).

One possibility is a northward propagation of wildfires. The effect starts from Venezuela anticipating the USA wildfires by $6\ months$, while the intermediate Central America wildfires anticipate the USA events by $4\ months$.

The alternative possibility, in terms of a southward propagation, ought to imply that the USA wildfires anticipate by $7\ months$ the wildfires both in Central America and in Venezuela.

The first possibility seems to be more credible. In fact, consider the intricate and essentially mysterious tectonic perturbation occurring in Central America (Gregori and Leybourne, 2025j) - including the Gulf of Mexico, the Bahamas, Lesser Antilles, etc. - that ought to be reasonably expected to originate a crustal stress that propagates northward. In addition, consider the location on top of a region that "plugs" the underlying edge of the planetary tetrahedron pattern of *MOR*s (see Gregori and Leybourne, 2021; Gregori et al., 2025x). This ought to occur indicatively along the line between Dallas-Winnipeg, as it is displayed by the frequency of wildfires (see Fig. 16). In addition, consider the large density of lighting (Lake Maracaibo – Catatumbo lightning) in northern South America (Figs 1 through 6).

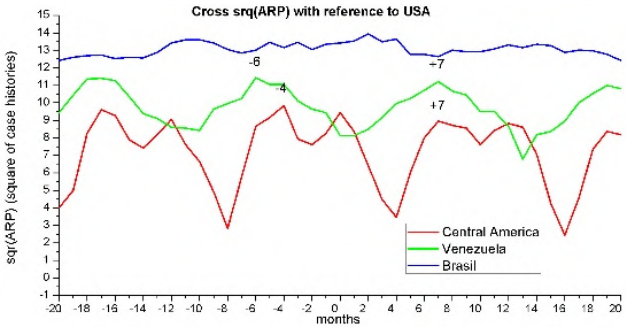

Fig. 25. Time-delayed correlation between the USA wildfire time series and the wildfire time series of Central America, Venezuela, and Brazil. The error bars are = *±1/2*. Detail of Fig. 24. See text. Unpublished figure.

In either case, the Brazil series seems completely unrelated to the others. This could be a consequence of the relevant anthropic disturbance, which is particularly intense in this region. However, a sound and likely explanation can be in terms of the peculiar feature of the *SAA*, which determines the clockwise rotation of South America (see Gregori and Leybourne, 2021 and Gregori et al., 2025a).

No better inference can be achieved until better information and monitoring is available. The best evidence can be, perhaps, by direct monitoring of crustal stress propagation by means arrays of *AE* stations (Gregori et al., 2025a).

In addition, two case histories are analyzed of one couple of time series. Fig. 26 refers to Karakoram ("pole series") *vs.* Siberia, and Fig. 27 to Botswana ("pole series") *vs.* equatorial Africa.

Apart the aforementioned obvious seasonal modulation shared by every series, one can choose whether the Karakoram "flash" is preceded by $6\ months$, or it is followed by $5\ months$, by the Siberia wildfires. Note that it is possible that these time delays could be only a mathematical consequence of the respective different seasonal modulation. This is a simple mathematical inference derived from an analysis of the available database – i.e., just objective formal evidence of the data series. The dilemma can be solved only by speculating suitable

NCGT Journal
New Concepts in Global Tectonics
New Concepts in Global Tectonics Journal
Volume 13, Number 6, August 2025
ISSN number; ISSN 2202-0039

mechanisms that, in any case, should take into account this observational matter of fact.

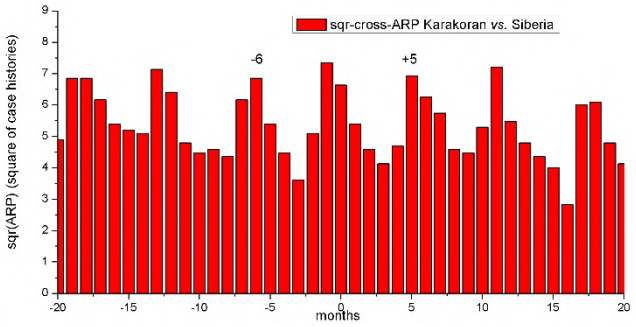

Fig. 26. Time-delayed correlation between the Karakoram wildfire "flash" time series ("pole series") and the Siberia wildfire time series. The error bars are = ±*1/2*. See text. Unpublished figure.

A similar comment applies to the case of Fig. 27, as the wildfires in equatorial Africa can either precede by $6\,months$, or follow by $5\,months$, the Botswana series. According to the aforementioned speculation about the specific role of the Botswana bunch of sea-urchin spikes etc., the hypothesis of a propagation from Botswana towards equatorial Africa, spending $5\,months$, seems, perhaps, more credible. But this is only speculative.

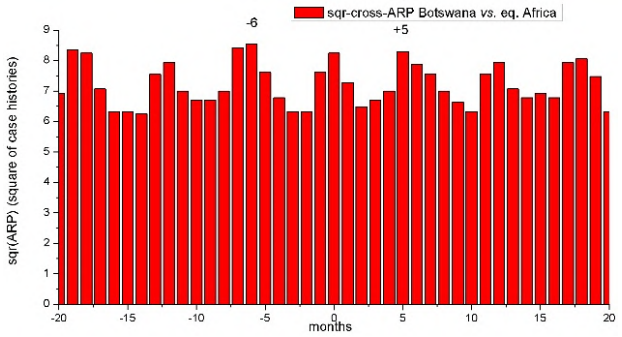

Fig. 27. Time-delayed correlation between the Botswana wildfire time series ("pole series") and the equatorial Africa wildfire time series. The error bars is = ±*1/2*. See text. Unpublished figure.

The estimates of a few to several months of time delay are consistent, in terms of order of magnitude, with the aforementioned roughly $\sim 4\,months$ estimate - and, in any case, this is the feeling, which is clearly guessed by direct visual inspection of the wildfire movie. The subjective criterion may be used to assign a score to wildfire intensity. In addition, wildfire information alone can be "polluted" by anthropic disturbance. Therefore, in order to validate either one interpretation or another, there is need for additional information concerning, e.g., crustal stress propagation, or local soil exhalation through shallow geotherms (Gregori et al., 2025h).

Summarizing, the analysis and interpretation, which is here proposed, requires some harder thinking, and mostly an expanded observational database, including information on crustal stress propagation. Even in this case, a crucial issue deals with the need for monitoring the real amount of fluid exhalation from soil. For instance, effects - that were unexpected until a few years ago - deal with earthquake precursors associated with the coupling between soil and atmosphere (see Gregori and Hovland, 2025; Straser et al., 2025; Wu, 2025; Gregori et al., 2025h; and references therein), or with the Quinn's inversion of the *CHAMP* records (see section Quinn et al., 2025).

However, the evidence given by the *NASA*'s *Earth Observatory* movie on wildfires is of paramount importance in order to understand planetary-scale phenomena that involve air-earth currents and several crucial aspects of Earth's science, much more than just a simple control on atmospheric pollution by the burning exhaust of vegetation.

Geophysical implications of wildfires, biomass burning, and other related proxies

Some additional concern is reported. Marlon et al. (2008) investigated the role of the anthropic impact during historical time. However - for completeness sake - it should be mentioned that a few years ago the feeling was quite different. For instance, Finneran (2010) stated that, according to the "NASA *biomass burning program that ran from 1985 to 1999, ... 90% of biomass burning is human instigated."* They claimed having *"traveled to wildfires in Canada, California, Russia, South Africa, Mexico and the wetlands of* NASA*'s* Kennedy Space Center *in Florida*."

More interesting is his comment about the "*northern exposure*", as he states that "*whether biomass burning is on the rise globally is not clear. But it definitely is increasing in far northern latitudes, in 'boreal' forests comprised largely of coniferous trees and peatlands.* [Indeed, peatlands are a well-known source of inflammable CH_4 exhalation, and this phenomenon is quite sensible to changes of endogenous heat release, and to permafrost thawing. See also the *OCO-2* spring-time map of atmospheric CO_2 concentration (Gregori, 2020; Gregori and Leybourne, 2021).]

The reason is that, unlike the tropics, northern latitudes are warming [this is consistent with some other evidence that emphasize that the northern polar cap is experiencing a steady increase of endogenous heat release; see Gregori and Leybourne, 2021] *and experiencing less precipitation, making them more susceptible to fire. Coniferous trees shed needles, which are stored in deep organic layers over time, providing abundant fuel for fires ...*

Fires in different ecosystems burn at different temperatures due to the nature and structure of the biomass and its moisture content. Burning biomass varies from very thin, dry grasses in savannahs to the very dense and massive, moister trees of the boreal, temperate and tropical forests.

Fire combustion products vary over a range depending on the degree of combustion ...

Flaming combustion like the kind in thin, small, dry grasses in savannahs results in near-complete combustion and produces mostly CO_2. *Smoldering combustion in moist, larger fuels like those in forest and peatlands results in incomplete combustion and dirtier emission products such as* CO. *Boreal fires burn the hottest and contribute more pollutants per unit area burned ...* "

ISSN number; ISSN 2202-0039

Summer 2010 was characterized by a huge extension of wildfires throughout Russia. Therefore, according to Finneran (2010), he claimed that "*the wildfires are believed caused by a warming climate that made the current summer the hottest on record. The hotter weather increases the incidence of lightning, the major cause of naturally occurring biomass burning*." [Note that hotter weather implies a greater amount of atmospheric convection, hence also a more efficient Cowling dynamo that favors lightning activity. In addition, a greater soil exhalation implies heat transport by advection, more intense atmospheric convection etc. However, new records of maximum atmospheric temperature occurred in the years after 2010, while no equivalent wave of wildfires occurred through Eurasia. Why?]

Indeed, wildfires are one facet of the changing "climate", which is closely related to the increase of endogenous heat release underneath the northern polar cap. The incorrect feeling, reportedly "believed" in 2010, was that anthropic pollution is the main responsible driver for global warming. In contrast, according to general objective inference, all evidence – that cannot be here reported in detail - are clearly in close agreement with the fact that - on the one hand - humankind is part of the environment with its associated responsibilities, even other than greenhouse gas production. However, on the other hand, natural phenomena certainly play the real leading role, consistently with the explanation of palæoclimatic variations that can be explained only in this way, when dealing with epochs when humankind certainly played no role.

A warning is that several people still seem to "believe" that anthropic pollution - and mainly greenhouse gas production - is the main element responsible for "global warming". Consider that - as often happened in the past - it is easier to guess one "simple" cause, rather than to argue about an intricate ensemble of phenomena and different drivers. In addition, consider that Einstein claimed that physics is like a detective story (Einstein and Infeld, 1953). We may liken palæoclimatology to the case of a serial killer, with circumstantial evidence, and with the impossibility to find the "smoking gun" proof. If a detective finds a logical way to "explain" the whole available circumstantial evidence, his explanation must be considered, at least as long as no better detective envisages some comparably detailed and more convincing explanation.

The mechanisms are presently largely ununderstood. For instance, Juselius-Rajamäki et al. (2023), is illustrated by *University of Helsinki* (2024) that claims they "*revealed that the northern peatlands have been expanding in size over the past centuries. This finding contrasts with the previous belief that the growth of peatlands in Fennoscandia had either stopped or slowed down considerably, as it was assumed that all the flat regions conducive to peat development had already been transformed into peatlands.*"

On the other hand, the challenge is disquieting. Del Vecchio et al. (2024) envisage a "*carbon bomb*". Their study is illustrated by *Dartmouth College* (2024) that claims that their "*findings … reveal groundbreaking evidence that the Arctic's permafrost significantly influences the region's river systems …* [and] *… highlight how permafrost … causes rivers in the Arctic to flow through narrower and shallower valleys compared to their southern counterparts. But permafrost also is an increasingly fragile reservoir of vast amounts of carbon. As climate change weakens Arctic permafrost, … every* $1°C$ *of global warming could release as much carbon as* 35 $million$ *cars emit in a year as polar waterways expand and churn up the thawing soil.*"

In any case, the role of wildfires - whatever the prime cause - is certainly a primary driver. According to Janssen et al. (2024), illustrated by *University of East Anglia* (2023) and by *University of Leeds* (2023), "*lightning ignitions are a major cause of wildfires in intact extratropical forests. Utilizing machine learning, the study found that* 77% *of fires in these areas are due to lightning, a stark contrast to human-caused fires in tropical regions. With climate change increasing lightning frequency and forest flammability, these forests, crucial for carbon storage, face heightened wildfire risks*" (*University of East Anglia,* 2023). That is, they "*…identified lightning as the primary cause of fires in intact extratropical forests in contrast to human-induced fires in tropical regions …*" (*University of Leeds,* 2023).

Concerning "climate", the explanation, which is here proposed, was derived - almost unwillingly and even with surprise - from a study on the origin of the geomagnetic field (Gregori, 2002; see, e.g., Gregori and Leybourne, 2021; Gregori et al., 2025a). The "climate" explanation is a necessary and strictly compulsory logical byproduct of an investigation focused on a substantially different problem. As long as no proof is raised against the cogent arguments of this inference, this explanation must be temporarily accepted.

The role of humankind, however, was eventually very different during the history of progressive land usage and occupation of territory. This key item was focused on by Zennaro et al. (2015) who investigated an ice core from Greenland. They use the "*specific biomarker levoglucosan to produce the first high-temporal resolution hemispheric reconstruction of Holocene fire emissions inferred from ice core analyses. Levoglucosan recorded in the Greenland North Greenland Eemian ice core significantly increases since the last glacial, resulting in a maximum around* ~2.5 ka *and then decreasing until the present.*"

They carried out a thorough discussion of possible natural causes. But every attempt and/or model resulted essentially unsuccessful. Therefore, they favor anthropic action. Their discussion of this item seems particularly incisive and wide-looking. It is here reported as an example of a realistic approach to this often improperly harsh debate.

"*Boreal forests in North America and Eurasia are likely the most important sources of fire products in Greenland ice cores during the present day and the past two millennia (Zennaro et al., 2014). Currently, forests at* NH *midlatitudes are not a major fire source due to few remaining forests and dense populations. Millennia ago midlatitude* NH *forests were still extensive and humans may have burned this vegetation, even in the upper midlatitude regions (north of* $45°N$*) of Europe and China (Kaplan et*

ISSN number; ISSN 2202-0039

al., 2009, 2011). Global circulation remained relatively stable during the middle to late Holocene, as suggested by stable oxygen isotope data demonstrating that circulation patterns of air masses reaching the Greenland Ice Sheet did not significantly change during the past 10 *ka (*NGRIP *Project Members, 2004; Vinther et al., 2006).*

However, the previous southern extension of boreal forests several thousand years ago changed the location of large-scale fire sources where fire products may have followed trajectories starting from sources farther south. The possibility of such transport from the midlatitudes is supported by Chernobyl radiation products (Davidson et al., 1987; Dibb, 1989) and volcanic tephra from Vesuvius (Barbante et al., 2013) which are traced from their source well into the Arctic.

The scientific literature supports the possibility that forest clearance rates culminated $2.5 - 2.0\ ka$ *in much of Europe (Ellis et al., 2013; Kaplan et al., 2009, 2011). A pollen-based reconstruction of land cover change demonstrates quantifiable forest clearance across much of Europe beginning ~4 ka (Fyfe et al., 2015). Forests were reduced to near-modern levels by* 2.5 *ka BP in England (Woodbridge et al., 2014) and* 2.2 *ka in France (Fyfe et al., 2015). This drop in the forest clearance rate in northwest Europe during the last* $2500 - 2000\ years$ *is consistent with the decreasing levoglucosan flux after* 2.5 *ka.*

Land cover change model results suggest that trends in fire history inferred from charcoal records are best explained by a substantial human influence on the climate system from biomass burning starting from the mid-Holocene (Kaplan et al., 2009, 2011). When models take into account the increasing efficiency of land use (Kaplan et al., 2009), deforestation rates are higher between $3.0 - 1.5\ ka$ *than model results that do not incorporate technological changes and that indicate greater deforestation levels after ~*1.5 *ka.*

In a newer work, Kaplan et al. (2011) compare results from two land cover change models, one based on the HYDE 3.1 *land use database (Goldewijk et al., 2011) and one based on* KK10 *(Kaplan et al., 2011) in which* per capita *land use declines with population density. Results substantially differ between the two models; the* KK10 *scenario estimates greater deforestation when land use* per capita *declines as population density increases, whereas the* HYDE *database predicts relatively low land use until the industrial era (*10% *of global land area is used at AD 1850). In the* HYDE *scenario land clearing in northeastern China, the Middle East, Europe, and South America began ~*3 *ka, while according to the* KK10 *scenario ~*40% *of land in these regions was already influenced by humans (Kaplan et al., 2011). At ~*2 *ka ~*60% *of the total land area of Europe and China was cleared of forest vegetation in* KK10, *while in the* HYDE *scenario anthropogenically induced land cover change only slightly increased (Kaplan et al., 2011)."*

Also, geological evidence is available concerning huge crises recorded by the biosphere caused by local large wildfire. Witman (2018a) introduces the study by Beck et al. (2018), and states that "*in 1973, the renowned Canadian ecologist C. S. Holling introduced the idea of ecosystem resilience. An ecosystem's resilience refers to its ability to withstand environmental pressures, or perturbations - such as fires, floods, storms, deforestation, fracking, pesticide spraying, or the introduction of an invasive species - and the time it takes for the ecosystem to return to a stable, functioning state. According to Holling, all ecological systems go through cycles of good and poor health. Scientists study these cycles in detail to better understand and predict the overall health of an ecosystem.*

Beck et al. (2018) examined a shift in an ecosystem to a stable state that can occur in response to a perturbation. Such shifts are known as 'critical transitions', and they are often sudden and unpredictable - examples include an influx of nutrients, a land use change, or a change in climate. The team identified a series of early warning signals that - if detected in time - can alert observers to an impending critical transition.

Detecting these signals, such as a lowered resilience or a sluggish recovery time, can be challenging. This is especially true for ecosystems with long generational life spans, such as temperate forests, some of which have trees that are thousands of years old. Knowing this, the researchers decided to use palæoecological data, which provide ecological data over long timescales.

Using palæoecological data collected from a meter-long core extracted in 2011 from Australia's Lake Vera in Tasmania, [note that Australia is on top of a vertex of the deep tetrahedron, hence allocation particularly sensible to variations of endogenous heat release; see Gregori and Leybourne (2021) and Fig. 14] *the researchers examined the interrelated changes in vegetation, pollen, charcoal, soil, and other components of the sediments over the past* 2,400 *years. In particular, they investigated the impact of fire, a major driver of ecosystem changes on land, on the aquatic ecosystem. Aquatic ecosystems, generally speaking, are highly sensitive and respond rapidly to environmental pressures.*

Lake Vera is home to a thriving community of a species of diatom, or alga, called Discostella stelligera. *The researchers found that the diatom community experienced a critical transition about* 820 *years ago that was likely caused by wildfires disrupting local vegetation around the same time. They also found that an increased rate of change, as well as increasing shifts in species composition - more oligotrophic (nutrient-poor) and acidic species of diatoms began to replace existing species – had preceded this critical transition.*

This study shows that a disturbance on land, such as a wildfire, can drive a critical transition in a lake within that ecosystem. It also illustrates several early warning signals, namely, rate of change and variability of species composition that scientists can potentially use to predict critical transitions in an ecosystem. The study also highlights the important role of palæoecological data, which provide evidence for ecosystem changes due to critical transitions and for distinguishing these changes from other kinds of abrupt change. This may also help researchers to understand the parameters that can be used to identify and measure early-warning signals with greater precision."

ISSN number; ISSN 2202-0039

A few better details are given in the abstract by Beck et al. (2018). "*Critical transitions in ecosystem states are often sudden and unpredictable. Consequently, there is a concerted effort to identify measurable early warning signals (*EWS*) for these important events.*

Aquatic ecosystems provide an opportunity to observe critical transitions due to their high sensitivity and rapid response times. Using palæoecological techniques, we can measure properties of time series data to determine if critical transitions are preceded by any measurable ecosystem metrics, that is, identify EWS.

Using a suite of palæoenvironmental data spanning the last $2{,}400\ years$ *(diatoms, pollen, geochemistry, and charcoal influx), we assess whether a critical transition in diatom community structure was preceded by measurable* EWS. *Lake Vera, in the temperate rain forest of western Tasmania, Australia, has a diatom community dominated by* Discostella stelligera *and undergoes an abrupt compositional shift at* $\sim 820\ cal\ year\ BP$ *that is concomitant with increased fire disturbance of the local vegetation.*

*This shift is manifest as a transition from less oligotrophic acidic diatom flora (*Achnanthidium minutissimum, Brachysira styriaca, *and* Fragilaria capucina*) to more oligotrophic acidic taxa (*Frustulia elongatissima, Eunotia diodon, *and* Gomphonema multiforme*). We observe a marked increase in compositional variance and rate-of-change prior to this critical transition, revealing these metrics are useful* EWS *in this system.*

Interestingly, vegetation remains complacent to fire disturbance until after the shift in the diatom community. Disturbance taxa invade and the vegetation system experiences an increase in both compositional variance and rate-of-change. These trends imply an approaching critical transition in the vegetation and the probable collapse of the local rain forest system."

These events are very unlikely to be caused by anthropic pollution. In any case, additional information ought to be collected wherever possible, analogous to the Lake Vera analysis in Tasmania. These data can be important in order to check models for reconstructing past "climate" and the drivers that caused climate change. In any case, living forms have an endemic great capability to change for survival, according to the principle of antifragility (see Gregori et al., 2025w).

This completes the present discussion of wildfires. But also, other phenomena envisage some anomalous release of endogenous heat.

Occurrences of deep-water fauna beaching like squid are seldom reported by mass media (Gregori et al., 2025b). Every kind of fauna acquainted to live within some very high environmental pressure - i.e. at $\sim several\ 100\ atm$, i.e., at $\sim several\ 10\ megaPa$ - has no reason to "escape" up to shallow waters, other than because its living ecosystem was poisoned by some ocean floor exhalation: unavoidably, this fauna dies by embolisms. The concern is not about the occasional report of these rarely observed events, rather about the apparent clustering in time and space of these reports referring to different parts of the world. It is unfortunate, however, that such a kind of information about fauna beaching is presently being systematically neglected by the generally accepted "official science".

In this same respect, let us recall that there is clear evidence that the largest extinctions occurred during the entire Earth's history were associated with tremendous planetary ocean floor heating (Earth's heartbeats; see Gregori, 2022; Gregori and Leybourne, 2021; and Gregori et al., 2025a), and consequent blast-exhalation of CH_4 from clathrates, etc.

The realm of these "exotic" reports should include - maybe - also the *TLE*s, e.g., the "hot weather flashes" mentioned in Gregori and Leybourne (2025g).

Even a catalogue of trees (or buildings or other) that suffered by a lightning strike ought to be kept within the data centers, much like data centers keep the information about earthquakes, volcanic eruptions, floods, etc. (Gregori et al., 2025b). The ancient Romans kept records of the sites that appeared prone to being stricken by lightning discharges, although their concern was ritual in honor of Jupiter. Also in this respect, suitable consideration ought to be given for the three concurrent factors: the presence of a sea-urchin spike, a sufficient electrostatic charge of the ionosphere, and suitable electrical conductivity in the atmospheric condenser. The spike is a local feature, unlike the electrostatic charge of the ionosphere that simultaneously characterizes some large area.

These kinds of exceptional events - or extreme conditions - are normally considered a matter of sensational curiosity, a "mystery" almost like UFOs, etc. Instead, this information can have relevant geophysical and environmental implications. They are sporadic occurrences - analogously to earthquakes, floods, volcanic eruptions, landslides, iceberg detachment, etc. - and suitable systematic records of these reports ought to be used for scientific investigation, as every extreme event occurring in nature has a specific reason that determines its occurrence.

Suitable account should be given for the presently available detection efficiency of these rare phenomena, and for the space- and time-coverage of the detecting network and facilities (e.g., sometimes even some huge volcanic eruptions may be almost unnoticed, when they occur in some area with no population; see, e.g., Simkin et al., 1981, 1984, and Simkin and Siebert, 1994). The statistics of seldom occurring reports can result in relevant interest for "forecasting" epochs of comparatively greater hazard, etc.

At present these items are considered only like anecdotes. For instance, a very unusual phenomenon was reported by mass media during the same period that included several different "critical" phenomena. These anomalous and unusual phenomena were the Caronia phenomenon (see Gregori et al., 2025b), the exceptional heat wave that hit Europe in 2003, and the marine circulation inversion in the Adriatic Sea mentioned in Gregori et al. (2025b) and Leybourne et al. (2006, 2020). According to mass-media reports (which however cannot be checked), somewhere in Sardinia a young man and a young woman were walking, close to each other along a sandy beach. The man had his feet in a few centimeters of

NCGT Journal
New Concepts in Global Tectonics

New Concepts in Global Tectonics Journal
Volume 13, Number 6, August 2025

ISSN number; ISSN 2202-0039

water, unlike the woman. According to mass media report, with clear sky an abrupt atmospheric electric discharge killed the man while the woman suffered no injury. In those same days somebody incidentally reported about two lightning discharges exceptionally hit two trees, in central and southern Italy, etc. Trees that are stricken by lightning are considered a comparatively common phenomenon, which is not worthy of record. The concern is, however, about why these phenomena occur at some given time, and only very seldom, although their frequency seemingly increases synchronously over some comparatively wide area.

A more reliable, uniform, and objective information could be available by means of dense arrays of recorders of atmospheric potential-gradient - of the correct kind as discussed in Gregori and Leybourne (2025d). However, if no arrays are available of this kind, the information is important that is provided by the density of trees stricken by lightning discharges.

If we want to understand these comparably less frequent phenomena, we must collect a statistical database and investigate it accordingly, much like what is presently done for earthquakes, floods, landslides, snowslides (avalanches), volcanic eruptions, hurricanes or tornadoes, wind surges, etc. and several kinds of so-called environmental extreme events.

Appendix – Defining the operators Arp, $b-Arp$, $cross-ARP$, and $\sqrt{Arp}$

The rationale of all these algorithms relies on superposition operators, and - for simplicity - it can be briefly explained by means of a simple imaginative case history. Consider Fig. A-1. The uppermost line is the available time-series of events. The events are "point-like-events", i.e., characterized only by occurrence or not - i.e., either YES or NO – and every listed event is *independent* of the intensity of the event. For instance, choose a threshold and call YES every event with intensity above the threshold.

Start the stopwatch at the instant of time of every event – which is called "pole-position" event - and consider all subsequent events. Consider every such a series of events (everyone defined by one given "pole position" event) and treat it as an *independent experiment* and time-series of events. Every line in decreasing order in Fig. A-1 shows these additional time-series of events. The rationale is that, if a cycle occurs of period T, upon superposition of all time-series of events one must find relative maxima at T, $2T$, $3T$, …, nT, … Therefore, construct the histograms of all time-series, and draw the very last plot in Fig. A-1. This operator is called Arp (acronym for "automatic research of periodicities"). The final histogram is briefly called "*arp*".

The identical rationale can be applied to events that occur either (as above) *after* the "pole-position" event, or also *before* it. This is the case history of Fig. A-2, which is self-explanatory. This operator is called "*bilateral Arp*" of $b-Arp$, and the final histogram is again called "$b-arp$".

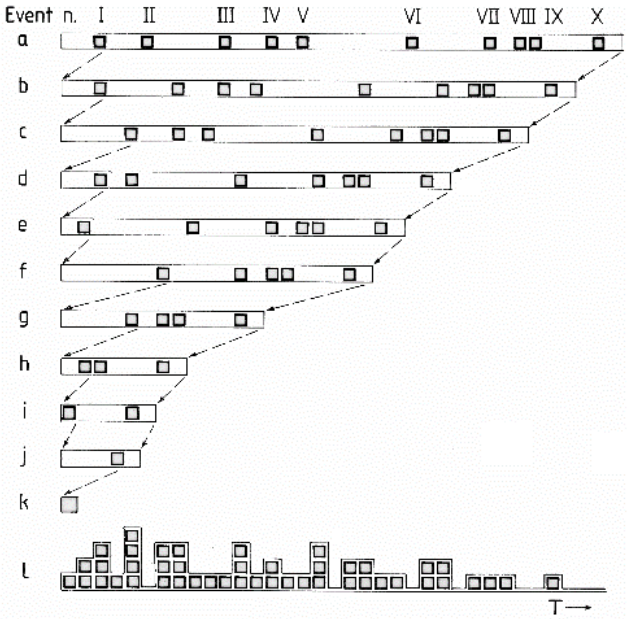

Fig. A-1 – Definition of the operator *Arp*. Refer to an arbitrary data series *H* (e.g., *vs.* time) composed, e.g., of *10* point-like events (row *a*). For simplicity, all events are here supposed to have an equal time duration (although this assumption can be dropped, see text). Change the origin on the time axis, and restart the stopwatch immediately after the occurrence of the *1st* event and get strip *b*. Similarly, restart the stopwatch after the *2nd* event, and get strip *c*, … restart the stopwatch after the *10th* event and get strip *k*. Sum up all such strips *b,c, … ,k* (but not strip *a*) to get the histogram *l*, which is called *arp*. This operation is said to be carried out by the operator *Arp*, and it is indicated by $Arp \otimes H$. In the case of a random distribution of the *10* events within *H*, the final result, i.e., *arp*, approximately looks like a right triangle with right angle in the origin. After Gregori *et al*. (1988) and Gregori (1990).

The standard error in every final "arp" or "$b-arp$" is $\sqrt{N_j}$, where N_j is the *j*-th ordinate value of the histogram. Hence, owing to the varying error-bars *vs. j*, it is difficult to assess the location of a relative maximum that ought to be indicative of a possible cycle of period T.

A simple procedure can get rid of this inconvenience. In fact, when one deals with a histogram N_j $(j = 1, 2, ...)$ formally compute the histogram $\sqrt{N_j}$ $(j = 1, 2, ...)$ that can be shown to have a standard error $\pm 1/2$ independent of j. Refer to Gregori *et al.* (1988) and Gregori (1990) for details.

Acknowledgements

We want to acknowledge all co-workers that, in different ways and at different times, contributed to the exploitation of the analyses mentioned in the present study. It is impossible to list all of them. We like also to thank them for the warm encouragement we had during several decades from several outstanding scientists.

Funding Information

G. P. Gregori retired since 2005. B. A. Leybourne is a semi-retired self-funded independent researcher.

ISSN number; ISSN 2202-0039

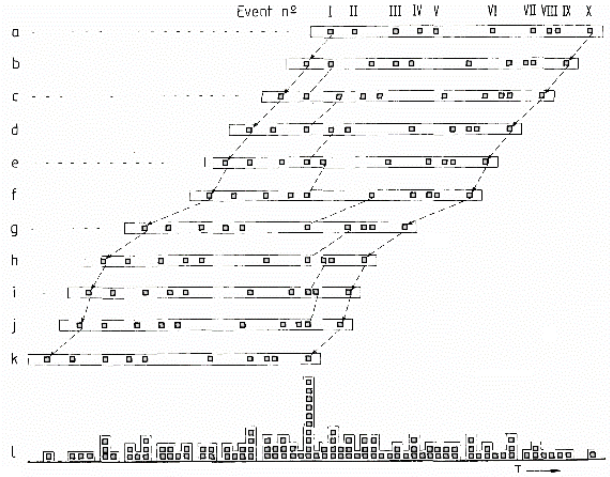

Fig. A-2 - Definition of bilateral *Arp* or $b-Arp$. The same data sequence *H* is considered as in Figs A-1. Restart the stopwatch immediately after every event, exactly like in Fig. A-1. However, don't reject the events for $t < 0$ within every strip. The final histogram (*b-arp*) is shown in *l*, and it is the sum of all strips *b,c,d, …, k*. In the case of a random distribution of the *10* events within *H*, *b-arp* approximately looks like an isosceles triangle. After Gregori *et al.* (1988) and Gregori (1990).

Author's Contributions

This study derived from a long-lasting cooperation by both authors and resulted from the emergence of long-lasting discussions.

Ethics

This article is original and contains unpublished material. Authors declare that there are no ethical issues and no conflict of interest that may arise after the publication of this manuscript.

References

Aich, V., R. Holzworth, S.J. Goodman, Y. Kuleshov, C. Price, and E. Williams, 2018. Lightning: a new essential climate variable, *EOS, Transactions of the American Geophysical Union*, 99; DOI:10.1029/2018EO104583

Albrecht, R.I., S.J. Goodman, D.E. Buechler, R.J. Blakeslee, and H.J. Christian, 2016. Where are the lightning hotspots on Earth? Bulletin of the American Meteorology Society, DOI:10.1175/BAMS-D-14-00193.1

Anonymous, 2011i. View a sea of wildfires in 2011, website of *NOAA Environmental Visualization Lab*

Anonymous, 2015k. Stratospheric accomplice for Santa Ana winds and California wildfires, *AGU Press release*, 8 July 2015

Anonymous, 2015m. Stratosphere pushes Santa Ana wind wildfires, *EarthSky*, issued July 16, 2015

Anonymous, 2018m. *La mappa stradale di La Gabella, Calci, Pisa, Toscana, website of Reti e Sistemi, Trapani*, retrieved October 8, 2018

Arley, N., and K.R. Buch, 1950. *Introduction to the Theory of Probability and Statistics*. Science Editions, John Wiley and Sons, Inc., New York, pp: 240

Bailey, D., 1995. *Ecosystem geography*, Springer, New York

Barbante, C., N.M. Kehrwald, P. Marianelli, B.M. Vinther, J.P. Steffensen, G. Cozzi, C.U. Hammer, H.B. Clausen, and M.L. Siggaard-Andersen, 2013. Greenland ice core evidence of the 79 AD Vesuvius eruption, *Climate of the Past*, 9 (3): 1221–1232

Beck, K.K., M.-S. Fletcher, P.S. Gadd, H. Heijnis, K.M. Saunders, G.L. Simpson, and A. Zawadzki, 2018. Variance and rate-of-change as early warning signals for a critical transition in an aquatic ecosystem state: a test case from Tasmania, Australia, *Journal of Geophyscal Research: Biogeosciences*, 123 (2): 495-508; DOI:10.1002/2017JG004135

Cai, Wenju, T. Cowan, and M. Raupach, 2009. Positive Indian Ocean Dipole events precondition southeast Australia bushfires, *Geophysical Research Letters*, 36: L19710 [6 pp.]; DOI:10.1029/2009GL039902

Canadian Committee on Forest Management, 2012. National Forestry Database, Forest Fires-National Tables. [online] Available from: http://nfdp.ccfm.org/fires/national_e.php (Accessed 25 April 2012)

Dartmouth College, 2024. Global warming's new threat: Arctic permafrost's carbon bomb, *SciTechDaily*, issued February 14, 2024

Davidson, C.I., J.R. Harrington, M.J. Stephenson, M.C. Monaghan, J. Pudykiewicz, and W.R. Schell, 1987. Radioactive cesium from the Cernobyl accident in the Greenland Ice Sheet, *Science*, 237 (4815): 633–634

Del Vecchio, J.M., M.C. Palucis, and C.R. Meyer, 2024. Permafrost extent sets drainage density in the Arctic, *Proceedings of the National Academy of Sciences*; DOI:10.1073/pnas.2307072120

Dennison, P.E., S.C. Brewer, J.D. Arnold, and M.A. Moritz, 2014. Large wildfire trends in the western United States, 1984–2011, *Geophysical Research Letters*, 41: 2928–2933; DOI:10.1002/2014GL059576

Diakakis, M., E.I. Nikolopoulos, S. Mavroulis, E. Vassilakis, and E. Korakaki, 2017. Observational evidence on the effects of mega-fires on the frequency of hydrogeomorphic hazards. The case of the Peloponnese fires of 2007 in Greece, *Science of The Total Environment*, 592: 262-276; DOI:10.1016/j.scitotenv.2017.03.070

Dibb, J., 1989. The Chernobyl reference horizon in the Greenland Ice Sheet, *Geophysical Research Letters*, 16 (9): 987–990; DOI:10.1029/GL016i009p00987

Dooley, E.E., 2012. Biomass fires a major source of isocyanic acid, *Environmental Health Perspectives*, 120 (6): A231

Einstein, A., and L. Infeld, 1953. *L'Evoluzione della Fisica. Sviluppo delle Idee dai Concetti Primitivi alla Relatività ed ai Quanti*. Translated from English (original title The Evolution of Physics, IV ed.), Edizioni Scientifiche Einaudi, Torino, pp: 1-313

Ellis, E.C., J.O. Kaplan, D.Q. Fuller, S. Vavrus, K. Klein Goldewijk, and P.H. Verburg, 2013. Used planet: a global history, *Proceedings of the National Academy of Sciences*, 110 (20): 7978–7985

ISSN number; ISSN 2202-0039

Faynberg, E.B., and W.A. Sidorov, 1978. *Integral Conductivity of the Sedimentary Cover and Water Shell of the Earth* (in Russian), Izmiran, with 5 maps, Nauka, Moscow, p: 1-11

Finneran, M., 2010. Wildfires: a symptom of climate change, *NASA News & Features*, updated September 24, 2010

Gannon, M., 2018c. These 'dirty' thunderstorms fill the sky with as much smoke as a volcanic eruption, *Live Science*, issued April 20, 2018

George, C., C. Rowland, F. Gerard, and H. Balzter, 2006. Retrospective mapping of burnt areas in Central Siberia using a modification of the normalised difference water index, *Remote Sensing of Environment*, 104: 346–359

Goldewijk, K., A. Beusen, G. van Drecht, and M. de Vos, 2011. The HYDE 3.1 spatially explicit database of human-induced global land-use change over the past 12,000 years, *Global Ecology and Biogeography*, 20 (1): 73–86

Gregori G.P., and M.T. Hovland, 2025. Go for the anomaly – a golden strategy for discovery? Seepology & the origin and crucial role of the biosphere - Earth and planetary objects - Supercritical water and serpentinization, present issue

Gregori, G. P., 1990. A Few Mathematical Procedures for the Analysis of Incomplete Historical Data Series. In W. Schröder (ed.), *Advances in geosciences*, Interdivisional Commission on History of IAGA, Bremen-Roennebeck, pp: 80-127

Gregori, G. P., 2002. Galaxy – Sun – Earth relations. The Origin of the Magnetic Field and of the Endogenous Energy of the Earth, with Implications for Volcanism, Geodynamics and Climate Control, and Related Items of Concern for Stars, Planets, Satellites, and Other Planetary Objects. A Discussion in a Prologue and Two Parts. *Beiträge zur Geschichte der Geophysik und Kosmischen Physik*, Band 3, Heft 3: pp. 1-471 [Available at http://ncgtjournal.com/additional-resources.html]

Gregori, G. P., 2013a. Space-time constraints on earthquake predictability - A 10 cm/sec "domino effect" typical of every fracture phenomenon, *New Concepts in Global Tectonics, Journal*, 1 (2): 23-39

Gregori, G. P., 2016. Some reflections on science and on the management of environmental catastrophes. *New Concepts in Global Tectonics, Journal*, 4 (3): 456-472

Gregori, G. P., 2019. Catastrophes and mankind. Fake truth and mass media. Science and society: a commentary. *New Concepts in Global Tectonics, Journal*, 7 (2): 4-12

Gregori, G. P., 2020. Climate change, security, sensors. *Acoustics,* 2: 474-504; DOI:10.3390/acoustics2030026.[https://www.mdpi.com/2624-599X/2/3/26/htm]

Gregori, G. P., and B. A. Leybourne, 2021. An unprecedented challenge for humankind survival. Energy exploitation from the atmospheric electrical circuit, *American Journal of Engineering and Applied Science*, 14 (2): 258-291; DOI:10.3844/ajeassp.2021.258.291

Gregori, G. P., and B. A. Leybourne, 2025b. The electrostatic Sun. In press in *New Concepts in Global Tectonics, Journal*

Gregori, G. P., and B. A. Leybourne, 2025c. The solar cycle and MiniMax - Effects on other planets. In press in *New Concepts in Global Tectonics, Journal*

Gregori, G.P., and B.A. Leybourne, 2025d. Measuring the electric field at ground, present issue

Gregori, G. P., and B. A. Leybourne, 2025e. The physics of electrical discharges – 1. Small-scale phenomena - Fog - atmospheric precipitation – BLs. In press in *New Concepts in Global Tectonics, Journal*

Gregori, G. P., and B. A. Leybourne, 2025f. The physics of electrical discharges – 2. RB & TGFs - Runaway breakdown – terrestrial gamma flashes – GK effect. In press in *New Concepts in Global Tectonics, Journal*

Gregori, G. P., and B. A. Leybourne, 2025g. The physics of electrical discharges – 3. Sparks and lightning - electrostatics of the ionosphere – TLEs - plasma jets collimation – Birkeland currents & sea-urchin spikes - stellar and galactic alignments. In press in *New Concepts in Global Tectonics, Journal*

Gregori, G. P., and B. A. Leybourne, 2025j. The energy supply to hurricanes. *New Concepts in Global Tectonics, Journal,* 13, (5): 731-786

Gregori, G. P., B. A. Leybourne, and F. F. Bonavia, 2025v. The origin of lavakas. *New Concepts in Global Tectonics, Journal,* 13, (5): 787-811

Gregori, G. P., B. A. Leybourne, and G. Paparo†, 2025b. Introduction – Anomalous lesser air-earth phenomena. In press in *New Concepts in Global Tectonics, Journal*

Gregori, G. P., and B. A. Leybourne, 2025c. The solar cycle and MiniMax - Effects on other planets. In press in *New Concepts in Global Tectonics, Journal*

Gregori, G. P., B. A. Leybourne, and J. R. Wright, 2025d. Generalized Cowling theorem and the Cowling dynamo. In press in *New Concepts in Global Tectonics, Journal*

Gregori, G. P., B. A. Leybourne, Dong Wenjie, and Gao Xiaoqing, 2025h. Shallow geotherms. In press in *New Concepts in Global Tectonics, Journal*

Gregori, G. P., B. A. Leybourne, G. Paparo†, and M. Poscolieri, 2025a. The global Sun-Earth circuit. In press in *New Concepts in Global Tectonics, Journal*

Gregori, G. P., B. A. Leybourne, U. Coppa, and G. Luongo, 2025t. Lightning and volcanic plumes. In press on *New Concept of Global Tectonics*

Gregori, G. P., B. A. Leybourne, W. Soon, and V. Straser, 2025e. The heuristic meaning of variational principles. In press in *New Concepts in Global Tectonics, Journal*

Gregori, G. P., F .F. Bonavia, and B. A. Leybourne, 2025x. Geoelectrical geology in North America, *New Concepts in Global Tectonics, Journal*, 13, (2): 252-269

Gregori, G. P., M. T. Hovland, B. A. Leybourne, S. Pellis, V. Straser, B. G. Gregori, G. M. Gregori, and A. R. Simonelli, 2025w. Air-earth currents and a universal "law": filamentary and spiral structures - Repetitiveness, fractality, golden ratio, fine-structure constant, antifragility and "statistics" - The origin of life, *New Concepts in Global Tectonics, Journal*, 3, (1): 106-225

Gregori, G. P., R. Santoleri, M. P. Pavese, M. Colacino, E. Fiorentino and G. de Franceschi, 1988. The analysis of point-like data series. In W. Schröder (ed.), *Past, Present and Future Trends in Geophysical Research,* Interdivisional Commission on History of IAGA, Bremen-Roennebeck, pp.: 146-211

Gregori, G. P., W. Soon, V. Straser, and B. A. Leybourne, 2022a. Golden ratio, fractals, and the arrow of time. Irreversibility vs. reversibility - Space, time, antitime - The foundations of physics. *New Concepts in Global Tectonics, Journal*, 10 (3): 158-201

Hansen, K., 2015. Global lightning activity, *NASA Earth Obs.*, issued March 31, 2015

Hickok, K., 2018a. Tons of major quakes have rattled the world recently. Does that mean anything? *Live Science*, issued August 23, 2018

Janssen, T.A.J., M.W. Jones, D. Finney, G.R. van der Werf, D. van Wees, Wenxuan Xu, and S. Veraverbeke, 2023. Extratropical forests increasingly at risk due to lightning fires, *Nature Geoscience*; DOI:10.1038/s41561-023-01322-z

Jenner, L., 2015. Northwestern fires by night, *NASA, Image feature*, August 21, 2015. ahttp://www.nasa.gov/imagefeature/goddard/northwestern-fires-by-night

Jin, Yufang, J.T. Randerson, M.L. Goulden, and S.J. Goetz, 2012. Post-fire changes in net shortwave radiation along a latitudinal gradient in boreal North America, *Geophysical Research Letters*, 39: L13403 [7 pp.]; DOI:10.1029/2012GL051790

Juselius-Rajamäki, T., M. Väliranta, and A. Korhola, 2023. The ongoing lateral expansion of peatlands in Finland, *Global Change Biology*; DOI:10.1111/gcb.16988

Kaplan, J.O. and K.H.-K. Lau, 2022. World Wide Lightning Location Network (WWLLN) Global Lightning Climatology (WGLC) and time series, 2022 update, *Earth System Science Data*, 14: 5665–5670; https://doi.org/10.5194/essd-14-5665-2022, 2022

Kaplan, J.O., and K.H.-K. Lau, 2021. The WGLC global gridded lightning climatology and timeseries. *Earth System Science Data Discussion*, pp: 1-25. DOI:10.5194/essd-2021-89

Kaplan, J.O., K.M. Krumhardt, and N. Zimmermann, 2009. The prehistoric and preindustrial deforestation of Europe, *Quaternary Science Reviews*, 28 (27/28): 3016–3034

Kaplan, J.O., K.M. Krumhardt, E.C. Ellis, W.F. Ruddiman, C. Lemmen, and K.K. Goldewijk, 2011. Holocene carbon emissions as a result of anthropogenic land cover change, *Holocene*, 21 (5): 775–791

Kehrwald, N.M., C. Whitlock, C. Barbante, V. Brovkin, A.-L. Daniau, J.O. Kaplan, J.R. Marlon, M.J. Power, K. Thonicke, and G.R. van der Werf, 2013. Fire research: linking past, present, and future data. *EOS, Transactions of the American Geophysical Union,* 94 (46): 421-422; DOI:10.1002/2013EO460001

Kim, Do-Hyung, J.O. Sexton, and J.R. Townshend, 2015. Accelerated deforestation in the humid tropics from the 1990s to the 2000s, *Geophysical Research Letters*, 42 (9): 3495-350; DOI:10.1002/2014GL062777

Kitzberger, T., D.A. Falk, A.L. Westerling, and T.W. Swetnam, 2017. Direct and indirect climate controls predict heterogeneous early-mid 21st century wildfire burned area across western and boreal North America. *PLoS ONE*, 12 (12): e0188486; DOI:10.1371/journal.pone.0188486

Langford, A.O., R.B. Pierce, and P.J. Schultz, 2015. Stratospheric intrusions, the Santa Ana winds, and wildland fires in Southern California, *Geophysical Research Letters*, 42; DOI:10.1002/2015GL064964

Lanzerotti, L. J., and G. P. Gregori, 1986. Telluric currents: the natural environment and interactions with man-made systems. In E. P. Krider, and R.G. Roble, (eds), *The Earth's Electrical Environment*, National Academy Press, Washington, D. C.; DOI:10.17226/898, pp.: 232-257

Lau, K., 2020. WGLC global lightning climatology, posted on October 23, 2020, *TERRACES, Climate and Vegetation Modelling Lab*

Lehsten, V., W.J. de Groot, M. Flannigan, C. George, P. Harmand, and H. Balzter, 2014. Wildfires in boreal ecoregions: Evaluating the power law assumption and intra-annual and interannual variations, *Journal of Geophysical Research: Biogeosciences*, 119: 14-23; DOI:10.1002/2012JG002252

Letzter, R., 2018g. A whole lot of the planet is on fire right now, *Live Science*, issued August 23, 2018

Leybourne, B. A., A. Haas, B. Orr, C. Smoot, I. Bhat, D. Lewis, G. P. Gregori, and T. Reed, 2020a. Electrical wildfire propagation along geomagnetic anomalies: a solar induction process, *The 8th World Multi-Conference on Systemics, Cybernetics and Informatics,* Orlando, FL, 18 (4): 122-126

Leybourne, B. A., A. Haas, B. Orr, N. C. Smoot, M. I. Bhat, D. Lewis, G. P. Gregori, and T. Reed, 2004a. Electrical wildfire propagation along geomagnetic anomalies, *The 8th World Multi-Conference on Systemics, Cybernetics and Informatics*, Orlando, FL.; pp.: 298-299

Leybourne, B. A., and D. Orr, 2020. Global disaster forecasting with space weather & geophysical intelligence, *Journal of Systemics, Cybernetics and Informatics,* 18 (4): 66-71; https://www.iiisci.org/journal/sci/FullText.asp?var=&id=ZA689IO20)

Leybourne, B. A., and M. B. Adams, 2020. Modeling mantle dynamics in the Banda Sea Triple Junction - Exploring a possible link to El Niño Southern Oscillation (Revisited), *Journal of Systemics, Cybernetics and Informatics*, 18 (4): 97-106. Revisited - 1st published in Marine Technology Society Oceans '99 Conference Proceedings, Seattle, Washington, September 13-16, 1999, https://www.iiisci.org/journal/sci/FullText.asp?var=&id=IP093LL20

Leybourne, B. A., B. Orr, A. Haas, G. P. Gregori, D. Lewis, P. Gruszinskas, N. C. Smoot, and M. I. Bhat, 2004b. Four elements of coupled climate: evidence of an electromagnetic driver for global warming, *32nd International Geological Congress*, Florence, Italy, #316-4 (abstracts –part 2), pp.: 1407

ISSN number; ISSN 2202-0039

Leybourne, B. A., B. Orr, A. Haas, P. Gruzinskas, D. Lewis, G. P. Gregori, C. Smoot, and I. Bhat, 2020. Earthquakes linked to 2003 European heat wave: implications for global warming - Evidence in the Adriatic and Mediterranean Basins (Revisited), *Journal of Systemics, Cybernetics and Informatics*, 18 (4): 84-88. Originally presented as Leybourne et al. (2004b) and published as Leybourne et al. (2006). https://www.iiisci.org/journal/sci/FullText.asp?var=&id=IP090LL20

Leybourne, B. A., D. W. Johnson, and G. P. Gregori, 2025. Arc-blast as static electricity or interplanetary lightning short circuits in Stellar Transformers. A plausible North American scenario, *New Concepts in Global Tectonics, Journal*, 13, (2): 229-251

Leybourne, B. A., G. P. Gregori, and C. de Hoop, 2006. Gulf of California electrical hot-spot hypothesis: climate and wildfire teleconnections, *New Concepts in Global Tectonics, Newsletters*, (38): 3-8

Liang, X. San, 2014. Unraveling the cause-effect relation between time series, *Physical Review*, E 90: 052150; DOI:10.1103/PhysRevE.90.052150

Lopez, R.E., D.N. Baker, and J. Allen, 2004. Sun unleashes Halloween storm, *EOS, Transactions of the American Geophysical Union,* 85 (11): 105, 108

Lui, A.T.Y., 2001. Current controversies in magnetospheric physics, *Reviews of Geophysics*, 39 (4): 535-563

Lunsford, C., 2017a. In photos: the southern California wildfires of 2017 seen from space, *Space.com*, issued December 8, 2017

Maestrini, B., E.C. Alvey, M.D. Hurteau, H. Safford, and J.R. Miesel, 2018. Fire severity alters the distribution of pyrogenic carbon stocks across ecosystem pools in a Californian mixed-conifer forest, Journal of Geophysical Research: *Biogeosciences*, 123 (2); DOI:10.1002/2017JG003832

Magill, B., 2015. Firestorm leaves 'mass destruction' in California, Climate Central, *Live Science*, issued September 14, 2015

Marlon, J.R., P.J. Bartlein, C. Carcaillet, D.G. Gavin, S.P. Harrison, P.E. Higuera, F. Joos, M.J. Power, and I.C. Prentice, 2008. Climate and human influences on global biomass burning over the past two millennia, *Nature, Geoscience*, 1: 697-702; DOI:10.1038/ngeo313

McKenzie, D., N.H.F. French, and R.D. Ottmar, 2012. National database for calculating fuel available to wildfires. *EOS, Transactions of the American Geophysical Union*, 93 (6): 57-58

NGRIP Project Members, 2004. High-resolution record of Northern Hemisphere climate extending into the last interglacial period, *Nature*, 431 (7005): 147–151

Paparo, G., and G. P. Gregori, 2003. Multifrequency acoustic emissions (AE) for monitoring the time evolution of microprocesses within solids. Reviews of Quantitative Nondestructive Evaluation, 22, (*AIP Conference Proceedings ed. by D. O. Thompson and D. E. Chimenti)*, pp.: 1423-1430

Pappas, S., 2013. Earth from above: 101 stunning images from orbit, *Live Science*, issued June 7, 2013

Pappas, S., 2018a. California's deadliest fire is seen engulfing Paradise in 'astonishing' satellite images, *Live Science,* issued November 16, 2018

Parrot, M., 2025. DEMETER observations of the variations of the global electric circuit under various constraints, *New Concepts in Global Tectonics, Journal*, 13, (2): 355-366; ID 530865; DOI:10.1155/2013/530865

Potera, C., 2011. New device measures atmospheric isocyanic acid. *Environmental Health Perspectives*, 119 (8): A338; DOI:10.1289/ehp.119-a338a

Quinn, J. M.,† G. P. Gregori, and B. A. Leybourne, 2025. Satellite monitoring of air-earth currents. In press in *New Concepts in Global Tectonics, Journal*

Salazar, D.-E., 2018b. Watch Yellowstone recover from wildfires over 30 years in this NASA time-lapse video, *Space.com*, issued August 28, 2018

Santoso, A., 2018. Learning from an extreme El Niño, *EOS, Transactions of the American Geophysical Union*, 99; DOI:10.1029/2018EO089619

Seager, R., N. Lis, J. Feldman, Mingfang Ting, A.P. Williams, J. Nakamura, Haibo Liu, and N. Henderson, 2018. Whither the 100th meridian? The once and future physical and human geography of America's arid-humid divide. Part I: The story so far, *Earth Interactions*; DOI:10.1175/EI-D-17-0011.1

Seager, R., N. Lis, J. Feldman, Mingfang Ting, A.P. Williams, J. Nakamura, Haibo Liu, and N. Henderson, 2018a. Whither the 100th meridian? The once and future physical and human geography of America's arid-humid divide. Part II: The meridian moves east, *Earth Interactions*; DOI:10.1175/EI-D-17-0012.1

Simkin, T., and Siebert, L., 1994. *Volcanoes of the World*. Geosciences Press, Inc. Tucson, pp: 1-349

Simkin, T., L. Siebert, and L. McClelland, 1984. *Volcanoes of the World - Supplement 1984*. Smithsonian Institution Washington

Simkin, T., L. Siebert, L. McClelland, D. Bridge, C. Newhall, and J.H., Latter, 1981. *Volcanoes of the World: a Regional Directory, Gazetteer and Chronology of Volcanism during the last 10,000 years*. US Hutchinson Ross Publishing. ISBN-10: 0879334088, pp: 1-233

Smoot, N. C., and B. A. Leybourne, 2001. The Central Pacific megatrend, *International Geology Review*, 43 (4): 341-365

Smoot, N. C., and B. A. Leybourne, 2020. Orthogonal megatrend intersections: "coils" of a Stellar Transformer. *Journal of Systemics, Cybernetics and Informatics*, 18 (4): 61-66; https://www.iiisci.org/journal/sci/FullText.a

SOHO, 2003. Solar and Heliospheric Observatory, 2003. Extreme ultraviolent Imaging Telescope (EIT) 195 Ångstrom image *28 October 2003 Solar Flare*

Stoof, C.R., D. Moore, P.M. Fernandes, J.J. Stoorvogel, R.E.S. Fernandes, A,J.D. Ferreira, and C.J. Ritsema, 2013. Hot fire, cool soil, *Geophysical Research Letters*, 40 (8): 1534–1539; DOI:10.1002/grl.50299

Størmer, C., 1955. *The Polar Aurora*. Oxford, at the Clarendon Press, pp: 403+34

ISSN number; ISSN 2202-0039

Straser, V., G. Cataldi, and D. Cataldi, 2025. Space weather related to potentially destructive seismic activity, In press in *New Concepts in Global Tectonics, Journal*

Tang, Maocang, and Zhang Jian, 1990. Approach on the underground suddenly warming relative to short-term climatic variations, *Plateau Meteorology*, 9 (4): 364-370

Tang, Maocang, Xiaoqing Gao, Hao Jiang, Weidong Guo, and Yanxiang Liu, 1999. The advection and evolution processes of geothermal vortexes, *Advances in Earth Science*, (2)

Tosca, M.G., D.J. Diner, M.J. Garay, and O.V. Kalashnikova, 2015. Human-caused fires limit convection in tropical Africa: first temporal observations and attribution, *Geophysical Research Letters*, 4, (15): 6492–6501; DOI:10.1002/2015GL065063

Tsunoda, F., 2010. Habits of earthquakes – Part 2: Earthquakes corridors in East Asia, *New Concepts in Global Tectonics, Newletters*, (54): 45-56

Tsunoda, F., 2010a. Habits of earthquakes – Part 3: Earthquakes in the Japanese Islands, *New Concepts in Global Tectonics, Newletters*, (55): 35-65

University of East Anglia, 2023. Increased lightning fires threaten boreal forest carbon storage, *SciTechDaily,* issued November 11, 2023

University of Helsinki, 2024. Challenging assumptions: scientists discover that the northern peatlands are still expanding, *SciTechDaily*, issued January 25, 2024

University of Iowa, 2023. A step backward: wildfires undo 20 years of air quality progress in Western U.S., *SciTechDaily*, issued December 7, 2023

University of Leeds, 2023. Boreal forests at risk: lightning-induced wildfires threaten crucial carbon storage, *SciTechDaily*, issued November 25, 2023

USFS, 2003. *California fire siege 2003. The Story*. Dept. of Interior

Vinther, B.M., H.B. Clausen, S.J. Johnsen, S.O. Rasmussen, K.K. Andersen, S.L. Buchardt, D. Dahl-Jensen, I.K. Seierstad, M.-L. Siggaard-Andersen, J.P. Steffensen, A. Svensson, J. Olsen, and J. Heinemeier, 2006. A synchronized dating of three Greenland ice cores throughout the Holocene, *Journal of Geophysical Research*., 111: D13102; DOI:10.1029/2005JD006921

Virts, K.S., J.M. Wallace, M.L. Hutchins, and R.H. Holzworth, 2013: Highlights of a new ground-based, hourly global lightning climatology. *Bulletin of the American Meteorological Society*, 94: 1381–1391; DOI:10.1175/BAMS-D-12-00082.1

Voiland A., 2020. Extraordinary fires char the Pantanal, a vast floodplain in South America, *NASA Earth Observatory News*, issued September 19, 2020

Wall, M., 2017i. Northern California wildfires rage in new photo from space, *Space.com*, issued October 10, 2017

Wall, M., 2017j. Raging southern California wildfires seen from space (photos), *Space.com*, issued December 6, 2017

Wall, M., 2018n. Raging California wildfires spotted from space (photos), *Space.com*, issued November 10, 2018

Wei, Jing, Jun Wang, Zhanqing Li, S. Kondragunta, S. Anenberg, Yi Wang, Huanxin Zhang, D. Diner, J. Hand, A. Lyapustin, R. Kahn, P. Colarco, A. da Silva, and C. Ichoku, 2023. Long-term mortality burden trends attributed to black carbon and PM2·5 from wildfire emissions across the continental USA from 2000 to 2020: a deep learning modelling study, *The Lancet Planetary Health*; DOI:10.1016/S2542-5196(23)00235-8

Weisberger, M., 2017g. Inferno down below: satellites reveal burning California wildfires. *Live Science,* issued October 12, 2017

Weisberger, M., 2018a. As world warms, America's invisible 'climate curtain' creeps east, *Live Science*, issued April 16, 2018

Williams, E.R., and G.Sátori, 2004. Lightning, thermodynamic and hydrological comparison of the two tropical continental chimneys, *Journal of Atmospheric and Solar-Terrestrial Physics*, 676 (13/14): 1213-1231; DOI:10.1016/j.jastp.2004.05.015

Witman, S., 2018a. Australian algae aid understanding of ecosystem resilience, *EOS, Transactions of the American Geophysical Union*, 99; DOI:10.1029/2018EO096161

Woodbridge, J., R.M. Fyfe, N. Roberts, S. Downey, K. Edinborough, and S. Shennan, 2014. The impact of the Neolithic agricultural transition in Britain: a comparison of pollen-based land-cover and archaeological C-14 date-inferred population change, *Journal of Archaeological Science*, 51: 216–224

Wu, Hong-chun, 2025. Jet stream's disturbances as possible precursors of earthquakes, preprint

Yang, Jianling, Qinyu Liu, Zhengyu Liu, Lixin Wu, and Fei Huang, 2009. Basin mode of Indian Ocean sea surface temperature and Northern Hemisphere circumglobal teleconnection, *Geophysical Research Letters*, 36: L19705, DOI:10.1029/2009GL039559

Young, P.J., L.K. Emmons, J.M. Roberts, J.-F. Lamarque, C. Wiedinmyer, P. Veres, and T.C. Van den Boer, 2012. Isocyanic acid in a global chemistry transport model: tropospheric distribution, budget, and identification of regions with potential health impacts, *Journal of Geophysical Research.: Atmosphere (1984–2012)*, 117, (D10); DOI:10.1029/2011JD017393

Yuan, Wenping, Xianglan Li, Shunlin Liang, Xuefeng Cui, Wenjie Dong, Shuguang Liu, Jiangzhou Xia, Yang Chen, Dan Liu, and Wenquan Zhu, 2014. Characterization of locations and extents of afforestation from the Grain for Green Project in China, *Remote Sensing Letters*, 5 (3): 221-229; DOI:10.1080/2150704X.2014.894655

Zennaro, P., N. Kehrwald, J. Marlon, W.F. Ruddiman, T. Brücher, C. Agostinelli, D. Dahl-Jensen, R. Zangrando, A. Gambaro, and C. Barbante, 2015. Europe on fire three thousand years ago: Arson or climate? *Geophysical Research Letters*; DOI:10.1002/2015GL064259

Zennaro, P., N. Kehrwald, J.R. McConnell, S. Schüpbach, O.J. Maselli, J. Marlon, P. Vallelonga, D. Leuenberger, R. Zangrando, A. Spolaor, M. Borrotti, E. Barbaro, A. Gambaro, and C. Barbante, 2014. Fire in ice: two millennia of boreal forest fire history from the

ISSN number; ISSN 2202-0039

Greenland NEEM ice core, *Climate of the Past*, 10 (5): 1905–1924

Acronyms

AAD - Australian-Antarctic Discordance
AE –acoustic emission
AGU – American Geophysical Union
AOT - aerosol optical thickness
arp – automatic research for periodicities (histogram or operator)
AVHRR – Advanced Very-High-Resolution Radiometer (NOAA's instrument)
b-arp – bilateral arp (histogram or operator)
BBA - boreal burned area
Cal Fire - California Department of Forestry and Fire Protection
CGT - circumglobal teleconnection
CHAMP - Challenging Minisatellite Payload, German satellite
CME – coronal mass ejection
CNFDB - Canadian National Fire Database
d.o.f. - degree of freedom
DUPAL – Duprè and Allègre (anomaly of basalt isotopic chemism)
e.m. - electromagnetic
EGU –European Geophysical Union
EIT - Extreme ultraviolet Imaging Telescope
ENSO –El Niño Southern Oscillation
EPR – East Pacific Rise
EQL - earthquake lights
ESA – European Space Agency
EWS - early warning signals
FAO – Food and Agriculture Organization
FR – (geomagnetic) field reversal
GA-SAW - geothermal abnormal soil abrupt warming
GGP - Grain for Green Project
GOES – Geostationary Operational Environmental Satellite (operated by *NOAA*)
GSFC – Goddard Space Flight center (*NASA*)
HYDE - History database of the Global Environment
IOBM - Indian Ocean Basin Mode
IOD - Indian Ocean Dipole (index)
KK10 – anthropogenic deforestation database
LIS - Lightning Imaging Sensor on *NASA's Tropical Rainfall Measuring Mission* satellite
MODIS - Moderate Resolution Imaging Spectroradiometer on NASA's TERRA satellite
MOR – mid-ocean ridge
NASA –National Atmospheric and Space Administration
NDVI - normalized difference vegetation index
NGDC –National Geophysical Data Center (of NOAA)
NH - Northern Hemisphere
NIFC - National Interagency Fire Center
NOAA – National Oceanographic and Atmospheric Administration
NSSTC - National Space Science and Technology Center
OCO-2 - Orbiting Carbon Observatory 2, NASA satellite
OTD - Optical Transient Detector on the *OrbView-1/Microlab* satellite
pIOD - positive Indian Ocean Dipole
PyC - Pyrogenic carbon
pyroCbs - pyrocumulonimbus storms
SAA - South Atlantic Anomaly or South American Anomaly
SEIR - Southeast Indian Ridge
Sentinel-5 Precursor – ESA satellite
SOHO - Solar and Heliospheric Observatory
SSF - surface shortwave forcing
Suomi NPP - Suomi National Polar-Orbiting satellite
SV - secular variation
TD - tide-driven (dynamo)
TEC - total electron content
TERRA – or *EOS AM-1*, multi-national *NASA* scientific research satellite
TLE - transient luminous event
UFO – unidentified flying object
VIIRS - Visible Infrared Imaging Radiometer Suite sensor on the *Suomi NPP* satellite
WGCL - World Wide Lightning Location Network
WHO – World Health Organization
WMT – warm mud tectonics

NCGT Journal
New Concepts in Global Tectonics

New Concepts in Global Tectonics Journal
Volume 13, Number 6, August 2025

ISSN number; ISSN 2202-0039

Geomagnetic anomalies: double-eyes in volcanic areas, and lineaments

Giovanni Pietro Gregori[1], Bruce Allen Leybourne[2], Ugo Coppa[3], Giuseppe Luongo[4]

[1] Former Senior Researcher at *IDASC-Institute of Acoustics and Sensors O. M. Corbino (CNR), Rome,* now merged with the *INM-Institute of Marine Engineering "Section of Acoustics and Sensors O.M. Corbino"- (CNR Rome)*; and *ISSO-International Seismic Safety Organization*, Italy
[2]*GeoPlasma Research Institute-(GeoPlasmaResearchInstitute.org),* Aurora, CO 80014, USA
[3]*Researcher at INGV – Osservatorio Vesuviano*
[4] Emeritus Professor of Physics of Volcanism at the *University Federico II* in Naples, Associate of *INGV – Osservatorio Vesuviano* - Former Director of the *Osseratorio Vesuviano*

Corresponding Author: G.P. Gregori, *DASC-Istituto di Acustica e Sensoristica O. M. Corbino (CNR)*, Roma, now merged into *IMM-Istituto per la Microelettronica e Microsistemi (CNR)*; B.A. Leybourne, *GeoPlasma Research Institute-(GeoPlasmaResearchInstitute.org)*; U. Coppa, *Osservatorio Vesuviano;*G. Luongo, *Osservatorio Vesuviano*
Email:
giovannipgregori38@gmail.com
leybourneb@iascc.org;
ugo.coppa@ingv.it;
luongius@unina.it

Abstract: Geomagnetic anomaly maps in volcanic areas can be interpreted according to the sea-urchin rationale. A few case studies are illustrated, while several examples of "double-eye" features in volcanic areas. Appendix A contains several case histories of geomagnetic double eye anomaly pattern. Appendix B contains a short discussion of geomagnetic lineaments observed in several part of the world, which are suggestive of an analogous effect on the planetary scale. In fact, geomagnetic anomaly maps can be interpreted according either *(i)* to the electromagnetic (e.m.) induction by the solar wind that generates telluric currents aimed to oppose the geomagnetic field originated by the deep geomagnetic dynamo, or *(ii)* by stray currents that outflow from the deep Earth's circuitry. The results correlate with other morphological, geodynamic, and tectonic features, which represent a tool for the investigation of Earth's interior. A few case studies are illustrated.

Keywords: volcanic areas – geomagnetic anomalies – *TD*-dynamo – sea-urchin spikes- shallow DC currents –geomagnetic anomalies – lineaments – telluric currents – case studies – Africa – Scotia arc – Florida and Gulf of Mexico

Introduction

Geomagnetic anomaly maps show peculiar morphological features. It is customary in the literature to refer to different rock magnetization and/or electrical conductivity. These features refer, however, to comparatively shallow features, while the rationale that is here considered appeals to much deeper processes on the planetary scale, which are manifested like local features. The key argument is the sea-urchin spike propagation of endogenous energy for the deep Earth interior through Earth's surface (see Gregori, 2002; Gregori et al., 2025a).

A concise summary of the leading idea of principle relies on the origin of the geomagnetic field. The Earth is composed of disjoint components, which are ionized, and are displaced by the tidal interaction – originated mainly by the Moon. This is an effective tide-driven (*TD*) dynamo. The energy balance is impressive and is sufficient to justify all geodynamic, geothermal, and volcanic phenomena (see Gregori, 2002; Gregori et al., 2025a, and Gregori and Leybourne, 2021). Every current generated in any way inside deep Earth must expand as much as possible. Hence, every gentle uplift at the *CMB* (core-mantle boundary) propagates upward, while it shrinks in diameter. The Earth interior looks therefore like a sea-urchin with several spikes that slowly propagate through the mantle, at a mean speed of 10 $cm\ year^{-1}$, much like an electric soldering iron propagates through a block of ice (*ESI* process). On top of every spike, the lower electrical conductivity σ determines the Joule heat that must be extracted from the Earth's interior.

When a spike gets close to Earth's surface, if it finds fluids, fluid exhalation transports heat by advection. If the available fluids are insufficient, heat accumulates. If the depth is shallow, the small lithostatic pressure permits liquefaction of overburden or surrounding country rock. Thus, magma is formed like a specifically devoted new fluid. Lava effusion – or volcanic explosion, eventually associated to earthquake vapors (Wu, 2025) - ensures the thermal energy balance. A volcanic plume is the propagation through the atmosphere of a sea-urchin spike. A sea-urchin spike pattern can also result from friction heat in geodynamic areas, rather than by Joule heat.

NCGT Journal
New Concepts in Global Tectonics
New Concepts in Global Tectonics Journal
Volume 13, Number 6, August 2025
ISSN number; ISSN 2202-0039

Different sea-urchin spikes interact with one another, and this is the unique available explanation for the geographical distribution of *MOR*s (mid-ocean ridges; see Gregori and Leybourne, 2021). In addition, the entire *TD* rationale is consistent with the association of tectonic features and magnetic fields observed in all other bodies in the Solar System (see Table 2 and 3 of Gregori et al., 2025a).

Therefore, when dealing with the magnetization of rocks in a volcanic area, we must consider the presence of variable DC electric currents flowing at some suitable depth. The depth, however, can be different at different sites, due to the heterogeneity of the Earth's crust.

Consider how a geomagnetic anomaly is defined. One starts from a map of one given magnetic element (i.e., one given component of the geomagnetic field ***B***, or its total intensity *F*). Then, one chooses the seemingly best model for the planetary deep origin ***B***, in order to isolate the residual that ought to be representative of the magnetization of the crust. The anomaly map is the residual map. Therefore, some arbitrariness is involved - and different maps can display comparative differences.

No map, however, is claimed being the best possible choice, as the quality of a map depends on the progressively increasing amount of the observational database. Nevertheless, the geomagnetic anomaly maps, altogether with gravity maps, seismological maps, and the general tectonic morphology, are the fundamental observational information used to investigate geodynamics and the origin and evolution of solid Earth.

Therefore, we have to interpret the geomagnetic anomaly maps by means of suitable and reasonable assumptions and approximations, in order to develop physically indicative hunches.

Two kinds of evidence can be considered. One evidence deals with a general "double-eye" pattern that characterizes every volcano. Another evidence is considered in Appendix B. It deals with the general appearance of positive/negative alignments indicating the likely large-scale flow of telluric currents, which occurred and produced an anomaly integrated over time on the secular time-range.

The rationale of the present paper

Consider the top of a sea-urchin spike (Fig. 1). The ***B***, generated by this DC current ***j***, originates a local geomagnetic anomaly of opposite sign on either side of the "horizontal" segment of such a circuit.

The positive or negative sign depends on whether one considers either one hemisphere - because the conventional definition of positive and negative anomaly can have a different meaning in the two hemispheres. In any case, the process has no ambiguity.

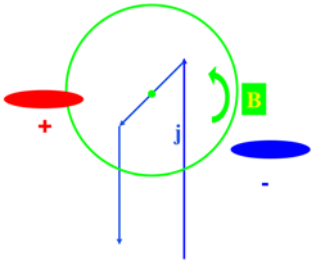

Fig. 1 - Cartoon showing the scheme of the shallowest extension of a DC circuit supplying the top point of a sea urchin spike. A field ***B*** is shown by a green circular pattern located in the plane of the figure. Positive and negative anomalies are indicated by red and blue colour, respectively. The DC electric current ***j*** of the spikes is perpendicular to the plane of the figure. After Gregori and Paparo (2021) with kind permission of *AJEAS*.

A case history

The "double-eye" pattern is a frequently observed matter-of-fact. Let us refer to a real case history for a better explanation of the rationale. When a spike reaches some shallow depth, its ***j***-pattern is shown in Fig. 1. If the volcano causes some local magma emplacement, the magma solidifies in the ambient ***B*** that is perturbed by the ***j*** of the spike. That is, the geomagnetic anomaly - within the region of the volcano supplied by the sea-urchin spike - should display some "double eye" structure, with a positive "eye" and a negative "eye" close to each other. The separation between the two "eyes" is sharp, i.e., the separation is the size of the cross-section of the conductor through which the DC ***j*** flows.

Fig. 2a shows one example. According to the usual procedure, the topographic correction should, however, be applied. In fact, owing to the ***B*** generated by the ***j*** of the spike, the outpoured lava - or the plutons if magma does not outpour at Earth's surface - are magnetized in some ordered way. Hence, the geomagnetic anomaly gets a contribution from the magnetostatic ***B*** generated by the solidified magma.

Therefore, it is customary to correct – approximately - the geomagnetic anomaly, recorded in a volcanic area, by subtracting the magnetostatic ***B*** generated by the volcanic edifice above sea-level, which is supposed to be composed of ordered, uniformly magnetized, and oriented ground. That is, the additional contribution is subtracted - or in this way, the so-called "*reduction for topography*" is

NCGT Journal
New Concepts in Global Tectonics

New Concepts in Global Tectonics Journal
Volume 13, Number 6, August 2025

ISSN number; ISSN 2202-0039

applied. The result in Fig. 2b shows that the ***B*** anomaly persists even after the approximate subtraction in this case. Fig. 2 is a detail of a wider aeromagnetic map presently available for the entire Tenerife Island, shown in Figs 3 and 4. Fig. 4 shows the same feature referring to El Hierro, which is the smallest island of the Canary Islands archipelago.

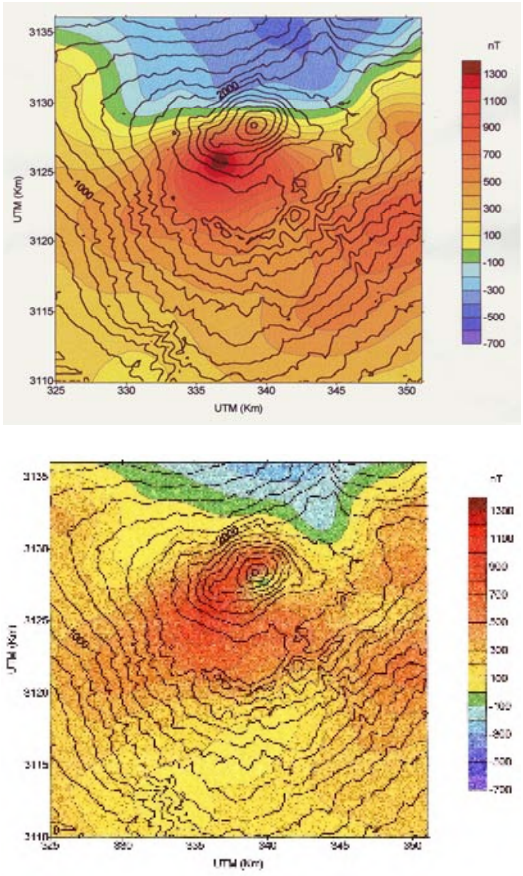

Fig. 2. The magnetic anomaly of every volcano has a typical "double-eye" structure, a pattern that - according to the hypothesis of a primary supply of these volcanoes by Joule heat - ought to be associated with DC ***j*** owing to the perpendicular axis joining the centers of these two "eyes". A usual data handling of magnetic anomalies in volcanic areas is concerned with the topographic reduction (see text). Even after applying this correction, the "double-eye" pattern remains. The present example represents the case history of Pico de Teide (Tenerife) non-reduced, and reduced [Fig. a) and b), respectively], for topography correction (after Garcìa et al., 1997, see also 2007). The color version of the figures is a courtesy by A. Garcìa, I. Blanco, and M. Torta). With kind permission of *Annals of Geophysics*.

To our knowledge, no explanation was ever proposed for this almost ubiquitous "double-eye" peculiarity, shared by the geomagnetic anomalies in almost every volcanic area. In addition, the rationale of the "*reduction for topography*" relies on substantial physically simplifying assumptions (Alberto Incoronato, private communication, 2021). Hence, this argument is not rigorous *per se*. In any case, as far as the implicit simplifying assumptions can be significant, some quantitative and indicative, approximate, estimates are possible.

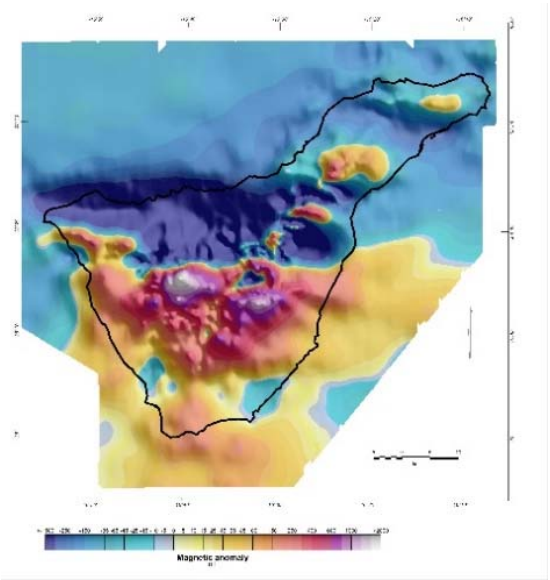

Fig. 3. Magnetic anomaly map (total intensity) of Tenerife Island plotted in two color density intervals, to highlight anomaly frequency and wavelength. Latitude and longitude are North and West from Greenwich respectively. After Garcìa et al. (2007). With kind permission of *Annals of Geophysics.*

The azimuthal orientation of the "double-eye" depends on the local orientation of the "horizontal" shallow segment of the DC ***j*** of the spike. Refer to the “simple” model outlined in Fig. 1. A quantitative approximate estimate can be made, referring to every observed case history - either associated to a volcano or not - such as *(i)* the mean depth of ***j***, *(ii)* the extension of the "horizontal" portion of the DC circuit, and *(iii)* the intensity of the ***j*** flowing inside it. To our knowledge, no analysis of this kind was ever exploited for any case history.

In addition, note that the explanation that is here proposed implies that the orientation of every "double-eye" pattern depends only on the local orientation of the DC circuit of every specific sea-urchin spike. Hence, there is no reason by which sea-urchin spikes located at different sites should display any regular pattern in their comparative orientation.

NCGT Journal
New Concepts in Global Tectonics

New Concepts in Global Tectonics Journal
Volume 13, Number 6, August 2025

ISSN number; ISSN 2202-0039

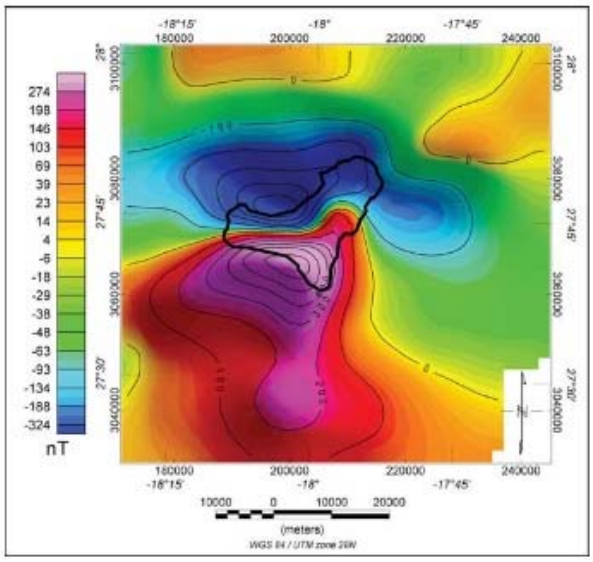

Fig. 4. "*Aeromagnetic anomaly map of El Hierro. Two main anomalies can be easily identified: an intense normal dipole over the island and a much weaker reverse dipole in the marine area to the northeast of the island. Coordinates correspond to the Universal Transverse Mercator projection (zone 28°N).*" Figure and captions after Blanco-Montenegro et al. (2008). With kind permission of *Geophysical Journal International*.

In contrast, if one supposes that the "double-eye" pattern depends on the orientation of the main field at the time of the magma outpouring activity, one should observe some regular planetary-scale pattern of the relative orientation of the "double-eye" patterns, and – to our knowledge - no such regularity seems recognizable in the available data.

Hence, the "local" spike interpretation, which is here proposed, seems to be more credible than any alternative "planetary" main-field hypothesis. Several case histories are shown in Appendix A.

For the sake of completeness, other double-eye patterns must be recalled – although on a much larger spatial scale – observed by Quinn's inversion technique.

When this technique is applied to magnetic satellite records, this double eye pattern is likely associated to intense air-earth currents due to large soil exhalation, mainly from areas with heavily fractured crust (see Quinn et al. (2025).

Appendix A

Case histories

Fig. A-1 shows the geomagnetic anomaly map of the Tyrrhenian Sea, which is well-known to be characterized by a large number of seamounts or (sometimes extinct?) volcanoes. No topographic correction, however, was applied in Fig. A-1. Figs A-2, A-3, A-4, A-5, and A-6 show the detailed map, respectively, for Vesuvius, for Etna, for the Vulcano Island in the Æolian archipelago, and for the Palinuro *STEP*,[1] obtained by recent and more precise surveys. The bathymetry of the area shown in Fig. A-6 is shown in better detail in Fig. A-7.

The "double-eye" pattern is also displayed by Etna (Fig. A-3). Note that this can be in agreement with the possibility of a speculated primary heat supply to Etna (see Gregori and Leybourne, 2021) deriving from friction heat by the "hinge" along the Moroccan megashear between the African and Eurasian lithosphere. In fact, friction heat ought to increase the local electrical conductivity σ thus favoring an easier release at Earth's surface of the endogenous heat that, in any case, propagates according to Hamilton's principle applied to electric currents (see Gregori et al., 2025e).

The comparison between Figs. A-4 and A-5 shows the role of the reduction-to-the-pole that corresponds to a loss of one degree of freedom (*d.o.f.*). Therefore, in terms of objective physical content, Fig. A-4 is more representative than Fig. A-5. The existence of sea-urchin spikes can be recognized (perhaps) also by seismic methods that should correlate with the "double-eye" feature. This correlation is envisaged by considering Fig. A-9, dealing with the islands of Lipari and Vulcano (also see Fig. A-8). Refer to Fig. A-10 for seismic station acronyms, and to Fig. A-9 for observational evidence.

Ventura et al. (1999) explain the derivation by means of the spatial distribution of travel time residuals, reckoned to a N-S profile through the Lipari-Vulcano volcanic complex (*LVVC*). They draw the spatial contour map. They find an average travel time difference considering the top advance (-240 msec), as recorded at La Fossa Cone, compared to the largest delay ($+400$ msec) that refers to Mt. Guardia depression located only few kilometers north of it. That is, a subsurface heterogeneity must explain a difference of 0.64 sec.

[1] *STEP* denotes "*subduction-transform edge propagators*" that "*are lithospheric tears bounding slabs and back-arc basins*" (Cocchi et al., 2017).

NCGT Journal
New Concepts in Global Tectonics

New Concepts in Global Tectonics Journal
Volume 13, Number 6, August 2025

ISSN number; ISSN 2202-0039

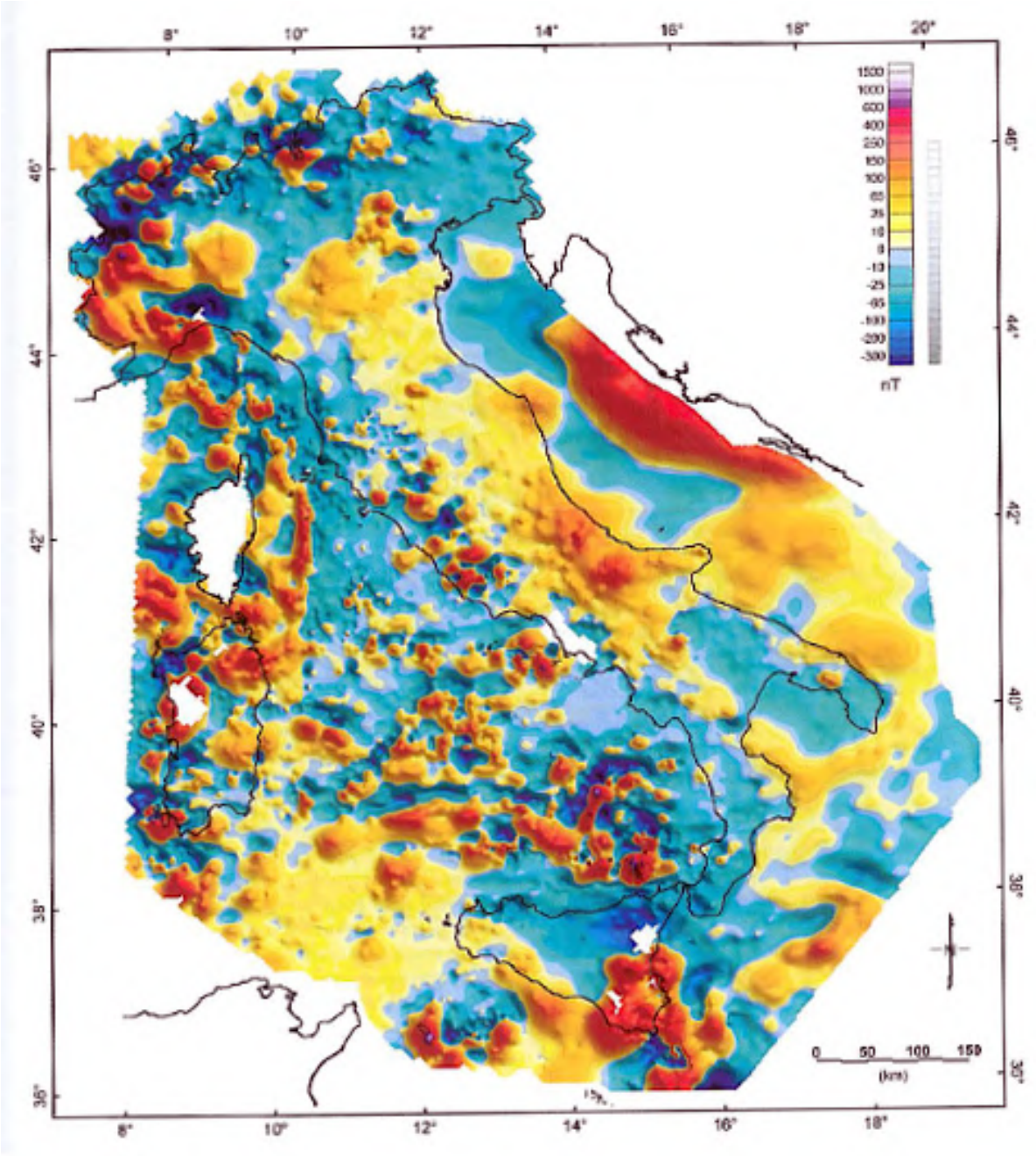

Fig. A-1. Magnetic anomaly map for the Italian area showing the "eyes" features associated with several seamounts, which make up the Tyrrhenian Sea to resemble much more to the Pacific than to other ocean floors. In fact, as it is well known, the Pacific Ocean floor contains a particularly large density of volcanic sea mounts, much more than the Indian or the Atlantic Ocean floor (figure after Chiappini et al., 2000). With kind permission of *Annals of Geophysics*.

The reference station - for computing travel time residuals - was the CHI station (see Fig. A-10), at the northern tip of the array. This is the oldest part of Lipari that is characterized by an outcrop of unfaulted massive lava flows. The definition of residuals is

$$R_j = \frac{1}{N}\left[\left(T_{ij}^{obs} - T_{ij}^{calc}\right) - \left(T_{iCHI}^{obs} - T_{iCHI}^{calc}\right)\right]$$

where the residual at the *given* station is R_j, and j refers to the event, the theoretical P-travel time, T^{calc}, is computed by means of the crustal velocity model and the Moho plunge according to the *DSS* (*Deep Seismic Sounding*), while the observed travel time is T^{obs}. The index CHI denotes the reference station.

NCGT Journal
New Concepts in Global Tectonics

New Concepts in Global Tectonics Journal
Volume 13, Number 6, August 2025

ISSN number; ISSN 2202-0039

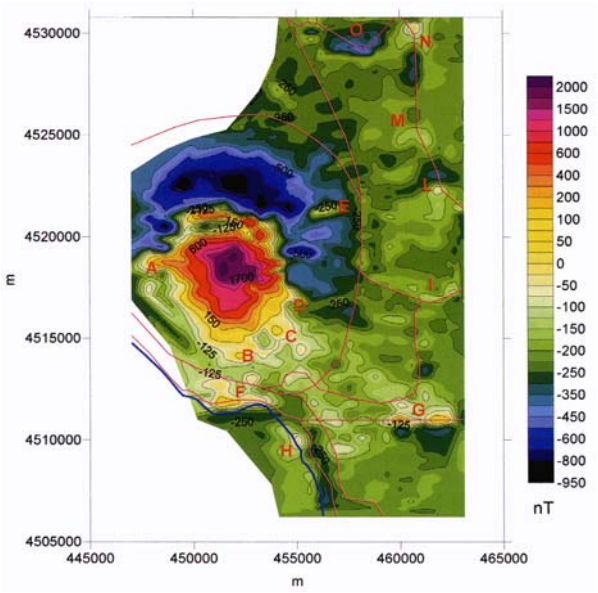

Fig. A-2. Magnetic anomaly map of Vesuvius by an aeromagnetic survey carried out in October 1999. Railways are denoted by red lines, and the coastline by a blue line. After Paoletti et al. (2005). With kind permission of *Annals of Geophysics.* I can see the image of the inline and collapse vortex structure outline in this image, also indicated as your double eye signature. The pattern shows the currently active and past remnant frozen signature in the magnetic anomaly of the air-earth e.m. vortex current. It has the lopsided collapse vortex shape also associated with hurricanes, the polar plasma vortices and many more. I discussed the collapsed vortex relationships and ubiquitous nature of these patterns extensively in my 2016 Electric Universe lecture. See https://www.youtube.com/watch?v=Q355Haapq-0

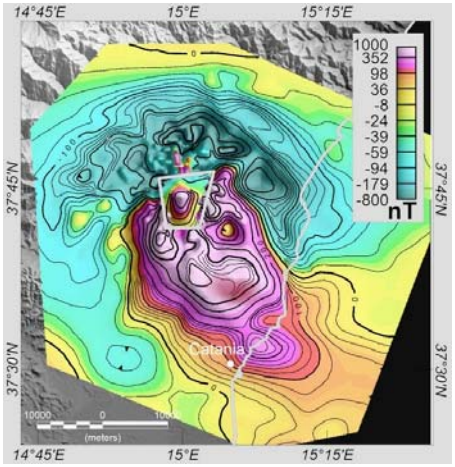

Fig. A-3. Shaded relief magnetic anomaly map (total intensity; no altimetry correction applied) of Etna. Isolines spacing 20 *nT*. After D'Ajello Caracciolo et al. (2014), with colors modified. Ditto – "*I can see the image of the inline and collapse vortex structure outline in this image, also indicated as your double eye signature. The pattern shows the currently active and past remnant frozen signature in the magnetic anomaly of the air-earth e.m. vortex current. It has the lopsided collapse vortex shape also associated with hurricanes, the polar plasma vortices and many more. I discussed the collapsed vortex relationships and ubiquitous nature of these patterns extensively in my 2016 Electric Universe lecture. See https://www.youtube.com/watch?v=Q355Haapq-0*"

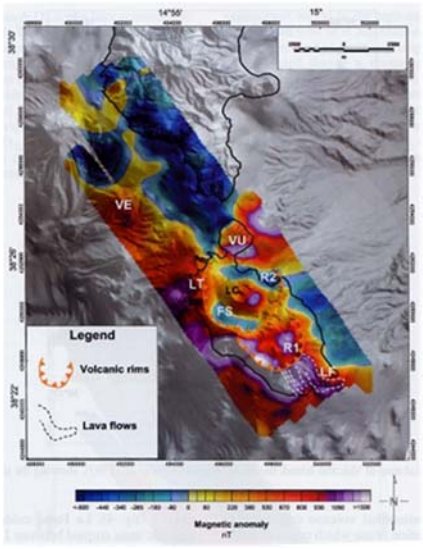

Fig. A-4. Aeromagnetic anomaly map of the Vulcano Island and of the southwestern Lipari Island in the Æolian archipelago. After Supper et al. (2004). With kind permission of *Annals of Geophysics.*

NCGT Journal
New Concepts in Global Tectonics

New Concepts in Global Tectonics Journal
Volume 13, Number 6, August 2025

ISSN number; ISSN 2202-0039

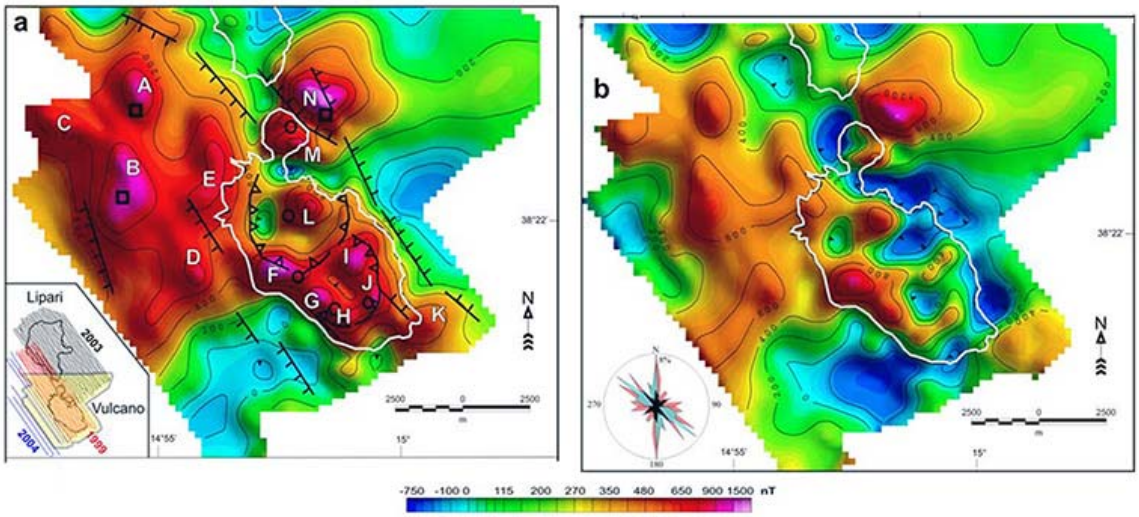

Fig. A-5. "(a) *Reduced-to-the-pole aeromagnetic anomaly map of Vulcano Island and offshore ... Capital letters evidence the positive magnetic anomalies ... 1999, 2003, and 2004 flight paths are reported in the inset.* (b) *Reduced-to-the-pole terrain-corrected magnetic anomaly map of Vulcano Island and offshore. The rose diagram in the inset summarizes the results of the spatial analysis on the location of the positive magnetic anomalies (red) and major volcanoes (blue). The azimuthal distribution of the strike of faults and fractures of Vulcano Island (in black) is from Chiarabba et al. (2004)."* Figure modified and captions after De Ritis et al. (2005). See text for comparison with Fig.A-4. *AGU* copyright free policy.

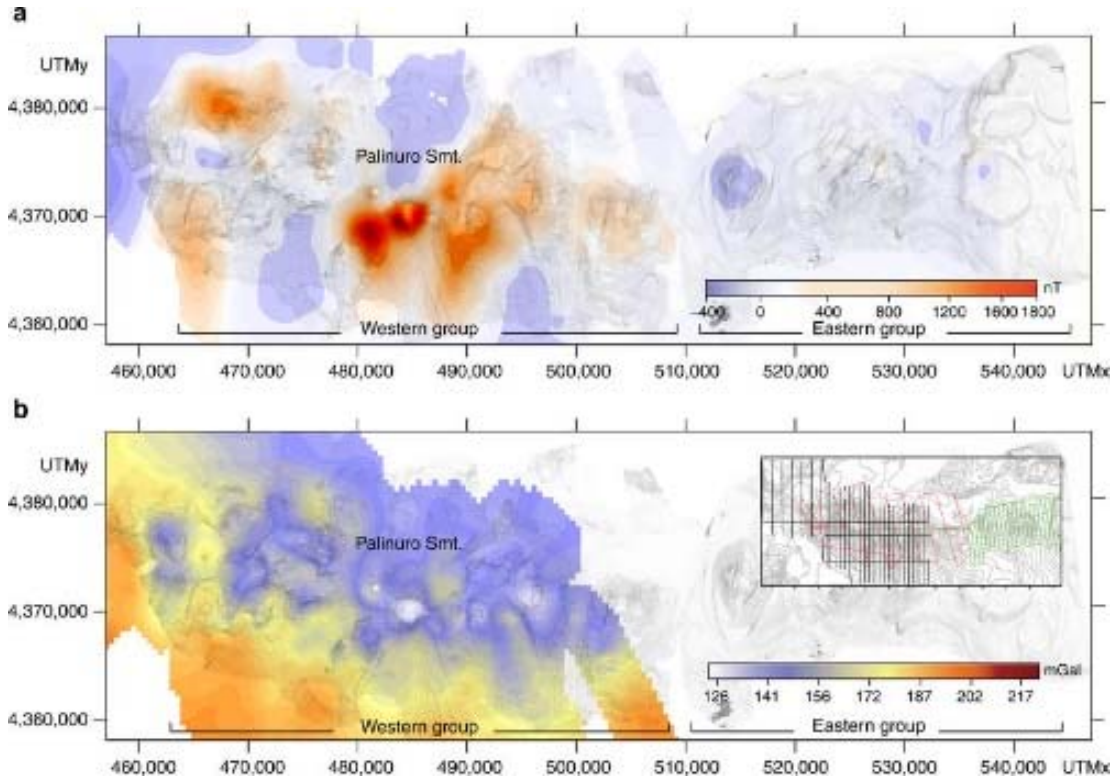

Fig. A-6. *"Magnetic and gravity anomaly maps.* (a) *reduced to the pole magnetic anomaly (grid cell size* 400 *m) overlaid on the shaded relief bathymetry of the* STEP *volcanic chain;* (b) *Bouguer gravity anomaly (grid cell size* 500 *m). Inset shows the survey lines: the gravity and magnetic survey acquired during* PALI2008 *cruise is reported in black, and the magnetic lines acquired during the* Æolian 2007 *and* SAFE 2015 *cruises are reported in red and green, respectively."* Figure and captions after Cocchi et al. (2017). Reproduced with kind permission of *Nature Communications* (CC BY 4.0).

NCGT Journal
New Concepts in Global Tectonics

New Concepts in Global Tectonics Journal
Volume 13, Number 6, August 2025

ISSN number; ISSN 2202-0039

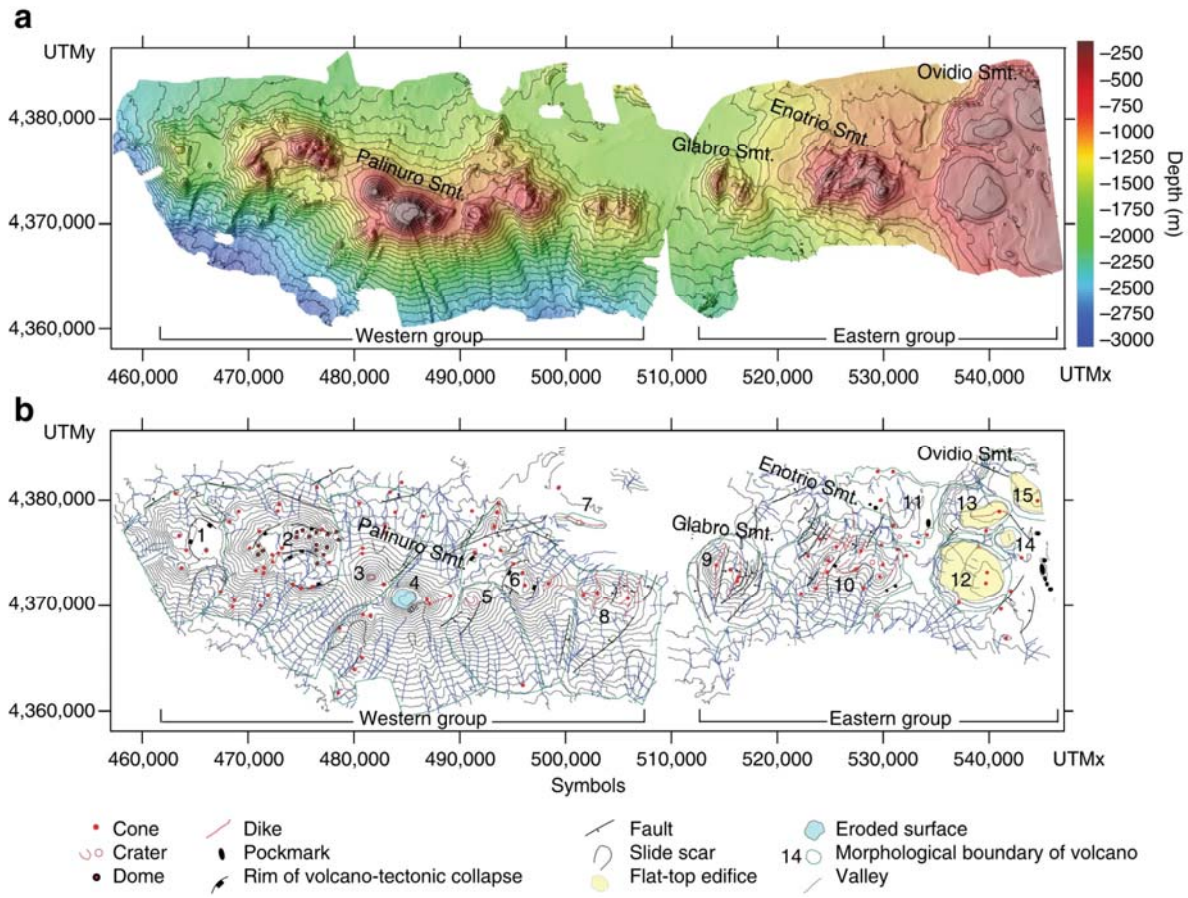

Fig. A-7. "*Bathymetry and morphostructural setting of the Palinuro* STEP *volcanic chain.* (a) *Shaded relief and bathymetry of the* $25\ m \times 25\ m$ STEP Volcanic Chain Digital Terrain Model *(WG105, UTM Zone* $33°N$ *…); the contour lines are* $100\ m$ *spaced.* (b) *Morphological map of the* STEP *volcanic chain with the main volcanoes marked by numbers.*" Figure and captions after Cocchi et al. (2017). Reproduced with kind permission of *Nature Communications*, (CC BY 4.0).

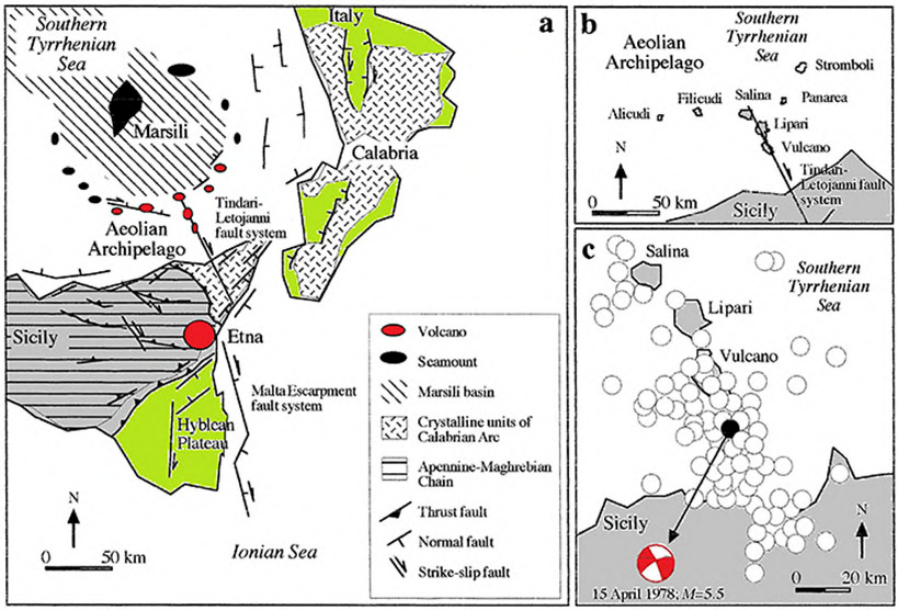

Fig. A-8. *(a,b)* Shows a sketch *of* the Southern Tyrrhenian Sea, Æolian Islands and Sicily with several toponyms and structural details. *(c)* This is a map of epicenters of shallow earthquakes (< 25 km) in the Lipari-Vulcano sector of the "Tindari-Letojanni" fault system. The 15 April 1978, $M = 5.5$ earthquake is shown by its epicenter and focal mechanism. Figure modified after Ventura et al. (1999).

NCGT Journal
New Concepts in Global Tectonics

New Concepts in Global Tectonics Journal
Volume 13, Number 6, August 2025

ISSN number; ISSN 2202-0039

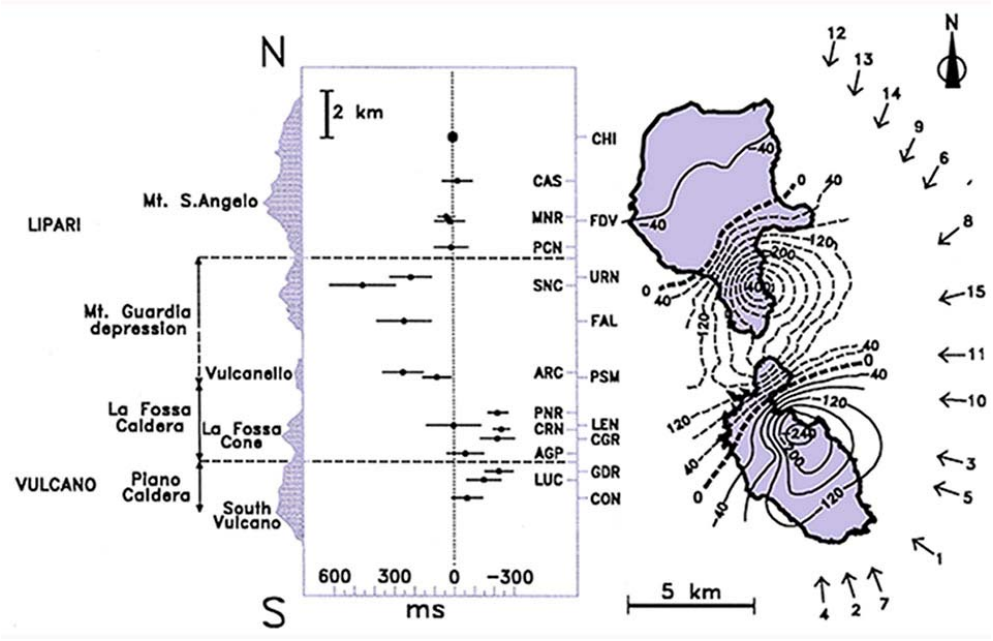

Fig. A-9. *[left]* The average residuals are shown projected along a N-S profile. The positive and negative values denote (in msec), respectively, the first arrival delays and advances. The standard deviations are indicated by bars. *[right]* The contour lines refer to averaged residuals. Thick dashed lines are contour values with $= 0\,msec$. The azimuths for the events are indicated by numbered arrows. Figure modified after Ventura et al. (1999).

Fig. A-10 - Locations of the array of seismic stations on the Lipari and Vulcano Islands. See text. Figure (modified) after Ventura et al. (1999).

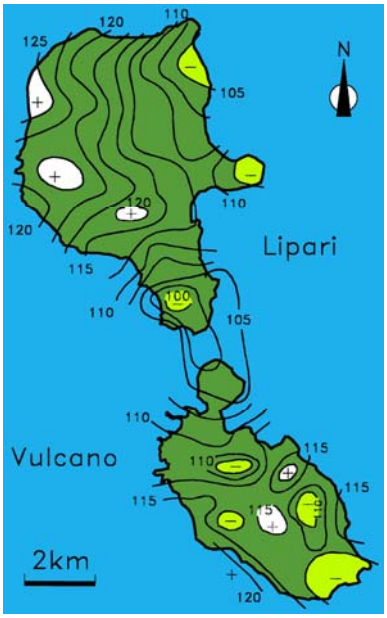

Fig. A-11 - Map of the Bouguer anomalies (mgal) of *LVVC*; with contour interval 2.5 mgal based on Bonasia et al. (1973). Figure (modified) after Ventura et al. (1999).

Ventura et al. (1999) applied the correction to the observed travel times for the station's altitude. They observed the largest standard deviations in the area of the Mt. Guardia depression (Fig. A-9). They claim that slightly smaller delays are expected to occur for teleseismic events compared to the closer events, even though all analyzed events show a uniform fast anomaly displayed by all arrival times.

They point out that Fig. A-9 shows a travel time anomaly, with a NE-SW-oriented short wavelength feature. The positive values, i.e., the slower area, clearly looks contained at the south of the sharp transition from positive to negative values. This transition occurs at the northern limit of La Fossa Caldera. As far as the northern boundary is concerned, the slower area is confined by the Mt. Guardia depression. They also comment that if one neglects the negative residual maximum observed at La Fossa Cone – due to the presence of a local dioritic intrusion - one finds a residuals pattern of travel times with an almost symmetrical NNW-SSE trend, by which the northwestern part of Lipari shows residuals that are similar to the residuals found at the southeastern part of Vulcano

Some related evidence can be observed also on the Bouguer anomaly map of the area (Fig. A-11).

That is, an apparent "double-eye" feature is shared either by geomagnetic anomalies, or by the aforementioned

ISSN number; ISSN 2202-0039

"*travel time residuals*", or by the Bouguer anomaly map. However, their specific local detailed correlation must be suitably investigated, as - in general - the ideal configuration, which is sketched in the cartoon of Fig. 1, is only indicative, while the eventual occurrence is expected to have several bunches of sea-urchin spikes.

Figs A-12, A-13, and A-14 show a detail of the Campi Flegrei (or Phlægrean Fields) volcanic complex, close to the island of Procida in the Bay of Naples. The rim of the hypothesized circular tuff structure in Fig. A-14 falls just halfway between the positive and negative "eye" of the geomagnetic anomaly, consistent with the argument of Fig. 1.

This whole area is characterized by huge amounts of volcanic ejecta, known as Campanian Ignimbrite (*CI*), erupted some $\sim 35 - 38\ ka$ ago (according to different estimates). Costa et al. (2012) modeled this event. They applied "*a novel computational approach to assess, for the first time, volcanic ash dispersal during the* CI *super-eruption providing insights into eruption dynamics and the impact of this gigantic event. The method uses a 3D time-dependent computational ash dispersion model, a set of wind fields, and more than* 100 *thickness measurements of the* CI *tephra deposit. Results reveal that the* CI *eruption dispersed* $250 - 300\ km^3$ *of ash over* $\sim 3.7 \times 10^6\ km^2$. *The injection of such a large quantity of ash (and volatiles) into the atmosphere would have caused a volcanic winter during the Heinrich event* 4, *the coldest and driest climatic episode of the Last Glacial period. Fluorine bearing leachate from the volcanic ash and acid rain would have further affected food sources and severely impacted Late Middle-Early Upper Palæolithic groups in Southern and Eastern Europe*." Concerning the Heinrich event *4*, refer to a figure in Jansen et al. (2007, p. 455).

Note that this *CI* gigantic paroxysm, which seemingly occurred just once, is consistent with the tentative inference - which is also guessed *passim* elsewhere while investigating volcanism all over the world - which applies to almost every volcanic area. Every area had a time of very intense eruptive activity, followed by a prolonged subsequent although much smaller activity. This behavior is suggestive of a time when the local bunch of sea-urchin spikes afforded to reach the Earth's surface for the first time - thus causing an intense eruptive activity. Later, the local sea-urchin spikes afforded to release their Joule heat much more regularly, displaying therefore no particularly intense activity, rather a comparably smooth heat release with some lesser and frequent small volcanic activity.

A synthetic scenario of this area is given by De Natale et al. (2016) (Fig. A-15). On the other hand, some puzzling uncertainties remain. Only some excerpts are here reported from their abstract.

"*The* $501\ m$ *deep hole of the Campi Flegrei Deep Drilling Project, located west of the Naples metropolitan area and inside the Campi Flegrei caldera, gives new insight to reconstruct the volcano-tectonic evolution of this highly populated volcano ... its tectonic structure, eruptive history, and size of the largest eruptions are intensely debated in the literature. New stratigraphic and* $^{40}Ar/^{39}Ar$ *geochronological dating allow us to determine, for the first time, the age of intracaldera deposits belonging to the two highest magnitude caldera-forming eruptions (i.e.,* CI, $39\ ka$, *and Neapolitan Yellow Tuff,* NYT, $14.9\ ka$*) and to estimate the amount of collapse. Tuffs from* $439\ m$ *of depth yield the first* $^{40}Ar/^{39}Ar$ *age of* $\sim 39\ ka$ *within the caldera, consistent with the* CI. *Volcanic rocks from the* NYT *were, moreover, detected between* $250 - 160\ m$.

Our findings highlight: (i) *a reduction of the area affected by caldera collapse, which appears not to include the city of Naples;* (ii) *a small volume of the infilling caldera deposits, particularly for the* CI, *and* (iii) *the need for reassessment of the collapse amounts and mechanisms related to larger eruptions ...* "

A clarifying picture is given in Fig. A-16, but see also Fig.A-17.

GPS and *DInSAR* records, including models, are shown in D'Auria et al. (2015), who also give several other figures (not here shown). In 2012-2013 the concern was about a rejuvenation of the phenomenon. They summarize their findings as follows. "*We found the first evidence, in the last* $30\ years$*, of a renewed magmatic activity at Campi Flegrei caldera from January 2012 to June 2013. The ground deformation, observed through* DInSAR *and* GPS *measurements, have been interpreted as the effect of the intrusion at shallow depth (*$3090 \pm 138\ m$*) of* $0.0042 \pm 0.0002\ km^3$ *of magma within a sill. This interrupts* $\sim 28\ years$ *of dominant hydrothermal activity and occurs in the context of an unrest phase which began in 2005 and within a more general ground uplift that goes on since 1950 ...* "

A model was computed by Kilburn et al. (2017) aimed to envisage a possible evolution of the system towards an eruption. Let us refer, rather, to a more recent model by Kilburn et al. (2023), which is an upgrade of the previous model. We report, however, only their Figs A-18, A-19, and A-20 that are self-explanatory, while - owing to brevity - we cannot report the entire model and related discussion. The interested reader should refer to the original paper. In any case, we stress that the interpretation, which is here envisaged, is not necessarily related to magma intrusion that can - or cannot - occur. Rather, a time-varying energy supply occurs to the bunch of sea-urchin spikes, with a consequent intensification of endogenous fluid flow. This can, or cannot, determine an expansion of the magma chamber (if any). The important physical point is that the endogenous heat release eventually increases, implying an effect on subsoil fluids – whether magma or others. Hence, the model always applies. This viewpoint is shared also by a recent paper (Vanorio et al., 2025), illustrated by Torrent Tucker (2025).

NCGT Journal
New Concepts in Global Tectonics

New Concepts in Global Tectonics Journal
Volume 13, Number 6, August 2025

ISSN number; ISSN 2202-0039

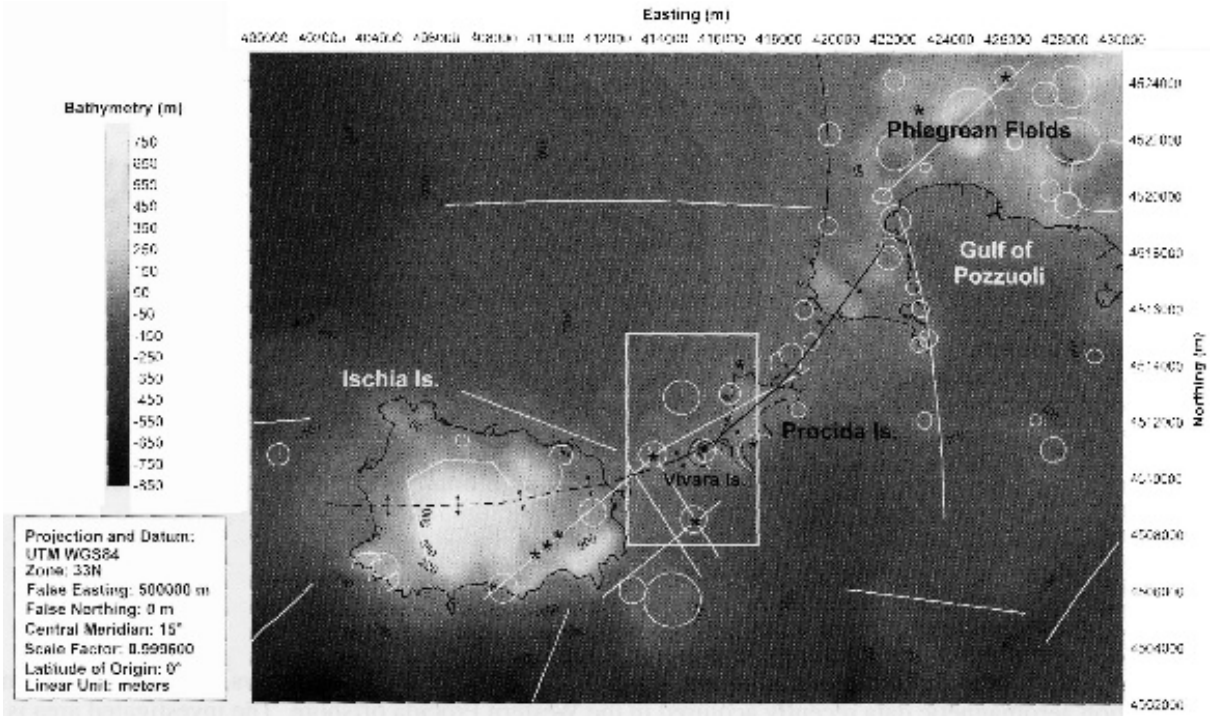

Fig. A-12. *"Topographic and bathymetric map of the Phlegrean Fields - Ischia Ridge. The main structural features are redrawn from di Girolamo and Rolandi (1975); white lines are fault, black lines are ridges, circles are crater rims, asterisks are latite basaltic and latite volcanoes. The spare shows the area"* shown in Figs A-13 and A-14. Figure and captions after Paoletti et al. (2008). With kind permission of *Annals of Geophysics*.

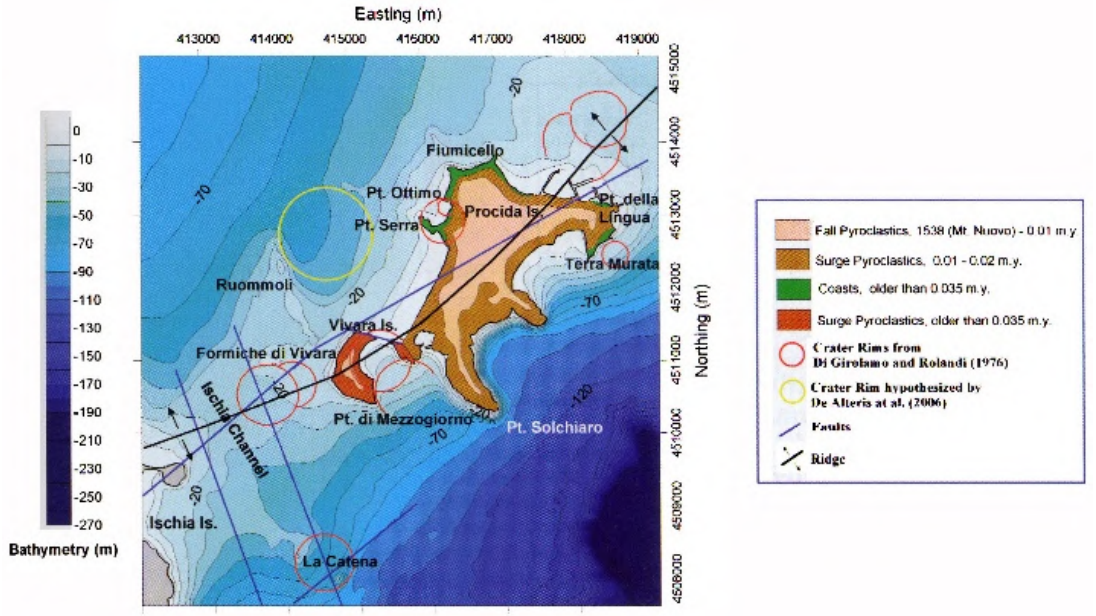

Fig. A-13. *"Geologic map of the Procida Island and bathymetric map of its western offshore. The geological units are from di Girolamo et al. (1984). The main lineaments are redrawn from di Girolamo and Rolandi (1975). The crater rims are from di Girolamo and Rolandi (1975) and de Alteris et al. (2006). Bathymetry digitized from de Alteris et al. (2006)."* Figure and captions after Paoletti et al. (2008). With kind permission of *Annals of Geophysics.*

NCGT Journal
New Concepts in Global Tectonics

New Concepts in Global Tectonics Journal
Volume 13, Number 6, August 2025

ISSN number; ISSN 2202-0039

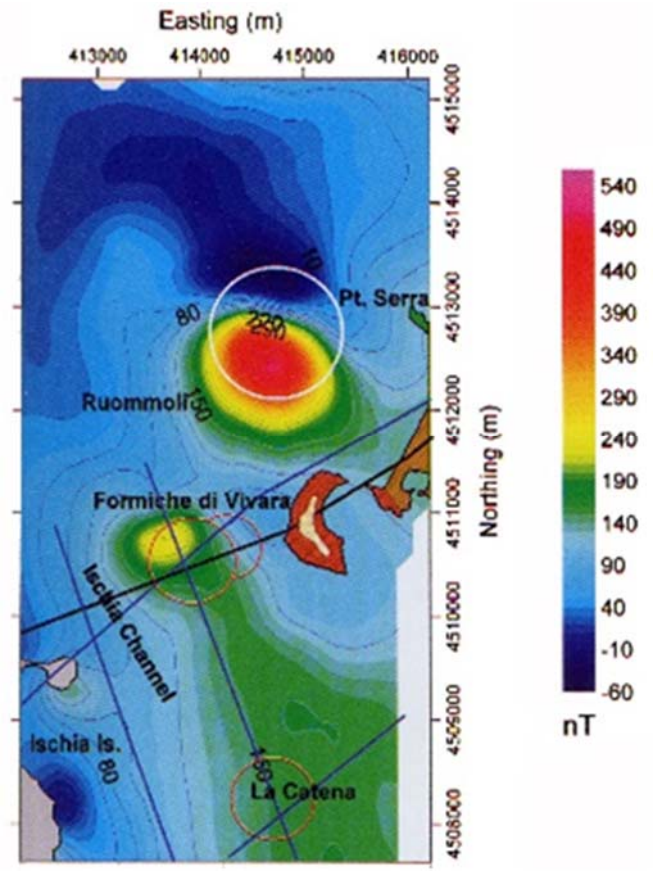

Fig. A-14. *"High resolution aeromagnetic field of the western Procida offshore. The rim of the tuff structure hypothesized by de Alteris et al. (2006) is drawn as a white circle, red circles show the rims of the Formiche di Vivara and La Catena volcanoes. The black line in the NE-SW ridge connecting Ischia and Phlegrean Fields. Fault are outlined by blue lines. For the geological units of the Procida Island refer to the legend of Fig. A-13."* Figure and captions after Paoletti et al. (2008). With kind permission of *Annals of Geophysics*. Here one can also see the inline and collapse vortex structure, but appears more separated than the previous images, i.e., low *nT* values in blue, tail away from the high *nT* values in red, whereas in the previous images the low *nT* values halfway surrounded the high *nT* values. The signature is still very obvious, and almost all vortices that aren't symmetrical have this collapsed signature, including the human heart. B.A. Leybourne discussed the collapsed vortex relationships extensively in his *2016 Electric Universe*. See https://www.youtube.com/watch?v=Q355Haapq-0

Fig. A-15. *"Morphological map of the Campi Flegrei caldera. The lines (dashed and solid, respectively, for* CI *and* NYT*) are the caldera limits as proposed by different authors. CFDDP drilling site (larger red star) is shown, together with the deep boreholes drilled by* ENEL-AGIP *(*SV1, SV3, MF1, MF5*) and* SAFEN*(*CF23*) companies (smaller red stars) and two shallower bore holes (smaller yellow stars)."* Figure and captions after De Natale et al. (2016). *AGU* copyright free policy.

NCGT Journal
New Concepts in Global Tectonics

New Concepts in Global Tectonics Journal
Volume 13, Number 6, August 2025

ISSN number; ISSN 2202-0039

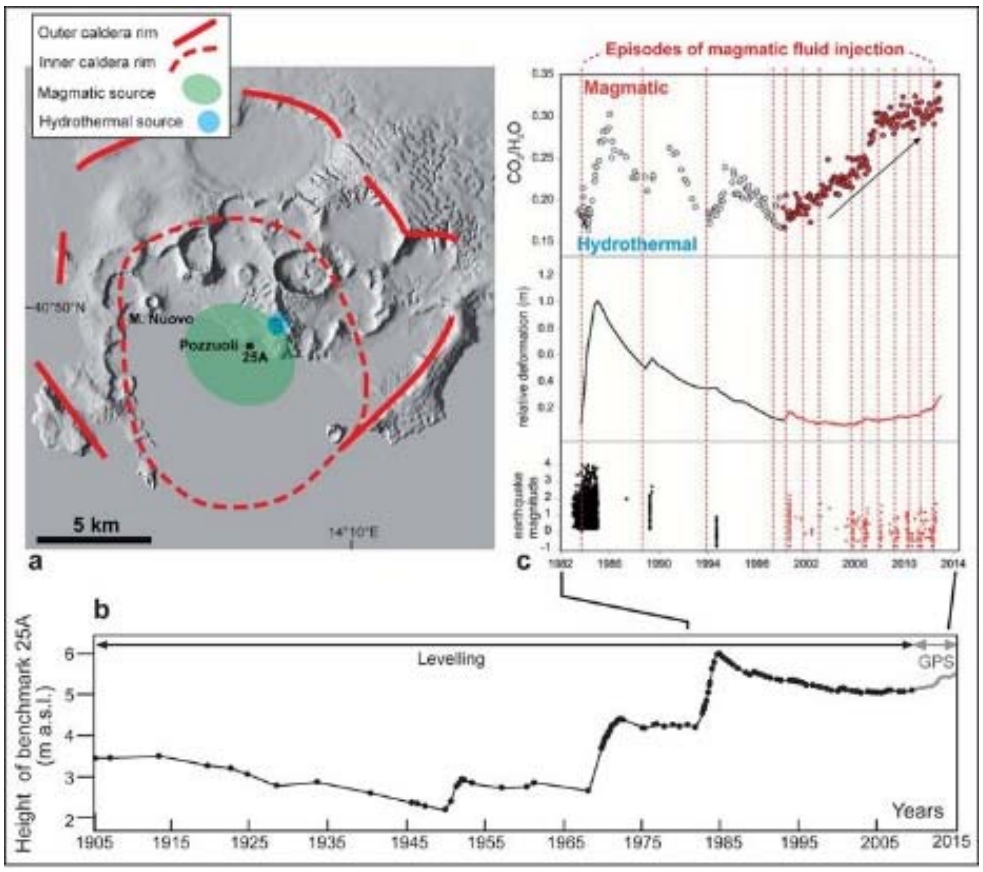

Fig. A-16. "(a) *Simplified structural map of Campi Flegrei caldera (Italy), including the map view location of the magmatic source (green ellipse,* 4 *km deep) and hydrothermal source (blue circle,* 2 *km below the Solfatara volcanic crater) responsible for the post-1980 deformation (Amoruso et al., 2014).* (b) *Elevation changes of benchmark* 25A *(shown in figure* (a); close to the center of the green circle*) from 1905 to 2009 (after Del Gaudio et al., 2010) merged with more recent (2009-2012)* GPS *data (De Martino et al., 2014);* $m\ a.s.l.$ *= meters above sea-level.* (c) *Measured and simulated fumarolic* CO_2*/water (*CO_2/H_2O*) ratio* [top], *ground deformation* [middle], *and earthquake magnitudes* [bottom]*; dashed lines refer to times of injection of magmatic fluids into the hydrothermal aquifer (after Chiodini et al., 2012). Credit: Acocella et al. (2015)."* Figure and captions after Acocella and Chiodini (2015). *AGU* copyright free policy.

The tectonism of this whole area is, maybe, the best-known historical case of bradyseism.[2]

The entire large caldera is characterized by piano tectonism, i.e., by small areas that seemingly - independently and occasionally - experience either uplift or subsidence.

The ancient former Pozzuoli fish-market, or several villas in the Baia area – both ones of classical Roman times - have well-known archæological remains, or also the recently found former artificial island of Calipso[3] that was originally created to exploit an underwater hot spring. It was made in the first half of the 1st century AD, and it has now been identified with La Secca delle Fumose (literally "*The shoal of the smoky floor*") offshore Lucrino.

Fig. A-21 shows the variation of soil level with respect to sea level in the harbor of Pozzuoli.

Compared to the typical time scale of this phenomenon, the total time interval spanned by the available records has a limited significance, and can provide no reliable long-range extrapolation, hence it has limited modeling purpose.

[2] Bradyseism is the gradual uplift (positive bradyseism) or descent (negative bradyseism) of part of the Earth's surface: In general, it is interpreted in terms of the filling or emptying of an underground magma chamber, even though it can be originated by hydrothermal activity, particularly in volcanic calderas. It can persist for millennia in between eruptions and each uplift event is normally accompanied by thousands of small to moderate earthquakes. The word - coined by Arturo Issel (1842–1922), Italian geologist, palæontologist, malacologist and archaeologist in 1883 - derives from the ancient Greek *bradús*, meaning "slow", and *seismós* meaning "movement". Campi Flegrei is the classical, historical, best known and investigated, area of bradyseism.

[3] Its evidence was found by means of a new high-resolution bathymetric map of the Pozzuoli Bay, carried out by a cooperation between the *Osservatorio Vesuviano* (*INGV*) and the *Istituto per l'ambiente marino costiero* (*IAMC*) of *CNR*. See Cangiano (2015).

NCGT Journal
New Concepts in Global Tectonics

New Concepts in Global Tectonics Journal
Volume 13, Number 6, August 2025

ISSN number; ISSN 2202-0039

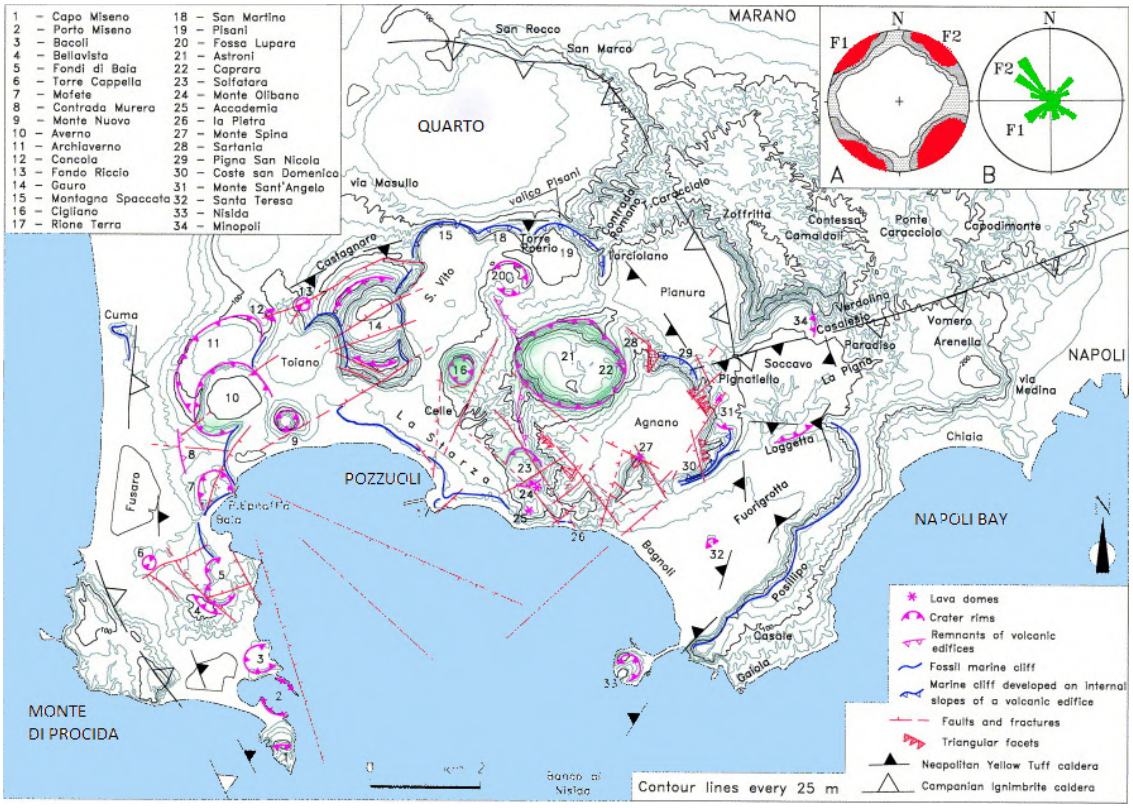

Fig. A-17. "*Structural sketch map of the Campi Flegrei caldera. In the insert, frequency diagrams of fault and fractures measured in the central part of the Neapolitan Yellow Tuff caldera:* (A) *equiareal projection of fracture poles;* (B) *Rose diagram relative to the same structures.* $F1 = N45°E$ *trending fractures;* $F2 = N50°W$ *trending fractures.*" Figure (modified according to suggestions by Di Vito) and captions after Di Vito et al. (1999).

Also, the volcano Monte Nuovo (see Fig. A-15, A-16, and number 9 in Fig. A-17, slightly East of Pozzuoli) is a well-known event, as it is the first reasonably well documented event of the birth of a new volcano. It is a cinder cone abruptly born during a one week event in September 29 - October 6, 1538. "*This took place on the western side of a raised marine terrace, la Starza ... in an area that has been strongly affected by tectonic movements over the past* 5000 years ... *Before the* 16^{th} *century, at least as far back as Roman times, this movement caused a net subsidence of the ground, modifying the coastline and submerging Roman ruins close to the shore.*

This phase of subsidence ended sometime before the eruption; precisely when is uncertain, but a clear uplift with the emergence of new land was observed by the inhabitants of Pozzuoli in 1502.

A further rapid uplift occurred 2 *days before the eruption in a more localized zone enclosing the immediate vent area and was accompanied by moderate seismic activity. The first* 2 *days of the eruption were characterized by explosive behavior, which produced pyroclastic deposits of limited areal extent and led to the growth of the main body of the cone around the vent ... Four days of relative quiescence with only minor explosive activity followed. The eruption finally ended on 6 October, the* 7^{th} *day, with a violent explosive phase and the emplacement of a small scoria flow. Twenty-four people, who were climbing up to the vent during this last phase, were killed by a sudden explosion ...* " (Di Vito et al., 1987).

Kilburn et al. (2017) summarize their achievement and stress that "… *volcanoes reawakening after long repose must rupture the crust before magma can erupt. Rupture is preceded by repeatable variations in the rate of seismicity with ground movement, which trace the amount of applied stress that is released by local earthquakes. A rupturing sequence has been developing across four episodes of ground uplift at Italy's Campi Flegrei caldera: in 1950-1952, 1969-1972, 1982-1984 and since 2004. We predicted in 2016 that the approach to rupture would continue after an additional uplift of* $30 - 40$ *cm at the location of largest movement. We have updated our analysis with new data on changes in the numbers of local earthquakes with amounts of ground movement. Here we show that subsequent events have confirmed our prediction and that the unrest has been changing the structure of Campi Flegrei's crust.* …" We stress that an *AE* array can effectively monitor the time-varying local stress (Gregori et al., 2025a), thus improving the long- and short-term predictability of the ongoing events.

NCGT Journal
New Concepts in Global Tectonics

New Concepts in Global Tectonics Journal
Volume 13, Number 6, August 2025

ISSN number; ISSN 2202-0039

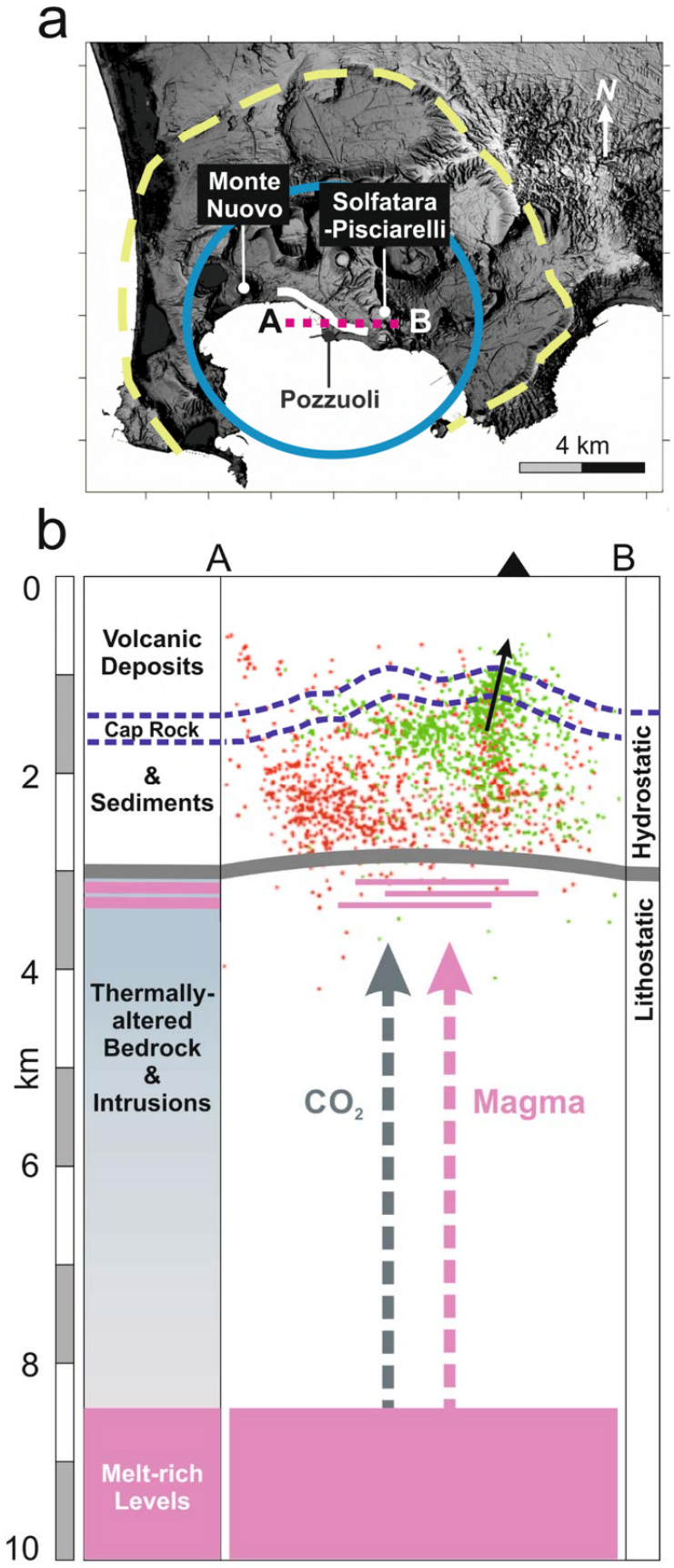

Fig. A-18. "*Unrest at Campi Flegrei since 1950.* (a) *Ground movement has occurred across the central* 80 km^2 *(blue ellipse) of the caldera (dashed outline). Most of the volcano/tectonic* (VT) *seismicity since 1983 (Fig. A-20) has been focused around the Starza marine terrace and fault system (white curve) between Monte Nuovo and the fumarolic fields of Solfatara and Pisciarelli, which are next to each other.* (b) *From the surface downwards, the crust beneath the central region of the caldera consists of predominantly pyroclastic volcanic deposits (primary and reworked) to depths of as much as* 2.3 *km, overlying marine silts and clays, which become thermally altered (thermometamorphosed) at depths of* ~2.5–3.0 *km and then grade (at unknown depth) into bedrock that contains solidified magmatic intrusions and extends to the top of a melt-rich layer* ~8 *km below the surface (magenta …). The melt-rich zone feeds magma and gas (notably* CO_2 *) to shallower depths. Measured temperatures of* ~400 °C *in the upper levels of the thermo-metamorphic horizon … favor silica mineralization and formation of low-permeability horizons (grey band) … Uplift between 1950 and 1984 is consistent with intrusions of magmatic sills to depths of* ~3 *km (pale magenta) … Pore pressures are expected to be hydrostatic above the thermo-metamorphic zone, but to reach higher values (that may approach lithostatic) where magmatic gas accumulates underneath … Precipitation of* Ca*-rich minerals favors the formation of a stronger cap rock at depths less than* 1.5 *km (outlined by the blue dashes). Almost all the seismicity during the 1982-1984 unrest (red dots) occurred in the hydrothermal system between the cap rock and thermo-metamorphic horizons. Since 2005 (green dots), seismicity has also occurred through the cap rock in the vicinity of Solfatara and Pisciarelli (black triangle; see also Fig. A-20) which may be favoring the escape of* CO_2 *(black arrow).*" Figure and captions after Kilburn et al. (2023). With kind permission of *Communications Earth Environment* ("Open Access").

NCGT Journal
New Concepts in Global Tectonics

New Concepts in Global Tectonics Journal
Volume 13, Number 6, August 2025

ISSN number; ISSN 2202-0039

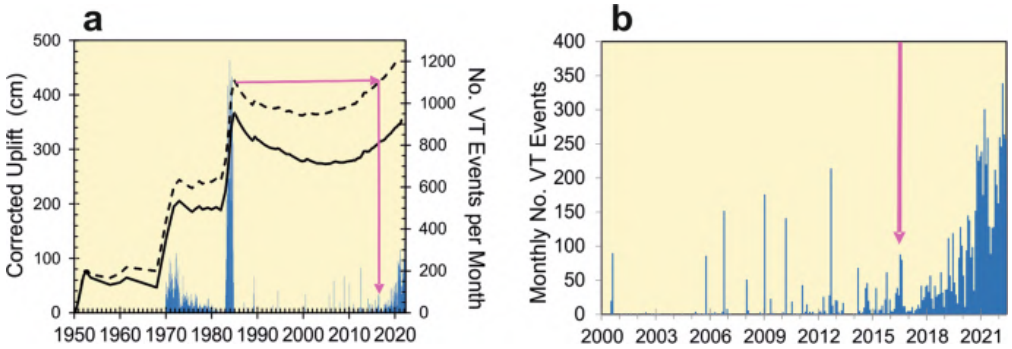

Fig. A-19. "*Variations in uplift and* VT *seismicity between 1950 and 2022.* (a) *Time series for measured and corrected uplift at Pozzuoli (solid and dashed black curves) and monthly rates of seismicity (columns). After the* VT *event rate reached a peak in 1984, Campi Flegrei remained almost aseismic during three decades of slow subsidence and uplift. Persistent* VT *seismicity recommenced in 2015–2016, when the corrected uplift returned to its position in 1984 (magenta arrows).We initially interpreted the decay in* VT *rate after 1972 as evidence of partial relaxation of the crust …; however, some or all of the events may have been caused by the illegal fishing practice of detonating explosives to drive sea-floor creatures to the surface.* (b) *Between 2015 and 2020,* VT *event rates accelerated to a steady mean value of about* 175 *events per month. The acceleration began when the corrected uplift had been restored to its 1984 position (magenta arrow). Data from* INGV-Sezione di Napoli (Osservatorio Vesuviano)…" Figure and captions after Kilburn et al. (2023). With kind permission of *Communications Earth Environment* ("Open Access").

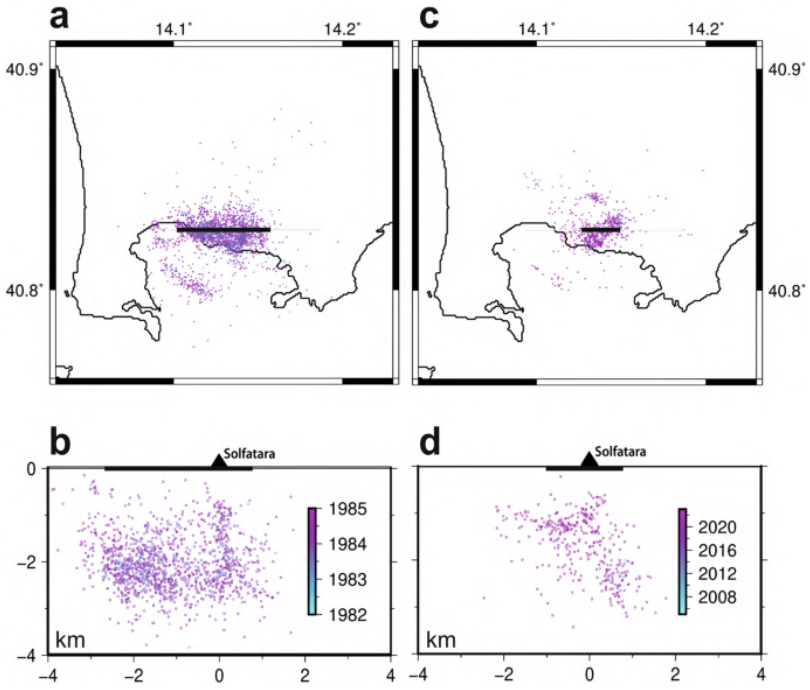

Fig. A-20. "*Distribution of* VT *events 1982-1985 and 2005-2022. Seismicity has been concentrated in the vicinity of the Starza fault system (Fig. A-18).* (a) *The 1982-1985 events occurred along the whole system,* (b) *at depths mostly between* 1 *and* 3 *km.* (c) *The 2005-2022 events have been restricted to a smaller volume at the eastern end of the system.* (d) *Most have occurred at depths less than* 1.5 *km , apart from an inclined trend* 1– 3 *km beneath Solfatara; the same trend may also have been present in 1982–1984. The black lines show the same distances in each pair of time intervals. Data from* INGV-Sezione di Napoli (Osservatorio Vesuviano)…" Figure and captions after Kilburn et al. (2023). With kind permission of *Communications Earth Environment* ("Open Access").

For the sake of completeness, let us mention Vesuvius, which is close to Campi Flegrei, although the two systems seem independent. Vesuvius is the historically best documented volcano of the world. The "quiet" time intervals between major eruptions display a disquieting regularity (Gregori, 1993b; 1996).

Longo et al. (2016) report (see figure not here shown) about a high-resolution aeromagnetic investigation of the Auca Mahuida volcano in Argentina. They also studied its underground structure, with various modeling, including a correlation with stratigraphy. No reduction to the pole was formerly applied. They show (maps not here shown) the total intensity anomaly map with no correction for topography, and with the topographic correction.

Longo et al. (2016) comment that "*most of the detected magnetic anomalies have a dipolar structure opposite to that of the present geomagnetic field. According to the available geochronological data and palæomagnetic measurements, the source bodies of Auca Mahuida mainly emplaced in the Matuyama reverse polarity chron. The reduction-to-the-pole map confirms that the magnetization direction is mainly reverse with only few anomalies normally magnetized ... Therefore, we model the measured anomaly field by applying analytical techniques that are*

NCGT Journal
New Concepts in Global Tectonics

New Concepts in Global Tectonics Journal
Volume 13, Number 6, August 2025

ISSN number; ISSN 2202-0039

independent of the magnetization direction. The obtained anomaly strikes and source geometries indicate an emplacement of intrusive bodies controlled by the regional faults affecting the Auca Mahuida basement and the sedimentary successions of the Neuque'n basin. Magma upraised along these faults and fractures feeding the volcanic activity and subsequently crystallized …

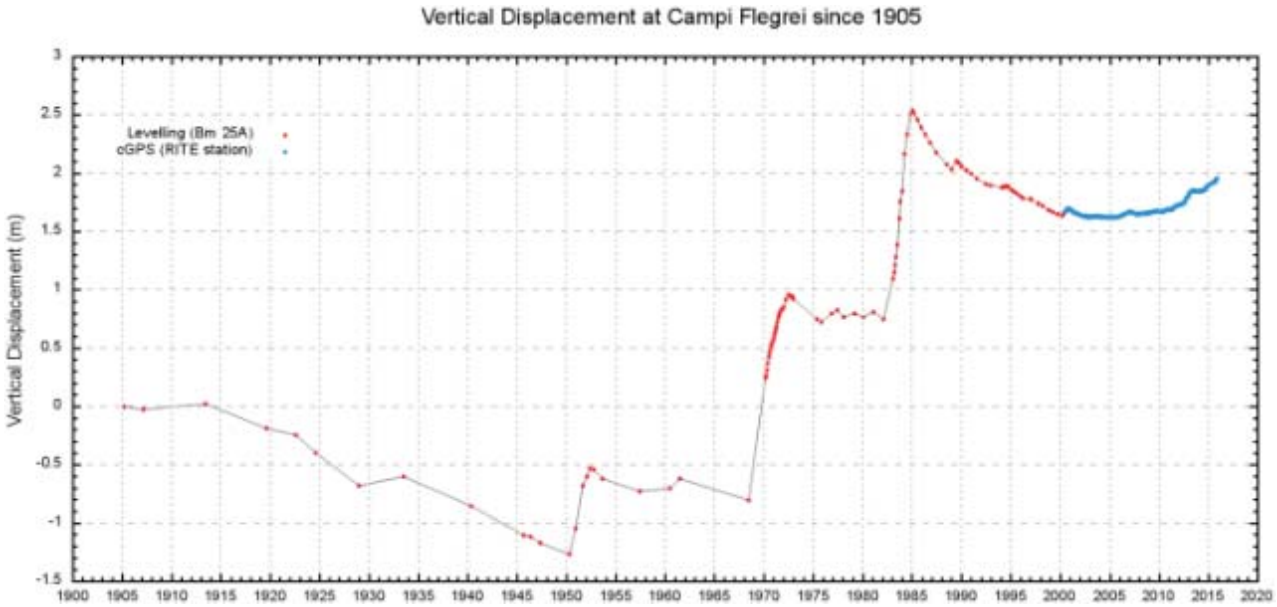

Fig. A-21. *"Ground displacement at Pozzuoli Porto since 1905, measured by precision leveling (until year 2000, in red) and at the close* GPS *benchmark of Rione Terra (since 2000, blue dots)."* Figure and captions after Moretti et al. (2017), also in De Natale et al. (2017). Figure and captions after Acocella and Chiodini (2015). *AGU* copyright free policy.

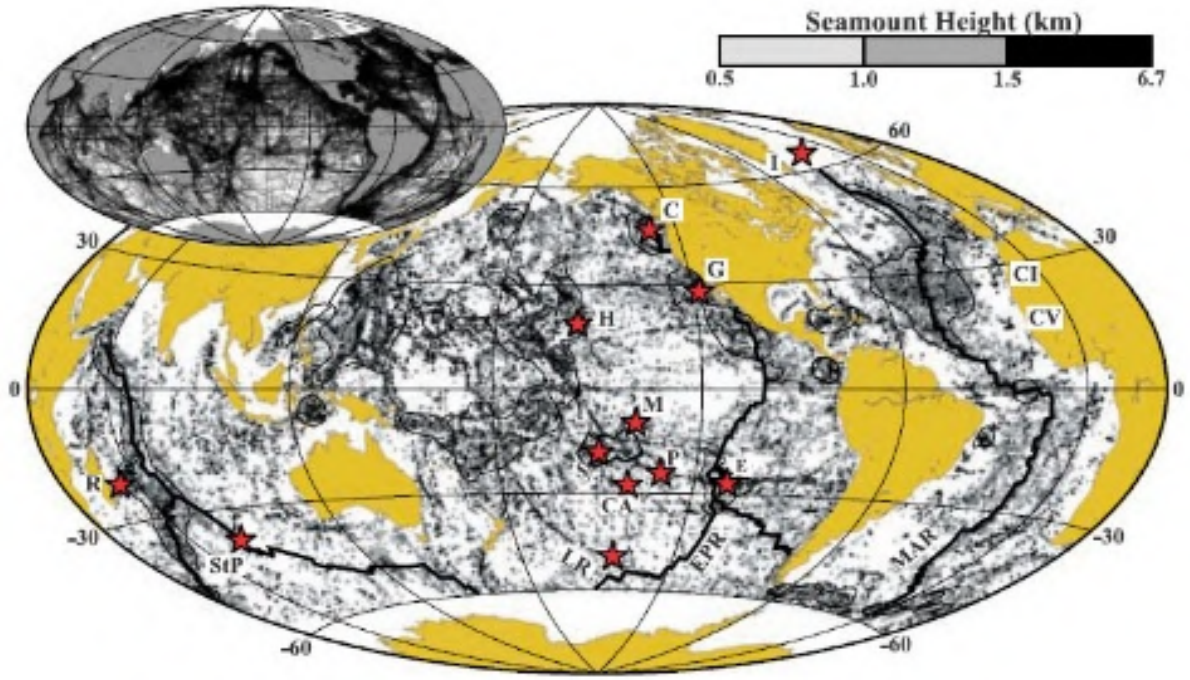

Fig. A-22. *"Spatial distribution of seamounts (dots):* $0.5 < h.1$ *km, light grey (*$n = 32{,}211$*);* $1 < h < h < h <$ *km, grey (*$n = 8{,}436$*);* $h > 1.5$ *km, black (*$n = 6{,}145$*). Thin black line delimits areas of high seamount density (defined as* 75 *seamounts of* $h >$ 1 *km* per10^6 km^2 *within a* 500 *km radius). Thick black lines are spreading ridges:* EPR, *East Pacific Rise;* MAR, *Mid-Atlantic Ridge. Stars locate commonly cited 'hotspots':* CA, *Cook-Austral;* CI, *Canary;* CV, *Cape Verde;* C, *Cobb;* E, *Easter Island;* G, *Guadaloupe;* H, *Hawai'i;* I, *Iceland;* LR, *Louisville;* M, *Marquesas;* P, *Pitcairn;* R, *Réunion;* S, *Society;* StP, *St. Paul's. Inset is coverage of bathymetric data measured along ship-tracks ... "* Figure and captions after Hillier and Watts (2007). *AGU* copyright free policy.

NCGT Journal
New Concepts in Global Tectonics

New Concepts in Global Tectonics Journal
Volume 13, Number 6, August 2025

ISSN number; ISSN 2202-0039

... The age of the Auca Mahuida rocks ... suggest that most of the sources emplaced during the reverse polarity Matuyama Chron. Auca Mahuida anomalies lie around the central crater with wavelengths between $1.5 - 5\ km$. *These anomalies do not correlate with any topographic effect shown on Fig. A-23, confirming their deep origin ...* " According to their modeling, a relevant amount of magnetic sources is located above, say, $\sim 2.5\ km$.

The whole volcano is therefore consistent with a "double-eye" pattern associated to a DC current on top of a sea-urchin spike, with solidification occurring in the upper layer $\sim 2.5\ km$ thick.

The difference in the density of volcanoes that occur in different oceans is shown in figure A-22, where, however - close to continental areas - some old volcanic edifices can be hidden by sediments. This figure was derived from a careful analysis of different sources of observational data, carried out by Hillier and Watts (2007), who also give Table A-1. They comment as follows. "*Table A-1 summarizes*[4] *the number of seamounts within the height bands used in Fig. A-22 and counts corrected for data coverage. Wessel's (2001)* 14,164 *seamounts with* $h > 1.5\ km$ *compare well to our* 13,995 *, although we predict* $\sim 25\%$ *fewer seamounts of* $1.75 \leq h \leq 5\ km$. *In the Pacific we expect* $\sim 22{,}000$ *large* ($h > 1\ km$) *volcanoes, and* $\sim 39 \pm 1 \times 10^3$ *globally, the accuracy estimated from the variance of predictions using a randomly selected* 10% *of seamounts ... we believe the result is a significant constraint upon the current estimates that range from* $\sim 15{,}000$ *(Marova, 2002) to* $\sim 100{,}000$ *(Wessel, 2001). More speculatively, we expect around* ~ 3 *million seamounts of* $h > 0.1\ km$."

Table A-1 - Number of seamounts in ocean areas within height bins[a]

	height (km)			
ocean	$0.5 < h < 1$	$1 < h < 1.5$	$h > 1.5$	total ($h > 0.1$)
Indian[b]	*5,705 (35,238)*	*1,571 (5,985)*	*973 (2,647)*	*30,873 (729,070)*
Pacific[c]	*15,925 (73,942)*	*4,519 (13,805)*	*3,874 (8,654)*	*120,456 (2,140,063)*
Atlantic[d]	*10,581 (42,647)*	*2,346 (6,291)*	*1,298 (2,694)*	*49,726 (608,270)*
global total	*32,211 (151,827)*	*8,436 (26,081)*	*6,145 (13,995)*	*201,055 (3,477,403)*
altimetry derived[e]	*0*	*170*	*14,164*	*14,334*

Legend [Table after Hillier and Watts (2007).]

- Counts corrected for seafloor data coverage are in brackets.
- $20° - 130°\ E$, $-60°$ to $20°\ N$ (no ocean north of this). *689* ship tracks - $5.8 \times 10^6\ km$.
- $130 - 290°\ E$, $\pm 60°\ N$. *3098* tracks - $21.7 \times 10^6\ km$.
- $70°W - 20°\ E$, $\pm 60°$ *N*. *1704* tracks - $12.0 \times 10^6\ km$.
- Wessel (2001), $\pm 60°\ N$.

Hillier (2006) states that "*up to* 50,000 *seamounts taller than* 1 *km are estimated to exist in the Pacific (Menard, 1964; Wessel and Lyons, 1997),* 12,000 *of which have been counted on maps (Batiza, 1982). Unfortunately, only* ~ 250 *are radiometrically dated after direct sampling, and these samples favor recent hotspot volcanism (*39% *of ages are* $< 10\ Ma$, 3.8 *times larger than in any other* 10 Ma *interval), so the distribution of seamount volcanism in space and time is not representatively sampled*."

That is, the space distribution is impressive, of all sea-urchin spikes - upon integrating over the long interval of the activity displayed by all volcanoes that are known at present.

A related item deals with the local monitoring in volcanic areas of telluric currents, and with the investigation on the correlation of their time variations with the time varying supply to volcanoes. An intriguing investigation of this kind was carried out by Maurizio Fedi and Ciro Del Negro who[5] carried out (private communication) magnetometric records, simultaneously at two sites. One of them was at $\sim 4\ km$ from a boca of Etna that was active (with lava effusion), while the other magnetometer was operated a few tens of kilometers apart. Each data series of records, collected at either one site, appeared like white noise.

When they searched for possible correlation between the two signals, they found a surprising and clear correlation.

After excluding all possibilities, they concluded that the only reasonable explanation was in terms of a simultaneous variation of the ***j*** that ought to supply Etna: in fact, the same temporal variation of the **j** either close to the boca or far apart - where leakage fringes of the ***j*** are observed - implies that the two feeble magnetic signals that can appear to be mere noise, in reality are correlated with each other.

[4] *AGU* copyright free policy.

[5] They are, respectively, from *University Federico II*, Napoli and from *INGV*, Catania. See Del Negro and Currenti (2003), Fedi et al. (2003) and Del Negro et al. (2004 and 2013).

NCGT Journal
New Concepts in Global Tectonics

New Concepts in Global Tectonics Journal
Volume 13, Number 6, August 2025

ISSN number; ISSN 2202-0039

Note that, even if Etna is mainly supplied by friction heat (Gregori and Leybourne, 2021), electric currents flow inside the hot conducting matter that propagates heat from the deep source to Earth's surface.

A last case history is reported by Pester (2024) dealing with Lake Rotorua (Fig. A-23) that sits at the heart of a massive ancient crater of a dormant volcano on New Zealand's North Island. The area is well known for hydrothermal activity, and clouds of steam drift around the lake's shore, and sulfur gives a "magical green-blue" color to the water. Researchers "*have now mapped Lake Rotorua's floor in never-before-seen detail, revealing eruption craters, an ancient river and a large magnetic anomaly in the southern part of the lake ... These new maps prove for the first time that Rotorua's mainland hydrothermal systems extend into the lake's hidden depths … Despite all of this activity, water temperatures near the bottom of the lake are usually around* $14°C$ …" In fact, the lake is large and contains enough cool water to counteract endogenous. The temperature only fluctuates by $\sim 1°C$ over a month.

Fig. A-23 shows an intricate multiple "double-eye" pattern.

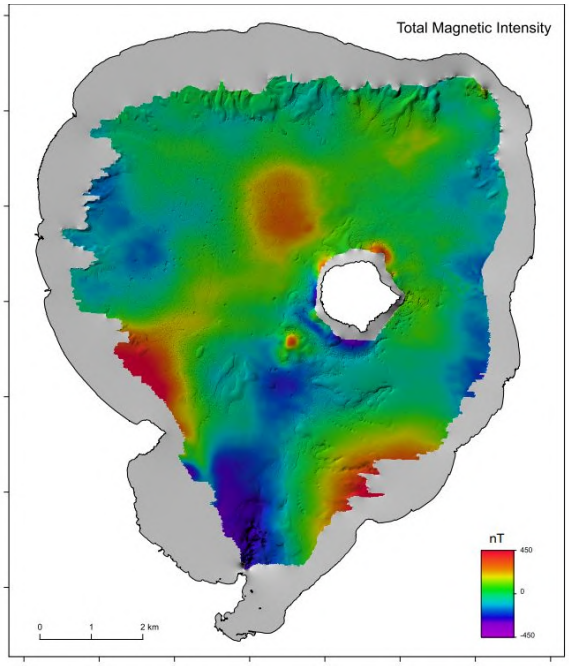

Fig. A-23 – "*Image showing the large magnetic anomaly in the southern part of the lake. (Image credit: Institute of Geological and Nuclear Sciences Limited (*GNS Science*).*" Figure and captions after Pester (2024). Reproduce with *NASA* copyright free policy. A multiple "double-eye" pattern is clearly shown.

Appendix B

Background

The content of the present Appendix B was formerly born as a separate paper that, owing to some unfortunate misunderstanding, was published with no authors' approval and with several mistakes (Gregori et al., 2025s). Since it was impossible to obtain that the paper is substituted by a new version, by cancelling the several mistakes, we decided to include – for reference purpose - the results of that paper in the present Appendix B, because the rationale is the same. We apologize for the unusual, although unavoidable, procedure.

Introduction

A frequent unexplained feature of geomagnetic anomalies maps deals with lineaments red/blue for positive/negative geomagnetic anomalies, which are generally observed and that are indicative, maybe, of a steady – or in any case - variable over long time intervals, but persistent - action by deep telluric currents that, on the long time-range, orient the magnetic components of the crust.

For the sake of completeness, let us mention a few items related to the surge tectonics model (see Meyerhoff and Meyerhoff, 1972; 1972a; 1974; Meyerhoff Hull, 1996; Meyerhoff *et al.,* 1992; 1996; 1996a), i.e., speculating about stream flow processes that occur in the lithosphere, which ought to simulate, perhaps, some features similar to the lineaments that are here considered. Meyerhoff did not necessarily speculate much about electric currents, at least in his writings. He expressed more conventional terms of mass (kinetic) transport of classical physics, i.e., he relied on fluid dynamics applied to solid Earth, analogously to fluid dynamics applied to the oceans or to the atmosphere. Conversely, he considered e.m. phenomena an ancillary driver. In any case, he must have assumed that e.m. energy was involved in leaving magnetic signatures. In any event, he indicated that these magnetic lineaments mostly represent susceptibility contrasts of magnitude and do not necessarily represent reversals of the global magnetic field (*FR*). However, he agrees that these are more likely related to local magma and/or mantle currents (geostreams) - and are not ridge parallel in many cases. *DSDP* results never confirmed the existence of these global reversals, as only a few boreholes reached what is considered magnetic basement - and the ones that did, were not able to extract a sample in situ, i.e., oriented in its original position. Consider that many magnetic surveys from ships or even planes use scalar

NCGT Journal
New Concepts in Global Tectonics
New Concepts in Global Tectonics Journal
Volume 13, Number 6, August 2025
ISSN number; ISSN 2202-0039

magnetometers, which cannot determine magnetic direction. They only measure magnitude - and even the ones that use vector magnetometers do not measure the ***B*** of deep Earth rock. Conversely, they are measuring ***B*** at whatever altitude they are located. They use what is called downward continuation (i.e., a mathematical trick) to project stronger values at depth greater than what is measured at altitude (airborne) or sea surface (marine). For instance, Quinn's data (Quinn et al., 2025) do not show *FR*s, and one would not expect to detect *FR*s in orbital space. This is another tectonic hoax perpetuated by the plate tectonic paradigm that must speculate that seafloor spreading creates new seafloor and provides continental drift/motions. According to Leybourne et al. (2025), the seafloor was magnetically reset (Curie temperature) during Arc Blast Birkeland currents that stripped off the lithosphere carving out the seafloor. That is, continents should not really move large distances, except when thrust faulting due to Arc Blast or some large bolide impact, while during the rest of the time they vibrate maybe shifting slightly. Thus, a global scale rotating plasma (electric) current leaves the double layer signature, i.e., charge vs. lack of charge resulting in a susceptibility contrast. It should be stressed, however, that all these models can explain some lineament features. However, they do not explain the main morphological feature, which is the main focus in the present paper, i.e., red/blue lineaments in one hemisphere that look reversed blue/red in the opposite hemisphere (Fig. B-1).

Reference is made to the serpentosphere (see Gregori and Hovland, 2025 and Gregori et al., 2025a, 2025t), which is a highly conductive layer at the base of the crust. The *ALB* (asthenosphere lithosphere boundary) is the upper boundary of the serpentosphere. See Gregori et al. (2025a, 2025t). It is reasonable to expect that this conducting layer is crossed by intense currents that tend to oppose the e.m. induction action by the solar wind.

Another expected effect is associated with some comparably shallower large region of telluric currents. Since these currents attempt to oppose the planetary geomagnetic field ***B*** of deep origin, these patterns – in restricted unperturbed regions - are expected to look like large blue patches in the geomagnetic anomaly maps.

We show examples of the sum of both these features, which are generally unexplained – and that cannot be simply interpreted in terms of local rock magnetization or electrical conductivity anomalies, as every local property of this kind ought to be irregularly distributed, rather than have regular patterns.

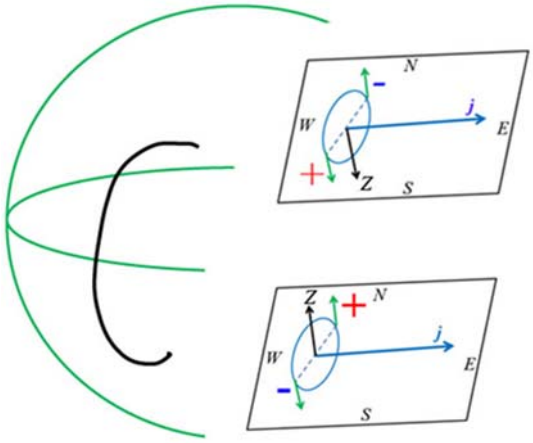

Fig. B-1. The cartoon shows both the Earth and the geomagnetic equator in green lines. The black line is a geomagnetic field line. A supposedly eastward telluric current ***j*** originates an anomalous perturbation, of opposite sign - in the two hemispheres - of the vertical component *Z*. A positive anomaly is denoted in red and a negative anomaly in blue. One should observe - on the geomagnetic anomaly maps – red/blue alignments, roughly running east-west at constant latitude, with red strip closer to the equator. See text

The sea-urchin spikes derive from the propagation of endogenous energy for the deep Earth interior through Earth's surface (see Gregori, 2002; Gregori et al., 2025a., 2025t; and, for a concise summary, Gregori et al., 2025r).

A geomagnetic anomaly map is drawn, starting from a map of one given magnetic element (i.e., one component of the geomagnetic field ***B***, or its total intensity *F*). Then, one chooses the seemingly best model for the planetary deep-origin ***B*** for isolating the residual that ought to be representative of the magnetization of the crust. The residual map is the "anomaly map". Therefore, some arbitrariness is involved, as different maps display comparative differences. No map, however, represents the best possible choice, as the quality of a map depends on the progressively increasing amount of the observed database. In any case, the geomagnetic anomaly maps, altogether with gravity maps, with seismological maps, and with the general tectonic morphology, are the fundamental observational information used for investigating geodynamics and the origin and evolution of solid Earth. Therefore, we must interpret the geomagnetic anomaly maps by means of suitable and reasonable assumptions and approximations, in order to get evidence of physically indicative hunches.

NCGT Journal
New Concepts in Global Tectonics

New Concepts in Global Tectonics Journal
Volume 13, Number 6, August 2025

ISSN number; ISSN 2202-0039

Lineaments of geomagnetic anomalies: a rationale for the interpretation

Consider an eastward telluric current $\boldsymbol{j}$ that flows at approximately constant latitude (Fig. B-1). The effect has an opposing spin direction – i.e., is specular - in the two geomagnetic hemispheres. In the northern geomagnetic hemisphere, the vertical component is $Z < 0$, i.e., the anomaly field (in green), which is produced by an eastward $\boldsymbol{j}$, increases the total field F equatorward to $\boldsymbol{j}$, and it decreases the total field F poleward to $\boldsymbol{j}$. A similar result is found with reversed sign in the southern geomagnetic hemisphere, where $Z > 0$.

In fact, the identical rationale applies to every telluric current, with any direction (Fig. B-2). That is, in the northern geomagnetic hemisphere, the vertical component $Z > 0$, which is produced by $\boldsymbol{j}$, is positive on the right side of $\boldsymbol{j}$. In contrast, on the left side of $\boldsymbol{j}$ the vertical component is $Z < 0$. A similar result holds in the southern geomagnetic hemisphere, where the signs are exchanged between right and left side relative to $\boldsymbol{j}$.

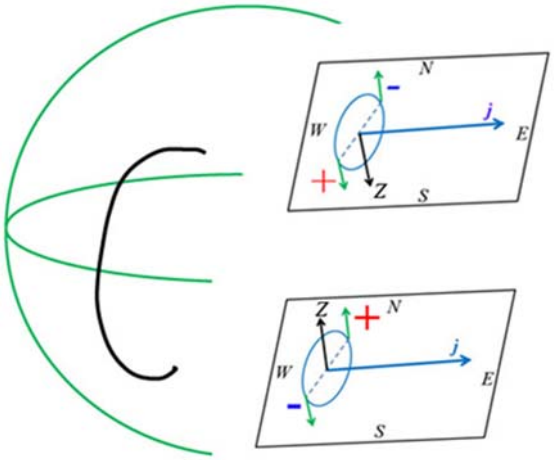

Fig. B-1. The cartoon shows both the Earth and the geomagnetic equator in green lines. The black line is a geomagnetic field line. A supposedly eastward telluric current $\boldsymbol{j}$ originates an anomalous perturbation, of opposite sign - in the two hemispheres - of the vertical component Z. A positive anomaly is denoted in red and a negative anomaly in blue. One should observe - on the geomagnetic anomaly maps – red/blue alignments, roughly running east-west at constant latitude, with red strip closer to the equator. See text.

Suppose that some *mean* eastward telluric current $\boldsymbol{j}$ has been the leading current during some relevant time interval of the past – and still at present. One ought to observe red/blue lineaments in the planetary maps of the geomagnetic anomalies. In general, at every location, the red/blue lineaments are indicative of peculiar local features that determined some typical mean direction of $\boldsymbol{j}$ during some long-time interval. In any case, all observational matters-of-fact are unquestionable, and denote that, during some geological time-lag, a *mean* flow of $\boldsymbol{j}$ determined the formation of the observed red/blue lineaments.

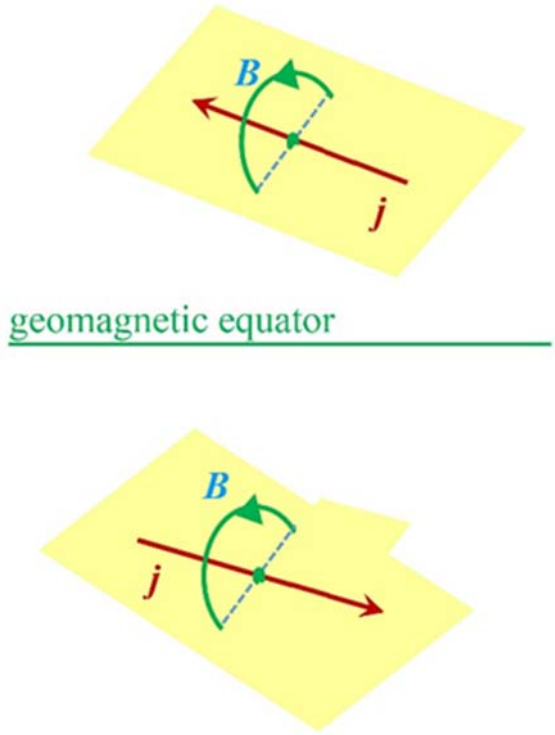

Fig. B-2. A general telluric current $\boldsymbol{j}$ generates an anomaly with $Z < 0$ on the right side of $\boldsymbol{j}$ in the northern hemisphere (*NH*), and an anomaly with $Z > 0$ on the left side of $\boldsymbol{j}$. In the southern hemisphere (*SH*), the signs of the Z anomaly are reversed between the right and left side of $\boldsymbol{j}$. See text.

The mean observed eastward telluric currents $\boldsymbol{j}$ are tentatively justified by the following argument (Fig. B-3). The Earth's dipole moment $\boldsymbol{M}$ is oriented southward (Fig. B-3a) - and can be symbolically represented by an equivalent circuit composed of a loop L of current (Fig. B-3b). When the solar wind interacts with the Earth - owing to electromagnetic (e.m.) induction and to the Hamilton variational principle (see Gregori et al., 2025e) - the solar wind attempts to minimize the effect of $\boldsymbol{M}$. This means that the result amounts to generate a mean current opposite to L (Fig. B-3c).

NCGT Journal
New Concepts in Global Tectonics
New Concepts in Global Tectonics Journal
Volume 13, Number 6, August 2025
ISSN number; ISSN 2202-0039

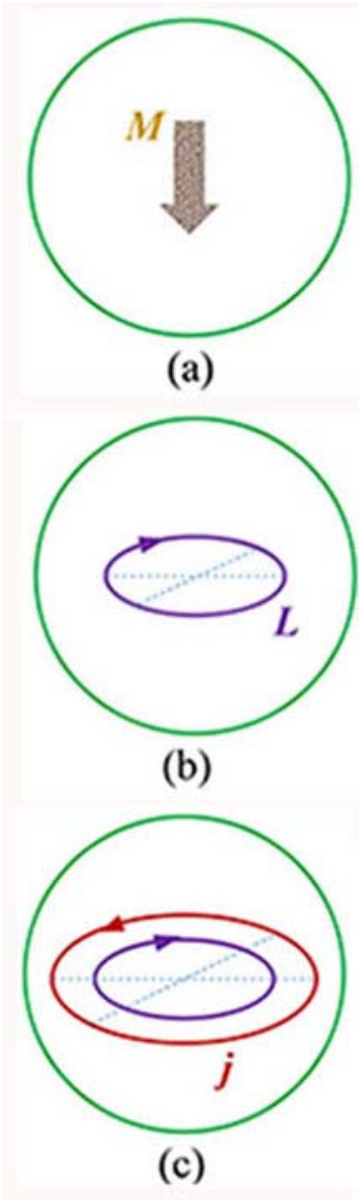

Fig. B-3. The Earth is shown in green. *(a)* The geomagnetic field has a moment $\boldsymbol{M}$. *(b)* In terms of an equivalent circuit, $\boldsymbol{M}$ can be substituted by an ideal loop *L*. *(c)* The e.m. induction by the solar wind attempts to oppose - as much as possible and as an *average* effect on some long time lag - the current that flows in the loop *L*. Thus, it generates a telluric current $\boldsymbol{j}$ in the serpentosphere that is approximately concentric and opposite to the *L* current. Hence, during a normal "chron", $\boldsymbol{j}$ is eastward, and, during a reversed "chron", $\boldsymbol{j}$ is westward. See text.

During a period ("chron") of normal field orientation, the induced current is eastward, and it is westward during a reversed "chron". At present, we are during a long lasting "chron" ($\sim 700\ ka$). Therefore, a reasonable guess is that the present red/blue lineaments refer to processes that occurred during the last long "chron". In addition, as it is well known, no statistical analysis of the time series of *FR*s afforded to evidence any regularity or periodicity. [6] According to the interpretation here given (see Gregori et al., 2025a), a *FR* is caused by an erratic encounter of the Solar System with a dense cloud of interstellar matter. Therefore, all phenomena that eventually happened during the long time-lag preceding the last *FR* are unlikely to be reckoned to the present observed red/blue lineaments. [7]

In the case of magma effusion (like lava flow or pluton), the crustal magnetization depends on the polarization of $\boldsymbol{B}$ at the time of eruption. Otherwise, erosion generates fragmented material that is deposited in sediments aligned according to the local $\boldsymbol{B}$. Hence, the evidence of mean eastward telluric currents ought to refer to the crustal fragmented material that accumulated in sediments during some time-lag of the last "chron".

In any case, the phenomenon is quite intricate. For completeness sake, we recall some other investigations of linear morphologies of the crust. (Smoot and Heffner (1986) showed the first NW SE trending of the Kashima fracture zone (*FZ*) in the NW Pacific. After that, other areas were investigated, such as the Marcus-Wake seamounts and guyots and their relation to the Dutton Ridge (Smoot, 1989), and the plate-wide Pacific trends of orthogonal fracture intersections (Smoot, 1994). Fracture zones were shown to cross to the western Pacific trenches, such as (Smoot, 1995, 1998a) the Chinook Trough, which is a trans-Pacific fracture zone.

In the Darwin Rise – in western Pacific - guyot heights trace the trans-Pacific Mendocino Fracture Zone, (Smoot and King, 1997). Many seafloor experts already knew about the Emperor Seamount chain, and the Adak and Amelia fracture zones in the Gulf of Alaska. The *GEOSAT* lineaments were used and compared to total coverage bathymetry (Leybourne and Smoot, 1997). The stage was set for examining entire basins between $72°N$ and $72°S$ worldwide. The focus was on examining *(i)* Vortex structures on the world-encircling vortex street (Smoot and Leybourne, 1997), *(ii)* magma floods,

[6] The literature is very large and cannot be here recalled.

[7] Concerning all possible connections of red/blue lineaments with the speculated Arc Blast phenomena on the long geological time scale, refer to the discussion in Leybourne et al. (2025).

NCGT Journal
New Concepts in Global Tectonics

New Concepts in Global Tectonics Journal
Volume 13, Number 6, August 2025

ISSN number; ISSN 2202-0039

microplates, and orthogonal intersections (Smoot, 1997*), (iii)* WNW-ESE Pacific lineation's (Smoot, 1998), and *(iv)* orthogonal intersections of megatrends in the Mesozoic Pacific Ocean basin (Smoot, 1999).

Upon considering the trends established - and by including the accurate bathymetry - a multitude of trends was displayed. Thus, NNW-ESE megatrends were shown for the north and central Pacific basin (Smoot and Leybourne, 2001; Smoot and Choi, 2003). By including the previously known NE Pacific Moonless Mountains - and the NE-SW trending of four seamount chains to the north of the Hess Rise - it was possible to construct such a diagram and to refute any sort of organized motion of the lithosphere in the Pacific basin (Smoot, 2012). Around that time "*the persistent mantle plume myth*" was explored (Anderson, 2013). The question was: do mantle plumes exist? A later e.m. synthesis of this problem was explored with the *Stellar Transformer* concept (Leybourne *et. al*., 2017; Leybourne and Gregori, 2020) resulting in the examination of "Orthogonal Megatrend Intersections" as "Coils of a Stellar Transformer" (Smoot and Leybourne, 2020). We stress, however, that a *FZ* is physically other than an alignment on a geomagnetic anomaly map.

Observed case histories

Concerning the geomagnetic anomaly maps, every region of the globe can be analysed according to the rationale of Figs B-1, B-2 and B-3. Only a few indicative highlights are here shown, relying on two magnetic anomaly maps of the world.

One map was implemented by Purucker (2007). The same map is reported by Thébault et al. (2010), who call it "*World Digital Magnetic Anomaly Map*" (*WDMAM*) and quote Khorhonen et al. (2007). The anomaly field is plotted at an altitude of *5 km* above the WGS84 ellipsoid. A distinction is made between near-surface compilations, satellite-based, and oceanic-model data. The entire data set is displayed by the natural color scale (red = high, blue = low) with a shaded relief effect using artificial illumination. The original map is at a scale of $1:50\ million$.

The other map, which is the main source used here, is the *Global Earth Magnetic Anomaly Grid* (*EMAG2*) compiled by satellite, ship, and airborne magnetic measurements, and is available at http://geomag.org and http://noaa.gov (Maus *et al*. 2008, Maus *et al*., 2009; Müller *et al*., 2008; Sabaka *et al*., 2004).

A few major case histories are here shown. Fig. B-4 is a detail of *EMAG2* dealing with Arabia, India, and the Sunda arc. Some general trends of east-west lineaments are evident. Conspicuous band thickening is shown, beginning in Iraq/Iran, through Himalaya, through Northern China and Japan. This is, maybe, correlated with the Moroccan megashear (Van Bemmelen, 1972) that, according to warm mud tectonics (*WMT*; see Gregori, 2002; Gregori and Leybourne, 2021; Gregori et al., 2024a), is a giant megasyncline crossing from Morocco through Japan. In addition, see the remarkable red/blue alignment in the Sunda archipelago.

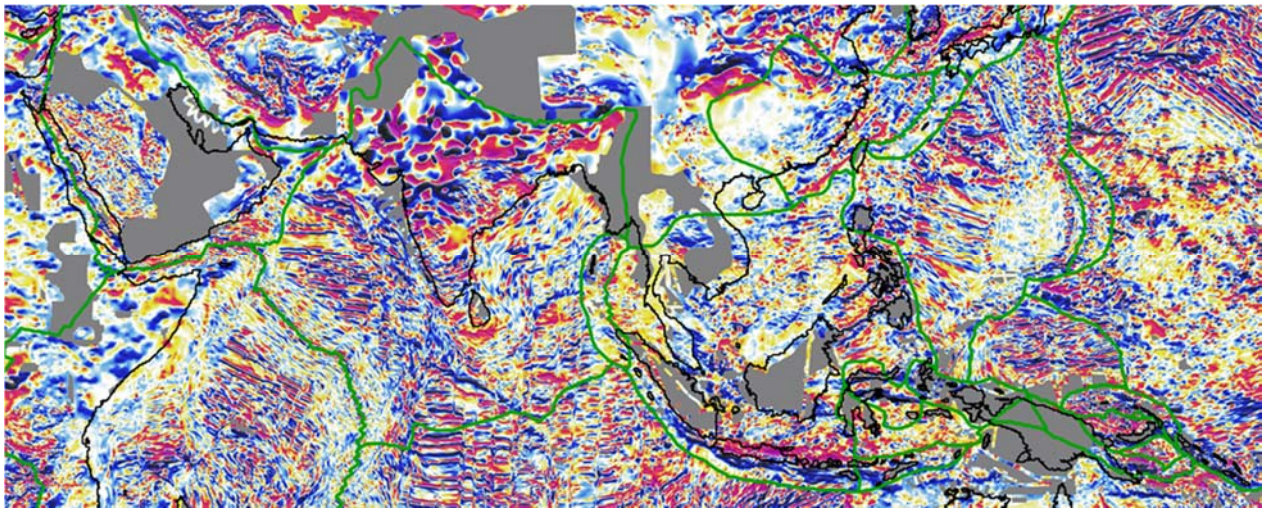

Fig. B-4. Detail of *EMAG2* dealing with Arabia, India, and the Sunda arc. See text. *NOAA* copyright free policy.

NCGT Journal
New Concepts in Global Tectonics

New Concepts in Global Tectonics Journal
Volume 13, Number 6, August 2025

ISSN number; ISSN 2202-0039

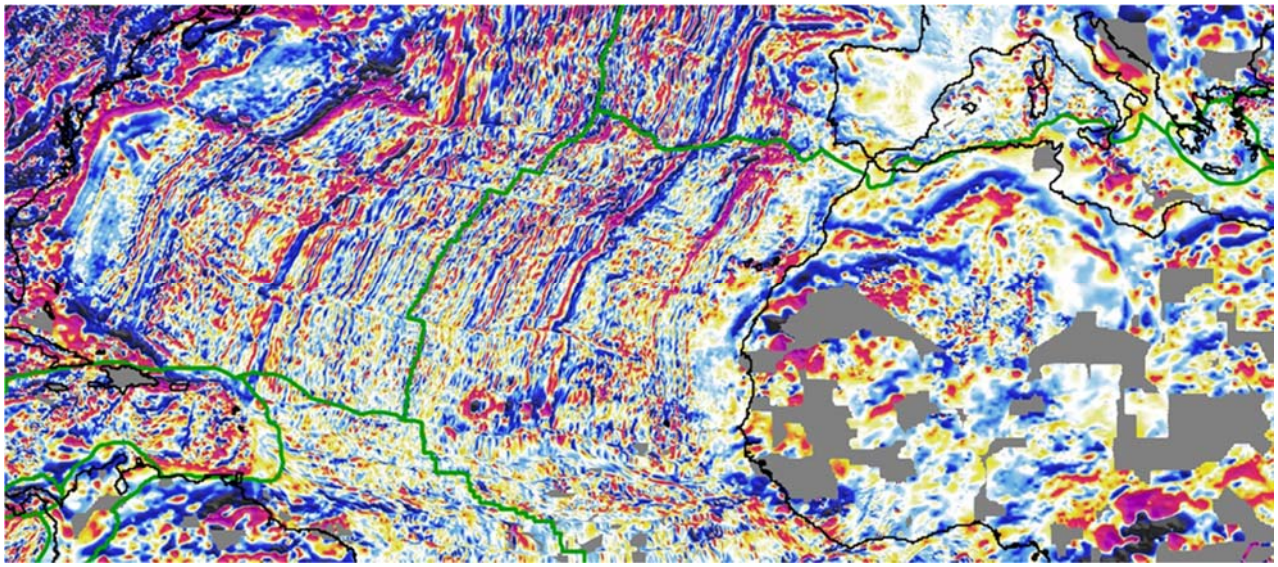

Fig. B-5. Detail of *EMAG2* dealing with central Atlantic. *NOAA* copyright free policy. Unpublished figure.

In contrast, in the Atlantic Ocean, the geodynamic and tectonic features are dominating (Fig. B-5). Intense telluric currents seem to flow in the crust, parallel to the *MAR* (Mid Atlantic Ridge), which is one edge of the tetrahedron that represents an alignment of sea-urchin spikes (Gregori and Leybourne, 2021).

Some regions give evidence of thicker red/blue bands, such as the Adriatic Sea/Balkan Peninsula, in Northern Venezuela area, and in some extended region in North Africa, which is part of the aforementioned Morocco/Japan megasyncline.

Africa seems to be the continent with the thicker lithosphere, denoting a comparably stronger link with the mantle (Chapman and Pollack, 1975; Pollack and Chapman, 1977, 1977a; Pollack et al., 1993). A long interdisciplinary discussion ought to refer to the whole set of morphological features of Africa.

For brevity, the focus is here only on geomagnetic anomalies. Fig. B-6 shows a detail of *EMAG2*, and Fig. B-7 addresses a few features that are concisely illustrated as follows.

Feature No. 1 is Zaïre's anomaly, clearly evidenced in Fig. B-8. Note that the comparative close location of Feature No. 7 (Bangui Magnetic Anomaly) may envisage that, perhaps, Features No. 1 and No. 7 are the signature of a unique large anomaly.

Feature No. 2 is analogous, although less extended.

Feature No. 3 shows a complicate pattern that displays two parallel red/blue double lines, beginning from Canary Islands and Western Sahara, and that - after a few bifurcations - join anew into a unique line at Suez and run northward until (maybe) joining the Iraq/Japan alignment. This feature approximately coincides with the Moroccan megashear, and is only slightly displaced southward, with respect to Earth's surface evidence. A relevant perturbation is caused by the rapid counterclockwise rotation of Anatolia into the Aegean Sea

Feature No. 4 is a similar doublet beginning in Guinea and Sierra Leone.

Feature No. 5 is analogous to feature No. 3. It is composed of 3 or 4 doublets crossing through South Africa and Namibia.

Feature No. 6 shows a curious "inverted V" pattern found on the ocean floor, south of South Africa. This feature should be considered in the framework of the justification of the planetary *MOR* (mid-ocean ridge) network, which is associated to the deep conducting tetrahedron (which is an alignment of sea-urchin spikes; Gregori and Leybourne, 2021). Note the curious pattern that corresponds to the southern tip of Africa, which is characterized by a high density of diamond-bearing kimberlites, and by a high atmospheric density of CO_2, which persists in every season (see, e.g. Gregori, 2020, and references therein), in addition to displaying a close correlation with the *DUPAL* anomaly of the isotopic chemism of basalt (see Gregori et al., 2025a).

Feature No. 7 is the Bangui Magnetic Anomaly, which is centered at Bangui, the capital of the Central African Republic. The magnetic anomaly is roughly elliptical, $\sim 700\ km \times 1{,}000\ km$, and covers most of the country, making it one of the "*largest and most intense crustal magnetic anomalies on the African continent*" (Wikipedia)..

NCGT Journal
New Concepts in Global Tectonics

New Concepts in Global Tectonics Journal
Volume 13, Number 6, August 2025

ISSN number; ISSN 2202-0039

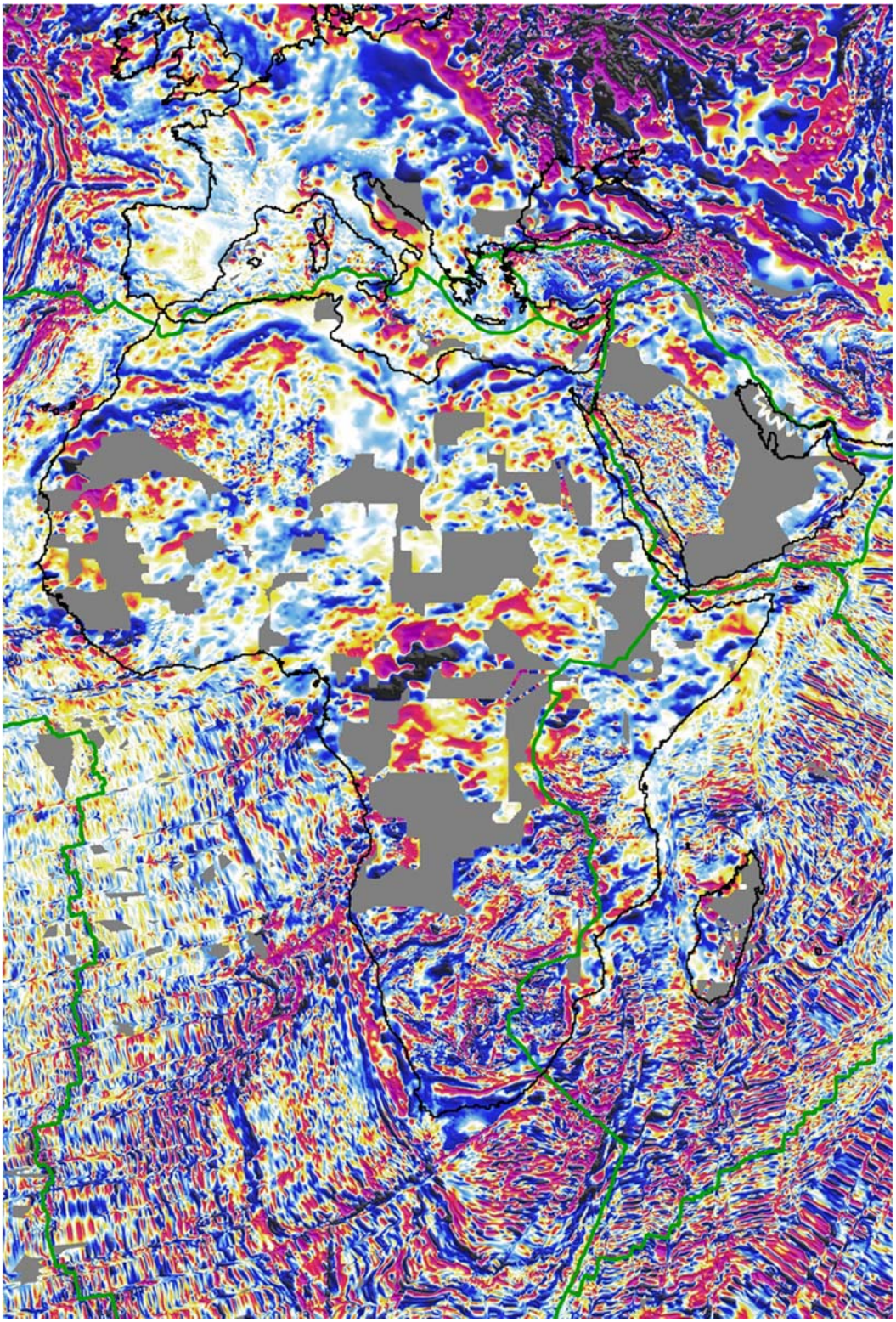

Fig. B-6. Africa and surroundings in *EMAG2*. See text. *NOAA* copyright free policy.

NCGT Journal
New Concepts in Global Tectonics
New Concepts in Global Tectonics Journal
Volume 13, Number 6, August 2025
ISSN number; ISSN 2202-0039

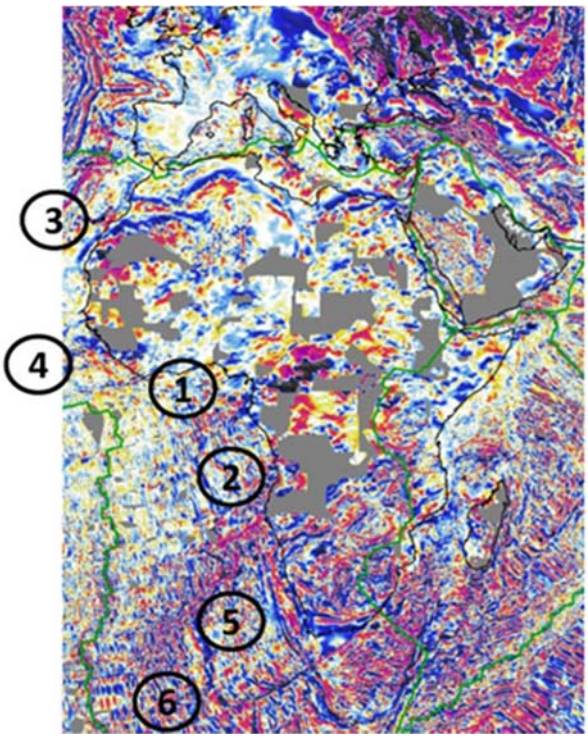

Fig. B-7. Africa and surroundings in *EMAG2*. The same as Fig. B-6 with superposed the indication of six peculiar features. See text. *NOAA* copyright free policy.

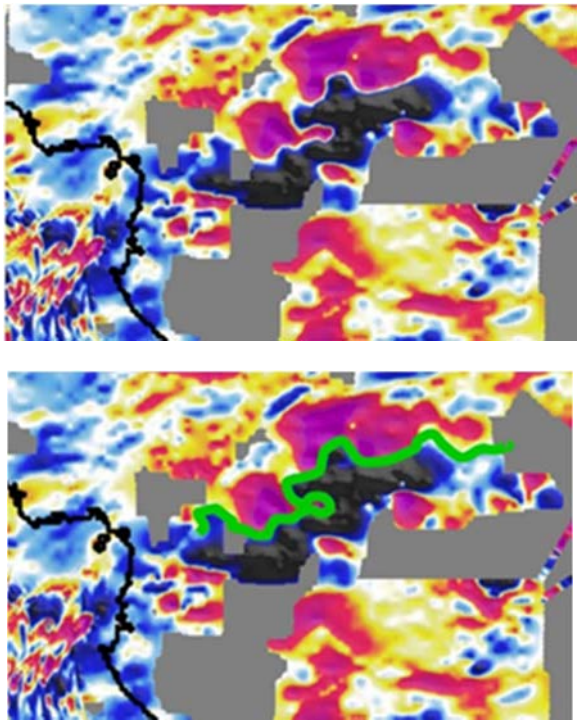

Fig. B-8. Zaïre geomagnetic anomaly map, a detail of *EMAG2*. *(a)* Original datum being a detail of Fig. B-6. *(b)* The same with superposed a semi-transparent green band to indicate the axis of the double-eye feature, corresponding to the Cameroon Volcanic Line (*CVL*). See text. *NOAA* copyright free policy. This feature is, maybe, connected with the Bangui anomaly.

Conclusion

These indications are only a concise premise for a much more extensive and far looking discussion that, owing to brevity, we cannot report in the present paper.

Telluric currents, however, can also flow inside ocean water, which has an electrical conductivity σ that is ~40,000 times larger than dry rocks (Lanzerotti and Gregori, 1986) - and oceans are the most important conductivity anomaly.

The mean pattern is therefore a large - or near global - double layered spherical condenser. One conductor is the ionosphere, while the atmosphere is an insulating layer. Oceans are a conductor, while the deep lithosphere and dry rocks are an insulating layer, with a layer underneath of great conductance represented by the serpentosphere. The upper boundary of the serpentosphere is the *ALB* (Gregori and Hovland, 2025; Gregori et al., 2025t). This huge condenser system responds to the e.m. induction by the solar wind.

Concerning additional features, Fig. B-9 shows, e.g., the geomagnetic anomaly of the Scotia Arc, where the red/blue lineaments associated to the Antarctic Peninsula are caused by the σ contrast between ocean water and ground. The large clockwise rotation of South America was the likely origin of the Scotia Arc, which, by that, broke the Circum-Antarctic *MOR* (Gregori and Leybourne, 2021) while rotating around a kingpin (see below).

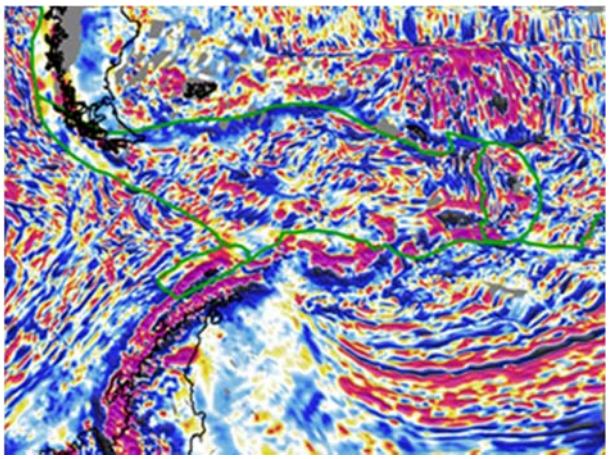

Fig. B-9. Scotia Arc detail in *EMAG2*. See text

The Gulf of Mexico is a singular case history, as it displays a huge blue patch, which envisages (maybe) a "hack" surviving after the huge Chicxulub impact (see Gregori and Leybourne, 2025j and the related discussion). In fact, see the huge blue patch roughly located in the Gulf of Mexico and in the surrounding areas (see Fig. B-10, which is identical to Fig. 10 of Gregori and Leybourne, 2025j).

This huge blue patch can be the "kingpin" associated with the impact of the Chicxulub astrobleme. Also note the large lineaments north of the blue patch. Refer to the extensive discussion in Quinn et al. (2025).

ISSN number; ISSN 2202-0039

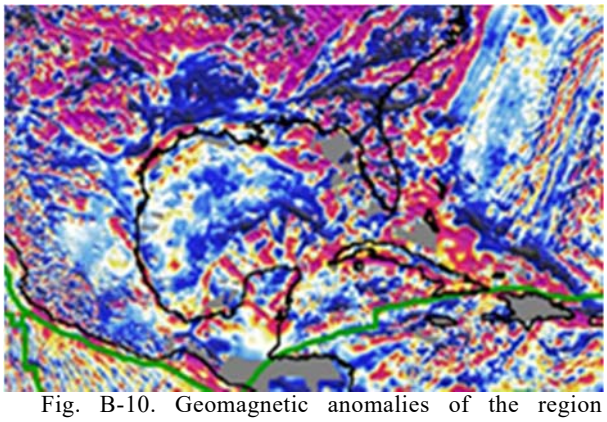

Fig. B-10. Geomagnetic anomalies of the region surrounding Florida. *EMAG2* detail. For other details, see Gregori et al. (2025r), and Gregori, and Leybourne (2025j). Note the large blue patch in the left side portion of this map. See text. *NOAA* copyright free policy

In addition, we could give a list of much evidence, although not here given, about morphological features that seem to be closely related to the sea-urchin spike mechanism. In fact, every item ought to request a long discussion of the correlation with local morphological features.

Summarizing, in general and in any case, the sea-urchin spike pattern, and the electric currents in the asthenosphere, envisage an unprecedented criterion suited to interpret the geomagnetic anomaly maps, for possible correlation with other geophysical evidence.

Acknowledgement

Fig. A-2 was kindly provided by I. Blanco. We thank her very much.

We want to thank N.C. Smoot for the relevant and authoritative information on tectonic fabric of fault systems throughout the Pacific Ocean seafloor.

We thank Professor Alberto Incoronato for some specific discussion.

We want also to acknowledge all co-workers that, in different ways and at different times, contributed to the exploitation of the analyses mentioned in the present study.

We also thank for the warm encouragement we had from several outstanding scientists.

Funding Information

The funding derives from the respective Institutions. G.P. Gregori has been retired since 2005. B.A. Leybourne is a semi-retired self-funded independent researcher. U. Coppa is a retired researcher at the *Osservatorio Vesuviano*. G. Luongo is at present Emeritus Professor of Physics of Volcanism at the *University Federico II* in Naples, Associate of *INGV – Osservatorio Vesuviano*, and a former Director of the *Osseratorio Vesuviano* retired since 2010.

Author's Contributions

Giovanni P. Gregori: Main responsibility. Bruce A. Leybourne: Contribution with relevant discussion. Ugo Coppa: Contribution with relevant discussion. Giuseppe Luongo: Contribution with relevant discussion.

Ethics

This article is original and contains unpublished material. Authors declare that there are no ethical issues and no conflict of interest that may arise after the publication of this manuscript.

References

Acocella, V., and G. Chiodini, 2015. Better forecasting for the next volcanic eruption, *EOS, Transactions of the American Geophysical Union*, 96; DOI:10.1029/2015EO039135. Published on 12 November 2015

Acocella, V., R. Di Lorenzo, C. Newhall, and R. Scandone, 2015. An overview of recent (1988 to 2014) caldera unrest: knowledge and perspectives, *Reviews of Geophysics*, 53: 896–955; DOI:10.1002/2015RG000492

Amoruso, A., L. Crescentini, and I. Sabbetta, 2014. Paired deformation sources of the Campi Flegrei caldera (Italy) required by recent (1980–2010) deformation history, *Journal of Geophysical Research,* 119: 858–879; DOI:10.1002/2013JB010392

Anderson, D. L., 2013. The persistent mantle plume myth, *Australian Journal of Earth Sciences*, 60 (6–7): 657–673; http://dx.doi.org/10.1080/08120099.2013.835283

Batiza, R., 1982. Abundances, distribution and sizes of volcanoes in the Pacific Ocean and implications for the origin of non-hotspot volcanoes, *Earth and Planetary Science Letters*, 60: 195–206

Blanco-Montenegro, I., I. Nicolosi, A. Pignatelli, and M. Chiappini, 2008. Magnetic imaging of the feeding system of oceanic volcanic islands: El Hierro (Canary Islands), *Geophysical Journal International*, 173: 339–350; DOI:10.1111/j.1365-246X.2008.03723.x

Bonasia, V., G. Luongo, and S. Montagna, 1973. A land gravity survey of the Aeolian Islands. *Bulletin of Volcanology*, 37: 134–146; DOI:10.1007/BF02596885

Cangiano, A., 2015. Nuove fumarole nella Baia di Pozzuoli: è l'antica isola termale di Calipso, *Napoli.com*, (107), issued 16 April 2015

Chapman, D. S., and H. N. Pollack, 1975. Global heat flow: a new look. *Earth and Planetary Science Letters*, 28 (1): 23-32

Chiappini, M., A. Meloni, E. Boschi, O. Faggioni, N. Beverini, C. Carmisciano, and I. Marson, 2000. Onshore-offshore integrated shaded relief magnetic anomaly map at sea level of Italy and surrounding

areas: *Annali di Geofisica*, 43 (5): 983-989, scale 1/1,500,000

Chiarabba, C., N. A. Pino, G. Ventura, and G. Vilardo, 2004. Structural features of the shallow plumbing system of Vulcano Island (Italy), *Bulletin of Volcanology*, 66: 477–484

Chiodini, G., S. Caliro, P. De Martino, R. Avino, and F. Gherardi, 2012. Early signals of new volcanic unrest at Campi Flegrei caldera? Insights from geochemical data and physical simulations. *Geology*, 40: 943–946; DOI:10.1130/G33251.1

Cocchi, L., S. Passaro, F. Caratori Tontini, and G. Ventura, 2017. Volcanism in slab tear faults is larger than in island-arcs and back-arcs, *Nature, Communications*, 8: 1451; DOI:10.1038/s41467-017-01626-w

Costa, A., A. Folch, G. Macedonio, B. Giaccio, R. Isaia, and V. C. Smith, 2012. Quantifying volcanic ash dispersal and impact of the Campanian Ignimbrite super-eruption, *Geophysical Research Letters*, 39 (10); DOI:10.1029/2012GL051605

D'Ajello Caracciolo, F., I. Nicolosi, R. Carluccio, S. Chiappini, R. De Ritis, A. Giuntini, V. Materni, A. Messina, M. Chiappini, 2014. High resolution aeromagnetic anomaly map of Mount Etna volcano, Southern Italy, *Journal of Volcanology and Geothermal Research*, 277: 36–40; DOI:10.1016/j.jvolgeores.2014.03.008

D'Auria, L., S. Pepe, R. Castaldo, F. Giudicepietro, G. Macedonio, P. Ricciolino, P. Tizzani, F. Casu, R. Lanari, M. R. Manzo, M. Martini, E. Sansosti, and I. Zinno, 2015. Magma injection beneath the urban area of Naples: a new mechanism for the 2012-2013 volcanic unrest at Campi Flegrei caldera, *Scientific Reports*, 5: Article no. 13100; DOI:10.1038/srep13100

de Alteris, G., R. Tondelli, S. Passaro, and M. de Lauro, 2006. *Isole Flegree (Ischia e Procida)*, Liguori, Napoli; pp: 1-73

De Martino, P., U. Tammaro, and F. Obrizzo, 2014. GPS time series at Campi Flegrei caldera (2000–2013), *Annals of Geophysics*, 57 (2): S0213; DOI:10.4401/ag-6431

De Natale, G., C. Torise, R. Somma, and R. Moretti, 2017. Nella caldera dei Campi Flegrei, *Le Scienze*, (585): 30-35

De Natale, G., C. Troise, D. Mark, A. Mormone, M. Piochi, M. A. Di Vito, R. Isaia, S. Carlino, D. Barra, and R. Somma, 2016. The Campi Flegrei Deep Drilling Project (CFDDP): new insight on caldera structure, evolution and hazard implications for the Naples area (Southern Italy), *Geochemistry, Geophysics, Geosystems*, 17: 4836–4847; *DOI:10.1002/2015GC006183*

De Ritis, R., I. Blanco-Montenegro, G. Ventura, and M. Chiappini, 2005. Aeromagnetic data provide new insights on the volcanism and tectonics of Vulcano Island and offshore areas (southern Tyrrhenian Sea, Italy), *Geophysical Research Letters*, 32: L15305 [4 pp.]; DOI:10.1029/2005GL023465

Del Gaudio, C., I. Aquino, G. P. Ricciardi, C. Ricco, and R. Scandone, 2010. Unrest episodes at Campi Flegrei: a reconstruction of vertical ground movements during 1905–2009, *Journal of Volcanology and Geothermal Research*, 195: 48–56; DOI:10.1016/j.jvolgeores.2010.05.014

Del Negro, C., and G. Currenti, 2003. Volcanomagnetic signals associated with the 2001 flank eruption of Mt. Etna (Italy), *Geophysical Research Letters*, 30 (7): 1357 [4 pp.]; DOI:10.1029/2002GL015481, 2003

Del Negro, C., G. Currenti, G. Solaro, F. Greco, A. Pepe, R. Napoli, S. Pepe, F. Casu, and E. Sansosti, 2013. Capturing the fingerprint of Etna volcano activity in gravity and satellite radar data, *Scientific Reports*, 3: 3089; DOI:10.1038/srep03089

Del Negro, C., G. Currenti, R. Napoli, and A. M. Vicari, 2004. Volcanomagnetic changes accompanying the onset of the 2002–2003 eruption of Mt. Etna (Italy), *Earth and Planetary Science Letters*, 229: 1–14; DOI:10.1016/j.epsl.2004.10.033

di Girolamo, P., and G. Rolandi, 1975. Vulcanismo sottomarino latitebasaltico-latitico (serie potassica) nel Canale d'Ischia (Campania), *Rendiconto dell'Accademia delle Scienze Fisiche e Matematiche (Società Nazionale di Scienze Lettere ed Arti in Napoli)*, S. 4, 42: 561-596

di Girolamo, P., M. R. Ghiara, L. Lirer, R. Munno, G. Rolandi, and D. Stanzione, 1984. Vulcanologia e petrologia dei Campi Flegrei, *Bollettino della Società geologica italiana*, 103, 349-413

Di Vito, M. A., R. Isaia, G. Orsi, J. Southon, S. de Vita, M. D'Antonio, L. Pappalardo, and M. Piochi, 1999. Volcanism and deformation since 12,000 years at the Campi Flegrei caldera (Italy), *Journal of Volcanology and Geothermal Research*, 91 (2/4): 221–246; DOI:10.1016/S0377-0273(99)00037-2

Di Vito, M., L. Lirer, G. Mastrolorenzo, and G. Rolandi, 1987. The 1538 Monte Nuovo eruption (Campi Flegrei, Italy), *Bulletin of Volcanology*, 49 (4): 608–615; DOI:10.1007/bf01079966

Fedi, M., M. La Manna, and F. Palmieri, 2003. Nonstationary analysis of geomagnetic time sequences from Mount Etna and North Palm Springs earthquake, *Journal of Geophysical Research*, 108, (B10): 2493; DOI:10.1029/2001JB000820

Garcìa, A., I. Blanco, J. M. Torta, and I. Socìas, 1997. High-resolution aeromagnetic survey of the Teide volcano (Canary Islands): a preliminary analysis. *Annali di Geofisica*, 40 (2): 329-340

Garcìa, A., M. Chiappini, I. Blanco-Montenegro, R. Carluccio, F. D'Ajello Caracciolo, R. De Ritis, I. Nicolosi, A. Pignatelli, N. Sánchez, and E. Boschi, 2007. High resolution aeromagnetic anomaly map of Tenerife, Canary Islands, *Annals of Geophysics*, 50

(5): 689-697

Gregori, G. P., 1993b. The next eruption of Somma-Vesuvius. In W. Schröder (ed.), The Earth and the universe, Festschrift in honour of Prof. H.-J. Treder, *Newsletter of IDCH-IAGA*, (20), Science Edition, Bremen-Roennebeck; pp: 191-213

Gregori, G. P., 1996. The next eruption of Somma-Vesuvius. In V. Piccione, and C. Antonelli (eds), *Proceedings of the 4th Workshop of Progetto Strategico Clima, Ambiente e Territorio nel Mezzogiorno*, Lecce, November 11-14, 1991, 2 vol., CNR, Roma; pp.: 399-468

Gregori, G. P., 2002. Galaxy – Sun – Earth relations. The Origin of the Magnetic Field and of the Endogenous Energy of the Earth, with Implications for Volcanism, Geodynamics and Climate Control, and Related Items of Concern for Stars, Planets, Satellites, and Other Planetary Objects. A Discussion in a Prologue and Two Parts. *Beiträge zur Geschichte der Geophysik und Kosmischen Physik*, Band 3, Heft 3: pp. 1-471 [Available at http://ncgtjournal.com/additional-resources.html]

Gregori, G. P., 2020. Climate change, security, sensors. *Acoustics,* 2: 474-504; DOI:10.3390/acoustics2030026.[https://www.mdpi.com/2624-599X/2/3/26/htm]

Gregori, G. P., and B. A. Leybourne, 2021. An unprecedented challenge for humankind survival. Energy exploitation from the atmospheric electrical circuit, *American Journal of Engineering and Applied Science*, 14 (2): 258-291; DOI:10.3844/ajeassp.2021.258.291

Gregori, G. P., and B. A. Leybourne, 2025j. The energy supply to hurricanes. *New Concepts in Global Tectonics, Journal,* 13, (5): 731-786

Gregori, G. P., and G. Paparo, 2021. Time-resolution of climate change monitoring volcanic cycles, Stromboli, ocean floor biota and pandemics (?), *American Journal of Engineering and Applied Science*, 14 (2): 351-363; DOI:10.3844/ajeassp.2021.351.363

Gregori, G. P., and G. Paparo, 2021. Time-resolution of climate change monitoring volcanic cycles, Stromboli, ocean floor biota and pandemics (?), *American Journal of Engineering and Applied Science*, 14 (2): 351-363; DOI:10.3844/ajeassp.2021.351.363

Gregori, G. P., and M. T. Hovland, 2025. Go for the anomaly – a golden strategy for discovery? Seepology & the origin and crucial role of the biosphere - Earth and planetary objects - Supercritical water and serpentinization. In press in *New Concepts in Global Tectonics, Journal*

Gregori, G. P., B. A. Leybourne, U. Coppa, and G. Luongo, 2025s. Geomagnetic anomalies: lineaments. *American Journal of Engineering and Applied Sciences*, 18 (1): 1-10. https://doi.org/10.3844/ajeassp.2025.1.10

Gregori, G. P., B. A. Leybourne, U. Coppa, and G. Luongo, 2025t. Lightning and volcanic plumes. In press on *New Concept of Global Tectonics*

Gregori, G. P., B. A. Leybourne, W. Soon, and V. Straser, 2025e. The heuristic meaning of variational principles. In press in *New Concepts in Global Tectonics, Journal*

Hillier, J. K., 2006. Pacific seamount volcanism in space and time. *Geophysical Journal International*, 168 (2): 877-889; DOI:10.1111/j.1365-246X.2006.03250.x

Hillier, J. K., and A. B. Watts, 2007. Global distribution of seamounts from ship-track bathymetry data, *Geophysical Research Letters*, 34: L13304; DOI:10.1029/2007GL029874

Jansen, E., J. Overpeck, K. R. Briffa, J.-C. Duplessy, F. Joos, V. Masson-Delmotte, D. Olago, B. Otto-Bliesner, W. R. Peltier, S. Rahmstorf, R. Ramesh, D. Raynaud, D. Rind, O. Solomina, R. Villalba, and D. Zhang, 2007. Palaeoclimate. In *S.* Solomon, D. Qin, M. Manning, Z. Chen, M. Marquis, K.B. Averyt, M. Tignor and H.L. Miller (eds.), *Climate Change 2007: the Physical Science Basis. Contribution of Working Group I to the Fourth Assessment Report of the IPCC*. Cambridge University Press, Cambridge and New York; pp: 433-497

Khorhonen, J. K., J. D. Fairhead, M. Hamoudi, K. Hemant, V. Lesur, M. Mandea, S. Maus, M.E. Purucker, D. Ravat, T. Sazonova, and E. Thébault, 2007. *Magnetic Anomaly Map of the World-Carte des Anomalies Magnétiques du Monde. Scale: 1:50,000,000*, 1st edn., Commission for the Geological Map of the World

Kilburn, C. R. J., G. De Natale, and S. Carlino, 2017. Progressive approach to eruption at Campi Flegrei caldera in southern Italy. *Nature Communications*, 8: 15312; DOI:10.1038/ncomms15312

Kilburn, C. R. J., S. Carlino, S. Danesi, and N. A. Pino, 20232024. Potential for rupture before eruption at Campi Flegrei caldera, Southern Italy. *Communications Earth Environment*, 4: 190; DOI: 10.1038/s43247-023-00842-1

Lanzerotti, L. J., and G. P. Gregori, 1986. Telluric currents: the natural environment and interactions with man-made systems. In E. P. Krider, and R.G. Roble, (eds), *The Earth's Electrical Environment*, National Academy Press, Washington, D. C.; DOI:10.17226/898, pp.: 232-257

Leybourne, B. A. and G. P. Gregori, 2020. Introduction to plasma tectonics & electric geology: solar wind coupling to planetary circuits lightning tells the stellar transformer story, *Journal of Systemics, Cybernetics and Informatics*, pp.: 7-13 https://www.iiisci.org/journal/sci/FullText.asp?var=&id=ZA424OY20

Leybourne, B. A., and N. C. Smoot, 1997. Ocean basin structural trends based on GEOSAT altimetry data. In *Ocean Technology at Stennis Space Center*, Proceedings of the Gulf Coast Chapter Marine Technology Society, pp: 135-140

Leybourne, B. A., D. W. Johnson, and G. P. Gregori, 2025. Arc-blast as static electricity or interplanetary lightning short circuits in Stellar Transformers. A plausible North American scenario, *New Concepts in Global Tectonics, Journal*, 13, (2): 229-251

Leybourne, B. A., J. M. Davis, G. P. Gregori, J. M. Quinn, and N. C. Smoot, 2017. Evolution of Earth as a Stellar Transformer, *New Concepts in Global Tectonics Journal*, 5 (1): 144-155

Longo, L. M., R. De Ritis, G. Ventura, G., and M. Chiappini, 2016. Analysis of the aeromagnetic anomalies of the Auca Mahuida volcano, Patagonia, Argentina, *Pure and Applied Geophysics*, 173 (10): 3273–3290; DOI:10.1007/s00024-015-1161-3

Marova, N. A., 2002. Seamounts of the world ocean, *Oceanology*, 42 (3): 409-413

Maus, S., F. Yin, H. Lühr, C. Manoj, M. Rother, J. Rauberg, I. Michaelis, C. Stolle, and R. D. Müller, 2008. Resolution of direction of oceanic magnetic lineations by the sixth-generation lithospheric magnetic field model from CHAMP satellite magnetic measurements. *Geochemistry, Geophysics, Geosystems*, 9 (7): Q07021; https://doi.org/10.1029/2008gc001949

Maus, S., U. Barckhausen, H. Berkenbosch, N. Bournas, J. Brozena, V. Childers, F. Dostaler, J. D. Fairhead, C. Finn, R. B. von Frese, C. Gaina, S. Golynsky, R. Kucks, H. Lühr, P. Milligan, S. Mogren, R. D. Müller, O. Olesen, M. Pilkington, R. Saltus, B. Schreckenberger, E. Thébault, and F. Caratori Tontini, 2009. EMAG2: a 2-arc-minute resolution Earth Magnetic Anomaly Grid compiled from satellite, airborne and marine magnetic measurements, *Geochemistry, Geophysics, Geosystems*, 10: Q08005; https://doi.org/10.1029/2009gc002471

Menard, H. W., 1964. *Marine Geology of the Pacific*. McGraw-Hill Book Co., New York; pp:1-271

Meyerhoff Hull, D., (ed.), 1996. *Surge tectonics: a new hypothesis of global geodynamics*. Kluwer Academic Publ., Dordrecht, etc.; pp: 1-348

Meyerhoff, A. A., and H. A. Meyerhoff, 1972. The new global tectonics: major inconsistencies, *American Association of Petroleum Geologists Bulletin*, 56 (2): 337–359. https://doi.org/10.1306/819a3e5c-16c5-11d7-8645000102c1865d

Meyerhoff, A. A., and H. A. Meyerhoff, 1972a. The new global tectonics: age of linear magnetic anomalies of ocean basins. *American Association of Petroleum Geologists Bulletin*, 52 (2): 337-359

Meyerhoff, A. A., and H. A. Meyerhoff, 1974. Tests of Plate Tectonics, *Special volume of the Bulletin of the American Association of Petroleum Geologists*, 56: 269-336

Meyerhoff, A. A., I. Taner, A. E. L. Morris, B. D. Martin, W. B. Agocs, and H. A. Meyerhoff, 1992. Surge tectonics: a new hypothesis of Earth dynamics. In Chatterjee, and N. Hotton III (eds), *New concepts on global tectonics*, Texas Technical University Press, Lubbock, TX; pp: 309-409

Meyerhoff, A. A., I. Taner, A. E. L. Morris, W. B. Agocs, D. Meyerhoff Hull, M. Kamen-Kaye, M. I. Bhat, N. C. Smoot, D. R. Choi, 1996. Surge tectonics. In D. Meyerhoff Hull, (ed.), *Surge Tectonics: a New Hypothesis of Global Geodynamics*. Kluwer Academic Publ., Dordrecht, etc.; Vol. 9, Springer Verlag, Berlin etc.; pp: 68-123

Meyerhoff, A. A., I. Taner, A. E. L. Morris, W. B. Agocs, D. Meyerhoff Hull, M. Kamen-Kaye, M. I. Bhat, N. C. Smoot, D. R. Choi, 1996a. *Surge tectonics: a new hypothesis of global geodynamics*, Springer Verlag, Berlin etc. ISBN 0792341562, 9780792341567; pp: 1-323

Moretti, R., G. De Natale, and C. Troise, 2017. A geochemical and geophysical reappraisal to the significance of the recent unrest at Campi Flegrei caldera (Southern Italy). *Geochemistry, Geophysics, Geosystems*, 18 (3): 1244-1269; DOI:10.1002/2016GC006569

Müller, R. D., M. Sdrolias, C. Gaina, and W. R. Roest, 2008. Age, spreading rates and spreading symmetry of the world's ocean crust, *Geochemistry, Geophysics, Geosystems*, 9 (4): Q04006; https://doi.org/10.1029/2007gc001743

Paoletti, V., A. Rapolla, and M. Secomandi, 2008. Magnetic signature of submarine volcanoes in the Phlegrean Fields-Ischia ridge (north-western side of the Bay of Naples, southern Italy), *Annals of Geophysics*, 51 (4): 575-584

Paoletti, V., R. Supper, M. Chiappini, M. Fedi, G. Florio, and A. Rapolla, 2005. Aeromagnetic survey of the Somma-Vesuvius volcanic area, *Annals of Geophysics*, 48 (2): 199-213

Pester, 2024. Major 'magnetic anomaly' discovered deep below New Zealand's Lake Rotorua, *Space.com, News*, issued February 4th 2024

Pollack, H. N., and D. S. Chapman, 1977. On the regional variation of heat flow, geotherms, and lithospheric thickness. *Tectonophysics*, 38: 279–296

Pollack, H. N., and D. S. Chapman, 1977a. The flow of heat from the Earth interior. *Scientific American*, 237 (2): 60-76

Pollack, H. N., S. J. Hurter, and J. R. Johnson, 1993. Heat flow from the Earth's interior: analysis of the global data set. *Reviews of Geophysics*, 31 (3): 267-280; https://doi.org/10.1029/93rg01249

Purucker, M. E., 2007. Magnetic anomaly map of the world, *EOS, Transactions of the American Geophysical Union*, 88 (25): 263-263. https://doi.org/10.1029/2007eo250003

Quinn, J. M.,† G. P. Gregori, and B. A. Leybourne, 2025. Satellite monitoring of air-earth currents. In press in *New Concepts in Global Tectonics, Journal*

Sabaka, T. J., N. Olsen, and M. E. Purucker, 2004. Extending comprehensive models of the Earth's magnetic field with Ørsted and CHAMP data, *Geophysical Journal International*, 159: 521-547;

https://doi.org/10.1111/j.1365-246x.2004.02421.x
Smoot, N. C., 1989. The Marcus-Wake seamounts and guyots as paleofracture indicators and their relation to the Dutton Ridge, *Marine Geology*, 88 (1/2): 117-131
Smoot, N. C., 1994. Plate-wide Pacific trends--orthogonal fracture intersections, *EOS, Transactions, of the American Geophysical Union*, 75 (25): 69
Smoot, N. C., 1995. The Chinook Trough: a trans-Pacific fracture zone, in *Proceedings of the Third Thematic Conference on Remote Sensing for Marine and Coastal Environments*, Vol. II, pp.: 539-550
Smoot, N. C., 1997. Magma floods, microplates, and orthogonal intersections, *New Concepts in Global Tectonics Newsletter*, (5): 8-13
Smoot, N. C., 1998. WNW-ESE Pacific lineations, *New Concepts in Global Tectonics Newsletter*, (9): 7-11
Smoot, N. C., 1998a. The trans-Pacific Chinook Trough megatrend, *Geomorphology*, 24 (4): 333-351
Smoot, N. C., 1999. Orthogonal intersections of megatrends in the Western Pacific Ocean basin: a case study of the Mid-Pacific Mountains, *Geomorphology*, 30: 323-356
Smoot, N. C., 2012. North-central Pacific basin lineaments and mobilism: Really? *New Concepts in Global Tectonics Newsletter*, (62): 5-21
Smoot, N. C., and B. A. Leybourne, 1997. Vortex structures on the world-encircling vortex street: Case study of the South Adriatic basin, *Marine Technology Society Journal*, 31 (2): 21-35
Smoot, N. C., and B. A. Leybourne, 2001. The Central Pacific megatrend. *International Geology Review*, 43 (4): 341-365
Smoot, N. C., and B. A. Leybourne, 2020. Orthogonal megatrend intersections: "coils" of a Stellar Transformer. *Journal of Systemics, Cybernetics and Informatics*, 18 (4): 61-66; https://www.iiisci.org/journal/sci/FullText.a
Smoot, N. C., and D. R. Choi, 2003. The North Pacific megatrend, *International Geology Review*, 45 (4): 346-370
Smoot, N. C., and K. J. Heffner, 1986. Bathymetry and possible tectonic interaction of the Uyeda Ridge with its environment, *Tectonophysics*, 124 (1/2): 23-36; https://doi.org/10.1016/0040-1951(86)90135-6
Supper, R., R. de Ritis, K. Motschka, and M. Chiappini, 2004. Aeromagnetic anomaly images of Vulcano and southern Lipari islands (Æolian archipelago, Italy), *Annals of Geophysics*, 47 (6): 1803-1810
Thébault, E., M. Purucker, K.A. Whaler, B. Langlais, and T. J. Sabaka, 2010. The magnetic field of the Earth's lithosphere, *Space Science Review*, 155 (1/4): 95–127. https://doi.org/10.1007/s11214-010-9667-6
Torrent Tucker, D., 2025. Scientists may have found a way to stop Italy's awakening supervolcano, *SciTechDaily*, issued May 20, 2025
van Bemmelen, R.W., 1972. *Geodynamic models. An Evaluation and a Synthesis*. Elsevier Publ. Co., Amsterdam etc., 2; pp.: 1-267
Vanorio, T., D. Geremia, G. De Landro, and Tianyang Guo, 2025 The recurrence of geophysical manifestations at the Campi Flegrei caldera", *Science Advances*; DOI:10.1126/sciadv.adt2067
Ventura, G., G. Vilardo, G. Milano, N. A. Pino, 1999. Relationships among crustal structure, volcanism and strike–slip tectonics in the Lipari-Vulcano volcanic complex – Aeolian Islands, southern Tyrrhenian sea, Italy, *Physics of the Earth and Planetary Interiors*, 116: 31–52; DOI:10.1016/S0031-9201(99)00117-X
Wessel, P., 2001. Global distribution of seamounts inferred from gridded Geosat/ERS-1 altimetry, *Journal of Geophysical Research*, 106: 19,431-19,441
Wessel, P., and S. Lyons, 1997. Distribution of large Pacific seamounts from Geosat/ERS-1, *Journal of Geophysical Research*, 102: 22459-22475
Wu, Hong-chun, 2025. Jet stream's disturbances as possible precursors of earthquakes, preprint

Acronyms

AE – acoustic emission
AGU – American Geophysical Union
ALB - asthenosphere lithosphere boundary).
CFDDP - Campi Flegrei Deep Drilling Project
CI - Campanian Ignimbrite
CMB – core-mantle boundary
CNR- Consiglio Nazionale delle Ricerche
CVL - Cameroon Volcanic Line
d.o.f. - degree of freedom
DC – direct current
DC – direct current
DInSAR - Synthetic Aperture Radar Differential Interferometry
DSDP - Deep-Sea Drilling Project
DSS - Deep Seismic Sounding (program)
DUPAL –Dupré-Allègre (basalt isotopic chemism anomaly)
EMAG2 - Global Earth Magnetic Anomaly Grid
EPR - East Pacific Rise
ESI - electric soldering iron (process).
FR – field reversals (geomagnetic)
FZ - fracture zone
GEOSAT - GEOdetic SATellite; a former *US Navy Earth* observation satellite, launched on March 12, 1985
GPS – Global Positioning System
IAMC - Istituto per l'ambiente marino costiero
INGV – Istituto Nazionale di Geofisica e Vulcanologia
LVVC - Lipari-Vulcano volcanic complex
MAR - Mid Atlantic Ridge
MOR - mid-ocean ridge
NH – northern hemisphere
NYT - Neapolitan Yellow Tuff
SH – Southern Hemisphere
STEP - subduction-transform edge propagators
TD - tide-driven (dynamo)

ISSN number; ISSN 2202-0039

VT - volcano-tectonic (seismicity)
WDMAM - World Digital Magnetic Anomaly Map
WGS-84 - World Geodetic System, 1984 ellipsoid
WMT - warm mud tectonics

NCGT Journal
New Concepts in Global Tectonics

New Concepts in Global Tectonics Journal
Volume 13, Number 6, August 2025

ISSN number; ISSN 2202-0039

Lightning in volcanic plumes

Giovanni Pietro Gregori[1], Bruce Allen Leybourne[2], Ugo Coppa[3], Giuseppe Luongo[4]

[1] Former Senior Researcher at *IDASC-Institute of Acoustics and Sensors O. M. Corbino (CNR), Rome,* now merged with the *INM-Institute of Marine Engineering "Section of Acoustics and Sensors O.M. Corbino"- (CNR Rome)*; and *ISSO-International Seismic Safety Organization*, Italy
[2]*GeoPlasma Research Institute-(GeoPlasmaResearchInstitute.org),* Aurora, CO 80014, USA
[3]*Researcher at INGV – Osservatorio Vesuviano*
[4] Emeritus Professor of Physics of Volcanism at the *University Federico II* in Naples, Associate of INGV – *Osservatorio Vesuviano* - Former Director of the *Osseratorio Vesuviano*

Corresponding Author: G.P. Gregori, *DASC-Istituto di Acustica e Sensoristica O. M. Corbino (CNR)*, Roma, now merged into *IMM-Istituto per la Microelettronica e Microsistemi (CNR)*; B.A. Leybourne, *GeoPlasma Research Institute-(GeoPlasmaResearchInstitute.org)*; U. Coppa, *Osservatorio Vesuviano;*G. Luongo, *Osservatorio Vesuviano*
Email:
giovannipgregori38@gmail.com
leybourneb@iascc.org;
ugo.coppa@ingv.it;
luongius@unina.it

Dedication: We dedicate this paper to the memory of Luigi Palmieri (1807-1896), the second historical and glorious Director of the *Osservatorio Vesuviano*, in charge from December 1854 until his death, at a time of great political difficulties that followed the fall of Napoleon. Luigi Palmieri was a true scientist, who observed phenomena with unprecedented instruments and approach. His studies were later forgotten but are still up to date. We want to pay homage to his contributions, which represent a forgotten benchmark in volcanology.

Abstract: A volcanic plume is the prolongation above Earth's surface of the underground electrical circuit, up to the ionosphere, where, as a standard, a positive charge is located. A plume is highly ionized, hence very conducting. No visible lightning can occur inside it, rather visible lightning occur on its boundaries. Inside the plume a large friction occurs between the components of pyroclastic. However, owing to the high temperature, the great availability of free electrons determines an immediate short-circuiting of every potential difference, through micro-discharges that are the source for a radio emission, while the plume is totally opaque and no micro-spark can be observed. Hence, visible lightning can be observed only at the boundaries of the plume. A plume contains free electrons, and both positive and negative ions and ash particles. Electrons immediately short-circuit the plume with the ionosphere, through "*e*"-discharges and an ensemble of comparatively smaller lightning. Positive ions and particles are pushed downward by gravity and by electrostatic repulsion from the ionosphere. In contrast, negative ions, or particles "float" in air, due to the competing role of gravity and of the upward electric field. Wind occasionally blows them far from the vent. Then, they eventually fall down and cause an intense lightning of the kind that is here called an "*ion*"-discharge. The current interpretation of volcanic plume lightning is biased by an incorrect current model for the atmospheric electrical circuit, which neglects the crucial role of the Cowling dynamo, which transforms the huge kinetic energy of cloud convection cells into electromagnetic (e.m.) energy By this, the phenomenon is primarily responsible for the positive charge of the ionosphere. Some astute and precise measurements by the second Director of the *Osservatorio Vesuviano*, Luigi Palmieri, which were later forgotten, were on the right path of discovery. In contrast, the current interpretation of volcanic plumes gives no justice for the precursory Palmieri's investigations. The entire topic is here reset, with a specific discussion mainly of the Surtsey eruption in 1963-1964 that was carefully investigated also by records of atmospheric electric field. Several additional case histories are also shown in the Appendix. A mention is given also about volcanic rings, as they are closely related to the Cowling dynamo mechanism, which is a leading anthem in the present set of papers concerning air-earth currents. The Appendix A shows set of examples of

NCGT Journal
New Concepts in Global Tectonics

New Concepts in Global Tectonics Journal
Volume 13, Number 6, August 2025

ISSN number; ISSN 2202-0039

lightning in volcanic plumes, chosen among several pictures available in the literature or on the web.

Keywords: volcanic plume; lightning; ionosphere; "*e*"-discharge and "*ion*"-discharge; Luigi Palmieri; Vesuvius 1944; Surtsey 1963-1964; radio lightning discharges; flight security; Mount Spurr 1992; electrification by friction; volcanic rings

Introduction

Several clear - although generally unnoticed - morphological features are observed at Earth's surface. We first recall about the origin of endogenous heat, and about how it is transferred to - and released at - Earth's surface, according to the sea-urchin pattern. Another related topic deals with geomagnetic anomalies, which are a twofold general and diffuse proxy. On the one hand, every volcano is characterized by a "double-eye" pattern, on the other the general appearance of positive/negative alignments are a clear hunch for large-scale flow of telluric currents, on the secular time-range. Geomagnetic anomalies are discussed in separate articles (Gregori et al., 2025r, and Gregori et al., 2025s). We discuss here volcanic plumes as an extension into the atmosphere of sea-urchin spikes that supply the volcano, while a volcano is a "catastrophic" manifestation of air-earth currents. We also stress a few other more or less spectacular effects. The present generally agreed interpretation of volcanism seems to forget about these proxies.

The Moho (Fig. 1) is defined by a transition between a lower-to-higher speed of seismic waves, consistently (perhaps) with a different water concentration in ground. Typical velocities of primary seismic waves (P-waves) are consistent, above the Moho, with those through basalt ($6.7-7.2\ km\ sec^{-1}$), while below they are similar to those through peridotite or dunite ($7.6-8.6\ km\ sec^{-1}$). See Gregori and Hovland (2025).

The asthenosphere is the upper layer of the mantle and can be associated - or identified with - the serpentosphere, i.e., the layer of unknown thickness where water penetrates through dehydrated rocks and has streamflow properties like oceans and atmosphere from embedded e.m. currents. The chemical reaction, i.e., serpentinization, produces hydration and high fracturing of rocks, which are embedded in supercritical water. Thus, the asthenosphere has a high electrical conductivity σ. Therefore, the electric currents that originate in deep Earth tend to expand as much as possible, due to Hamilton's variation principle (see Gregori et al., 2025e).

Owing to the increasing gravitational compression, the trend of temperature is to increase *vs.* depth through the mantle. The higher temperature produces an increasing ionization, i.e., free electrons that are extracted from progressively deeper atomic shells. Electrons are stripped from their respective nucleus. The state-of-matter is no longer solid – such as in the crust - because crystalline bonds no more exist. The large availability of electrons makes the medium highly conductive - i.e., the state of matter is similar to the interior of a large planet, such as it occurs inside Jupiter where the state is conventionally called "metallic". The Earth's mantle is therefore a fluid of decreasing viscosity *vs.* depth, being in a state that more correctly is "metallic". The outer core (*OC*) is basically completely fluid, or "metallic", and it is observed by the absence of S waves that cannot propagate. In any case, the electrical conductivity σ in the deep Earth's interior can be estimated only with large error-bars, by means of computations of induced electromagnetic (e.m.) currents of very, very low frequency waves (see Gregori, 2002, and references therein).

When atomic nuclei are "naked" - as they are completely stripped of their electrons - the "naked" nuclei interact through their nuclear magnetic moments, although present theoretical physics has still several uncertainties concerning the detailed interaction mechanism (see, however, Gregori et al., 2025w). The state-of-matter is very compact and characterized by cohesion forces much stronger that crystalline (or chemical) bonds. Owing to the complete absence of electrons, electrical conductivity σ is null. At the same time, nuclei experience a strong electrostatic repulsion. However, they are compressed by gravitation, while the attraction by nuclear magnetic moments overwhelms Coulomb's repulsion. Thus, this state-of-matter can be called "*magpol*" state, acronym for magnetic-polarized state. All nuclear magnetic moments therefore result into some kind of compacted "fibrous" pattern, due to the alignment of magnetic moments. The magpol state releases no photons, i.e., it is "dark matter".[1] Thus, the inner core (*IC*) is the source for the leading part of the observed geomagnetic field, i.e., of the dipole field.

[1] The concept of "dark matter" has much wider implications, referring to the whole realm of elementary particles and cosmology (see Gregori et al., 2023w for some additional detail).

NCGT Journal
New Concepts in Global Tectonics

New Concepts in Global Tectonics Journal
Volume 13, Number 6, August 2025

ISSN number; ISSN 2202-0039

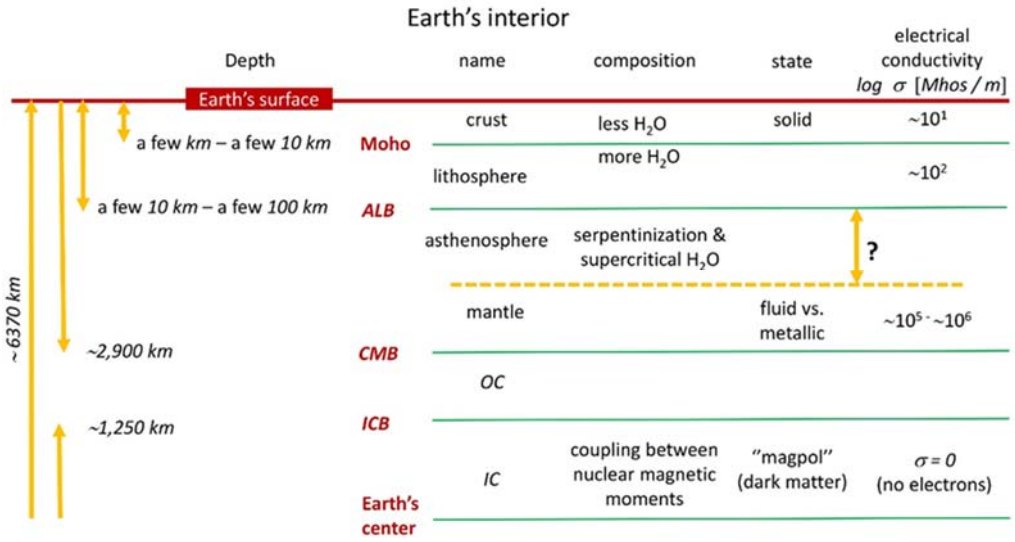

Fig. 1 – Indicative terms here adopted to describe the Earth's interior. No general agreement exists in the literature. The present figure aims to indicate what every term means here, the only purpose being to avoid misunderstanding, with no presumption that this is the correct definition. Note the, depending on whether it is below a Mid-Ocean Ridge (*MOR*) or under a continent, Moho is generally defined as a transition zone just above the mantle within the upper asthenosphere under *MOR*s, while under continents Moho is within the lithosphere. One should consider, however, that *MOR*s cannot by compared either to ocean floors or to continental lithosphere. In fact, *MOR*s, as an observational matter-of-fact, is the locus where the geomagnetic secular variation (*SV*) is neither westward, neither eastward (Janackova et al. 1989; Janackova and Urban, 1990; Urban and Janackova, 1990; Gregori, G.P., 1993). Obviously, every geodynamic model (plate tectonics, surge tectonics, wrench tectonics, etc.) speculates some explanation. However, the present paper is not suited for such an extensive review. This figure aims only to explain the meaning of terms, according to the choice made in the present set of papers. Conversely, the reference model in the present set of papers is a different focus, and is irrelevant for the discussion of visible lightning in volcanic plumes. In any case, the reference model here used is *warm-mud tectonics* (*WMT*). Therefore, *MOR*s are located on top of superswells, and the regions - that according to plate tectonics are plate boundaries - are here considered like regions of higher fracturing, so that serpentinization can more freely propagate (Gregori and Hovland, 2014), while *MOR*s are explained by sea-urchin spikes (Gregori and Leybourne, 2021), and serpentinization plays a secondary role, if any role at all. Unpublished figure.

Different components of the planet Earth move with respect to one another, due to the varying tidal forces and to the non-compact structure of the planet. Since various Earth's components are ionized, this process amounts to operate like a dynamo, i.e., this is the tide-driven (*TD*) dynamo. The energy balance (Gregori, 2002) is impressive (see Fig. 3 and Table 1 in Gregori et al., 2025a).

Another observational hunch derives from the so-called spatial spectrum of the geomagnetic field $\boldsymbol{B}$ (Lowes, 1974), as expressed by the Lowes-Nevanlinna's (*LN*'s) plot (Gregori, 2002, Fig. 2). When air-earth currents can be neglected (see Gregori et al., 2025a), the $\boldsymbol{B}$ observed at Earth's surface (i.e., at $r = a$) can be described by means of a potential, which is expressed in terms of a spherical harmonic expansion (*SHE*). Every term of the expansion is denoted by a couple of indices (i.e. degree n and order m), with coefficients g_n^m and h_n^m that, in principle, can be arbitrary. In contrast, from a physical viewpoint, their trend *vs.* n and m reflects the physics of the dynamo. The m dependence reflects the choice of the frame of reference, unlike the n dependence, which is invariant with respect to change of reference.

Fig. 2 displays on abscissas n and on ordinates its corresponding associated fraction of $\boldsymbol{B^2}$, when measured at $r = a$ and averaged over the entire planet (i.e., it is proportional to the mean magnetic energy density associated to all *SHE* terms of degree n). Such a fraction is defined by considering, once at a time, every contribution by all terms, and for every fixed n by summing up over all $m = 0, 1, \ldots, n$. The *SHE* considered in Fig. 2 is based on the $\boldsymbol{B}$ records collected by the *MAGSAT* satellite, epoch 1979.85, which are well suited for getting rid of the bias by crustal sources (Gregori *et al*., 1999).

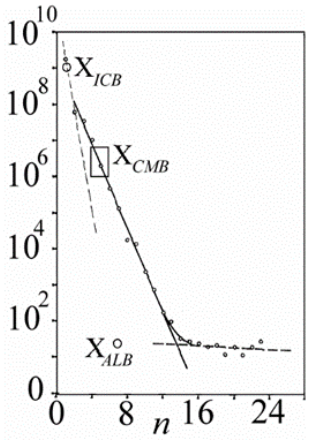

Fig. 2 - Figure redrawn after Gregori *et al*. (2000c) and Gregori (2002). See text for explanation. *ESA* copyright free policy, and kind permission of the late Wilfried Schröder.

NCGT Journal
New Concepts in Global Tectonics
New Concepts in Global Tectonics Journal
Volume 13, Number 6, August 2025
ISSN number; ISSN 2202-0039

All points result to be aligned along *3* straight lines. One line through $n = 1, 2$ is called *Nevanlinna's line*, (formerly envisaged by Nevanlinna, 1987), and it is denoted by an index $k = 0$. The line $k = 1$ is called *first Lowes' line* and it goes through points with $n = 3, 4, \ldots, 13$. The third line, $k = 2$, is called *second Lowes' line* and it goes through points with $n = 14, \ldots$ The three lines altogether are called *LN* lines (Gregori, 2002).

The energy balance can be computed by considering that every electric current $\boldsymbol{j}$, which is generated inside deep Earth, must expand as much as possible (by Hamilton's, see Gregori et al., 2025e). Therefore, assume that the three lines in Fig. 2 correspond to three spherical shells (*ss*) of currents that are thus defined like equivalent circuits suited for energy computation. Compute the $\boldsymbol{j}$ that must flow on every respective *ss*, and compute the associated energy, which is function of the radius of the *ss*. It is thus found that the energy diverges for an asymptote.

The radius of the asymptote – which is related to the tilt of every *LN* line – is surprisingly found to correspond to the lower bound for the (seismically determined) radii R_{ICB}, R_{CMB}, and R_{ALB}, respectively, of *ICB* $(k = 0)$, *CMB* $(k = 1)$, and *ALB* $(k = 2)$. The difference between every asymptote and the corresponding seismically determined radius is just a very few percent.

When considering *SHE*s that refer to different epochs, it is found that the tilt of every line change *vs.* time, even by some relevant amount. However, every such "historical" line always results to cross through some fixed cross-point denoted in Fig. 2 as X_{ICB}, X_{CMB}, and X_{ALB}, respectively. This implies that every line ought to be associated to some relevant change of the internal structure of the Earth, although always allowing for one specific n, and a corresponding energy contribution by that given n, that results invariant in time.

The energy argument can be easily explained and understood as far as R_{CMB} and R_{ALB} are concerned, as they correspond to the stepwise change of electrical conductivity σ (Fig. 1), because the $\boldsymbol{j}$ expand and decay by Joule heat. In contrast, it is interesting to note that the difference between R_{ICB} and the seismically determined *IC* radius is a slightly larger percent than for R_{CMB} and R_{ALB}. In fact, R_{ICB} depends on the maximum and unknown compressibility of matter in the magpol state of the *IC*.

During the last few centuries the values of R_{ICB} changed by a relevant amount (see Fig. 6 of Gregori et al., 2025a), denoting that the energy that is produced by the *TD* dynamo is stored inside the Earth's "battery", through a change of the state-of-matter from the metallic state of the *OC* to the magpol state of the *IC*, and viceversa (see Gregori and Leybourne, 2021, and Gregori et al., 2025a).

Energy transfer to Earth's surface

Refer to a given *ss* (e.g., the *CMB*), and consider some minor bump with respect to perfect spherical symmetry (Fig. 3). Owing to Hamilton's (see Gregori et al., 2025e), the currents $\boldsymbol{j}$ tend to concentrate on the top of such a bump, where they release a comparatively larger amount of Joule heat. Since the local thermal conductivity is very low, such a heat cannot propagate. Hence, the local temperature increases, and by it also the local electrical conductivity σ, by which, owing to Hamilton's, an additional and ever-increasing amount of $\boldsymbol{j}$ can concentrate on the top of the bump. The process is therefore self-amplifying.

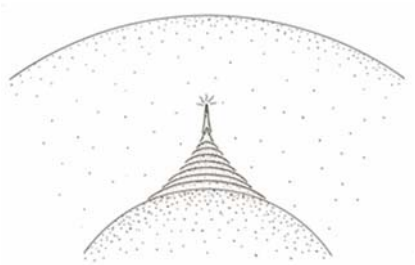

Fig. 3 - Consider a given *ss* inside the Earth (e.g., the *CMB*), and some minor bump with respect to perfect spherical symmetry. See text. After Gregori (1993, 2002). With kind permission of *Physics of the Earth and Planetary Interiors* (GPG is co-author).

The result is that the mechanism looks much like in the case of an *"electric soldering iron"* (*ESI*) that is pushed into a block of ice. The entire Earth ought thus to be depicted, in terms of the mass density, almost reminding about an onion - and in terms of σ almost reminding about a "sea urchin" or an "octopus", with every spike that shrinks while propagating upward. It must be clearly stressed that several sea-urchin spikes can rise at the same time from the *CMB*. However, owing to the same mechanism of Fig. 3, they cannot be very close to each other. Their distance must be at least as large as the distance of two starting large - and low-elevation - bumps from the *CMB*. Otherwise, all currents that supply the *ESI* mechanism contribute to supply the first-born spike. The interaction between sea-urchin spikes is specifically discussed in Gregori and Leybourne (2021).

It can be shown (see Fig. 7 of Gregori et al., 2025a) that the mean speed of upward propagation is $\sim 10\ cm\ year^{-1}$. It ought to be stressed that such a propagation strictly implies no transport of matter (no magma, no ions, etc.), rather only - and strictly only – transport of conduction charges (electrons). That is, the process is merely electrodynamic, rather than thermodynamic.

It should be stressed that $\boldsymbol{j}$ flows along the spike like a DC current - and owing to the Cowling dynamo (see Gregori et al., 2025d) it also experiences a self-collimation effect (Fig. 4).

The sea-urchin spikes have a twofold implication. On the one hand, they transfer energy from deep Earth up to Earth's surface, through a flow of electrons that move at a speed comparable to light speed. On the other, the spikes act like effective antennæ that permit e.m. coupling between deep Earth and the e.m. field induced by the solar wind, by getting rid of the Faraday screening represented

New Concepts in Global Tectonics Journal
Volume 13, Number 6, August 2025
ISSN number; ISSN 2202-0039

by the outer Earth's layers. This justifies the solar control on volcanism (Gregori, 2002; Gregori and Leybourne, 2021).

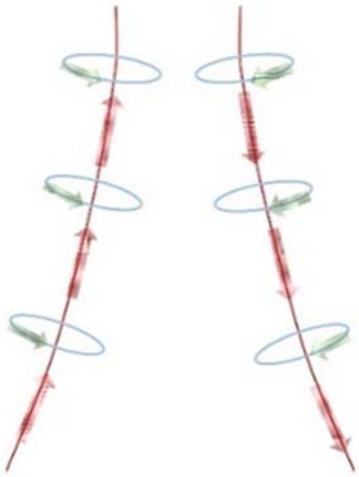

Fig. 4 - Self-collimation, due to the Cowling dynamo, of the electric current that flows on one given side of a sea-urchin spike. Unpublished figure. See text.

When a "spike" of the sea-urchin approaches Earth's surface, as soon as it finds some fluids (water, oil, CO_2, CH_4, geogas, etc.), such fluids transport heat by advection and exhalation - thus eventually ensuring the energy balance. In contrast, when the available fluids are insufficient, the local system warms up, and the "spike" further propagates upward, until it reaches some comparatively shallow depth where the equation-of-state, and the reduced lithostatic pressure, allows for melt. Thus, an additional fluid is formed, i.e., magma that samples, therefore, the chemism of the layer where it is formed (see Gregori et al., 2025a). The magma can now operate much like any other fluid, in the fact that, through an eruption, it transports heat by advection.

Differently stated, the former mere electrodynamic process, as soon as some fluid (lava or other) is available, transforms into a fluid- and thermo-dynamic process. This whole process inside a volcano can be called the "calorimetric" explanation of volcanism. Note that the so-called magma chamber is only a strictly local phenomenon, and no connection exists between magma chambers of different volcanoes.

A typical feature of every volcano is represented by the geomagnetic anomalies that display a double-eye pattern (see Gregori et al., 2025r). The $\boldsymbol{B}$, which is generated, causes a local geomagnetic anomaly of opposite sign on either side of the "horizontal" segment of such a circuit.

Lightning and volcanic plumes

Several morphological features of volcanic plumes are a physically significant and expressive check of such an entire rationale. Several details can be easily explained, that – according to every other explanation of volcanism – are generally reported like a mysterious feature.

A short reminder about previous investigations on lightning discharges in volcanic plumes is as follows. Lightning discharges in volcanic plumes deal with a very large, catastrophic amount of energy. McNutt and Davis (2000) contain a detailed list (also given, and adapted, by Mather and Harrison, 2006) of *55* volcanoes that - either on one or on several occasions - displayed lightning discharges during an eruption. They complain that this is "*a common yet poorly studied phenomenon*". At present, these very spectacular happenings are generally reported as being intuitively explained because of friction electricity that eventually generates electric fields $\boldsymbol{E}$. Authors often mention rock fracturing that they claim is caused by magma pressure, with eventual contribution by water, etc. They suppose that rock fragments, ash, and ice particles collide inside the plume and generate static charges, just like ice particles that collide and create charge in regular thunderstorms (i.e., this is part of the so-called "cloud generator"; see Gregori and Leybourne, 2025e).

For instance, Mather and Harrison (2006) make a review and claim that both remote sensing and surface observations of the atmospheric electric potential gradient - altogether with the electric charge of volcanic ash - show that a substantial electrification is present in volcanic plumes, independent of the occurrence of lightning. Little evidence seems to be related to ash composition. They refer to different conceptual theories, although they claim that the ash fragmentation mechanism seems to be a key process. However, it is unclear what effect is dominant in every different case history. They stress, however, that electrostatics are a dominant factor for the control of dry fall-out of ash from a volcanic plume. The electrical impact of a volcanic plume may also affect the global atmospheric electrical circuit – hence, in the case of violent eruptions, also global climate and local meteorological conditions. They also comment that the local hazard is generally low compared to other volcanic impacts.

These explanations, however, look vague, intuitive, and *ad hoc*. On the other hand, according to the general framework of the present general understanding of atmospheric phenomena, no explanation seems to be seemingly possible other than in terms of speculation. In contrast, we propose a new original explanation that seems supported by observational evidence.

A concern is about justifying the fact that some volcanoes produce lightning while others don't - and that some volcanoes with large dusty plumes produce little or no lightning, while others with small or mediocre plumes produce much lightning.

We propose a seemingly better inference in the framework of the model that is here envisaged in terms of an atmospheric condenser supplied at both capacitance plates (see Gregori et al., 2025a, and Gregori and Hovland, 2025). In addition, the very large spatial gradient plays a key role, of the electrical conductivity σ through the plume. This model is also capable of explaining several observed features that, to our knowledge, previous models cannot explain.

The occurrence of lightning inside a volcanic plume is

ISSN number; ISSN 2202-0039

not determined by the volcanic eruption *per se*, rather it depends on two items. *(i)* A primary control factor is the electrostatic state of the ionosphere, either locally or inside some larger spatial range around the volcano. In addition, *(ii)* the eventual presence is crucial of a sea-urchin spike, which is likely to be an (almost) ubiquitous occurrence in a volcano - although on some occasion it can be less effective in terms of soil/ionosphere coupling.

As far as the underground σ structure is concerned that characterizes a given volcano, all volcanoes are not analogous to one another. Every two different volcanoes can be characterized by eventually quite different primary heat sources. Joule heat is the primary supply of hotspot volcanism, while friction heat supplies island arc volcanoes. Island arc volcanoes, however, have their own electric circuit, because their primary heat source produces magma melt, and ionization, hence conduction charges, etc. However, island arc volcanoes show no specific correlation with geomagnetic patters, and are therefore very likely to derive from mere friction heat, according to the mechanisms of Figs 9 and 10 of Gregori et al. (2025a) - and consistently with the evidence that also the Hawai'i hotspot volcanism has a ~50,000-100,000 years delay with respect to the increase of kinetic energy of the lithospheric slab (Gregori, 2002; Gregori and Leybourne, 2021; Gregori et al., 2025n). In contrast, the electric circuit of a hotspot volcano is directly powered by the deep *TD* geodynamo – while, in the case of a volcano supplied by friction heat, the source is much shallower, mainly in the crust and lithosphere. Therefore, different volcanoes interact in a different way with the upper capacitance plate of the atmospheric condenser.

If the volcano is the top point of a sea-urchin spike, the volcanic plume is the upward prolongation of the deep underground ***j***-system. Therefore, specific e.m. phenomena involve the plume, its ash, and lapilli. In contrast, if the volcano is supplied by friction heat (see above) - and e.m. phenomena play only a comparatively less crucial role – the probability to observe lightning discharges ought to be expected to be (perhaps) lower, or in any case to respond to a different primary electrostatic mechanism. This does not mean that no lightning are observed, because the atmospheric electrical circuit is always severely affected by the volcanic eruption. Rather, it is meant that in hotspot volcanoes the e.m coupling is direct with the deep *TD* dynamo, while the e.m coupling is with a much shallower source in volcanoes supplied by friction heat.

Historical information

Since the early dawn of civilization, lightning in volcanic plumes were well-known. Thus, they entered in the mythology of ancient societies. No explicit mention is here given about the Norse mythology, which relied on the witness of great eruptions from some Icelandic volcanoes (e.g., Thorarinsson, 1967, 1984), or about the classical ancient Greek mythology, which relied on volcanic eruptions observed in the Mediterranean area. Only remind about the great Santorini (Thera) eruption that in ~1450 BC destroyed the Minoan civilization (LaMoreaux, 1995). According to Sivertsen (2009), it can be associated (maybe) with the Exodus of the Jews from Egypt. "*Then the Lord said to Moses, '* Stretch out your hand toward the sky, that there may be darkness over the land of Egypt, even a darkness which may be felt.*' So Moses stretched out his hand toward the sky, and there was thick darkness in all the land of Egypt for three days*" (*Exodus*, 10:21-22). We do not enter into the almost endless number of papers that hypothesize various phenomena to be possibly associated to the Bible that reported anomalous and intense events. On the other hand, the dating of these phenomena is generally uncertain, and other catastrophes mentioned either in the Bible or by ancient classic authors were sometimes tentatively associated with the catastrophic Santorini event. There is no need to enter here into this debate.

Only note that if Moses directly watched the Santorini explosion from a site located, say, $\sim 1000 - 1200\ km$ from Santorini, the "cloud" that he could observe above the horizon ought to have an altitude of at least $\sim 80 - 115\ km$. That is, we should suppose that the effects of the explosion reached the lower ionosphere. However, maybe Moses observed no actual volcanic plume. Rather, he observed only intense electric discharges (i.e., something analogous to, although much stronger than, the "Andes lights"; see Gregori and Leybourne, 2025g). On the other hand, maybe Moses did not directly watch the event, while the stratospheric cloud rather later obscured Egypt for three days.[2]

Titus Lucretius Carus (~99 BC - ~55 BC) described volcanoes as follows: ["*De rerum natura*", I, 722-725] "… *et hic Ætnæa minantur/ murmura flammarum rursum se colligere iras, /faucibus eruptos iterum vis ut vomat ignis/ad cælumque ferat ammai fulgura rursum."* ["… and the rumblings of Etna that threaten a new awakening of its hanger, a new eruption that would vomit fire from its jaws bringing up to the sky the ashes of flames."].[3]

The AD 79 eruption of Vesuvius is, maybe, the best known and complete account of an old volcanic catastrophe, given in some detail by Pliny the Younger [Plinius Caecilius Secundus (Gaius), AD 61 - ~AD 112] in a few letters that he wrote to the famous Roman historian Publius (or Gaius) Cornelius Tacitus (AD 56 – AD 117). He described the action by his uncle Pliny the Elder [Gaius Plinius Secundus, AD 23 or 24 - AD 79] who died while trying to rescue people and to observe the eruption at close distance. As far as lightning in the plume are concerned,

[2] Luce (1969); Friedrich et al. (1990); LaMoreaux (1995); Bruins and van der Plicht (1996); Kuniholm et al. (1996); Renfrew (1996); Greene (2000).

[3] Our English translation from the Latin original.

NCGT Journal
New Concepts in Global Tectonics
New Concepts in Global Tectonics Journal
Volume 13, Number 6, August 2025
ISSN number; ISSN 2202-0039

only the following statements are contained in these letters.

"*Plinius Cœcilius Secundus (Caius) to Cornelius Tacitus … they were surrounded with darkness blacker and more dismal than night, which however was sometimes dispersed by several ashes and eruptions from the mountain* …. [This is a "primary" kind of lightning discharge observed at the outer boundary of the plume; see below.] *On the land side a dark and horrible cloud, charged with combustible matter, suddenly broke and shot forth a long trail of fire, in the nature of lightning, but in larger ashes* [This is the "secondary" kind of lightning discharges that he correctly claims are "*larger ashes*", outgoing from the boundary of the dust cloud moved by wind; see below] ... "[4]

Middle Age writers frequently reported lightning, always in terms of divine and awful intervention against the sins of humankind, etc.

Seemingly, the first true scientific measurements were carried out by Luigi Palmieri (1807-1896), second Director of the "*Osservatorio Vesuviano*", in charge from December 1854 until his death. [5] The first Director had been Macedonio Melloni (1798-1854). However, following the "Restoration"[6] after the Napoleon time (e.g., Gasparini[7] and Musella, 1991) and owing to political reasons, the king of Naples wanted to substitute him. The *Osservatorio* was being planned to be transformed into a hotel for tourists. Palmieri hesitated to accept and to become Director. Only when Melloni contracted cholera, he accepted. Thus, the *Osservatorio* survived: it was the very first ever established volcanological observatory in the world. In 1859 Palmieri published the very first issue of the "*Annali del Reale Osservatorio Meteorologico Vesuviano*" (see Fig. 5). On the frontispiece he quoted the statement: "*il faudrai qu'il se formàt dans Naples une société vésuvienne, un observatoire du Vesuve, un journal du Vesuve comme il y a deja des bibliothèques et des collections vesuviennes*" ["it is worthwhile that a Vesuvian Society is established in Naples, a Vesuvian Observatory, and a Vesuvian Journal, much like Vesuvian libraries and collections already exist"] (Ménard de la Groye).[8]

An investigation - that is still up to date and that was inexplicably forgotten by later volcanologists - was carried out by means of one instrument constructed by Palmieri, among several innovative devices that he envisaged for carrying out pioneering measurements on a volcano. In 1878 he constructed a double wire electrometer with mobile conductor (Fig. 6) ["*elettrometro bifilare a conduttore mobile*"]. The target was to measure electrostatic phenomena in volcanoes by comparing records collected at Naples downtown and/or at the *Osservatorio*. Later, he also used measurements carried out in Rome.

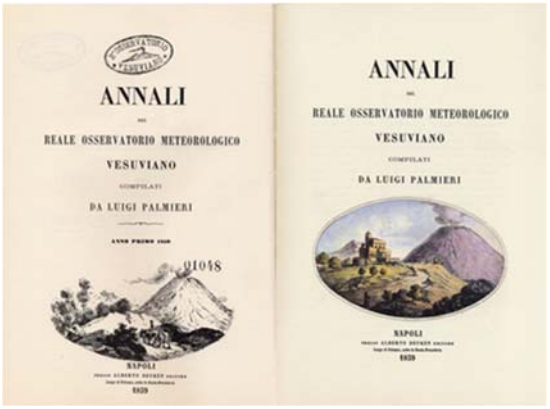

Fig. 5 - Frontispiece of the very first issue of the "*Annali del Reale Osservatorio Meteorologico Vesuviano*", published by L. Palmieri in 1859. With kind permission of *INGV, Osservatorio Vesuviano*.

At his time, this was pioneering research, as only in 1831 Faraday had discovered e.m. induction. The leading idea was very similar to a Volta's condensing electroscope, using two conducting leaves instead of two wires. The wires appeared less perturbed by an external shaking of the instrument. Since 1862, or maybe earlier, the Volta condensing electroscope was available on the market, from Carlo Jest (Torino) at a cost of 50 Lire.

Torreson (1939, p. 234) reports about the "*Wulf type of bifilar electrometer*" that he presents (Wulf, 1909, i.e., 31 *years* after Palmieri's) as "*one of the most suitable and convenient electrometers for field-measurements*." Israël (1951) also illustrated this instrument, which seems to be much like the Palmieri's double wire electrometer, where

[4] English translation after Logan Lobley (1889), who reported the "*Letters of Pliny the Younger, containing an account of the eruption of AD 79. From* 'The letters of Pliny the Younger' *by John Earl of Orrery.*"

[5] The following information mainly relies on Casertano (1999). This is the authoritative Palmieri's celebration written by the late Lorenzo Casertano (1921-2004), a nice gentleman, friend, and learned, authoritative volcanologist.

[6] During the Enlightenment, Naples, Paris, and St. Petersburg were considered as the leading European capitals of culture. During the "Restoration", however, the most important leaders of the learned class of Naples, who had followed Napoleon with enthusiasm, were hanged (in 1799-1800, altogether 119 people; while some nobles were beheaded), and later Naples never recovered to its former prestige. Thus, also the remarkable Palmieri's experiments were not acknowledged as they must deserve. See, e.g., Croce (1912), Ciarallo (1992), …

[7] Paolo Gasparini (1937-2016), former Director of the "*Osservatorio Vesuviano*".

[8] Ménard de la Groye (1794-1822), since 1810 professor of natural history at the university of Angers, and since 1818 professor of geology at the *Collège de France*; also member of the *Académie des sciences*. He is known for having reported about the Vesuvius eruption of 1813-1814.

New Concepts in Global Tectonics Journal
Volume 13, Number 6, August 2025
ISSN number; ISSN 2202-0039

however two quartz fibers are used, coated with a metallic layer. However, owing to the loss of prestige by Naples, the Palmieri's paternity was evidently forgotten. However, also the "*Wulf type of bifilar electrometer*" was seemingly forgotten by later volcanologists.

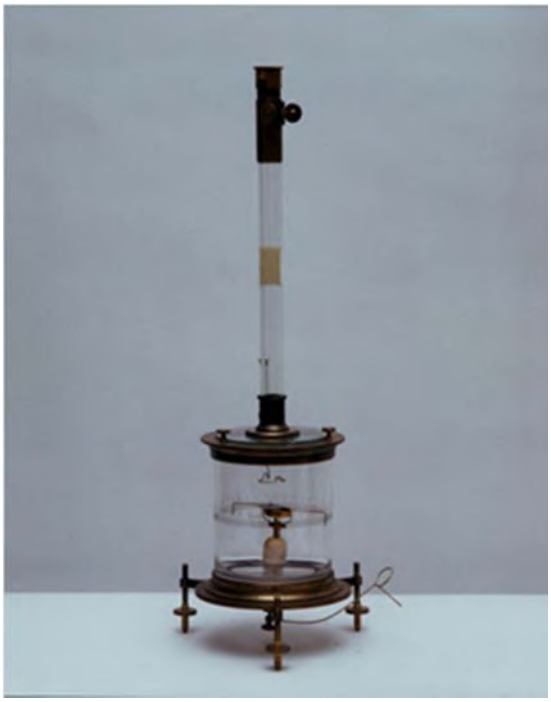

Fig. 6. Palmieri's double wire electrometer with mobile conductor. A Faraday cup collects charged ash particles. The Coulomb repulsion makes the two wires of the electrometer to detach from each other. This effect is calibrated to measure the electrostatic charge of the particles collected by the Faraday cup. This picture shows the original Palmieri instrument, which at present is at the Museum of the *Osservatorio Vesuviano*. With kind permission of *INGV, Osservatorio Vesuviano*.

For clarity purpose, before reporting the remarkable - and still up to date - findings by Palmieri, it is worthwhile to mention the results that must be expected according to the rationale of the model that is here envisaged.

Sea-urchin spikes projected through the atmosphere: Palmieri's measurements

The leading structure underground is a sea-urchin spike that represents a spatial distribution of a region of comparatively larger σ. The sea-urchin spike is propagated from underground through air, and inside a volcanic plume, until the region where the volcanic plume becomes less conductive. The boundary region of the plume - where σ decreases - is the site where eventual visible lightning occur. In fact, inside the plume a large friction occurs between the components of pyroclastics. On the other hand, owing to the high temperature, the great availability of free electrons determines an immediate short-circuiting of every potential difference. Thus, micro-discharges immediately occur, which are the source of radio emission. On the other hand, the plume is totally opaque for visible radiation, and no micro-spark can be observed as a *visible* micro-lightning. Hence, observed visible lightning occur only at the boundaries of the plume.

Note, however, that drawing boundaries between plume lightning, and near-vent lightning, can be challenging, as shown in several case histories included in the Appendix. We stress, however, that drawing boundaries between plume lightning and near-vent lightning is a bottom-up approach, while the argument here envisaged is a top-down approach. That is, we envisage a specific physical mechanism, and we show how the Palmieri forgotten measurements are a convincing confirmation of our guessed explanation. In addition, all case histories discussed in the Appendix show how the interpretation of volcanic plumes images – guided by our top-down rationale – can confirm our interpretation. See here below some details and a few examples.

It must be stressed, however, that the discussion about radio waves associated to volcanic plumes is a different phenomenon, and is here given in a separate section.

The top-point of the sea-urchin spike is the highest upward extension of the underground electric circuits, towards the upper plate of the atmospheric condenser (the ionosphere; see Gregori et al., 2025a and Gregori and Hovland, 2025). An electric discharge (not necessarily a lightning discharge) involves the motion of three kinds of charged particles: *(i)* electrons, *(ii)* positive ions and/or positive ash particles, and *(iii)* negative ions and/or negative ash particles (Fig. 7).

Electrons, owing to the greater mobility, are responsible for the main flow of electric charge between the two plates of the atmospheric condenser. The volcanic plume "breaks" any kind of "barrier" represented by meteorological clouds. The electrical coupling is therefore - in general - more directly concerned with a straight connection with the ionosphere, with no intermediate additional screening. This phenomenon is expected to involve a 2D widespread occurrence through the entire outer surface of the volcanic plume, eventually displaying diffuse lightning towards the ionosphere. These discharges are here denoted as "primary", or electron discharges, or briefly "*e*-discharge".

The loss of electrons towards the ionosphere implies that the remaining volcanic smoke and ash is enriched in negative and positive ions and heavier particles. Therefore, the particles collected by a Faraday cup must be expected to be mainly positively charged.

Concerning the negative ions and negative smoke and ash particles, their comparably smaller and more mobile particle-carriers eventually succeed (perhaps) to migrate towards the ionosphere, similarly to electrons, although with a much lower mobility. In contrast, the larger size negative particles are excessively heavy. Hence, they "float" in air as $\boldsymbol{E}$ compensates the weight of negative ions and particles. Wind eventually displaces these "floating" ions and ash particles. Whenever they can hardly be taken

NCGT Journal
New Concepts in Global Tectonics
New Concepts in Global Tectonics Journal
Volume 13, Number 6, August 2025
ISSN number; ISSN 2202-0039

suspended in air by the ***E*** originated in the ionosphere, owing to gravity, they finally precipitate. These are observed like more intense *CG* lightning, which occur at some distance from the volcanic plume. These are here called "*secondary*" or "*ion-discharges*".

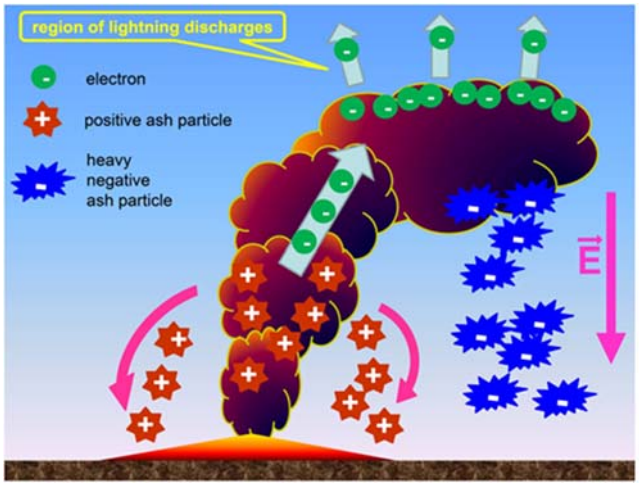

Fig. 7 -Electrically charged particles in a volcanic plume. Consider three kinds of particles: electrons (in green), positive ions and/or positive ash particles (in red), and negative ions and/or negative ash particles (in blue). Electrons have the greatest mobility and the main responsibility for causing a (partial) discharge of the electric potential difference between the two plates of the atmospheric condenser. These discharges cloud-to-ionosphere are here denoted like "primary", or "*e*-discharge". They occur either through a lightning, or not. In either case, the largest percent of electric charge that thus remains inside the volcanic plume will be composed of positively and negatively charged ions and ash particles. The positive ions and ash particles are rapidly pushed by gravity and by ***E*** towards Earth's surface. In contrast, the negative ions and negatively charged smoke and ash particles, of suitably small weight, behave like electrons, and are pushed towards the ionosphere and into the magnetosphere. However, the heavier negatively charged particles "float" in air, suspended by the ionospheric ***E*** that opposes gravity. The "floating" negatively charged particles are displaced by wind, and precipitate over Earth's surface, as, owing to their excessive weight, the ***E*** inside the atmospheric condenser is insufficient to keep them floating in air. Thus, negative ions and ash constitute a conducting channel through which one or several *CG* discharges occur. They are here denoted like "secondary" or "ion-discharge". See text. Unpublished figure.

Summarizing, when measuring the electric charge of smoke and ash particles, one should expect to find tiny particles bearing a positive charge. Heavier particles eventually manifest mainly negative electric charge, although they can be observed only whenever specific constraints are satisfied, i.e., whenever the main volcanic plume was blown apart by wind, or when the recording instrument monitors only particles left in the trail of the volcanic plume, etc. Differently stated, in general suitable environmental conditions must be satisfied in order that heavy negatively charged particles can freely precipitate due to gravity. This will occur eventually far from the volcano, depending on their ballistic trajectory, on the ***E***intensity of ionospheric origin at the time of the eruption, and on the wind speed and direction.

Two kinds of effects occur. One effect is concerned with anomalous atmospheric pollution downstream with respect to the volcano, with consequent eventual serious hazard for the inhabitants. Another effect is the occurrence of lightning of a particular kind and far away from the volcanic plume.

A case history of the first kind is reported by Ilyinskaya et al. (2017), who summarize as follows their observations. Note, however, that the focus of the present paper is on the electrostatic aspects, while the chemical pollution is a different concern. They report about one of the most intense and widespread air pollution, caused by a volcanic eruption, that occurred in 2014-2015 by volcano Holuhraun in Iceland, which injected $\sim 11\,Tg$ of SO_2 into the troposphere for over $6\,months$. The interested reader ought to refer to their original long paper. We report here only a few highlights.

Ilyinskaya et al. (2017) investigated the chemistry of aerosol particle matter (*PM*) and of gas, and the evolution when the plume dispersed. Samples were collected at the eruptive vent, and in two populated areas in Iceland. The hourly air quality standards ($350\ \mu g\ m^{-3}$) for SO_2 was exceeded on *88* occasions in Reykjahlõ town (at $100\ km$ distance), and on *34* occasions in Reykjavk's area (at $250\ km$ distance), while during $30\ days$ the mean daily concentration in Reykjavk of *PM* sulphate exceeded $5\ \mu g\ m^{-3}$, which is the maximum non-eruptive measured concentration. They measured the impact of the eruption on concentration of air pollutants (SO_2, SO_4^{2-} and $PM_{2.5}$) in the two populated areas. They identified two types of plume impact. One type has high concentrations of both SO_2 and S-bearing *PM*, with a highS_{gas}/S_{PM} mass ratio [$SO_{2(g)}/SO_{4(PM)}^{2-}$>10]. The other has a low S_{gas}/S_{PM} ratio (< 10), which they guess refers to a mature plume, when sulphur had undergone a significant gas-to-aerosol conversion. Several tracers characterized both kinds of plume, i.e., fine aerosol (mostly PM_1 and $PM_{2.5}$), sulphate (mean ~90% of *PM* mass), and various species, including heavy metals. The greatest hazard for health was by *PM*. However, public warnings and operational alert was only concerned with the dispersion of volcanic SO_2.

The lightning discharge phenomenon is even more hazardous. In fact, wherever these negative charged particles reach the end of their ballistic trajectory – eventually even at some comparatively large distance from the volcano – an intense lightning eventually occurs between volcanic plume and ground. This kind of discharges will be here denoted as "*secondary*", or also "*ion-discharges*", for distinction with the aforementioned "*primary*" or "e-*discharge*" between plume and the ionosphere.

ISSN number; ISSN 2202-0039

For future reference, also note that the mechanism of luminous emission from the two kinds of discharges can display a comparatively different morphology. An "*e*-discharge" implies electrons that are rapidly accelerated towards the ionosphere and originate a tiny light emission from the sporadic molecules and atoms with which they scatter. In contrast, an "ion-discharge" is concentrated within a comparatively large "tube" of falling negatively charged particles, which end their ballistic trajectory. They contain negative ions that are excited and release photons. Hence, the discharge ought to be expected to appear like a comparatively brighter lightning flash. In fact, this is observed, as shown in the subsequent sections. The same argument will be shown to be apply also to every other standard lightning flash, even other than phenomena related to a volcanic plume.

Note that, during the exposure-time needed for taking a photograph of a plume, several "ion-discharges" can occur, due to the large horizontal extension of the plume. According to the observational evidence shown here below, "ion-discharges" appear to be the comparatively brighter events in a volcanic plume. The fainter "*e*-discharge" - which in general appear to be almost uniformly distributed at the outer boundary of the volcanic plume - are eventually invisible, particularly with twilight illumination. In this case, only "ion-discharges" appear on the photo.

Before reporting some observations, for future reference, let us remind about the remarkable and clear synthesis made by Casertano (1999) of Palmieri's findings.

"*This study concluded that, even on fine day, the atmospheric electric current measured at Vesuvius was considerably higher than in Naples."*

This finding shows that a conspicuous electric discharge occurs through the volcanic edifice, much larger than through its nearby area, due to the presence of the sea-urchin spike. This is consistent with the existence of conspicuous air-earth currents that ought to be expected to occur on top of every sea-urchin spike, independent of the presence, or not, of a volcano or of lightning. In fact, this is consistent with the evidence provided by the *DEMETER* and post-*DEMETER* investigations (see Parrot, 2025) and by the Quinn's inversion technique (see Quinn et al., 2025).

Casertano (1999) further comments as follows. "*We do not know whether in the later half of the 18th century the idea of site variation* ['gradiente di campo', literally 'field gradient'] *was common scientific knowledge or whether Palmieri was the first to coin this term. Whatever the reply, the formulæ produced by Palmieri were without external influence. The research had to formulate common formulæ with regard to atmospheric electricity in which, as expressed by Pinto (1896),* 'the rain must rain even when it is positively charged surrounded by small and large negative charges, which in turn are surrounded by an area of strong positive charge as they are described to occur inside large temporal storms and whirling winds.' *The law was confirmed also for areas outside Italy, and was considered to be a standard formula, where it was contested as to who was its founder. The merit was given to Palmieri who received congratulations from Faraday.*

Palmieri claimed (1862a) that, as rain drops fall from clouds in the terrestrial gravity field, they would become positively charged due to electrostatic friction. Therefore, it can be assumed that the same process would also affect volcanic ash; ash that fell as rain would be positively charged; and ash that fell as volcanic projectiles (not reaching the upper atmosphere) would become negatively charged. This would create a situation in which a volcanic cloud could produce and discharge large quantities of electric energy as was observed by the young Pliny during the AD 79 eruption."

Compared to the model that here proposed, this Palmieri's explanation is different. He imagined a similarity between falling raindrops and falling ash or lapilli. On the other hand, he missed any possibility to envisage any atmospheric condenser, supplied on both external and internal plates. However, it is remarkable that he correctly focused on the role of electrostatics in the explanation of atmospheric precipitation.

This concept is here resumed, although in a substantially different framework, where the Cowling dynamo plays a three-fold role (see Gregori et al., 2025d). In fact, on the one hand the Cowling dynamo contributes to amplify by a substantial amount the positive charge of the ionosphere. On the other, micro-Cowling dynamos are responsible for water condensation and eventual precipitation in the atmosphere. The third role is the generation of large e.m. fields $\boldsymbol{E}$ inside clouds, including the supply of the "seed" $\boldsymbol{E}$ that through the *RB* process, produces the deadly *TGF*s (see Gregori and Leybourne, 2025f).

Casertano (1999) also mentions another finding by Palmieri, including his pioneering investigation on telluric currents.

"Pliny also noted for the first time that during the eruption the volcanic edifice tended to modify its position with respect to sea-level, which more or less surrounds the volcano. He noted that the sea-level dropped, due to isostatic uplift, with respect to its normal level. Two days after the eruption on 8th December 1861, Palmieri (1862b, 1862c) noted that the coastal area nearest to the vent had risen to a point at which sea algæ and shellfish which normally lie below sea-level were now exposed above sea-level.

The maximum relative lowering of sea-level, ~1.5 m, was seen at Torre del Greco with a gradual return to normal towards north and south. Therefore, from a reef in front of Torre del Greco, the maximum uplift was observed at Granatiello, ~4 km north, where there was no noted variation of sea-level. It was presumed that the eruption had caused an uplift of the volcanic edifice that gradually returned to 'normality' within a year from the eruption. It was therefore concluded that in general isostasy was caused by a variation in the land with respect to the sea, and not in the sea as it was previously assumed.

ISSN number; ISSN 2202-0039

Since 1859 Palmieri (1891) had been conducting experiments on this phenomenon, as well as on its possible relation with local meteorological, electrical and magnetic anomalies. This work was further stimulated after the 1872 eruption, when, to reward the Director and his staff, the first telegraph line was built connecting the Osservatorio *with the* Central Post Office *of Resina. For anyone else, this would have remained a simple telegraph line but for Palmieri it was a means of investigating the telluric current and its relation with the activity of Vesuvius. After establishing the relation between the telluric current and Vesuvius activity in 1894, two years before his death, he noted the variations in intensity and direction of the e.m. phenomena at Vesuvius … "*

Palmieri was also a pioneer in the investigation of the correlation between seismology and volcanism (also reviewed by Casertano, 1999). This item, however, is not pertinent for the present discussion.

J. Logan Lobley[9] (1889), in his lengthy and extensive discussion of Vesuvius and surrounding volcanoes, describes the electric discharges in volcanic plumes by reporting directly the original report given by Palmieri of his results.

"*Lightning, volcanic (Fulgori). Frequent observations of lightning, or electrical manifestation, in the cloud of smoke produced by volcanic eruptions leave no doubt whatever that this is not the ordinary lightning of meteorology, but is entirely due to electricity consequent upon volcanic action.*

An ingenious apparatus by which the electricity of eruptions can easily be studied was devised by Prof. Palmieri and installed at the Observatory. *It is named by the Professor* 'Apparecchio a conduttore mobile', *or apparatus with movable conductor, and possesses a bifilar electrometer of great delicacy. Palmieri says*: 'The *Observatory* is distant in a direct line from the central crater of Vesuvius 2.380 m, so that, when the smoke is copious, it is properly situated for the study of electricity, particularly when the wind inclines the pine-tree cloud[10] in the direction of the *Observatory*, as frequently happened on the last occasion (1872). With smoke alone, without ashes, we obtained strong tensions of positive electricity. With ashes only, which sometimes fell while the smoke turned in the other direction, we had strong negative electricity. When the smoke inclined towards the *Observatory*, accompanied with ashes and lapilli, we had sometimes one kind of electricity, and sometimes the other, just as the smoke or the ashes predominated - and often with a fixed conductor we obtained negative electricity, and with a 'movable conductor' positive electricity.

The conditions - under which ('fulgori') lightning flashes are seen from the cloud of smoke - are that it is conveying great abundance of ashes. In 1861 there were small flashes even from the line of eccentric mouths above Torre del Greco, although the smoke was not very great. And when these ceased to discharge - and the central crater became somewhat active, with a moderate amount of smoke but a great deal of flashes - small and frequent lightning flashes were observed in the twilight darting through the smoke, which was dark in color.' "

These Palmieri's results are in excellent agreement with the aforementioned expectation. He calls "smoke" the small ash particles, and "ash" and "lapilli" the larger particles. "Smoke" is therefore in general positively charged. "Ash" and "lapilli" look generally negative, although their observation is more erratic, depending on wind, etc.

Finally, let us report the seemingly very first account of this phenomenon, given by Palmieri (1859, p. 44) in the very first issue of the "*Annali del Reale Osservatorio Meteorologico Vesuviano*" (see Fig. 5).

"Atmospheric electricity is generally very intense at the time of great eruptions. It cancels all phases of the diurnal periodicity and it displays variations that are properly dependent on the direction where the smoke is pushed by wind. When the smoke is conspicuous and it is pushed over the Observatory, ***E*** *becomes very strong, while it fades off when the smoke either fades or moves away. This electricity is always positive: I measured it, not only close to the* Observatory … *but also close to the igneous bocas on the top of the cone, as well as by means of portable instruments at its base. I always found the same result. However, at the time of ash fall, I recorded negative electricity by means of fixed conductor, and positive electricity by a mobile conductor … In these circumstances, I am acquainted to use a large dish on top of the measuring device, instead of a globe. The dish is kept lowered: I observe negative electricity … but as soon as I take the dish off, abruptly I observe positive electricity."*

That is, as long as no ash is collected by the recording device, the instrument monitors the ***E*** of ionospheric origin. In contrast, when the ballistic trajectories of ash originate ash accumulation on top of the recorder, the negative charge of ash plays the leading role.

Palmieri, however, tentatively interprets his findings by means of a speculated friction inside the plume, and of the role of precipitating water, that he claims ought to derive from coagulation of the water vapor that is contained inside the plume. He did not even imagine the possibility of an externally applied ***E***.[11] Hence, he could speculate about no possible different role played by negative and positive ions. Thus, he envisaged his tentative interpretation that seemed to him the unique possible explanation. On the other hand, at the end of the 18th century, as a paradigm, interplanetary space was conceived as being vacuum, apart at most

[9] J. Logan Lobley (1833-1913), English geologist.

[10] At that time, following the term formerly used by Pliny the Elder (see above), "*pine-tree cloud*" denoted the volcanic plume.

[11] In addition, he could not hypothesize either the run-away breakdown (*RB*) process and/or the Cowling dynamo.

NCGT Journal
New Concepts in Global Tectonics

New Concepts in Global Tectonics Journal
Volume 13, Number 6, August 2025

ISSN number; ISSN 2202-0039

sporadic clouds of solar material (see Gregori and Leybourne, 2025b).

Vesuvius 1944 and Surtsey 1963

The literature reports a conspicuous number of (unexplained) case histories. The case history of the last historical eruption of Vesuvius (in 1944), and the birth of the Surtsey Island (in 1963/1964) close to Iceland, are here reported in some detail. The Appendix contains several additional case histories.

The Vesuvius 1944 eruption (Fig. 8) can be simply interpreted in terms of a prolongation through the atmosphere of the conducting spike of the sea-urchin spike. However, σ decreases through the atmosphere while crossing through the plume boundary to surrounding air. Hence, at some suitable height the plume has no more the large σ of the spine. Therefore, $\boldsymbol{j}$ can no more flow, and a spark is eventually triggered towards to ionosphere. That is, the volcanic plume inside the lower part is a perfect conductor, and at a higher altitude an imperfect conductor or an imperfect dielectric. Therefore, in every respect a volcanic plume looks like a lightning rod.

For future reference, note that only the "black" volcanic plume is observed, composed of lava and pyroclastic materials, while no "white" is supposedly associated with water vapor. In fact, no volcanic ejecta gets in contact with sea water.

A similar explanation applies to the Surtsey's case history (Fig. 9), which erupted on 8 November 1963, at $130\ m$ below sea-level (Thorarinsson and Vonnegut, 1964; Thorarinsson, 1967). To our knowledge, this is one of the best-monitored events from the electrical viewpoint. Therefore, we devote a specific discussion in the present study.

Fishermen first noticed smoke emerging from beneath the waves, and they thought a ship was on fire, but no SOS calls were received. Fig. 10 gives a perspective of the scale size of phenomena. Consider the tiny appearance of the Surtsey Island at the horizon, ~$23\ km$ from the observing site. Also consider the great left-right asymmetry of the plume, compared to the regular symmetry of the Vesuvius' plume. The Surtsey event was investigated with great care – maybe better than every other volcanic eruption - in terms of the associated atmospheric electricity.[12] Therefore, we devote particular care to the discussion of available observations.

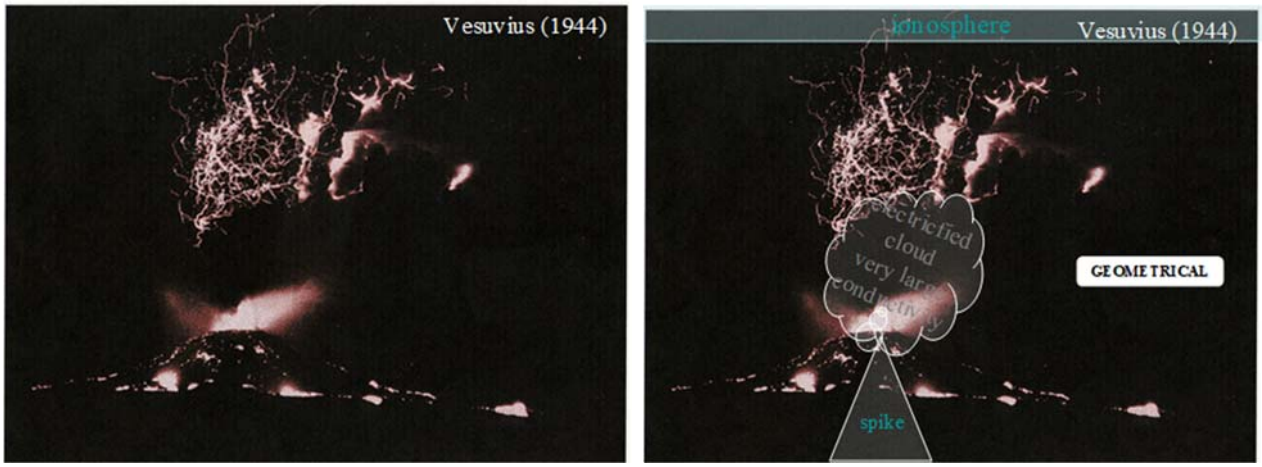

Fig. 8. Plume-ionosphere lightning of the Vesuvius 1944 eruption. The lower figure is the same as the upper figure and, in addition, it shows the guessed atmospheric prolongation of the sea-urchin spike. The phenomenon is explained as a straight geometrical upward prolongation of the sea-urchin spike that supplies the volcano. Note the glow of the lava fountain underneath the upward extension of the volcanic plume. Courtesy of Pino di Natale, *INGV*, *Osservatorio Vesuviano*, Napoli. With kind permission of *INGV*, *Osservatorio Vesuviano.*

[12] For completeness, let us mention that it seems that only Brook et al. (1974) is reported as another early monitoring of atmospheric electricity in volcanic plumes. However, they monitored the electric charge aloft by the clouds formed when molten lava meets seawater, reporting positive potential gradient values sometimes $> 7000\ V\ m^{-1}$. In addition, they rely on several standard concepts of atmospheric lighting and conclude: "*the charge appeared to be distributed in a vertical column extending upward from the sea to a height not exceeding* ~$100\ m$." This is evidently incompatible with the findings here considered.

NCGT Journal
New Concepts in Global Tectonics

New Concepts in Global Tectonics Journal
Volume 13, Number 6, August 2025

ISSN number; ISSN 2202-0039

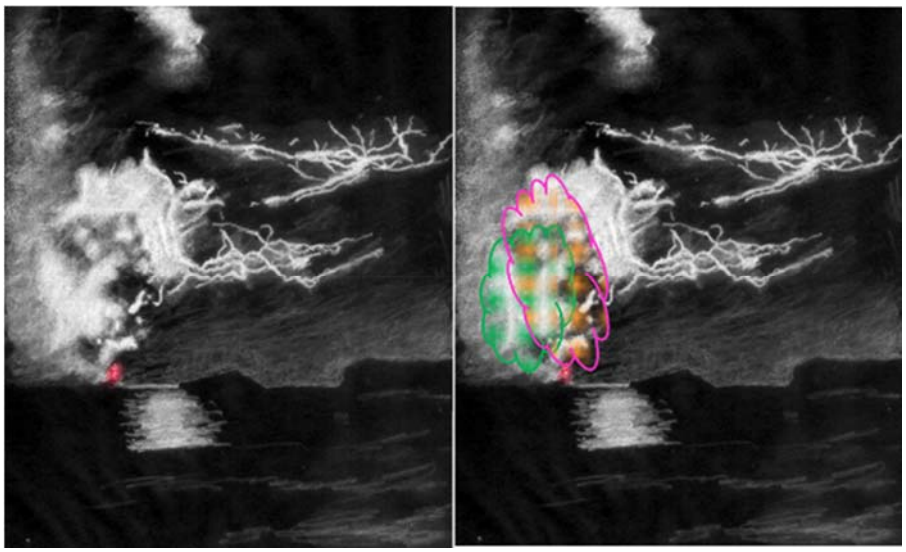

The background image is an artistic work, an Indian-ink-and-pencil sketch, based on a photograph shown in Salanave (1980, p. 46; © Sigurgeir Jònasson, Icelandair; see Fig. 5).

Fig. 9. Plume-ionosphere lightning of the Surtsey December 1963 eruption. The right figure is the same as the left figure and, in addition, it shows the atmospheric prolongation of the sea-urchin spike. Similarly to Vesuvius in Fig. 8, the phenomenon can be justified as a prolongation of the sea-urchin spike that supplies the volcano. In addition, it envisages that the anomalous ionospheric $\boldsymbol{E}$ field, associated with the auroral zone, justifies the large bending of electric discharges. The direction of the observed bending of the plume is not specified. The camera was located at $\sim 23\,km$ from the volcano. See text. Note the similarity with Fig. 6. Unpublished figure.

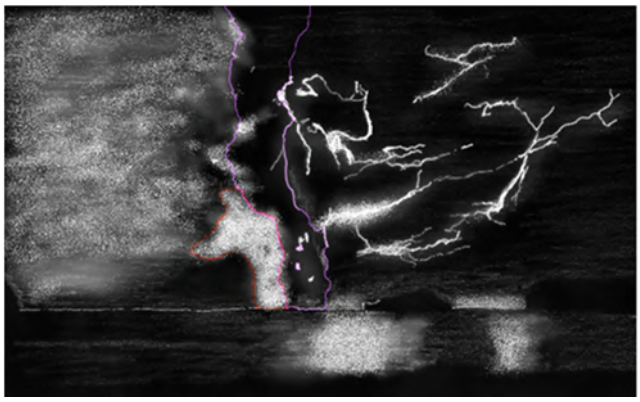

Fig. 10 - Plume-ionosphere lightning discharges of the Surtsey December 1963 eruption, published on the cover of the 28 May 1965 Science issue (vol. 148, No. 1674). Also reported by Uman (1987). The "ion-discharge" is (maybe) the comparably more intense lightning seen in the background, behind the plume. The original photograph is © 1965 by AAAS. Courtesy by Sigurgeir Jònasson, Icelandair. The present figure is an artistic work hand-made sketch that was drawn for focusing on the physical mechanism. See text.

The background of Fig. 9 is a hand-made sketch based on a black-and-white photograph (see the figure captions). The red color shows the likely lava fountain. An added pink callout-cloud indicates the "black" volcanic plume, while an added light-green callout-cloud indicates the "white" plume in the foreground, which is likely to be composed of water vapor. The intense white patch at the upper-right side of the "black" volcanic plume ought to be originated by the violent electric discharge between the plume and the ionosphere.

Compared to Vesuvius, the spatial asymmetry of lightning discharges is caused by the intense and non-uniform ionospheric e.m. field that always affects the auroral zone, which typically crosses over Iceland. The direction of the lightning sparks from the plume should be towards the instant location of the ionospheric region with a comparatively higher positive charge concentration. However, the bending direction shown in Fig. 9 was not measured in detail.

Also note, in the present image (Fig. 9), the more intense glow of the sky at the left side of the plume, compared to the right side. This is the likely effect of the strong lightning of negative ions ("ion-discharge", see Fig. 10) that occur behind the plume. They are also the likely source for the light of the intense curious white "plume" observed at the left of the main dark volcanic plume, which is probably composed of water-vapor.

Also Fig. 10 is a hand-made sketch based on a black-and-white photograph. A light-violet contour shows the black volcanic plume, which is the prolongation through the atmosphere of the sea-urchin spike. A much smaller "white" cloud is indicated by a light-red contour, being the likely water-vapor cloud due to the interaction between volcanic ejecta and ocean water.

The more intense light of the sky at the left of the plume ought to be explained by the "secondary" or "ion-discharge" that is expected to be hidden behind both the plume and the "white" cloud. The intense discharges at the right of the plume are plume-ionosphere "primary" or "*e*-discharges".

Salanave (1980) reports, together with his Fig. 5 (here Fig. 9), also the other similar figure, here shown as Fig. 11. The two Figs 9 and 11 seem almost identical. However, the intense lightning on the foreground seems to "fall down" before moving towards the right side. This can be an "ion-discharge". The original photograph is black-and-white. In the sketch here shown, we colored in red the presumable lava fountain.

A few additional details are given concerning Fig. 11. Let us quote Salanave (1980, p. 46). "*During November 1963 a series of eruptions on the ocean floor off the south coats of Iceland formed a new island, since called Surtsey*

NCGT Journal
New Concepts in Global Tectonics
New Concepts in Global Tectonics Journal
Volume 13, Number 6, August 2025
ISSN number; ISSN 2202-0039

… During the 14th day of its eruption Surtsey was first reported to be the scene of spectacular lightning discharges, and a few days later an especially vivid display occurred when a thunderstorm apparently gathered over the island."

Fig. 11. Plume-ionosphere lightning of the Surtsey December 1963 eruption. The lava fountain is red. See captions of Fig. 9 and see text. Artistic work, pencil hand-drawing, that we made based on a photo (© Sigurgeir J_onasson, Icelandair) in Salanave (1980). Unpublished figure.

Note that the lightning activity occurred only during the 14th day of the eruption. This means that (maybe) the electrostatic state of the ionosphere was not suited to trigger a discharge to connect the ionosphere with the electric currents supplied by the *TD* geodynamo inside sea-urchin spike of the volcanic plume. A suitable electrostatic monitoring of the local state of the ionosphere should be available to test this explanation.

Figs. 11 and 12 refer to two photos, with 5 min and 10 min exposure respectively, taken between 19h 27m LT and 19h 48m LT of December 1st, and with 6 min time lag in between them. Full Moon was above the horizon, to the left of the cloud. The camera was located at Vestmannaeyjar on the Icelandic coast, at a ~23 km distance from the volcano, pointed approximately SW. Hence, the lightning discharges are roughly oriented NE.[13] The instant location was not specified of the auroral electrojet at these instants of time.

Fig. 12 is remarkable due to two distinct lightning discharges. One – which is towards the ionosphere ("*e*-discharge" or "primary") as in Figs. 9 and 11 – is according to the argument of Fig. 7 and ought to be mostly associated with an electron flow. The "secondary" or "ion-discharge" - which appears more intense in Fig. 12 between plume and ocean surface - is likely to be associated with heavy "floating" negatively charged ions, ash particles, and lapilli that fall down due to gravity. The timing of Figs 11 and 12 (5 min exposure, 6 min time delay, 10 min exposure, respectively) is consistent with this mechanism. In fact, consider the timing of the slow ballistic trajectories of heavy ions, ash particles, and lapilli, compared to the much faster electron flux.

Fig. 12. Plume-ionosphere lightning of the Surtsey December 1963 eruption. The plume-ionosphere lightning is roughly NE oriented as in Fig. 11. The plume-ocean lightning discharges on the left ought to be associated with the fall by gravity of heavy negatively charged ions, ash particles and lapilli. The location of such a "secondary" plume-ocean lightning was caused by the wind direction that transported the heavy "floating" negatively charged particles. Therefore, this "secondary" lightning was detected due to the correct location of the observer relative to Surtsey. Note the faint glow on Surtsey Island, and the much dark plume that is violently illuminated by lightning. Also, the white, intense, water-vapor "plume" is seen at the left of the dark plume, which is lit by the intense "ion-discharge". Red color shows the lava fountain. A red-color contour shows the "white" plume due to water vapor. A light-violet contour shows the dark volcanic plume. See text. Artistic work, pencil hand-drawing that we made based on a photo (© Sigurgeir Jònasson, Icelandair) in Salanave (1980). Unpublished figure.

[13] The photos were taken by Sigurgeir Jònasson, Vestmannaeyjar, Iceland.

NCGT Journal
New Concepts in Global Tectonics
New Concepts in Global Tectonics Journal
Volume 13, Number 6, August 2025
ISSN number; ISSN 2202-0039

The location with respect to the erupting vent of the "secondary" lightning or "ion-discharge" depends on wind direction and on the transport of the heavy negatively charged particles.

The observer should, however, be suitably located with respect to the volcano in order to distinguish this "secondary" lightning as an independent phenomenon - compared to the "primary" lightning from the main plume towards the ionosphere.

In Fig. 11 the "secondary" lightning or "ion-discharge" occurs in the background, behind the plume. In contrast, the "secondary" discharge is clearly recognized in Figs 12 and 13 where it ends into the ocean. In addition, note in the Fig. 13 huge water-vapor white "plume" that is illuminated by the "ion-discharge", and that lights up the whole sky to the left of the white "plume".

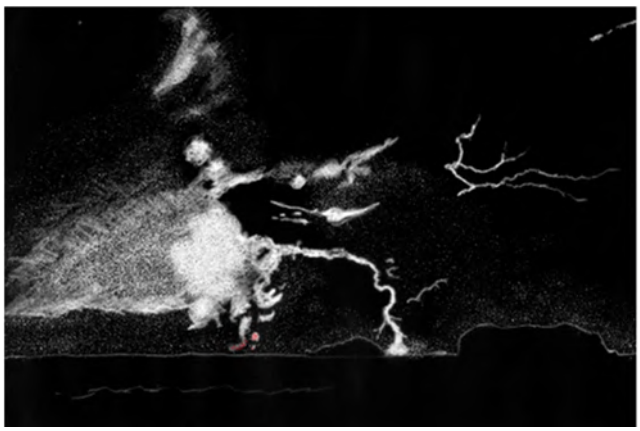

Fig. 13. Lightning discharges in the Surtsey volcanic plume, at 19 h 38 min to 19 h 48 min on 5 December 1963 (600 sec exposure). The top of the cloud was estimated to be ~8 km above Surtsey. The "secondary" lightning can be clearly recognized at the right side of the volcano. The lava fountain is colored in red. Note also the "white" water vapor cloud in the foreground that illuminates the sky at the left side. See text. Artistic work, pencil hand-drawing, that we made based on a photo (© Sigurgeir Jònasson, Icelandair) in Anderson et al. (1965). Unpublished figure.

Concerning the birth of Surtsey, Altschuler (1999) specifies that "*undersea volcanic eruptions began on the morning of 14 November 1963, only ~23 km from the southern coast of Iceland, where the water depth was ~130 m. Within 10 days an island was created which was nearly ~1 km long and ~100 m above sea-level.*

Motion pictures showed clouds rising vertically at ~12 m sec^{-1} to an altitude of ~9 km. The cloud of 1 December contained intense, almost continuous light, presumably the result of large dust particles and perhaps electret effects of sulfur. Aircraft flights through the volcanic cloud were made during periods of no lightning. Large electric fields $\boldsymbol{E}$ *were measured, sometimes exceeding 11,000 V m^{-1}*."

[His sources are Thorarinsson and Vonnegut (1964) and Anderson et al. (1965).]

The Haraldur *records*

Some atmospheric electricity measurements - seemingly being a unique experiment of this kind - were carried out during the Surtsey 1963-1964 eruption. Anderson et al. (1965) is a detailed report. A few highlights are here recalled that are relevant for the present discussion.

They used a boat (Fig. 14) - the fishing vessel *M. S. Haraldur* - with a portable electrometer, and a standard recorder of atmospheric potential-gradient using a radioactive Po (polonium) source (see Gregori and Leybourne, 2025d). In addition, they measured (both sign and intensity) of the electric current $\boldsymbol{j}$ associated with the corona discharge from the top point of the mainmast.

They carried out - near the volcano - also airborne measurements by flights of a *Constellation* airplane equipped by the *U.S. Naval Research Laboratory* with $\boldsymbol{E}$ meters in the wing tips. Four flights were made on 11, 12, 15, and 16 February, although no indications of lightning were detected during that time. Note that the occurrence of a lightning requires an intense ionospheric potential, which in general might not be available

Compared to airborne measurements, the *Haraldur* records look much more expressive, as they were measured during periods of lightning activity. In addition, measurements were carried out ~4m above sea surface, underneath the volcanic plume, rather than above it (see below).

The physical quantity recorded by the *Haraldur* devices - and the associated time-varying errors - are discussed elsewhere (see Figs 4 and 5 of Gregori and Leybourne, 2025d). They are generally related to the vertical component E_z of the atmospheric potential-gradient (see Gregori and Leybourne, 2025d), although they are biased by unknown factors. In any case, these items are not relevant for the present discussion. The concern is here about the *relative* spacetime variations of the records.

We deserve a few comments to explain how measurements and records ought to be interpreted according to the rationale of the present study. A qualitative explanation of the observations is according to the following argument (Fig. 15). The present case history is more intricate than the simple and ideal configuration considered in Fig. 4 of Gregori and Leybourne (2025d).

Consider the so-called "fair-weather" condition (Fig. 15a) over ocean surface. The electric equipotential surfaces are horizontal, while the termination of $\boldsymbol{E}$ field-lines is on the sea surface, which is supposed to be perfectly conducting. The space density of the electrons - which are electrostatically induced into sea water - depends on the local intensity of $\boldsymbol{E}$ (the two quantities are in fact related to each other through the Gauss theorem applied to an elementary volume that crosses through sea surface).

Suppose that a volcanic plume is located between the ionosphere and sea surface (Fig. 15b). In reality, the distance is very small between plume and sea surface. compared to its distance from the ionosphere.

NCGT Journal
New Concepts in Global Tectonics

New Concepts in Global Tectonics Journal
Volume 13, Number 6, August 2025

ISSN number; ISSN 2202-0039

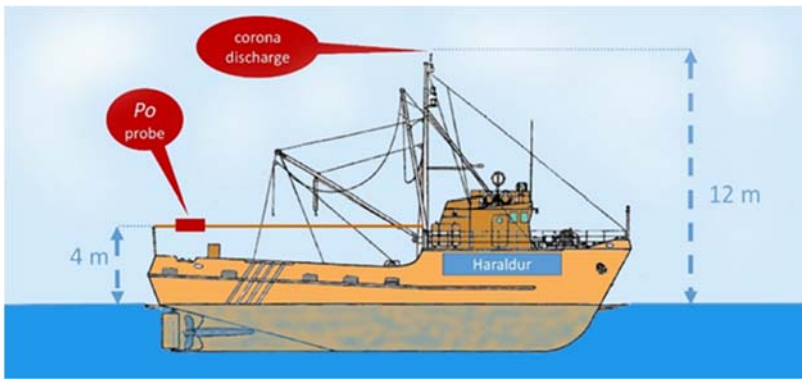

Fig. 14 – Simply indicative realistic sketch (not the original vessel), based on a simpler sketch in Anderson et al. (1965) showing a few elements of the monitoring apparatus. Unpublished figure.

The plume has a very large σ, as it contains a very large amount of free conduction charges (electrons). Owing to electrostatic induction, a violent charge separation occurs, and all electrons pile up on the upper side of the plume. The equipotential surfaces are consequently deformed. The local number density of $\boldsymbol{E}$ field-lines, which terminate on the surface of the plume at every given site, depends on the local density of electrostatically induced charge, which depends on the local curvature radius of the plume. Unlike in Fig. 4 of Gregori and Leybourne (2025d), these deformed equipotential surfaces and $\boldsymbol{E}$ field-lines look much asymmetric *vs.* altitude.

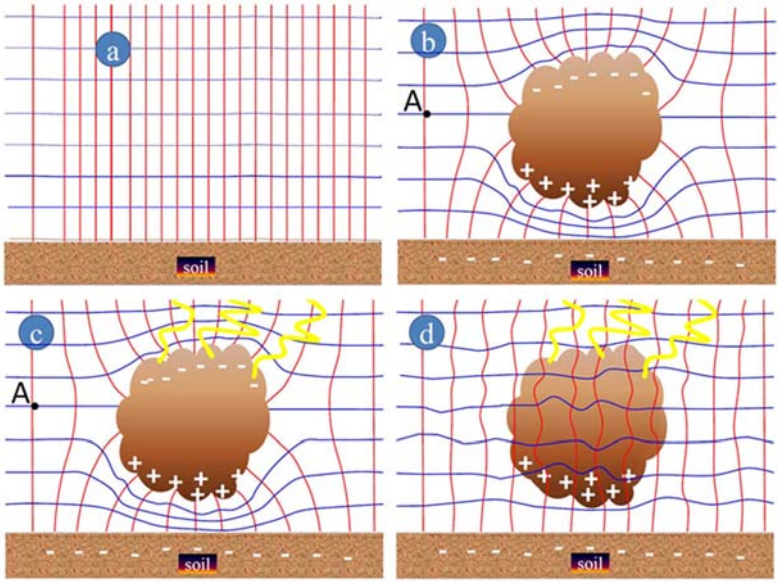

Fig. 15 - Atmospheric electricity perturbation caused by a volcanic plume at ground or over sea surface. *(a)* The unperturbed state is depicted at surface, which is approximately *perfectly* conducting, with equipotential surfaces (in blue) parallel to Earth's surface and $\boldsymbol{E}$ field lines (in red) that stop when crossing Earth's water. *(b)* A volcanic plume is located between Earth's surface (very close to it) and ionosphere. Equipotential surfaces and $\boldsymbol{E}$ field lines are deformed, and $\boldsymbol{E}$ is much more intense beneath than above the plume. *(c)* When one or several lightning occur between plume and ionosphere, free electrons move to the ionosphere, leaving inside the cloud both ions and charged particle. The reduced σ of the cloud implies that the plume is no more an equipotential surface, hence an abrupt change of the pattern of equipotential surfaces and of $\boldsymbol{E}$ field lines [Fig. *(d)*]. See text. Unpublished figure.

Above the clouds the final geometry of these equipotential surfaces (Fig. 15b) will depend on the ionospheric potential, and on its height. Hence, the transition from the structure, which is perturbed by the plume, towards the former unperturbed pattern occurs smoothly *vs.* height. In contrast, underneath the volcanic plume, almost all equipotential surfaces are compressed and must cross through the space between the lower boundary of the plume and ocean surface. If the σ of sea water is supposed infinite, the sea surface must be an equipotential surface, and all perturbed equipotential surface must therefore cross through the narrow neck between the plume and sea surface (Fig. 15b). In the case that the σ of sea water is finite, only a lesser amount of these equipotential surfaces will penetrate inside sea water.

Correspondingly, the $\boldsymbol{E}$ field-lines will terminate right at sea surface for a perfectly conducting sea water, or they will slightly penetrate inside it, as much as needed in order to find a total electrostatic screening by the conduction charges that are available inside sea water. That is, sea water with finite σ cannot fully screen, and some $\boldsymbol{E}$ field-lines afford to cross through sea surface. Hence, some tiny $E_z \neq 0$ exists across sea surface.

The electric potential of the plume - which is the same for the entire plume due to its very large σ - is the potential associated to a suitable surface that is indicatively denoted by A (compare this figure with Fig. 4 of Gregori and Leybourne, 2025d).

If the *Haraldur* is sailing beneath the cloud, it must measure a strong positive E_z (as a standard, the positive direction is defined by the "fair-weather" condition, i.e., with E_z pointing downward). At the same time, the $\boldsymbol{j}$ measured on top of the mainmast must be composed of

ISSN number; ISSN 2202-0039

electrons moving upward, due to the large electrostatic charge of the volcanic plume.

In addition, if the *Haraldur* is located beneath a "secondary" electric fallout, i.e., beneath the falling heavy negative ions and/or heavy aerosols, etc., the measured E_z must be negative, and the mainmast $\boldsymbol{j}$ must measure electrons flowing downward.

Conversely, airborne $\boldsymbol{E}$ measurements are not expected to be significantly affected by the volcanic plume, which is located beneath the aircraft. Or the recorded variations are certainly not as dramatic as for the *Haraldur* records. Consider that, owing to flight security, the aircraft must remain at a reasonable height above the plume.

Suppose that one or several lightning occur between the upper boundary of the plume and the ionosphere (Fig. 15c). A short-circuiting is thus triggered between the plume and the ionosphere. The very high mobility of the electrons - which are available inside the plume - is such that almost instantaneously, at a speed comparable to light's speed, the electric potential of the plume becomes equal to the potential of the region of the ionosphere with which the plume is short-circuited. Recall the fact that, in contrast with the usual assumption, the ionosphere is not an equipotential surface.

The plume, however, loses in this way some very large amount of its free electrons. Hence, its σ abruptly and dramatically decreases. This means that physics no more implies that the plume must be entirely at the same electric potential. Therefore, $\boldsymbol{E}$ must be completely redistributed. This implies that the final configuration of the equipotential surfaces again approximately resembles much more to the "fair-weather" state (Fig. 15d), rather than to the pre-lightning discharge configuration of Fig. 15b. That it, the geometry is the same, although - compared to Fig. 15b - the difference is only related to the role of positive and negative ions that, compared to electrons, have a much lower mobility. Hence, these ions and much heavier particles must obey the laws of thermodynamics and fluid dynamics, convection etc. The σ inside the plume is thus certainly much smaller than before the occurrence of the lightning discharges.

Hence, if the *Haraldur* is located beneath the plume, when a lighting occurs, its Po recorder must abruptly measure a state that looks approximately identical to "fair-weather" conditions. Similarly, also the mainmast $\boldsymbol{j}$ must return to its previous standard unperturbed state.

Therefore, referring to the report, let us comment on a few statements, by Anderson et al. (1965). Their first observations started on 5 February 1964.

In early December a vivid lightning activity was seemingly associated to thunderstorms initiated by the eruptions. On the night of 1 December some long-time exposure photographs were taken from Vestmannaeyjar (see Figs 12 and 13). The volcanic cloud was almost continuously illuminated by intense lightning, while large dust-particles were blown by wind to Vestmannaeyjar. A varying eruptive activity continued through January 1964 and strong whirlwinds were often displayed beneath the eruption clouds. The first volcanic crater was plugged in mid-January, and Surtsey remained dormant for a short time, until the opening of a new fissure appeared to the west of the first crater associated with violent eruptions. It is interesting to point out that, during late winter, the atmosphere over a relevant fraction of the North Atlantic was thermally stable. In fact, in the Surtsey area no thunderstorms were observed, even though lightning frequently occurred, triggered by vigorous eruptions.

Anderson et al. (1965) reminds us about several past reports of lightning associated with volcanic eruptions, even though the investigations of thunderstorm electricity were seldom carried out. In recent times, atmospheric electricity measurements were carried out in Japan downwind of several volcanic eruptions. They envisaged a substantial difference, in several respects, compared to the electrical disturbances originated by thunderstorms.[14]

Some details of Anderson et al. (1965) are important. At 14:00 *IMT* (Icelandic Mean Time), *Haraldur* was $\sim 6\ km$ north of the island, with light wind and a thin overcast. The cloud plume looked almost vertical above the volcano, displaying a slow westward motion. During the approach to the volcano the potential-gradient was increasingly more intense with positive charge overhead, an as usual fine weather condition. Then, for a short time, the potential-gradient became negative, while a few minutes later a very light rain fell on *Haraldur*, which was composed of drops, black with tephra. However, after a brief reversal, the potential-gradient continued to increase until 14:50 *IMT* - when the *Haraldur* stopped $\sim 200\ m$ NW of the island. At that time, the recorded potential-gradient amounted at least to *10* times the gradient measured with fine weather (i.e., the "fine weather" value).

That is, as long as *Haraldur* was not beneath the volcanic cloud, the potential-gradient steadily increased while approaching the volcano. In fact, the volcano was the cause of an intense convection cell that, owing to the Cowling dynamo (Gregori et al., 2025d), caused a large increase of the positive electrostatic charge of the local ionosphere. However - as soon as *Haraldur* crossed beneath a "secondary" or "ion-discharge" in a fallout region of “floating” negative ions and heavy aerosols - the potential-gradient reversed the trend. In fact, Anderson et al. (1965) relies on later observations of the eruption carried out from Vestmannaeyjar (see below). They also later comment that, when passing under the edge of the cloud, they detected precipitation of a mixture of tephra and sea salt particles, altogether with drops of dirty rain, they guess caused by

[14] Hatakeyama and Kubo (1943, 1943a); Nagata et al. (1946); Hatakeyama (1949, 1949a, 1958); Hatakeyama and Uchikawa (1951); and Ishikawa et al. (1951).

ISSN number; ISSN 2202-0039

water coalescence when the superheated steam cooled (thus, micro-Cowling dynamo caused condensation). When the cloud moved ~10 km downwind of the volcano, the plume contained only fine and slowly falling tephra, plus sea salt particles, although no more rain. Such a dry precipitation was often reported by aircraft to be observed downwind for hundreds of kilometers.

Upon returning to their 5 February description, Anderson et al. (1965) state that at 15:35 *IMT* an eruption of steam and tephra intensified during several lightning observations, indicating an increase of air-earth currents associated with a large flux of hot fluids. Following the lightning occurrence, the potential-gradient was briefly negative, likely the consequence of a cloud transition over top of *Haraldur*. Afterwards, as soon as the detector was no longer under the cloud, the potential-gradient reset to the steady large positive value. Subsequently, after nightfall, a large increase of eruptive activity occurred, while lightning frequency rose to ~10 $discharges\ min^{-1}$. However, the electrometer insulation had become wet with sea spray, and no electrical records were possible.

On 16 February 1964 *Haraldur* carried out new observations with the equipment in Fig. 14. However, the Po probe was shielded by the mainmast and boom above. Hence, over open-ocean, away the volcano, the fine-weather potential-gradient was appreciably lower than the value usually recorded by a more exposed probe. This bias was, however, calibrated during the 85 min voyage from Vestmannaeyjar to Surtsey.

When *Haraldur* approached the volcano, the eruption activity became vigorous with rapidly rising large black clouds. At intervals, a sharp noise was heard sounding like the firing of artillery but was thunder that followed a visible lightning by 2 sec or so. The interesting strip-chart records (not here shown) are reproduced in the original paper (Anderson et al., 1965), referenced for the interested reader.

The potential-gradient started to increase, altogether with a flow of negative charge by corona effect from the *Haraldur* mast point. The phenomenon began while *Haraldur* was at $> 1\ km$ from the island. The potential-gradient even went off the positive scale when *Haraldur* approached closer to the volcano while the eruption was in progress. Lightning occurred, while the measured potential-gradient decreased abruptly, and reset to about the fine-weather value that was recorded during the voyage to the volcano (as per Fig. 15c). That is, an increased air-earth current produced an intensification of the electrical activity of the plume. However, the *e*-discharge rapidly reset the condition to the same state that preceded the intensification of eruptions.

Similar trends were also observed on other occasions. Refer to Anderson et al. (1965) for details.

When, at about 13:28 *IMT*, a *Naval Research Laboratory* airplane was in the Surtsey area, when a vigorous eruption occurred while the potential-gradient recorded by *Haraldur* was ~30 $times$ the fine-weather value. See Anderson et al. (1965) for the strip-chart record. However, no lightning occurred during this period. After 13:35 *IMT* the volcano was quiet with no eruption until 15:00, while *Haraldur* approached the crater to within 100 m . Note that air-earth currents are not always associated with lightning.

At 15:04 *IMT* a violent series of eruptions began, with frequent lightning, followed by other eruptions and after $\sim 10 - 60\ sec$, the formation of a black cloud. Lightning was also observed at an elevation of about three island heights, consistent with an extended electrical plume. In addition, several "secondary" or "*ion*-discharges" cloud/Earth discharges were observed that were in fact, occasionally observed to strike at some distance from the crater. As expected, the largest number of discharges were, however, of the "primary" or "*e*-type".

A 24 frames/sec movie taken at close range, showed two different eruption sequences, with lightning that flashed ~10 *sec* after the start of the eruption. This is suggestive of a timing between the breaking of the plug by solid and non-conductive material, and the subsequent ejection of the endogenous hot fluids that are the primary driver of the explosion. Thunder physics is not yet understood (see, however, a guessed explanation explained in Gregori et al., 2025v). A sharp crack of thunder was heard, being characteristically short, correlated with every lightning, even though thunders were about twice the observed number of lightning. Both thunders and lightning occurred with a timing independent of the motion of the cloud, which was composed of solid material, while electrical phenomena followed a different and much more rapid evolution.

Between 15:16 *IMT* and 15:36 *IMT* the strip-chart record displays *26* discontinuities of the lightning type. The most intense eruptions showed *5* discharges in *135 sec*, with 11 sec shortest interval between discharges. In another part of the strip-chart *13* lightning occurred in 9 min.

The most intense recorded potential-gradient was $\sim 60\ times$ the fine-weather value that had been measured during the voyage to the island. The maximum occurred at 15:27 *IMT*, preceding a lightning, and 34 sec after an earlier discharge. However, most of the potential-gradient maxima were found to be ~30 $times$ the fine-weather value, although the records appeared limited, and approaching an asymptote. At the same time, however, usually the trace of the corona-discharge displayed a continued increase until the occurrence of the discharge.

It was excessively hazardous to sail under the cloud. Hence, beginning at 16:00 *IMT*, a series of measurements was carried out upwind from the volcano, at progressively increasing distance, while eruptions and lightning persisted. Therefore, *Haraldur* never was beneath the cloud. In fact, no polarity-reversal either of the potential-gradient or of the corona discharge occurred. The flow of negative charge from the exposed point persisted as long as *Haraldur* was at ~2.6 km from the island. This denotes that the effect was the likely consequence of the intense $\boldsymbol{E}$-field associated to the huge Cowling dynamo supplied by the volcano, which

ISSN number; ISSN 2202-0039

causes an increasing electrostatic charge of the local ionosphere.

The phenomenon was even more evident by means of additional observations carried out on 22 March 1964. In the morning of 22 March, *Haraldur* was at ~63 km from the island. Periodic increases of potential-gradient occurred in the positive direction. The authors interpreted this result as the consequence of the steady activity of the volcano that produced a plume ~3 km high, displayed in an otherwise cloudless sky. That is, the balance periodically changed *vs.* time, between the charging of the ionosphere by the volcanic Cowling dynamo, and the $\boldsymbol{E}$-damping associated to the "*e*-discharge". Thus, the availability of electrical conduction by endogenous hot fluids displayed some kind of "Strombolian" timing, although with a short period.

In fact, the surges of potential-gradient were irregular, with a period of a minute or so. The magnitude consistently increased when *Haraldur* approached the volcano. A light wind carried some tephra in the direction of *Haraldur* that eventually passed beneath the volcanic cloud, while it was located ~ 2 km west of the island. The strip-chart (not here shown) displays an increase of potential-gradient in the positive direction as *Haraldur* approached the volcano. The gradient finally suddenly reversed when the ship was close to, and partly under, the cloud - and became again strongly positive when *Haraldur* went beyond the volcano. The potential-gradient increased in the positive direction when *Haraldur* turned upwind, southeast of the crater.

Two abrupt transients were, however, recorded - two negative transients shortly before a reversal and two positive transients while crossing beneath the cloud – that Anderson et al. (1965) guessed were caused by unobserved lightning. In any case, a strong electrical discharge can happen even with no luminous emission. A lightning occurs when the photon emission is above the background with a sufficient contrast against daylight. In addition, the location of the observer must be suitable, with no screening by cloud cover, etc.

A confirmation of the same processes was available when, later in the day, *Haraldur* was located downwind of the island, and the volcanic cloud passed overhead. See the strip-chart in Anderson et al. (1965) that indicates a negative charge of suspended negative ions floating in air above the ship.

Subsequent interesting observations were carried out from Vestmannaeyjar, at ~ 23 km from the volcano, located approximately SW of the observation point. When visibility was good, almost every night a lightning was observed over the volcano. Time-lapse motion pictures were taken on several nights with a 16 mm camera, which recorded volcanic activity and lightning.

In general, owing to fine, black tephra particles, the volcanic cloud looks far more opaque than ordinary clouds. Therefore, lightning over the volcano at night look somewhat different from lightning of ordinary thunderstorms. In addition, no illumination occurs originated from discharges inside the cloud. Anderson et al. (1965) interprets this as the result of opacity. On the other hand, no discharge occurs inside the volcanic plume. Rather, it occurs only on the outer boundary of the plume. In addition, the "primary" or "*e*-discharges" are cloud-to-ionosphere, while "secondary" or "*ion*-discharges" are cloud-to-ground (*CG*). In contrast, no volcanic plume discharge is cloud-to-cloud (*CC*), which is rather a typical feature associated to the different Cowling dynamos that are operative inside distinct convection cells of different meteorological clouds. Conversely, a volcanic plume is a unique cell. In any case, luminous regions that result from lightning can be readily distinguished - in the photographs - from the glowing lava, because of the blue or white color of lightning (see Surtsey and other volcanoes images here shown *passim*).

In any case, the distribution displayed by both kinds ("*e*-" and "*ion*-") discharges, with varied apparent length and extension, depends on several factors, i.e., on the location of the observer with respect to the width and orientation of the opaque cloud, as shown, e.g., in Fig. 13.

Anderson et al. (1965) points out that the location of lightning associated with a thunderstorm cloud is typically unpredictable. However, several clouds are associated to several convection cells, while a volcano is a unique highly conducting convection cell. Anderson et al. (1965) claim that lightning in the volcanic cloud - which as explained above are visible only on the boundary of the plume - occur only a rather small volume, upwind of the plume, because, downwind, the opaque cloud screens the visibility of "*e*-discharges". Thus, Anderson et al. (1965) carried out a frame-by-frame examination of a film for getting an average picture of the lightning distribution. By hand-drawing and visual inspection of the film, they plotted all lightning pictures on one plot, and all of them – as expected due to the aforementioned reasons - appear to occur on the outer boundary of the plume (figure not here shown) - and some of them extended well up into the top of the plume.

They report a mean of ~20 $discharges\ per\ hour$. The longest period with no observed lightning was ~20 min. In addition, several case histories showed lightning seen in two alternate frames, but never in successive frames. That is, a discharge is a domino effect applied to ball lightning (*BL*s; see Gregori and Leybourne, 2025e). The propagation speed of a discharge is much lower than e.m. phenomena. Hence, there is need for a recovery time, in order to generate anew the conditions for triggering a new *BL*-domino effect, i.e., a new lightning. That is, the physical reason of such an effect ought to be that the Cowling dynamo has a recovery time that is longer than the time interval between two successive frames.

They also comment that "*… short, sharp clicks of radio static were often detected with a small transistor radio tuned to* 550 $kcycles$. *At night it was often possible to correlate these with the appearance of lightning in the cloud over Surtsey*." That is, a lightning discharge is an emitting radio antenna.

ISSN number; ISSN 2202-0039

The final comments refer to a different stage of the evolution of the volcano. Since the time of early observations, the nature of Surtsey's activity changed, even though the activity never stopped. On 4 April 1964 a wall of scoria was formed, which prevented sea water to flow into the crater. When this wall formed, both violent eruptions and lightning ceased. That is, water is an essential component, being a source of the hot fluids that transport heat by advection, and these fluids have a great mobility. Water vapor is therefore a crucial ingredient for volcanic activity, and a source of free electrons that permit "*e*-discharges". With no water supply, the crater was therefore filled with molten lava, which sometimes flowed in streams down into the sea. This fact caused clouds of steam and, presumably of sea-salt particles.

Björnsson carried out, on 24 July, additional measurements of potential-gradient, carried out aboard another *Icelandic Coast Guard* vessel. A thin stream of hot lava had fallen into the sea, and generated a dense, white plume that at the beginning was ~10 m in diameter. Then, wind carried this plume along the shore, lifting it to ~200 m while it became a horizontal cylinder ~100 m in diameter. The vessel sailed beneath the cylindrical cloud and moving at a right angle with respect to it, ~800 m downwind from the cloud and ~200 m offshore. A positive potential-gradient of ~33 $V\ cm^{-1}$ was recorded offshore, under the cloud, as plotted in a figure not here shown. This ~33 $V\ cm^{-1}$ value was ~25 $times$ the fine-weather value over the ocean, which was ~1.3 $V\ cm^{-1}$. That is, a lightning implies no relevant e.m. coupling of the plume with the ionosphere, which has therefore a large charge originated by the Cowling dynamos inside the global cloud pattern (see Gregori et al., 2025d).

The presence of lava envisages a "quiet" emplacement of fluid (lava) that, through advection, affords to transport the needed amount of endogenous heat. No explosive eruption occurs, hence the volcanic plume seemingly is no longer the prolongation of the volcanic sea-urchin spike through the atmosphere. Maybe, also the electrostatic state of the ionosphere is not sufficiently intense. In any case, the e.m. coupling between volcano and ionosphere causes no direct lightning discharge.

The trend - displayed while crossing beneath the horizontal plume - means that the condition of Fig. 15b was found. However, the insufficient e.m. coupling with the ionosphere could not determine the phenomenon of Fig. 15c that, through a lightning discharge, had to cause the transition to the condition of Fig. 15d.

For completeness, also the tentative estimates of the net charge should be mentioned that were carried out by Anderson et al. (1965). They relied on all series of measurements, and on the aforementioned Björnsson's July ~1.3 $V\ cm^{-1}$ value for the fine-weather potential-gradient at ocean surface, and on the February ~40 − 80 $V\ cm^{-1}$ measurements at ~300–500 m upwind from the volcano. They applied the Gauss theorem (Chalmers, 1957, p. 213).

Anderson et al. (1965) were concerned with the disturbance produced by the corona discharge from the top-point of the mainmast, because it can affect the records carried out by the Po device. The rationale that they applied is pictorially represented by the transition between the condition of Fig. 15b to the condition of Fig. 15d, which is caused by the lightning represented by Fig. 15c. With reference to the whole set of their observations, they point out that, for a large fraction of the observed lightning, the top of the cloud above the ocean was at a height ~500–700 m and the tops of the visible discharges at ~200–300 m, while an elevation angle of ~40° − 45° was estimated for the lightning top.

They also considered the values for the potential-gradient changes that followed the lightning. Thus, they concluded that possibly ~0.1–0.5 C of positive charge was neutralized in many of these discharges. That is, the potential-gradient beneath the cloud was reversed, due to the negative charge of the "floating" suspended negative ions and/or tiny particles that are eventually responsible for "*ion*-discharges". They estimated the amount of positive charge, which is needed to compensate the negative charge of the cloud for getting fair-weather values. In addition, the high potential-gradients were typically regenerated in ~10 − 40 sec. Hence, they guessed that charging currents of ~30 mA ought to have accompanied this kind of events.

They likened the cloud to an ellipsoid of revolution about the vertical axis. They measured the dimensions of cloud images on the motion-picture films. Finally, they computed the volume enclosed by the cloud edges. At the times of a discharge, they estimated volumes of ~108 m^3, hence a charge concentration of ~2×10^4 $elementary\ charges\ cm^{-3}$.

The volume of the volcanic cloud increased by an impressive amount - as in several instances it exceeded ~10^7 $m^3\ sec^{-1}$, with a starting ascent velocity of the steam jets that often resulted ~150 $m\ sec^{-1}$. The area of the orifice, estimated from aerial views, was not larger than ~5000 m^2. Thus, the volume rate-of-flow of steam, which was released at ~150 $m\ sec^{-1}$, was not greater than ~10^6 $m^3\ sec^{-1}$, being only a small fraction of what was estimated from the growth of the outline of the cloud. Thus, they considered the high-speed jets rapidly expelled from the volcanic cloud. Finally, the concentration of the net positive charge in the effluent steam possibly resulted to be as much as 100 $times$ the previous estimate.

Finally, according to the relations discussed by Vonnegut (1963), they estimated ~10^6 J for the energy released in one of these discharges. This is ~1/1000 the energy estimated for a lightning in a thunderstorm. That is, compared to a volcanic plume, the Cowling dynamo inside a meteorological cloud is a much more effective e.m. device, maybe because it deals with light air-molecules, rather than with heavy particles of pyroclastic material. The smaller mass of particles is such that the preferential effect can be focused on the e.m. aspect, rather than on the kinetic and thermal energy of the massive particles.

ISSN number; ISSN 2202-0039

In fact, a volcanic cloud of this kind is composed of negative ions and heavy particles, suspended in air due to the positive charge of the ionosphere that opposes the gravity field. In any case, a warning is given about the reliability of a measurement of the potential-gradient by means of a Po source, by which error-bars can be a serious bias (see Gregori and Leybourne, 2025d).

In addition, concerning the period of active eruptions on 16 February 1964, the estimated ($\sim 1000\ kW$) average rate of released electrical energy is $< 1/1000$ the estimated rate for thermal energy released from the volcano. That is, the e.m. energy in a catastrophic volcanic eruption is a small percent of the total energy of the explosive phenomenon, which is, rather, manifested as mechanical (i.e., kinetic and thermal) energy. This is consistent with the aforementioned inference that the Cowling dynamo inside a cloud is much more effective than inside a volcanic plume.

A different estimate was carried out by means of the observations from Vestmannaeyjar, and of the aforementioned Björnsson's 22 March measurements aboard the *Icelandic Coast Guard* vessel, while sailing at $\sim 6\ m\ sec^{-1}$ and crossing $\sim 2\ km$ downwind beneath the plume, which was a horizontal cylinder $\sim 100\ m$ in diameter. At that time, the cloud top was at $\sim 3000\ m$ height.

According to measurements, the fine-weather gradient over the ocean was $\sim 1.3\ V\ cm^{-1}$, while - when the ship was directly under the plume - the surface potential was $\sim -20\ V\ cm^{-1}$, and zero when the ship was $\sim 700\ m$ on either side of the axis of the cloud line. At $\sim 2000\ m$ on either side of the plume the surface gradient was $\sim +30\ V\ cm^{-1}$. Evidently the *Icelandic Coast Guard* vessel was crossing beneath a "secondary" plume or "*ion*-discharge", which was only a horizontal cylinder $\sim 100\ m$ in diameter, mainly composed of “floating” negative ions and/or charged heavy particles, while, above the "secondary" plume of the "*ion*-discharge", the main plume did not perturb the standard positive potential-gradient. The "secondary" plume affords, however, to cancel - and to oppose the positive potential-gradient of the "primary" and main plume - only inside a belt of $\sim 700\ m$ on either side of the axis of its cylinder.

In contrast, Anderson et al. (1965) forgets about the fact that the ionosphere is well-known to have a positive charge - which is partially neutralized by a "primary" lightning discharge, i.e., by an "*e*-discharge". They just consider the formation of an electrical dipole inside the volcanic cloud due to a vertical separation of charges, consistently with the fashionable Wilson model for the electrostatic charging of the ionosphere (Gregori et al., 2025d). That is, Anderson et al. (1965) speculate about an electric dipole structure. They warn, however, that undoubtedly the true charge distribution is other than the simple model they assume. In fact, since they forgot about the positive charge of the ionosphere, their model could not fit observations. They conclude, however, that, compared to the negative charge, the positive charge shows a wider horizontal distribution - transverse to the plume. This is consistent with the much larger inertia of ions and dust particles, compared to the highly movable free electrons.

Therefore, the Anderson et al. (1965) model holds only indicatively. In any case, they comment that - at $\sim 2\ km$ downwind from the volcano - the cloud had vertical depth of $\sim 1500\ m$ according to estimates from photographs. Hence, the guessed mean charge concentration in the cylinder is $\sim 6000\ elementary\ charges\ cm^{-3}$, and, since the wind carried the cloud-plume horizontally at $\sim 3\ m\ sec^{-1}$, the positive charge flux was $\sim 3\ mA$. They also point out that the center of "gravity" of the lower charge was either inside or close to the cloud base, rather than closer to the ocean surface - as expected if it refers to the falling volcanic dust. In fact, the negative charges are the "floating" ions or tephra or dust particles that are responsible for an eventual "*ion*-discharge".

Then, Anderson et al. (1965) carry out another estimate. When, on 24 July, the lava flowed from the crater into the sea, the ionized cloud lost all electrons that immediately flew to the ionosphere. Thus, the cloud carried a net positive charge. Hence, the cylindrical plume of $\sim 100\ m$ diameter carried an estimated charge $\sim 0.01\ C\ km^{-1}$, or a net charge concentration of $\sim 10^4\ positive\ elementary\ charges\ cm^{-3}$. This value is consistent with estimates derived from the Björnsson's observation of 22 March. The diameter of the plume at its source was $\sim 10\ m$, where the charge concentration was therefore $\sim 10^6\ elementary\ charges\ cm^{-3}$.

They do not afford to make estimates from airborne measurements, because, compared to sea-level measurements, owing to Fig. 7, the observed $\boldsymbol{E}$ is considerably less perturbed while flying above a volcanic plume. They stress, however, the $\boldsymbol{E}$ records of 16 February. At that time the plane followed a charged cloud downwind, and the greatest $\boldsymbol{E}$ was around the cloud close to the crater. In fact, this is the central axis of the huge convection cell supplied by the whole volcano. The convection cell generates a violent Cowling dynamo that transports positive charge to the ionosphere (or negative charge, i.e., electrons, down from the ionosphere; see Gregori et al., 2025d).

In addition, Anderson et al. (1965) stress that $\boldsymbol{E}$ decreased by one order of magnitude within $10\ min$ after the eruption, and subsequently it relaxed with a time constant of $\sim 7\ min$. That is, the "*e*-discharge" that raises from the edge of the plume lowers the local positive charge in the ionosphere, and the estimated relaxation time is an interesting datum. They also stress that in no observed case history an $\boldsymbol{E}$-increase seemed to be associated to any charge generation that could be associated to tephra or charged fallout from the cloud downwind. In addition, they comment that a similar rate was monitored on 24 July from the *Coast Guard* ship, when it followed the plume downwind.

Anderson et al. (1965) conclude that the thermal-energy supply by Surtsey to the atmosphere is comparable to a thunderstorm input. They quote Braham (1952) for the estimated rate of energy release from heat of the condensing

ISSN number; ISSN 2202-0039

water in an average thunderstorm, being of order of $\sim 3x10^{18}\ erg\ sec^{-1}$, while, according to Thorarinsson and Vonnegut (1964), the thermal energy released by Surtsey was $\sim 10^{18}\ erg\ sec^{-1}$.

The Anderson et al. (1965) comments appear intriguing - and very pertinent to the discussion in the present study - that deal with the competing role of electrification by the standard cloud generator mechanism, compared to the role of the volcano. Indeed, they did not know about the Cowling dynamo, and about the distinct case histories of the Cowling dynamo inside a thunderstorm cloud compared to the Cowling dynamo inside a volcanic plume. In either case, the primary energy supply is thermal convection, although supplied by a different source, and applied to particles of different mass, i.e., to ionized air molecules and ions in a thunderstorm cloud, and to ash, lapilli, and pyroclastic materials in a volcanic plume. This basic physical difference determines all observed morphological distinctions.

The final comments by Anderson et al. (1965) denote several differences with the interpretation that is here given. They first comment that all aforementioned observations were not directly connected to standard thunderstorm activity. In addition, they stress that all evidence envisage a positive charge of the volcanic cloud. In fact, the electron component almost immediately propagates through the ionosphere by an "*e*-discharge", while the cloud remains positively charged. They also comment that lightning occurs shortly after an eruptive event, although the time lag is so short that it is very difficult to estimate. Indeed, this is what must be expected. In fact, unlike every different tentative belief, the friction inside the plume is not the source of electrification for visible lightning. It rather reflects a phenomenon supplied by the *TD* dynamo through the sea-urchin spike of the volcano.

They also stress that the records - carried out either at ocean surface or from the air - detect a potential-gradient that is more intense near the crater and that rapidly decreases with distance. That is, the phenomenon is very intense close to the axis of volcano, where the huge convection cell is more intense, as the volcano operates like an anomalous restricted and well-defined heat source that causes a convection cell. They also comment that the cloud had no detectable dipole structure.

Finally, they conclude and stress the similarity of their records, upwind of Surtsey, with those made near volcanic eruptions in Japan by Hatakeyama and Uchikawa (1951), by Ishikawa et al. (1951), and by Hatakeyama (1958).

Anderson et al. (1965) discuss the several tentative hypotheses that were envisaged for justifying the electrification process, maybe based on the contact between lava and water, although the process also occurs in absence of sea water, etc. This discussion is not here pertinent. They conclude that "*the mechanisms of particle formation and electrification are far from clear*."

Genge (2018) recently investigated the role on climate played by electrostatic effects on volcanic ash. Genge (2018) summarizes his conclusion and claims that the convective rise of fine ash and aerosols into the stratosphere causes short-term climate change triggered by large volcanic eruptions. He warns, however, about the large net electrical charges inside volcanic plumes that can influence the dynamics of ash particles. He estimates that, during large eruptions lasting more than a few hours, ash inside plumes $< 500\ nm$ in diameter can be lifted into the ionosphere by electrostatic levitation.

Genge (2018) comments that the ash levitation into the mesosphere is consistent with the disturbances observed in the ionosphere during eruptions – and, in addition, also with the polar mesospheric clouds observed after the AD 1883 Krakatau eruption. Therefore, huge volcanic eruptions likely put significant quantities of charged ash into the ionosphere. The effect ought to be - on time scales of $100\ sec$ – a disturbance, redistribution of charge, or a collapse of the global electrical circuit.

In addition, Genge (2018) stresses that the atmospheric electrical potential can affect cloud formation. Indeed, according to the mechanism that is here envisaged (Gregori et al., 2025d), this is a vague statement. Therefore, also this indirect effect can originate radiative forcing and abrupt effects on climate. This is, rather, the effect of a so-called nuclear winter scenario, which is an effect of the atmospheric electrical circuit. The most typical example is shown, e.g., by the well-known average air temperature and precipitation records following the 1883 eruption of Krakatau.

Radio lightning discharges and flight security. Mount Spurr 1992

Radio lightning discharges require an independent discussion, as the primary phenomena are substantially different. In fact, friction inside pyroclastics within the volcanic plume causes emission of radio waves, even though no visible phenomena can be observed, due to the composition of a huge number of micro-sparks inside the plume that cannot be observed through the opaque medium.

Consistently with the impact on the atmospheric electrical circuit, a different kind of measurement was carried out during three eruptions of Mount Spurr, Alaska (see Fig. 16). They showed that the atmospheric electric discharges - detected by radio emission and by triangulation by different receivers - only occurred along the outer boundary of the plume (Fig. 17), showing that, at least in this case, radio emission are originated only at the boundary of the plume. Measurements were carried out during an active period of Mount Spurr that, after $39\ years$ dormancy, displayed three eruptive paroxysms in 1992 (*Alaska Volcano Observatory*, 1993).

According to Riehle et al. (1994), on 27 June 1992, after a conspicuous series of tremors and earthquakes, the eruption started at ~ 15:05 UT. "*... Pilot reports estimated the plume to be as high as* ~9 *km, and the* National Weather Service *(*NWS*) estimated a plume height of* ~14.5 *km*

NCGT Journal
New Concepts in Global Tectonics

New Concepts in Global Tectonics Journal
Volume 13, Number 6, August 2025

ISSN number; ISSN 2202-0039

*based on C-band radar measurements ... The eruption lasted ~4 hours … Tephra volume was ~50×10^6 m^3 [~20×10^6 m^3 dense-rock equivalent (*DRE*)], and was mostly juvenile andesite ... "*

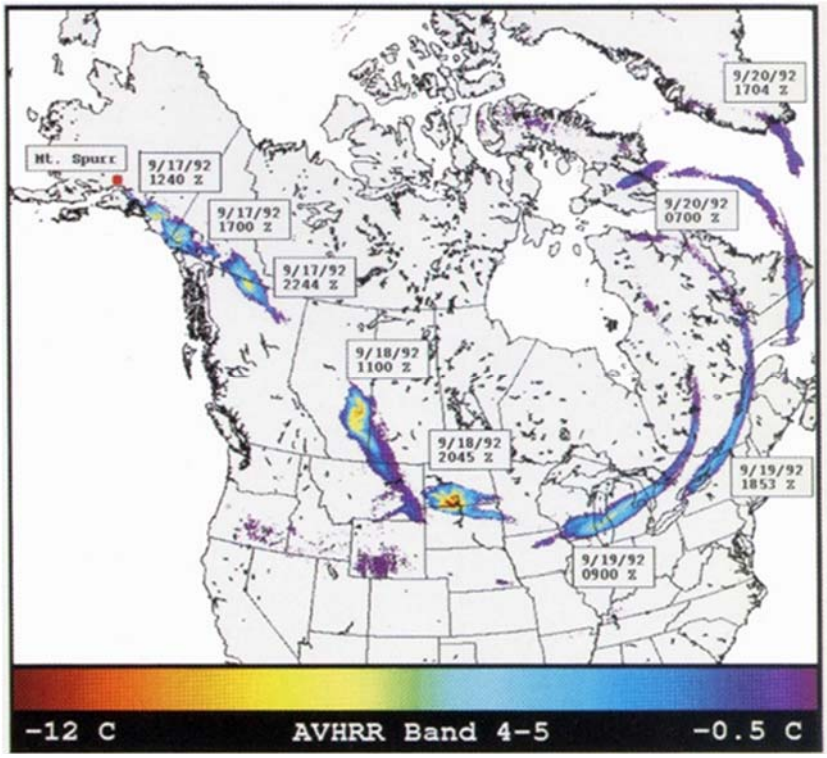

Fig. 16. "*A composite of nine* NOAA-AVHRR *(*Advanced Very High Resolution Radiometer*) images of the September 1992 cloud erupted by Alaska's Mount Spurr. Multispectral* AVHRR *can map ash clouds for days after the eruption, possibly even after they cease being a hazard to aviation. If the concentration of ash can be determined by image characteristics, then the degree of hazard posed by the plume can be assessed by satellite data. (Courtesy by D. J. Schneider).*" Figure and captions after Riehle et al. (1994). With kind permission of *AGU.*

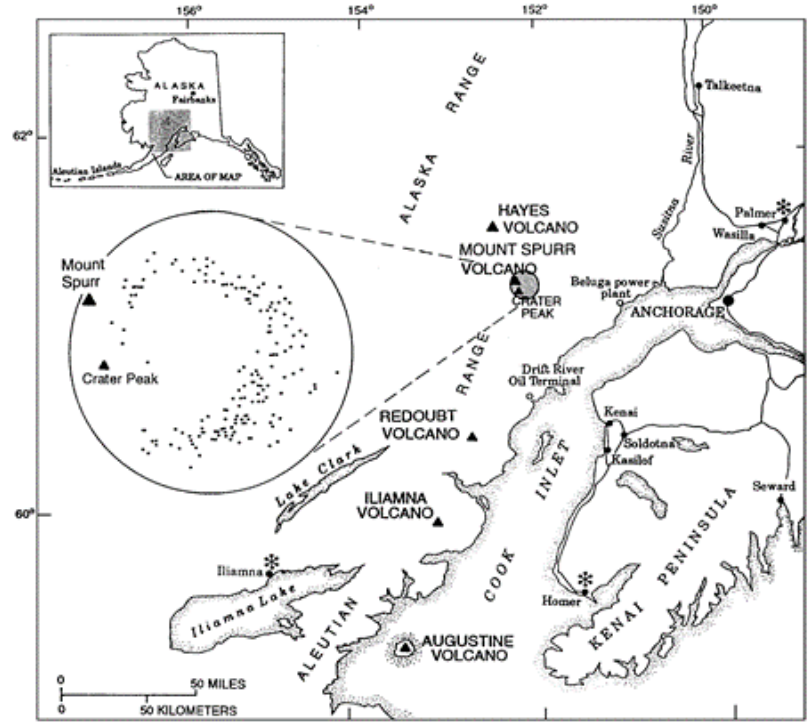

Fig. 17 - Cook Inlet area and locations of the active volcanoes. Asterisks show locations of *LDS* (lightning detection system) receivers. Enlarged view (inset) of area surrounding Mount Spurr shows *171* lightning strokes. Figure and captions after Paskievitch et al. (1995). Note that the radio emissions seem to occur almost along a spiral, instead of ring. In this respect, B.A. Leybourne also noticed some similar effects in Florida, where lightning seemed to concentrate mostly along the edges of the geomagnetic anomalies. Maybe this is a coincidence. However, one wonders if a very large effect may also have lightning inside an air-earth current, such as in an arc blast scenario (Leybourne et al., 2025). Also, possibly a storm - i.e., a large cloud system associated to a large Cowling dynamo (Gregori et al., 2025d) - may exhibit comparable spiral features. With kind permission of *USGS.*

The second eruption occurred on 18 August 1992. "*At 23:48 UT a pilot reported an ash-rich plume. The main eruption began at 00:42 UT (of August 19) ... By 00:58 UT a sub-Plinian column thrust through low clouds to reach ~11 km altitude ... Ultimately, the radar-determined plume top reached ~14 km - pilot reports were higher ... More*

NCGT Journal
New Concepts in Global Tectonics
New Concepts in Global Tectonics Journal
Volume 13, Number 6, August 2025
ISSN number; ISSN 2202-0039

than 170 *lightning strikes were detected by the* AVO (Alaska Volcano Observatory*) lightning detection system (*LDS*) during the second half of the eruption. Eruption ended after ~3 hours 28 min at 04:11 UT ... ... The volume of August tephra is ~*$110 \times 10^6\ m^3$* [~*$40 \times 10^6\ m^3$* DRE] ...".*

The third eruption occurred on 16-17 September 1992. *"… An eruption, accompanied by brief incandescence, began at 06:36 UT (of September 17th) but lasted only* 11 *min ... At 08:04 UT on 17 September the main phase ... began impulsively, accompanied by intermittent bright incandescence ... This eruption lasted* 3 *hours* 36 *min ... The ash cloud rose to a radar-determined height of nearly* 14 *km ... Tephra volume is ~*$50 \times 10^6\ m^3$ [$20 \times 10^6\ m^3$ DRE]."

During the first eruption the (radio) *LDS* was not deployed, although lightning discharges were visually observed. However, recording instruments were set up to monitor the location of the volcanic plume even in overcast weather, for flight security applications. This is considered a well-known real great hazard (Casadevall, 1991; Riehle et al., 1994), particularly in Alaska, due to the large number of volcanoes and of flight paths crossing that area, and due to the adverse meteorological conditions, that often occur in polar regions (Fig. 18).

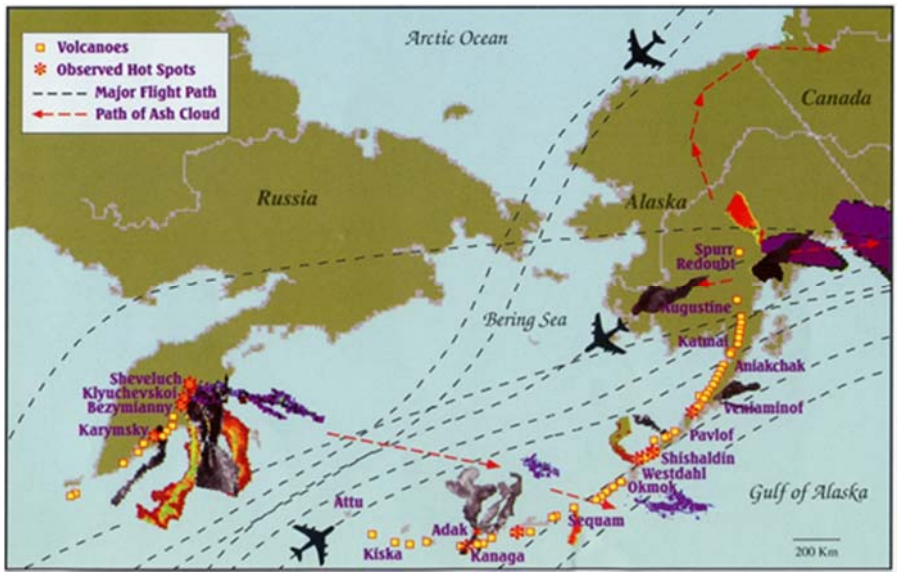

Fig. 18 - Air traffic in North Pacific, showing volcanoes and their plumes observed with their respective eruptions. After Berry (1997). With kind permission of *Geophysical Institute, University of Alaska.*

During the second eruption the measurements were collected that are shown in Fig. 17.

Paskievitch et al. (1995) comment that they "*detected and located* 171 *lightning strokes during the August 18, 1992, eruption of the Crater Peak vent of Mount Spurr ... The strokes, predominantly intracloud (*IC) [see comment below], *were detected during a* 70 *min interval that began more than an hour into the eruption. All detected strokes were of positive polarity.*

*The spatial distribution of the strokes in the horizontal plane defines a ring-like pattern ~*10 *km in diameter, and displaced roughly ~*5 *km to the east of Crater Peak ... This displacement is consistent with the migration of the eruption cloud resulting from the westerly winds during the eruption (Neal et al., 1995) ... Although lightning was observed during the September 16-17, 1992, eruption of Crater Peak, no lightning was detected by the* LDS."

That is, lightning was observed, although it was anomalous because it was not detected by the *LDS*, and the radio signals originated from "*strokes, predominantly* IC". They call (see below) "strokes" the *IC* discharges, and "strikes" the cloud-ground (*CG*) discharges. That is, this is an e.m. phenomenon, although substantially other than all other lightning discharges. Since the phenomenon is mainly *IC*, it is the likely consequence of the Cowling dynamo inside the volcanic plume, while it is not concerned either with a cloud/ionosphere discharge ("primary" lightning) or with a cloud/ground discharge ("secondary" lightning).

Paskievitch et al. (1995) also specify that "*at the time of lightning detection, the eruption column had extended to its maximum altitude of ~*14 *km on the basis of C-band radar estimates (Rose et al., 1995), or* 18 *km (unpublished pilot reports). Satellite imagery near this time depicts an elongate plume extending to the east. The* National Weather Service's *C-band radar provides a cross-sectional view of the plume (not the eruption column) displaced to the east of the vent. The image shows zones that are defined by regions of like particle size (Rose et al., 1995)."*

That is, the radio source, identified with the electric discharges, occurred only at the boundary of the volcanic plume, i.e., where the σ of the environment rapidly decreases from the electrically very conductive plume interior to the almost non-conducting surrounding air. The plume appears to be only slightly bent, by a modest amount, similarly to what occurs to every volcanic plume that is bent by meteorological circulation. It would be interesting to

ISSN number; ISSN 2202-0039

know the state of the auroral electrojet at the time of this eruption in order to guess the possible role of $\boldsymbol{E}$ field of ionospheric origin.

The following specifications are also important, in order to point out the meaning of the classification into "strike" or "stroke", into *IC* and *CG*, etc.

"*The spatial pattern made by the stroke locations is very uniform, which suggests that it is not a random function. Stroke occurrence and location are most likely controlled by concentrations of particle-size fractions or particle densities within the plume that in turn control charge densities and polarities.*

Analyses of stroke signals suggest that $> 70\%$ *of the strokes were intracloud (*IC*), and the remaining* 30% *were ground strokes, or strikes* [i.e., cloud-ground, *CG*]. *However, caution must be exercised when considering the distinction between these* IC *and* CG *strokes. The* LDS *determines stroke type with a model that is based on typical meteorological lightning. The time between peak stroke signal and the first polarity change is measured. If this time interval is* $< 10\ \mu sec$*, the stroke is classified as* IC. *If the time interval exceeds* $10\ \mu sec$*, a* CG *is indicated. However, volcanogenic lightning might behave quite differently than meteorological lightning in this regard. For instance, the conductive ionized channel that precedes volcanogenic lightning could perhaps be a slower path than that for meteorological lightning (Rodney Bent,* Atmospheric Research Systems, Inc*., oral commun., 1992). If this were the case, some volcanogenic* IC *strokes could be misclassified as* CG.

Stroke amplitudes, calculated by AVO*'s central analyzer, for the* 50 *detected* GC*s ranged from* $15\ kA$ *to* $40\ kA$ *with an average amplitude of* $22\ kA$*. These values fall within the range of* CG*s observed in local area thunderstorms but approach neither the low nor high values that describe this observed range (*$3.5\ kA - 350\ kA$*). The* LDS *is unable to calculate amplitudes for* IC*s.*"

The "mystery" of the non-detection of discharges during the third eruption period originated some concern that these authors, comment as follows.

"Lightning was neither detected nor observed during the June eruption. Although the occurrence of lightning was observed during the September eruption, none was detected by the LDS *even though the system appeared to be operational. Indeed, the system probably did not detect all of the lightning that occurred during the August 18 eruption, even when the system was fully operational. There are several possibilities for this. The simplest explanation is that the signal from* IC *lightning has a lower amplitude than* CG *lightning.* [This is reasonable, as *IC*s are "*e*"-discharges, and *CG*s "*ion*"-discharges.] *Data from the August 18 eruption indicate that* IC*s predominate. Possibly the typical signal levels from these strokes fall below the detection threshold of the* LDS. *The subset of strokes recorded for the August 18 eruption may have produced greater signal strengths and were therefore the only ones detected.* [In fact, a crucial control factor is the local electrostatic charge of the ionosphere (Gregori et al., 2025d).]

Considering the similarities between the three eruptions, it is puzzling the strokes were detected for only the August eruption. Perhaps subtle factors are involved in an eruption that would raise the stroke amplitudes or affect other stroke characteristics that would allow for detection. Also, atmospheric and meteorological conditions at the time of an eruption may influence volcanogenic lightning characteristics."

This shows that several different kinds of e.m. phenomena are associated with a volcanic plume, even other than a spectacular lightning discharge. Every different observed phenomenon is a possible diagnostic information, and every phenomenon should be independently interpreted. Only the information on the state of the ionosphere can give a better possibility to assess the real physical mechanism.

In fact, as mentioned above, during the third eruption the *LDS* monitoring system was in operation, but it detected no electric discharges. The plume certainly existed. However, no radio signals emission occurred analogous to the occurrences observed during the second eruption. This shows that the same volcano - on the occasion of subsequent paroxysms during the same eruptive cycle - implies a substantially different σ inside its plume. Maybe, these comparatively different meteorological and/or ionospheric conditions were responsible for a different behavior. Maybe, a different e.m. supply occurred from the underground source. In either case, the plume was substantially different in different case histories. Or, more likely, since lightning discharges in volcanic plumes occur only during some restricted time intervals of an intense eruption period, it is possible that the characteristics of the electrostatic coupling between volcano and ionosphere eventually experiences an evolution. In this way, identical conditions, which should have identical electrical phenomena, give rise to eventually different morphological features.

It is worthwhile mentioning some details of the experimental setting, in order to understand the kind of the detected signal. Paskievitch et al. (1995) refer to the *LDS* installed by *AVO* in 1991, and comment as follows.

"The typical lightning discharge, or flash, is composed of a number of strokes. The series of strokes associated with a lightning flash occur within a $few\ 10^{-1}\ sec$. [These strokes are generated by the e.m. field produced by Cowling dynamos operative inside different atmospheric clouds and are independent of volcanic activity. In addition, every lightning is an oscillatory phenomenon up-and-down from the ionosphere.] *A lightning discharge is termed a 'strike' only if it makes contact with some conductive surface such as the Earth, trees, or aircraft.* [Note that trees must be considered as part of Earth's surface. In contrast, an aircraft is a conducting object inside an externally applied $\boldsymbol{E}$. Electrostatic induction generates a charge separation on its surface. A discharge occurs when the intensity is such as to

ISSN number; ISSN 2202-0039

overwhelm the air insulator. In some respect a slow-motion and a reduced energy-scale - a film-sequence of this process - is displayed by the interaction of a *BL* (ball lightning) with an aircraft (Gregori and Leybourne, 2025e).] *Each discrete stroke of lightning generates a broadband radio signal that radiates at the speed of light in an omnidirectional pattern.*

The LDS *at* AVO *incorporates lightning stroke detectors in the Alaska cities of Palmer, Iliamna, and Homer (Fig. 17). These detectors monitor a portion of the radio frequency spectrum for a lightning-induced instantaneous rise in signal amplitude. A stroke that generates a radio signal with an amplitude exceeding the detector's threshold will be recorded at each detector at a different instant in time. The time of arrival of a signal is measured and recorded to sub-* μsec *resolution. Using these precise times of arrival and the known locations of the detector sites, a lightning stroke's location can be determined."*

Concerning the morphology of the eruption, they specify that "*following* ~10 $months$ *of elevated seismicity, the volcano erupted explosively on June 27, August 18, and September 16-17, 1992. The site of the three eruptions was Crater Peak, a satellite cone at* 2,300 m *elevation on the southern margin of the caldera and* 3.2 km *south of Mount Spurr's summit cone (Nye and Turner, 1990). The three eruptions of Crater Peak were similar in character. The eruptions were explosive with sudden and impulsive onsets to each main phase. Duration of the main phase of each eruption were* $3.5-4$ $hours$ *, material ejected largely consisted of andesitic tephra, dense-rock equivalent erupted volumes for each of the eruptions were similar (Neal et al., 1995), and maximum radar-discernible column heights were* $\sim 13-15$ km *above sea-level (Rose et al., 1995).*"

In addition, "*the main phase of the August 18 eruption began at 4:42 pm* ADT *(Alaska daylight time). The* LDS *was unable to establish communication with the detector at Iliamna and therefore was not fully operational prior to 6:30 pm* ADT. *This prevented direct comparison of the onset of the eruption with the onset of lightning. Although the* LDS *first detected and located lightning at 6:30 pm* ADT*, it is known that lightning did occur before this time ... Once communication to all three detectors was established, the* LDS *recorded* 171 *strokes during a* 70 min *interval*."

Also lightning, as mentioned above, were observed during this eruption series. McNutt and Davis (2000) comment that seismograms recorded simultaneous spikes, and a gain-ranging, i.e., a lowering of the gain at a station that occurs when the signal level begins to saturate. The records showed spikes of typical duration ~0.04– 0.05 sec. According to a uniform criterion, they report *28* lightning on June 27th (weakest activity), *29* on August 18th (strongest activity), and *3* on September 17th (intermediate activity). The three eruptive series showed the first lightning $\sim 21-26$ min after the onset of the eruption. They envisaged that "*the charge separation occurred in the convecting cloud rather than at the vent*." This fact envisages that, according to the interpretation here proposed, some physical and non-vanishing time is required by the atmosphere to acquire a suitable structure, through air convection etc. in order to supply an intense Cowling dynamo. An alternative possibility is that the electric potential - required to trigger a discharge - needs some time lag to attain its discharge-threshold through the underground circuitry related to the *TD* dynamo.

According to our rationale, no significance should be attributed to the negative or positive polarity of discharges, as the direction of the discharge depends on where the trigger occurs, because the phenomenon occurs like a domino effect in both directions of the conducting column. It is an oscillatory phenomenon (Gregori and Leybourne, 2025g).

"All three eruptions had similar durations of $\sim 3.5-4$ $hours$*, and tephra volumes of* $\sim 44-56 \times 10^6$ m^3*. The August eruption, however, produced stronger volcanic tremor,* 30 cm^2 *reduced displacement as compared with* 16 cm^2 *for June, and greater gas,* $\sim 400 \pm 120$ kt SO_2 *for August and* $\sim 200 \pm 60$ kt *for June."* McNutt and Davis (2000) claim, therefore, that tremor amplitude and magmatic gas content seem to correlate with lightning strength. We contend this interpretation, being a matter of a coincidence. Winds, more or less intense, influence the evolution of lightning.

In addition, notwithstanding a careful analysis, no simple correlation was evidenced relating to other eruption parameters such as volcanic lightning timing and morphology. In addition, also the comparison gave no result with analogous case histories studied by other investigations. Therefore, a more exhaustive model and explanation of radio signals and/or lightning discharges is likely to be needed in order to use – if possible, at all - these e.m. emissions are like tools for monitoring the state of activity of a volcano for application to flight security.

The comparatively different behavior must be stressed of discharge detection either by radio waves or by lightning. Phenomena are physically very complicated, including meteorological and/or ionospheric factors, and no simplifying model can explain the variety of observations.

Mather and Harrison (2006, p. 405-407) review as follows some previous observations of this same kind. Hoblitt (1994) temporarily installed in 1990 in Alaska a commercially available *LDS* around Redoubt Volcano. The nearest detectors to the volcano were at ~ *100 km*. Broad-band radio waves were recorded by the *LDS* antennæ, and the hardware then filtered out the records that did not show the characteristic waveform of *CG* lightning. Then, *AVO* installed their own *LDS* aimed to monitor the Cook Inlet volcanoes. Then, Mather and Harrison (2006) remind us about the McNutt and Davis (2000) finding of a $\sim 21-26$ min delay after the onset of the eruption. Hoblitt (1994) at Redoubt measured a time delay ~2.5 smaller.

Then, Mather and Harrison (2006) remind us about the eruption of Grimsvötn in November 2004, which was

ISSN number; ISSN 2202-0039

monitored by different remote sensing techniques by the *Icelandic Meteorological Office* (Arason 2005a, b; Vogfjör et al., 2005). They used Arrival Time Difference (*ATD*) lightning location system of the *UK Met Office*, and detected the lightning from the Grimsvötn plume, simultaneously with tracking by the Icelandic weather radar. They detected *250* lightning strikes over Vatnajökull, during the first 36 $hours$ of the eruption. The waveform was measured for *152* lightning events (*70 IC*, and *82 CG*). *IC* events are likely from "*e*"-discharges, *CG* events "*ion*"-discharges. According to the explanation here given, every *IC* lightning should be associated to a direct Cowling dynamo process, while every *CG* event can be caused either by a direct Cowling dynamo process or by a positive "*ion*-discharge" lightning. Mather and Harrison (2006) also stress that the *CG* fraction is greater than what usually occurs in thunderstorms. Indeed, compared to what occurs inside a volcanic plume, usually a much smaller number of positive ions is available inside standard clouds. The maximum observed event rate was for plume heights of ~10 km.

Mather and Harrison (2006) give a Table where they compare terrestrial atmospheric electrical parameters in fair weather, or in thunderclouds, or in volcanic plumes. There is no need to report here these details. In any case, the physics of a volcanic plume is certainly much different, compared to cloud phenomena (Gregori et al., 2025d).

Mather and Harrison (2006, p. 397) also mention measurements carried out during the eruption of Parìcutin (in 1943-1952), Mexico. The ejecta composition changed progressively from basaltic andesite ($55wt\%\ SiO_2$) in 1943 to andesite ($> 60wt\%\ SiO_2$) in 1952 (Luhr and Simkin, 1993). Lightning were always reported, although the phenomenon was not constant. This is reasonable, as the electric potential changed, of the two plates of the atmospheric condenser. Fries and Gutiérrez (1950) recorded electric discharges on 2 $days$ in July, 3 $days$ in August, 3 $days$ in September, 1 day in October, and 3 $days$ in December in 1949. One should check, however, whether the atmospheric potential gradient changed in a large area even further from the volcano, denoting the state of the ionospheric electrostatic field (Gregori et al., 2025d). In any case, an association was reported of lightning with the plume feature, looking more ash-rich. In fact, "*e*"-discharges depend on the ionospheric electrostatic potential, while "*ion*"-discharges depend on the ions and ash particles of the plume. "*Forshag and Gonzàlez-Reyna (1956) observed that lightning on 27th May 1945 was only associated with occasional ash-rich plumes, but none was seen in the steam column.*" Mather and Harrison (2006) also report an information after Fries and Gutiérrez (1950), who claimed that discharges seemed "*more common*" within the column (i.e., within the plume), although they observed also lightning from the rim of the cone. In fact, as explained above, owing to physical facts, no visible lightning can occur inside the plume, and they got a false feeling while interpreting plume images.

In any case, the composition of the plume is irrelevant for discriminating among different plume-lightning physical occurrences. Rather, the size and electrification of ash particles and ions - and their weight - is relevant to determine the "floatation" of negative particles according to the rationale of Fig. 9. Friction phenomena between different materials is not important. Only plume ionization is relevant for a Cowling dynamo process, i.e., the number densities are important for electrons and for positive and negative ions, respectively, independent of composition and of the size-spectrum of dust grains etc.

Behnke et al. (2012) report about a spectacular lightning observed in 2009 during the Mount Redoubt eruption. According to the rationale here envisaged, the violent lightning was an intense "*ion*"-discharge. In contrast, they favor "*separate electrification processes for the explosive and plume phases. During the explosive phase, nearly continuous electrical discharges were observed occurring close to the vent.* [These are "e"-discharges] *Further, the onset of the lightning activity was concurrent with the volcanic explosion, indicating that the ejecta were already highly electrified as they exited the vent* [pyroclastics are certainly highly electrified] …. *a silica-based charging process, in which ash is charged as magma fractures within the volcano, was acting during the explosive phase … The continuation of large-scale lightning in the downwind plume* [i.e. "*ion*"-discharge] *suggests that the same gravitational sedimentation processes that electrify thunderstorms dominated during the plume phase.* [Thunderstorm phenomena are dominated by the Cowling dynamo process, which – should always be stressed – is the *main* cause for the electrification of the ionosphere (see Gregori et al., 2025d). In addition, we emphasize that the Cowling dynamo is a *rigorous* result, *not* speculation. In contrast, the most fashionable Wilson electrification process of the ionosphere is an optional mechanism that can or cannot contribute.] *In this process, oppositely charged particles of different sizes become segregated because of their differing fall speeds.* [This statement to the aforementioned fashionable Wilson electrification mechanism, which is optional, although very likely fully unessential (Gregori et al., 2025d for extensive discussion).] … *Redoubt's plumes generally reached* > 10 *m in altitude, similar to thunderclouds, and contained abundant water and ice. Thus, contact electrification interactions among ice particles or ice-coated ash, water droplets, and supercooled ice pellets may also have played a role.*" That is, the general feeling is completely other than the mechanism that is here proposed. In any case, in general, authors consider a unique kind of visible lightning, while "*e*"-discharges and "*ion*"-discharges are substantially different phenomena.

The two-mode process - for explosive and plume phases - is also mentioned in the short note by Thomas et al. (2007). They are always biased by the reference to standard lightning models. They liken a volcanic plume to a "dirty" thunderstorm. The following comment is interesting.

ISSN number; ISSN 2202-0039

"*Although the plume was undoubtedly charged as a result of the explosion, the fact that the plume lightning was delayed and continued after and well downwind of the eruption indicates that* in situ *charging also occurred within the plume, e.g. as a result of particle interactions involving tephra, ash, and ice hydrometeors."* [Indeed, these are "*ion*"-discharges, physically very different than "*e*"-discharges. The confusion derives from the fact that the Palmieri investigations have been completely forgotten.]

Behnke et al. (2014) report about a very detailed monitoring of the lightning activity during the 2010 eruption of Eyjafjallajökull. They carried out their measurements by means of *6* lightning mapping stations in southern Iceland - and by a radar station they attempted to correlate the varying observed behavior with meteorological parameters. But, they found no clear dependence.

Therefore, a tentative reasonable final inference is that the behavior of the atmospheric electrical circuit in volcanic plumes is a response to three drivers: local meteorological conditions, state of the ionosphere, and electric supply by the *TD* dynamo. In any case, a volcanic plume is definitely other than a thunderstorm cloud, or other than any other kind of atmospheric discharge, either visible (lightning) or not.

In fact, a completely different phenomenon deals with radio emission. This is very clearly evidenced, e.g., Behnke et al. (2021), where the insistent reference must be pointed out made by the authors to a comparison between volcanic plume phenomena and meteorological cloud phenomena. In any case, the fundamental Palmieri measurements are completely forgotten. Quoting the introduction of Behnke et al. (2021), "*the onset of an explosive volcanic eruption is often signaled by a swarm of small electrical discharges originating from the vent, in the rising ash column (Behnke et al., 2013, 2014, 2018; Smith et al., 2018, 2020, 2021; Thomas et al., 2007, 2010). These small discharges, referred to as vent discharges, persist for seconds, depending on the duration of the explosion (Behnke et al., 2013). This long-lasting property creates a distinctive radio frequency (*RF*) signature in the very high frequency (*VHF*) band called continual radio frequency (*CRF*), which contrasts with the* VHF *signature produced by lightning (volcanic or meteorological) over comparable time scales of seconds or longer. The* CRF *impulses persist at relatively high rates for seconds or tens of seconds, while lightning is inherently intermittent, typically creating a burst of high-rate impulses for hundreds of milliseconds, with gaps of time with no impulses between successive discharges. Moreover, the* CRF *signature is unique to explosive volcanic eruptions, i.e., the signature is not observed in thunderstorms (Behnke et al., 2013)."*

Thus they found that "VHF *emissions of vent discharges and volcanic lightning have a mean pulse width of* $50\ nsec$. *Vent discharge impulses are more isolated in time than volcanic lightning impulses, and vent discharges and volcanic lightning have similar* VHF *spectral content."* That is, when dealing with micro-discharges inside an electrified hot fluid – such as inside a volcanic plume or inside a thunderstorm cloud – some similarities are observed, as expected. However, this is other than a Cowling dynamo mechanism inside a cloud, and other than a visible lightning associated to a volcanic plume.

We report here the abstract of Behnke et al. (2021). "*In this study, we analyze the pulse width and spectral content of vent discharges and volcanic lightning flashes. We made measurements of electrical activity with a broadband* VHF *antenna (*$20-80\ MHz$*) during an explosive eruption of Sakurajima volcano on November 8, 2019. The individual impulses that comprise vent discharges and volcanic lightning were analyzed to determine the fundamental width of the impulses and the rate of fall-off of their energy spectral density. The results show that vent discharges are more similar to volcanic lightning than they are different. The mean pulse width for both vent discharges and volcanic lightning was* $50\ nsec$. *Both types of electrical activity had similar spectral content; the average slope of the amplitude spectra was* -3.4 *for both. Further, examination of the pulse width and spectral slope distributions showed that while the distributions of volcanic lightning and vent discharges are statistically distinct from each other, the distribution of vent discharges is a subset of the distribution of volcanic lightning.*"

We must point out that they had no concern about carrying out records similar to the Palmieri measurements that are celebrated in the present paper. In addition, we stress that it is physically nonsensical to compare electrical phenomena inside a volcanic plume with phenomena inside a cloud.

The concern about flight security is seemingly solved by a different technique (Schneider et al., 1995). *Advanced Very High Resolution Radiometer* (*AVHRR*) images from polar-orbiting satellites are used with a two-channel technique (see Fig. 16). "*The frequency of data collection (about once every few hours) allows for an understanding of the patterns of change in spectral response that occur during the evolution of a volcanic cloud. Volcanic clouds imaged during and shortly after eruption are optically thick and can contain abundant water droplets and (or) ice, and these characteristics cause their spectral signal to closely resemble a meteorological cloud. As the volcanic cloud disperses, the spectral properties of the cloud change, first at the edge and then throughout. These changes produce a volcanic cloud signal that can be distinguished by using a brightness temperature difference determined from thermal bands* 4 *and* 5 *of the* AVHRR.*"* However, they warn that *"signal needs to be correlated with ash concentration and particle size to determine when drifting volcanic clouds are a threat to aircraft.*"

This curious behavior of Mount Spurr seems to suggest that the e.m. monitoring of the electric discharges inside volcanic plumes strictly requires to set up a device that simultaneously monitors a wide frequency spectrum. This information seems to be a fundamental parameter for

ISSN number; ISSN 2202-0039

envisaging the different physical features that characterize different volcanic plumes, even of the same volcano - and also for comparing different paroxysms observed during the same eruptive episode. In addition, the astute electrostatic aspects that were investigated by Palmieri were neglected in these investigations.

A recent investigation by Vossen et al. (2021) deals with extremely low frequency ($1-45\ Hz$) recorded during the persistent volcanic activity of Minamidake crater at Sakurajima volcano in Japan in July 2018 through January 2020 (see Fig. A-15). Two thunderstorm detectors were located at a distance of 3 and 4 km from the active vents. They compared the records with other detailed information concerned with monitoring the explosive activity. Their sensors detected discharges in 71% of *724* explosions. They successfully recognized the presence/absence of electrical discharges with an accuracy of 73%. They looked for correlation with the height of the plume, although such a detail is not relevant for the discussion here carried out. They conclude, however, *"fracto- and tribo-electrification appear to be the dominant plume electrification mechanisms.*" That is, they rely on the current present model of the atmospheric electrical circuit, which leads to an interpretation that forgets about the crucial role of the Cowling dynamo inside clouds, and about Palmieri's precursory investigations (see Gregori et al., 2025d).

For completeness, remind about Woodhouse and Behnke (2014), devoted to model volcanic plumes evolution and propagation, on the basis of records of lightning discharges, including the role of wind and the effects of moisture. The purpose is to provide an algorithm suited for flight security. They rely on current present model of the atmospheric electrical circuit, and envisage a *"thunderstorm-style ice-based charging mechanisms*", relying also on *"the availability of condensed water and low temperatures at high altitudes in the plume*". However, they conclude that *"overall this charging mechanism is believed to have had only a weak influence on the production of lightning*."

The electric charge and mass of particles inside a volcanic plume - Electrification by friction

Concerning Sakurajima volcano, the electric charge of ash particles was measured on the occasion of a 16 day eruption period in May 1990 (Gilbert et al., 1991; see also Lane and Gilbert, 1992). They resumed measurements that recall the aforementioned Palmieri pioneering investigations, although they do not mention Palmieri - and seemingly they did not know about his double-wire electrometer.

The concern of Gilbert et al. (1991) was to assess the possible role of electrostatic forces in particle agglomeration to form lapilli. A previous guess, discussed in the literature, dealt with the possible role of atmospheric water, but the evidence was not clear and conclusive. Kikuchi and Endoh (1982) had measured changes in the atmospheric $\boldsymbol{E}$ due to wind-blown erupted volcanic ash (i.e., the rationale ought to be according to Fig. 15). In contrast, Gilbert et al. (1991) focused on the electric charge of ash particles. They used two experimental settings for measuring the ratio between the electric charge q and the mass m of these particles.

In one setting, volcanic ash, while falling, crossed between two copper plates, parallel to each other, inside an earthed case. One plate was at ground potential, the other supplied at $\pm 3\ kV$ that generated an $\boldsymbol{E}$ of $1.2 \times 10^5\ V\ m^{-1}$ between the plates. The charge on ash particles that hit the ground plate was measured on a *Keithley 614* electrometer, which is standard commercial electronic equipment that can monitor electric charge in the range $0.01\ pC - 199.99\ nC$. A layer of oiled *Al* foil covered the plates in order to make ash particles to adhere. Then, the ash was removed from the oiled foil, and weighed in order to measure the q/m ratio.

They also measured the size distribution of the ash particles. In a second experiment, they estimated the average q/m ratio by means of an ion-screened Faraday cup in which the falling ash accumulated. A thin *Al* sheet covered the cup in order to weigh the collected ash. Thus, the two experiments measured, respectively, both the total magnitude of positive and negative charges, and the average charge on the collected ash. That is, the second experiment is much akin to the pioneering measurement carried out by Palmieri.

However, consider the difficulty of this kind of experiment, depending on several perturbing factors that are only partly taken into account, but that Gilbert et al. (1991) accordingly discussed. They considered leakage currents and corona effect, which depend *(i)* on humidity, *(ii)* on the different behavior of particles depending on their size, and, mostly, *(iii)* on the perturbation originated by the recording instrument, due to the progressive integrated electrostatic effect, which changes in time while the experiment is in progress. This drawback is particularly important in the Faraday cup setting, as the Faraday cup gets progressively electrostatically self-shielded, while its Coulomb field favors (or opposes) the collection of particles that, compared to its own charge, have a charge of opposite (or the same) sign.

An additional key effect, which Gilbert et al. (1991) seemingly did not take into account, deals with the different mobility of electrons and ions. Suppose that volcanic ash is electrically neutral. Hence, an equal number is available of positive and negative charges (mainly electrons). However, electrons have a much higher mobility and a very small mass. Hence, the absolute value of the observed q/m ratio (in the two-plates experimental setting) ought to be much larger when dealing with negative compared to positive charges.

They find a substantial asymmetry between positive and negative charges (see below). They (correctly) comment that, in principle, different eruptions could perform differently in terms of electrostatics. Hence, experiments

ISSN number; ISSN 2202-0039

carried out at different times have no strict requirement for being representative of similar physical conditions. In addition, one must always distinguish "*e*"-discharges and "*ion*"-discharges, a feeling that seems to be absent in the literature.

They plotted their results in three figures, not here shown.

In a first run of $100\ min$ the non-earthed plate was kept at a negative potential $-3\ kV$. A plot shows the charge (nC) *vs.* time for the parallel-plates experiment. When the plates are shielded from ash fallout, a flat trend is observed, with a slight decrease due to the electrical conductivity σ of air. The trend with unshielded plates is decreasing with an almost horizontal intermediate plateau that, they specify, corresponded to the time when the ash fall almost ceased. Every ash-fall episode, before and after the plateau, lasted a few to several minutes. They found $q/m = -2.7 \times 10^{-4}\ C\ kg^{-1}$. Temperatures and relative humidity at the start and finish of the experiment were $25\ °C$, 44 %, and $23°C$, 48 %.

The second plot shows the charge (nC) *vs.* time for the parallel-plates experiment using $+3\ kV$ supply. They measured $q/m = +4.9 \times 10^{-4}\ C\ kg^{-1}$. The trend is linear and increasing, and steeper with unshielded plates. Temperatures and relative humidity at the start and finish of the experiment were $20°C$, 66%, and $19°C$, 74%. The second run lasted $90\ min$. The non-earthed plate was at a positive potential $+3\ kV$, hence the positive ash particles were collected by the earthed plate. In either case, with shielded plates, the charge on the earthed plate changed in time due to air σ. Upon comparing the different ordinate scales of both plots, a gentle effect is observed when negative charges are collected by the earthed plate, while a linear and more vigorous increase is observed in the second plot. The very regular linear trend, interpolated during both periods of shielded plates, denotes - independent of ash particle fallout - a seemingly much regular availability of positive particles in air.

According to the aforementioned expectation, owing to the greater electron mobility, one should find a much higher $|q/m|$ ratio (i.e., consider the absolute value) when collecting negative compared to positive charges. The result is just the opposite. Then, if the two experiments can be considered to refer to similar physical case histories, the conclusion should be that a substantial lack of electrons characterizes the ash cloud, consistent with the aforementioned pioneering Palmieri measurements. In fact, electrons very rapidly flow into the ionosphere and reduce the electrostatic charge. This is the same phenomenon as "primary" lightning or "*e*-discharge" - although the discharge always occurs, even in the case that its intensity is insufficient to trigger an emission of light, perceived by the human eye as a lightning.

Gilbert et al. (1991), rather, envisage that measurements refer to different eruptions. That is, the preconceived paradigm of a strictly neutral total electric charge of the ash cloud is always assumed *a priori*, allowing for no possible doubt.

In contrast, the rationale here envisaged relies on the crucial role played by the positive electrostatic charge of the ionosphere (Gregori and Leybourne, 2025b and Gregori et al., 2025d). The positive sign is determined by the prevalent electrostatic charge of the solar wind. The effect is dramatically amplified by the Cowling dynamos that are ubiquitous inside the Earth's atmosphere and are very efficient in transforming kinetic energy of large cloud systems into e.m. energy. Thus, these Cowling dynamos amplify the electric charge of the ionosphere, with its identical sign. Since the charge is positive, the Cowling dynamos of clouds increase, locally, the total positive electric charge of the ionosphere.

To summarize, concerning the exhalations in volcanoes, phenomena are synthetically represented by the cartoon in Fig. 7. Electrons are mainly involved in the electrical circuit that connects the underground ***j*** with the ionosphere. Therefore, the participation of ash particles in the global electric circuitry should be manifested with a large percent of positive particles. They contribute in some way to close the main ***j*** flow between ground and ionosphere. However, electrons accomplish the most important flow. Indeed, this argument can justify the different results expressed in both Gilbert *et al.* (1991) plots. However, as a strict matter of principle, one should simultaneously carry out these two experiments by two identical experimental settings, with and without plate shielding, operated close each other during the same eruption.

This same inference and conclusion is given by the Faraday cup experimental setting shown by Gilbert *et al.* (1991) in a third plot (not here shown). When the cup was shielded from ash fallout, the trend denotes the effects associated with air σ. The result was $q/m = +4.6 \times 10^{-5}\ C\ kg^{-1}$, which confirms the greater role played by positive charges. Temperature and relative humidity were $23°C$ and 33%.

As a tentative working hypothesis, assume that two different measured eruptions can be approximately likened to each other. According to the aforementioned argument, one should find that the result of the Faraday cup experiment is the algebraic sum of the results of the two experiments carried out with vertical plates with opposite voltage supply. That is, the Faraday cup experiment should give $q/m = [+4.6 - 2.7] \times 10^{-4}\ C\ kg^{-1}$, which is $\sim 5\ times$ larger than what is actually measured ($q/m = +4.6 \times 10^{-5}\ C\ kg^{-1}$). This is, however, the consequence of the aforementioned self-shielding by the Faraday cup.

Summarizing, as long as no similar and simultaneous experiments are available, these results are consistent with the general logical framework and interpretation here envisaged of the atmospheric electrical circuit. Conversely, Gilbert et al. (1991) are biased by the paradigm of a speculated total electrical neutrality of the volcanic cloud. They vaguely mention different possible effects associated

ISSN number; ISSN 2202-0039

either to friction (triboelectric effect), or to piezoelectricity during deformation ("fractocharging"), or to fracturing ("fractoemission"). All these effects ought to be triggered "*between particles colliding in the turbulent environment of the ash plume*".

From the viewpoint of the model and interpretation that is here proposed, an additional argument must be pointed out. Different volcanoes can have a different primary heat supply. This same distinction can hold also for every single volcano, which could have a different kind of supply during its evolution, either during an eruption cycle, or on the historical or geological time scale.

One possible reason for this is that a volcano can be directly supplied by Joule heat of underground circuits. In this case, one should observe a specific and very intense e.m. coupling between underground phenomena and the ionosphere.

In contrast, other volcanic conditions ought to imply a prevalent primary supply by friction heat. For instance, the Hawai'i volcanism (Gregori, 2002; Gregori and Leybourne, 2021) is primarily triggered by an increase of Joule heat, which causes an increase of kinetic energy of the sliding lithosphere. This increased kinetic energy causes a larger amount of friction heat that, after a time delay of $\sim 50{,}000 - 100{,}000\ years$, generates an impulse of volcanism (see Gregori et al., 2025n).

Another case history deals with Etna that (maybe) can be the security valve for the friction heat associated with the "hinge" between the African-Sicilian lithospheric slab and peninsular Italy (see Gregori and Leybourne, 2021; Gregori et al., 2025b).

By this, it is meant that the e.m. nature of the coupling between a volcanic plume and the ionosphere can be substantially different when observing different volcanoes, or when observing one and the same volcano at different times of its evolution, either during an eruption cycle, or on the long-period on the either historical or geological time scale.

Gilbert et al. (1991) conclude that "*electrostatic effects greatly influence the dispersal and deposition of ash during explosive volcanic eruptions*".

It is surprising, however, that electrostatic phenomena in volcanism were only very seldom investigated, notwithstanding the remarkable and very intriguing Palmieri's investigations appearing as early as AD 1878.

This fact proves the strength of a subconscious paradigm, by which the present subconscious feeling is that a volcanic eruption must always be electrically neutral. Maybe, the unique (although generally undeclared) logical reason is the "principle of sufficient reason" that, however, is only a response to the human need for "simplicity". In contrast, the present available concepts and understanding are clearly suggestive of a remarkable asymmetry between negative and positive objects.

A physical concern - which has been neglected in the entire aforementioned discussion - deals with the mechanism by which particles inside volcanic plumes are ionized.

A specifically devoted study by Houghton et al. (2013) analyzed the ash of the 2011 Grìmsvötn eruption. Friction electricity certainly plays an important role, also because ash particles are definitely non-spherical. They summarize their findings as follows.

"*The plume from the 2011 eruption of Grìmsvötn was highly electrically charged, as shown by the considerable lightning activity measured by the United Kingdom* Met Office*'s low-frequency lightning detection network. Previous measurements of volcanic plumes have shown that ash particles are electrically charged up to hundreds of kilometers away from the vent, which indicates that the ash continues to charge in the plume (Harrison et al., 2010; Hatakeyama, 1949, 1949a).*

We study triboelectric charging of different size fractions of a sample of volcanic ash experimentally. Consistently with previous work, we find that the particle size distribution is a determining factor in the charging. Specifically, our laboratory experiments demonstrate that the normalized span of the particle size distribution plays an important role in the magnitude of charging generated. The influence of the normalized span on plume charging suggests that all ash plumes are likely to be charged, with implications for remote sensing and plume lifetime through scavenging effects."

The particle size distribution, together with the largely non-spherical shape of particles, play a crucial role, as the larger the contact surface is between different media, the more effective is the ionization by friction. In any case, friction ionization is important, but it is only one facet of a more complicated phenomenon.

Conversely, the fundamental leading role must be stressed of the Cowling dynamo process. The phenomenon is very similar to what occurs in every cloud. The only difference is that the huge thermal source determines a much stronger effect in meteorological clouds than in a single volcanic plume - in terms of energy content on every spatial scale from microscale through macro-scale.

In addition, the Cowling dynamo inside a standard cloud acts on ionized molecules and ions, while inside a volcanic plume it acts on heavier particles, i.e., ions, ash particles, lapilli and other pyroclastic material. Hence, the e.m. response is much more efficient in a standard cloud than in a volcanic plume.

Therefore, it is concluded that, since the Cowling dynamo inside a cloud is co-responsible for the electrostatic charging of the ionosphere (see Gregori et al., 2025d), the seldom occurring volcanic plumes are responsible for a similar effect, although with different efficiency in terms of transfer of kinetic energy into e.m. phenomena.

Note also that - compared to macro-convection - micro-convection is even more important, as it causes a more densely distributed, hence a more effective, friction between ash particles, hence a greater efficiency in terms of ionization.

NCGT Journal
New Concepts in Global Tectonics
New Concepts in Global Tectonics Journal
Volume 13, Number 6, August 2025
ISSN number; ISSN 2202-0039

Volcanic rings

Look at Figs 19 and 20. These volcanic rings are well known and reported from several volcanoes. The explanation is immediately related to a Cowling dynamo process (Gregori et al., 2025d), looking almost like a tutorial case history. In fact, whenever a heat source generates a temporary local convection pattern, a toroidal magnetic field is generated that acts like a "plasma bottle" that confines inside a torus the hot plasma that eventually releases light. The phenomenon is closely analogous – although much more energetic – than the generation of a ball lightning (*BL*). Refer to Gregori and Leybourne (2025e) for detailed discussion.

Suitable conditions must be satisfied, such as, e.g., the presence of highly ionized water vapor, etc. In Fig. 19 the raising column of water vapor is visible, following the snow fall. When the upwelling convection plume exhausts its upward movement, the condition are attained for the formation of the toroidal magnetic field, etc.

The present generally reported models rely on analogies with smoke rings, based on fluid-dynamics applied to neutral fluids, etc. See, e.g., Ichihara et al. (2023) and Pulvirenti et al. (2023).

Fig. 19. Splendid example of volcanic ring photographed over Etna on 18th December 2023, after a significant large snow fall. After Caridi (2023). Permission kindly granted by *MeteoWeb*.

Fig. 20. "*Examples of volcanic vortex rings having a radius of tens of meters observed at Etna (Italy). Photo courtesy of:* ***(a)*** *Giò Giusa;* ***(b)*** *Marisa Liotta;* ***(c)*** *Pippo Scarpinati.*" Figure and captions after Pulvirenti et al. (2023). Reproduce with kind permission of *Scientific Reports* ("Open Access").

Conclusion: past and present air-earth currents

In any case, the great difficulty must be pointed out that is implied by every kind of experiment dealing with a volcanic eruption. The structure, composition, evolution - and non-repetitiveness of the physical system - are such that different authors can propose different speculated explanations. No "final" proof can be given. Peculiar experiments, such as the Caronia phenomenon (see Gregori et al., 2025b; Gregori and Leybourne, 2025g), can eventually envisage a comparatively easier capability to observe (and sometimes control) the observed morphology in a "natural laboratory". That is, an apparent curious whim of nature gives us a facility to test our guessed model and explanation.

The correct approach to study the volcanic plume electrification is therefore to consider every realistic possible explanation, but we must avoid any paradigm. Then, we must compare expectation with observations, in the framework of other kinds of measurements and evidences inferred from other records exploited within the whole Earth system. That is, in the present case, one should

New Concepts in Global Tectonics Journal
Volume 13, Number 6, August 2025
ISSN number; ISSN 2202-0039

consider the entire so-called "atmospheric condenser". In fact, every model shares the concept of "atmospheric condenser", either according to the present old-fashioned standard interpretation, or according to the newly proposed scheme that is here envisaged. We must just avoid opinion science. We must "*read the book written by Nature*", and minimize every possible bias from "*the books written by men*".

Appendix

Introduction

Several photos are available of volcanic eruptions. Only a small fraction clearly shows visible lightning on the boundaries of volcanic plumes, where both kinds of primary or "*e*-discharges", and secondary of "*ion*-discharges", are recognizable. Consider that the plume is opaque, looking like a "black cloud" composed of pyroclastics and ash. A picture represents only one side of the plume. We show a set of examples, selected from several pictures available in the literature or on the web. The original photos are often protected by copyright, and are substituted by artistic works, aimed to emphasize the interpretation of the observed lightning. In general, every comparatively brighter lightning is likely to be a "secondary" or "*ion*-discharge". Every figure requires a careful analysis for recognizing the two kinds of lightning.

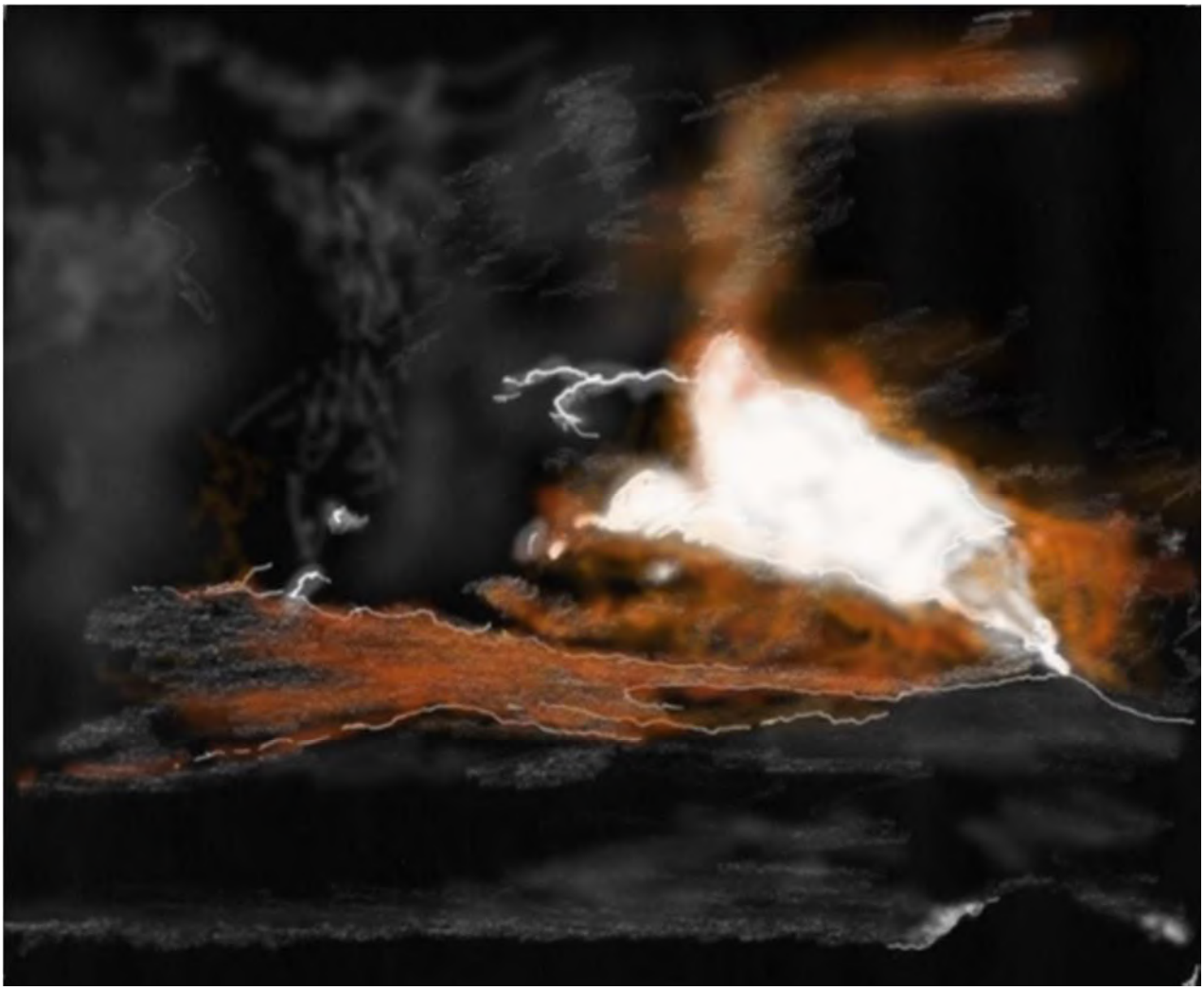

Fig. A-1. Lightning observation of the Eyjafjallajökull 2010 volcanic plume. Hand-made sketch, or artistic work based on a photograph, an April 17 image after Detay (2010). A "secondary" or "*ion*-discharge" is clearly visible to the left of the lava flow towards the ocean. Wind blows leftward. Unpublished figure.

New Concepts in Global Tectonics Journal
Volume 13, Number 6, August 2025

ISSN number; ISSN 2202-0039

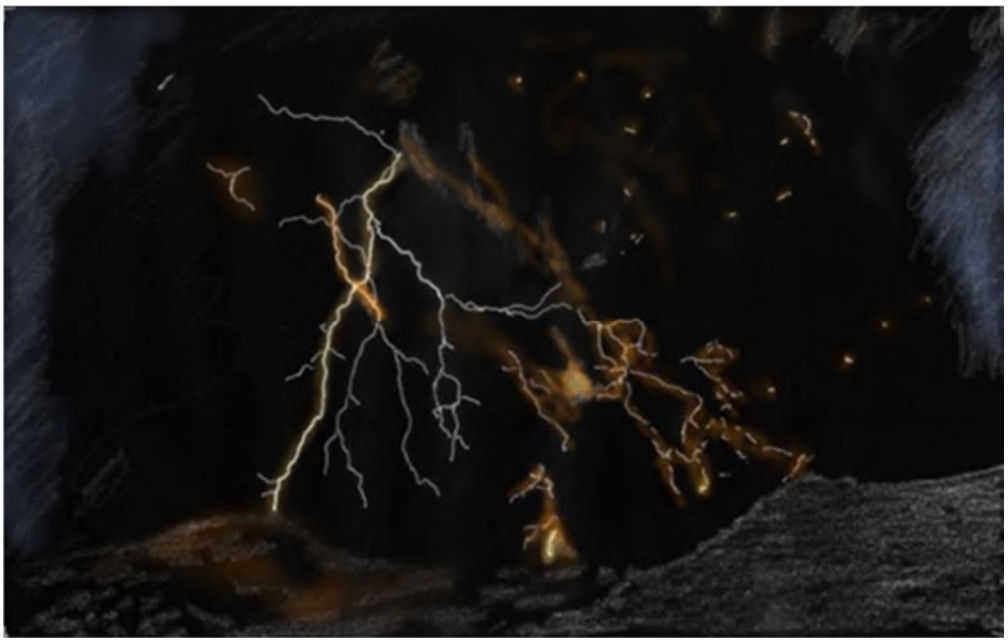

Fig. A-2. Lightning observation of the Eyjafjallajökull 2010 volcanic plume. Hand-made sketch, or artistic work based on a photograph, an April 17 (REUTERS/Lucas Jackson) picture. The branching of the lighting is downward, and these are likely "secondary" or "*ion*-discharges" associated with various amounts of ions as shown by lightning of various color and intensity. Unpublished figure.

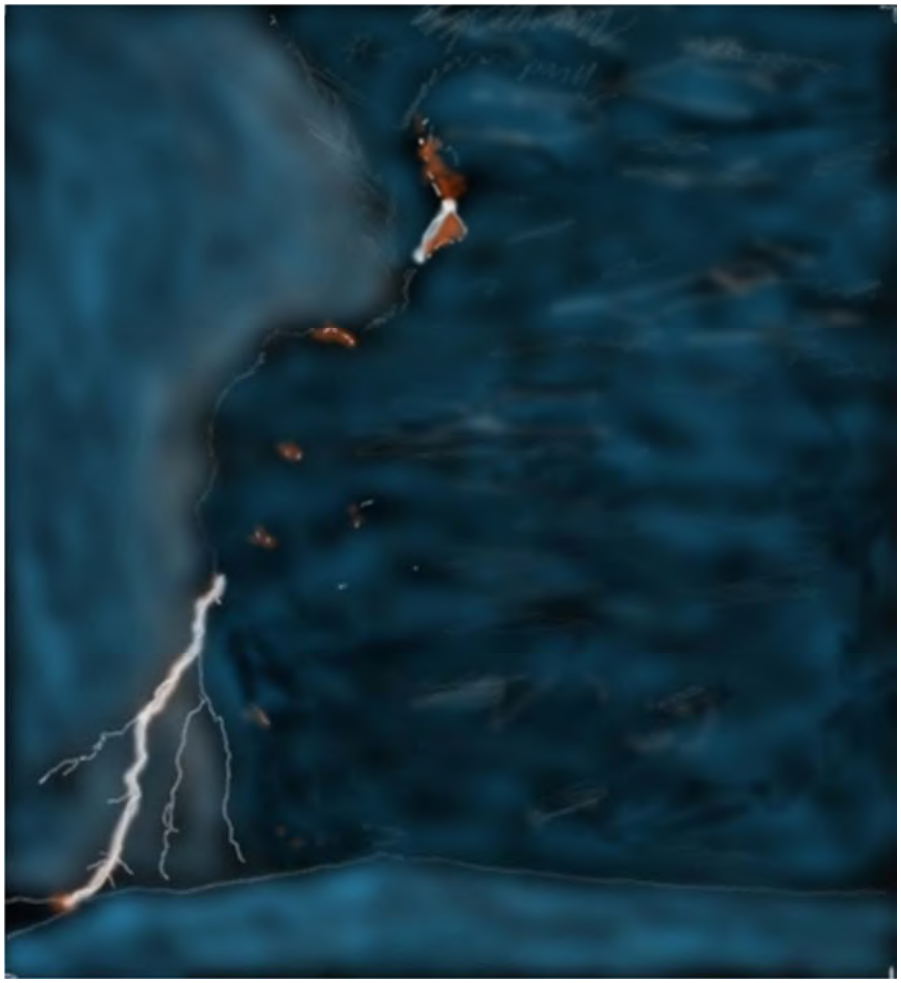

Fig. A-3. Lightning observation of the Eyjafjallajökull 2010 volcanic plume. Hand-made sketch, or artistic work based on a photograph by Olivier Vandeginste after a slide presentation by Martin Pegner provided by *Slideshare*, who gives the following captions "… 10 *km east of Hvosvollur at a distance* 25 *km from Eyjafjallajökull craters on April 18 …* 15 *sec exposure* ." (www.slideshare.net/pegner/eyjafjallajokull-volcano-4393037). The prominent feature is the "black cloud". No "*e*-discharges" are observed as they are expected to occur during the very early phase of the eruption. The "black cloud" partially hides an intense "*ion*-discharge", branching downward. Some red feeble glows are caused by the hot ions inside the "black cloud", i.e., inside the plume, even though visible lightning are observed only outside the plume. See text. Unpublished figure.

NCGT Journal
New Concepts in Global Tectonics

New Concepts in Global Tectonics Journal
Volume 13, Number 6, August 2025

ISSN number; ISSN 2202-0039

Fig. A-4. Lightning observation of the Eyjafjallajökull 2010 volcanic plume. Hand-made sketch, or artistic work based on a photograph by Olivier Vandeginste after a slide presentation by Martin Pegner provided by *Slideshare*, who gives the following captions " ... *taken* 25 *km from Eyjafjallajökull craters on April 18* ... 168 *sec exposure* ... " (www.slideshare.net/pegner/eyjafjallajokull- volcano-4393037). Several feeble possible "*e*-discharge" are probably observed, together with several more intense lightning that are probably "*ion*-discharges". The white cloud in the foreground is probably associated to the water vapor caused by lava entering into the ocean. Unpublished figure.

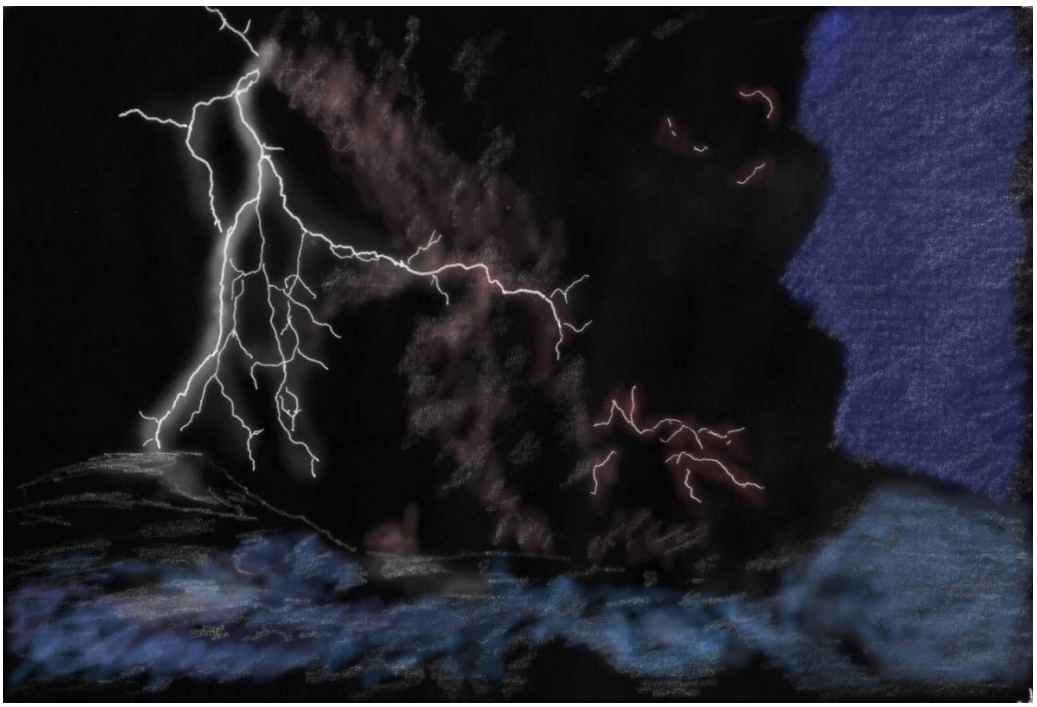

Fig. A-5. *"Lightning's in the ash plume in the volcanic eruption in Eyjafjallajökull glacier in Iceland (April 17, 2010).*" Handmade sketch, an artistic work, after a color photograph (and captions) in Stefnisson (2010), (© National Geographic). Also, in Zhang (2014). The branching of the lighting is downward, being likely "secondary" or "*ion*-discharges" associated with various fallout of ions. Unpublished figure.

New Concepts in Global Tectonics Journal
Volume 13, Number 6, August 2025

ISSN number; ISSN 2202-0039

Fig. A-6. "*A high column of ash and lava spewing from Chile's Calbuco volcano on April 23, 2015. Credit:* David Cortes Serey/Agence France-Presse Getty Images." The captions refer to a photograph in St. Fleur (2016), published by *The New York Times*. The figure is a hand-made sketch, an artistic work, aimed to explain the physical interpretation. The white cloud is probably water vapor. The red patch is probably the lava flow, while only a lesser amount of lightning is observed. Unpublished figure.

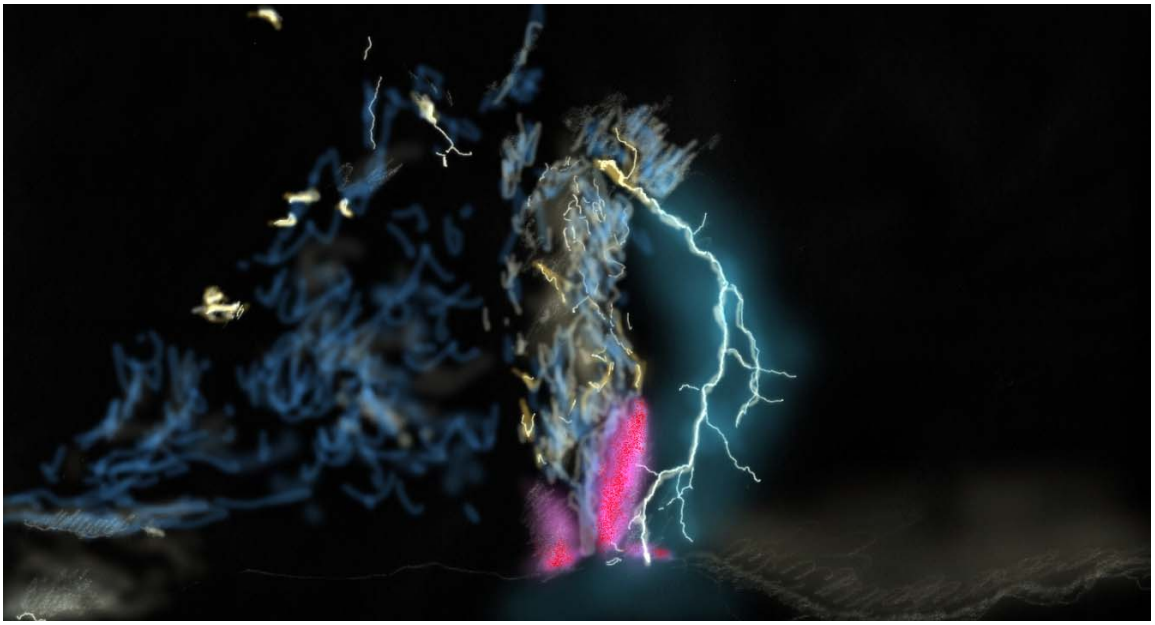

Fig. 7. *"Night eruption of Calbuco volcano in Chile*. Credit: *Verichip*, Monday, April 27, 2015; *posted by Terri at 1:53 PM*." The hand-made sketch - an artistic work here shown- is aimed to explain the physical processes. The lava fountains are red/pink. The intense lightning seen at the right, is branching downward, and is a "secondary" or "*ion*-discharge". But the main fraction of the plume is blown leftward. The short intense lightning at the boundary of the plume are likely to be lesser "*ion*-discharges", while no "*e*-discharge" seems to occur. The short visible lightning on the left upper boundary of the plume cannot be easily interpreted. Consider in fact, the challenge of distinguishing details in a simple picture alone. See main text. Unpublished figure.

NCGT Journal
New Concepts in Global Tectonics

New Concepts in Global Tectonics Journal
Volume 13, Number 6, August 2025

ISSN number; ISSN 2202-0039

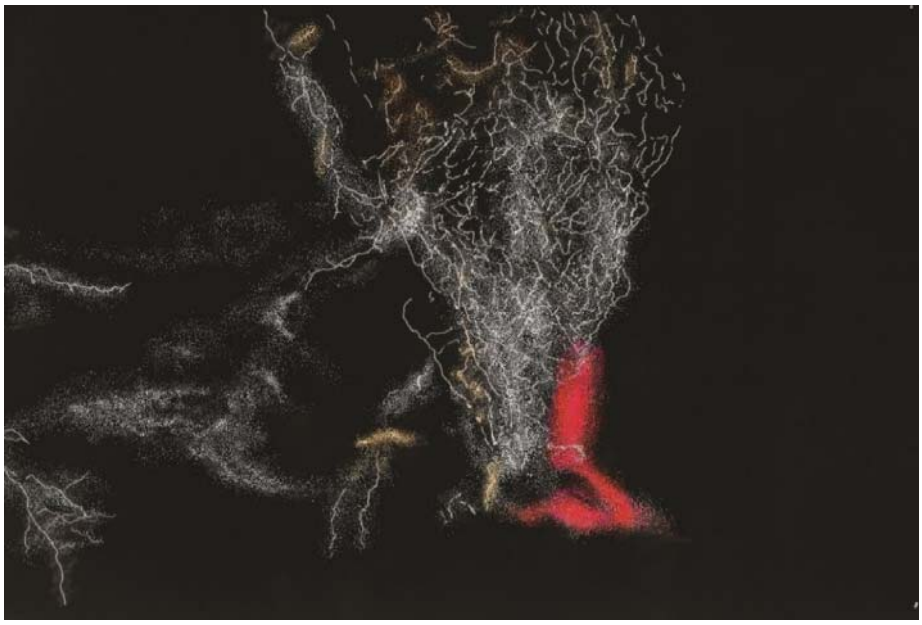

Fig. A-8. *"Calbuco Volcano is located in the lakes region south of Santiago, Chile's capital city, and is one of the* 10 *most dangerous volcanoes in the country. After more than* 40 *years of inactivity, the day April 23 the volcano erupted, spewing more than* 2×10^8 *tons of ash …. In the picture is seen one of the most violent moments of the eruption, which occurred in the early hours of April 24, 2015.* © Francisco Negroni / National Geographic Photo Contest." Captions after Taylor (2015). The figure is a hand-made sketch, an artistic work, aimed to highlight the leading physical mechanism. The lava fountain is red. A likely large "*ion*-discharge" is only partially seen at the left-lower corner of the image. A large number of "*e*-discharges" denotes the early stage of the eruption. Unpublished figure.

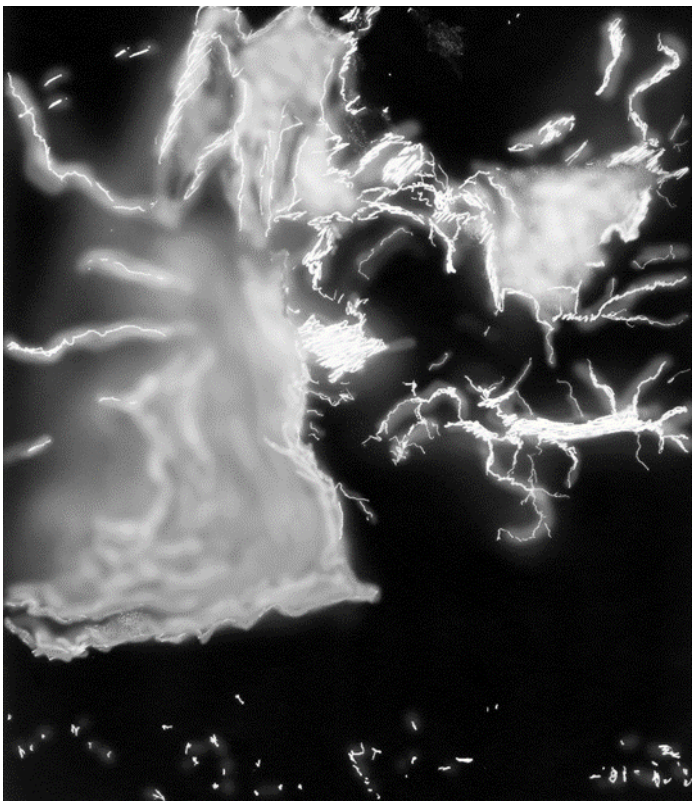

Fig. A-9. The eruption of Cerro Negro in Nicaragua, 1971. The "secondary" or "*ion*-discharge" is on the right. The original photograph is by F. Penalba, after *http://volcaniclightning.tripod.com/index.htm*. The figure is a hand-made sketch, an artistic work, aimed to highlight the physical explanation. Unpublished figure.

NCGT Journal
New Concepts in Global Tectonics

New Concepts in Global Tectonics Journal
Volume 13, Number 6, August 2025

ISSN number; ISSN 2202-0039

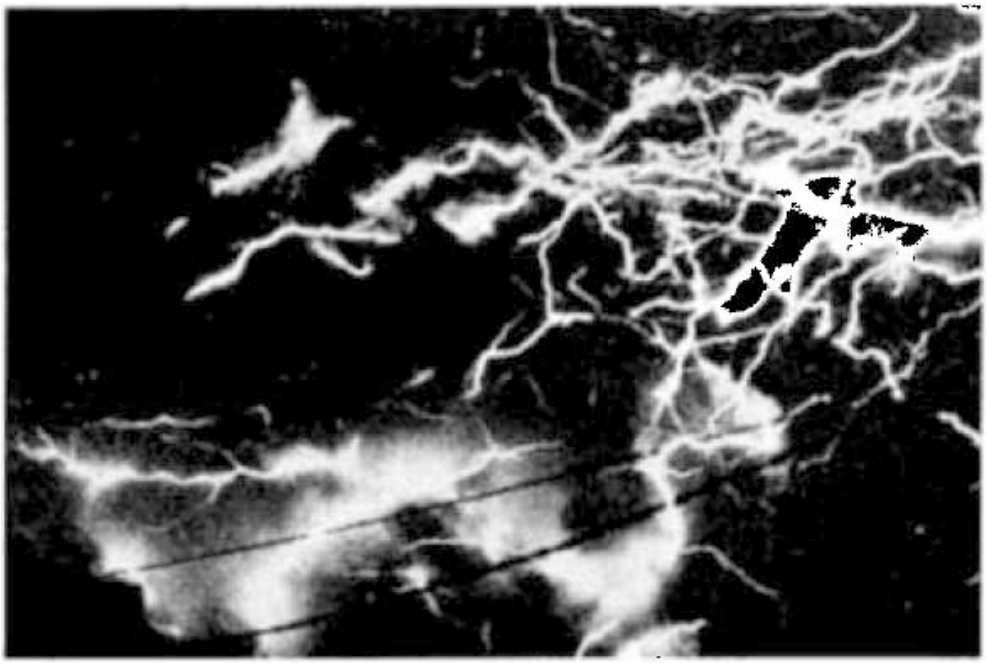

Fig. A-10. Volcanic lightning on Mount Usu (Hokkaidō), August 7, 1977 (I). Courtesy of Mr. K. Kijama. After Kikuchi and Endoh (1982). We point out the difficulty of interpreting the nature of the several lightning here shown, as the exposure time of the photograph is not specified. The dense lightning network at the right-upper side probably denotes "*e*-discharges", hence an early stage of the eruption. A leftward blowing wind is probably associated to the "*ion*-discharges" displayed at lower altitude on the left of the image, overlying the lava glow in the background. With kind permission of the *Journal of the Meteorological Society of Japan* (fully "*Open Access*" publication).

Fig. A-11. Volcanic lightning on Mount Usu (Hokkaidō), August 7, 1977 (I). Courtesy of Mr. S. Watanabe. After Kikuchi and Endoh (1982). The photograph (seemingly daytime image) shows a clear "secondary" or "*ion*-discharge", branching downward from a white cloud, maybe of water vapor, which hides the outer boundary of the plume. With kind permission of the *Journal of the Meteorological Society of Japan* (fully "*Open Access*" publication).

New Concepts in Global Tectonics Journal
Volume 13, Number 6, August 2025
ISSN number; ISSN 2202-0039

Fig. A-12. Volcanic lightning on Mount Usu (Hokkaidō), August 14, 1977 (II). Black and white photograph, courtesy of Prof. Y. Katsui. After Kikuchi and Endoh (1982). The luminous patch is likely to be illuminated by the lava fountain. An "*ion*-discharge" is visible close to, and at the left of, the luminous patch. The other small light patches are probably minor "*ion*-discharges", including the elongated lightning at the upper right corner of the image. The volcanic plume is bent rightward by the wind. With kind permission of the *Journal of the Meteorological Society of Japan* (fully "*Open Access*" publication).

Fig. A-13. Volcanic lightning on Mount Usu (Hokkaidō), August 14, 1977 (III). Courtesy of Prof. Y. Katsui. After Kikuchi and Endoh (1982). A clear "*ion*-discharge" is visible to the right of the luminous patch, which is caused by the lava fountain. The volcanic plume is blown rightward by the wind. The short lightning above the white cloud are likely to be "*e*"-discharges. With kind permission of the *Journal of the Meteorological Society of Japan* (fully "*Open Access*" publication).

New Concepts in Global Tectonics Journal
Volume 13, Number 6, August 2025
ISSN number; ISSN 2202-0039

Fig. A-14. Mount Galunggung (West Java, Indonesia) eruption in 1982. Photo: R. Hadian, *U.S. Geological Survey*. Courtesy of the *U.S. Geological Survey*. A dense activity of "*e*-discharge" is displayed, mainly at the left of the image, while the more intense lightning observed at the center of the image is probably an "*ion*-discharge". The wind is probably blowing towards the observer. In any case, the interpretation of this picture is not easy. *USGS* copyright free policy ("*Public Domain*").

Fig. A-15. Sakurajima volcanic lightning, May 18, 1991. Credit: *Sakurajima Volcananological Observatory*. The lightning are likely to be "*e*-discharges", hence denoting an early stage of the eruption, with wind blowing leftward. Reproduced according to free permission policy of *National Astronomical Observatory of Japan* (*NAOJ*).

New Concepts in Global Tectonics Journal
Volume 13, Number 6, August 2025
ISSN number; ISSN 2202-0039

Fig. A-16. Mount Rinjani (Lombok, Indonesia) eruption in 1995. Photo: Oliver Spalt. The large discharge in the background, branching downward, is an intense "*ion*-discharge" clearly separated from the uprising "black cloud". The volcano top, lava glow, and "black could" are clearly detected. Reproduced by permission under CC BY-SA 3.0 license of *Wikimedia Commons*.

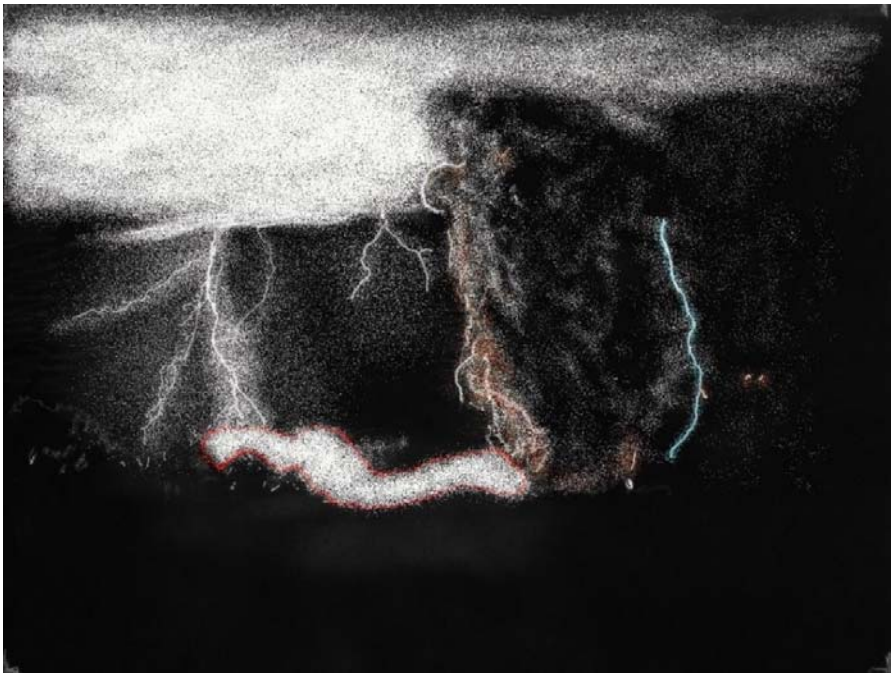

Fig. A-17. Lightning strikes associated with the volcanic plume of Chaitén's eruption in 2008. The "secondary" (branching downward, partially hidden by the white cloud) "*ion*-discharges" are clearly recognized, and they are the cause of the upper luminous patch. The original figure (credit: *UPI* photo by Carlos Gutierrez) is the basis for this hand-made sketch, artistic work, here shown is for explaining the interpretation here proposed. The "white" smaller cloud close to ground is evidenced by a red contour and is probably originated by water vapor. The wind blows leftward. Unpublished figure.

ISSN number; ISSN 2202-0039

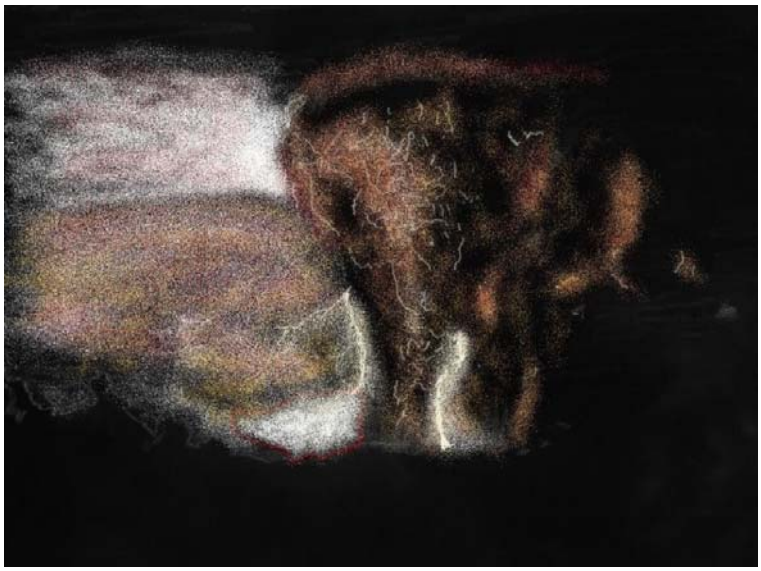

Fig. A-18. Lightning strikes associated with the volcanic plume of Chaitén's eruption in 2008. Only "secondary" "*ion*-discharges" are observed, partially hidden by the "black cloud" due to the location of the observer. The luminous patch at the upper left side is probably caused by an intense and partially hidden "*ion*-discharge". The white patch at the base of the plume is probably associated to water vapor that is illuminated by an intense hidden "*ion*-discharge". The original image (credit: *UPI* photo by Carlos Gutierrez) is the basis for this hand-made sketch, an artistic work, aimed to highlight the proposed interpretation. Unpublished figure.

Fig. A-19. Lightning flashes in a roiling cloud of ash over Mount Redoubt on March 27, 2009. The "*ion*-discharges" are partly screened by the thick pyroclastic cloud. The yellow glow is associated to the lava fountain. The wind blows rightward, and the visible "*ion*-discharge" is branching downward. Photo credit and copyright: Bretwood Higman, *Ground Truth Trekking*. After Dauna Coulter (ed. Tony Phillips), Credit: *Science@NASA* (4.03.2009). *NASA* copyright free policy.

New Concepts in Global Tectonics Journal
Volume 13, Number 6, August 2025

ISSN number; ISSN 2202-0039

Fig. A-20. Lightning in the pyroclastic cloud over Mount Redoubt from the 11:20 pm March 27 eruption at 11:26 pm. The ‘’secondary’’ “*ion*-discharges” are seen both at the left and right side of the plume. Wind seems to be blowing leftward. The yellow glow is associated with the lava fountain. The “*e*-discharges” are not seen, probably due to a comparatively late stage of the eruption. After *Ground Truth Trekking Blog*, a *WordPress* by Shaun Reynolds, based on *Craving4Green* made free by *Seven Jeans*. *NASA* copyright free policy.

Fig. A-21. Lightning in the pyroclastic cloud over Mount Redoubt from the 1:20 am March 28 eruption at 1:26 am. The image appears somewhat confused. The ‘’secondary’’ “*ion*-discharges” seemingly occur along the vertical extension of the plume, envisaging that no relevant wind was blowing at that time. They are seen to begin at low altitude, right beneath the mushroom opening of the plume, and to end on the eruption vent, although they are partly hidden by the thick horizontal spreading pyroclastic plume. The light emitted by the vent is comparatively lower, while some remnants of “*e*-discharges” are maybe, although not certainly, displayed all around the plume, even on its top, at a comparatively high altitude. After *Ground Truth Trekking Blog*, a *WordPress* by Shaun Reynolds, based on *Craving4Green* made free by *Seven Jeans*. *NASA* copyright free policy.

ISSN number; ISSN 2202-0039

Acknowledgement

We want to acknowledge all co-workers that, in different ways and at different times, contributed to the exploitation of the analyses mentioned in the present study. We are also thankful for the warm encouragement we had from several outstanding scientists.

Funding Information

The funding derived from the respective Institutions. G.P. Gregori has been retired since 2005. B.A. Leybourne is a semi-retired self-funded independent researcher. U. Coppa is a researcher at the *Osservatorio Vesuviano*. G. Luongo is at present Emeritus Professor of Physics of Volcanism at the *University Federico II* in Naples, Associate of *INGV – Osservatorio Vesuviano* , and a former Director of the *Osseratorio Vesuviano* retired since 2010.

Author's Contributions

The leading idea relies on a long lasting study by GPG. The entire content derived from mutual intense discussion between the authors.

Ethics

This article is original and contains unpublished material. Authors declare that there are no ethical issues and no conflict of interest that may arise after the publication of this manuscript.

References

Alaska Volcano Observatory, 1993. Mt. Spurr's 1992 eruptions, EOS, Transactions American Geophysical Union, 74 (19); 217 and 221-222

Altschuler, M. D., 1999. Atmospheric electricity and plasma interpretations of UFOs. In *Scientific Study of Unidentified Flying Objects,* E.U. Condon, (ed.), Regents of The University of Colorado, Ch. 7: 1156-1204

Anderson, R., S. Gathman, J. Hughes, S. Björnsson, S. Jónasson, D. C. Blanchard, C. B. Moore, H.J. Survilas, and B. Vonnegut , 1965. Electricity in volcanic clouds. Investigations show that lightning can result from charge-separation processes in a volcanic crater, Science, 148 (3674): 1179-1189; DOI:10.1126/science.148.3674.1179

Arason, P., 2005a. Volcanogenic lightning during the Grímsvötn 2004 subglacial eruption. Geophysical Research Abstracts, 7: 05355 (European Geosciences Union)

Arason, P., 2005b. Lightning during volcanic eruptions in Iceland. Geophysical Research Abstracts, 7: 05369 (European Geosciences Union)

Behnke, S. A., H. E, Edens, R. J. Thomas, C. M. Smith, S. R. McNutt, A. R.Van Eaton, C. Cimarelli, and V. Cigala, 2018. Investigating the origin of continual radio frequency impulses during explosive volcanic eruptions. Journal of Geophysical Research: Atmospheres, 123: 4157–4174; DOI:10. 1002/2017JD027990

Behnke, S. A., H. Edens, S. Senay, M. Iguchi, and D. Miki, 2021. Radio frequency characteristics of volcanic lightning and vent discharges. Journal of Geophysical Research: Atmospheres, 126: e2020JD034495; DOI:10.1029/2020JD034495

Behnke, S. A., R J. Thomas, H. E. Edens, P. R. Krehbiel, and W.Rison, 2014. The 2010 eruption of Eyjafjallajökull: lightning and plume charge structure, Journal of Geophysical Research, Atmospheres, 119 (2): 833–859; DOI:10.1002/2013JD020781

Behnke, S. A., R J. Thomas, P. R. Krehbiel, and S. R. McNutt, 2012. Spectacular lightning revealed in 2009 Mount Redoubt eruption, EOS, Transactions American Geophysical Union, 93 (20): 193–194; DOI:10.1029/2012EO200001

Behnke, S. A., R. J. Thomas, S. R. McNutt, D. J. Schneider, P. R. Krehbiel, W. Rison, and H. E. Edens, 2013. Observations of volcanic lightning during the 2009 eruption of Redoubt Volcano. Journal of Volcanology and Geothermal Research, 259: 214–234; DOI:10. 1016/j.jvolgeores.2011.12.010

Berry, K., 1997. Iceworm alerts seismologists to volcanic eruptions, Geophysical Institute Quarterly, 14 (3): 1-1

Braham, R. R.,Jr., 1952. The water and energy budgets of the thunderstorm and their relation to thunderstorm development. Journal of the Atmospheric Sciences, 9 (4): 227-242

Brook, M., C. B. Moore, and T. Sigurgeirsson, 1974. Lightning in volcanic clouds, Journal of Geophysical Research, 79 (3): 472-475; DOI:10.1029/JC079i003p00472

Bruins, H. J., and J. van der Plicht, 1996. The Exodus enigma. Nature, 382: 213-214

Caridi, P., 2023. Etna, straordinario anello vulcanico di dimensioni enormi dopo la neve del weekend | FOTO e VIDEO. Un bellissimo anello vulcanico stamani sull'Etna dopo la neve caduta nel weekend: immagini foto e video inedite e meravigliose, Meteoweb, Geo-Vulcanologia, issued 18 Dic 2023

Casadevall, T. J., (ed.), 1991. Volcanic ash and aviation safety. Proceedings of the First International Symposium on Volcanic Ash and Aviation Safety. Bulletin (2047), USGS, pp: 1-450; DOI: 10.3133/b2047. Also DIANE Publishing, 1994

Casertano, L., 1999. The scientific life of Luigi Palmieri, 100th Anniversary commemoration (21/04/1807-09/09/1986), *Annali di Geofisica*, 42 (3): 581-585

Chalmers, J. A., 1967. *Atmospheric electricity,* Pergamon Press, Oxford and New York [First edition appeared in 1957], pp: 1-515

Ciarallo, A. M., 1992. Domenico Cirillo, Medico e Naturalista Martire del '99, Procaccini, Napoli, pp:1-75

Croce, B., 1912. La Rivoluzione Napoletana del 1799. Biografie, Racconti e Ricerche, Laterza, Bari, reprinted in 1961

Detay, M., 2010. Eyjafjöll: radiografia di un'eruzione, *Le Scienze*, (503): 74-81

Forshag, W. F., and J .R. González-Reyna, 1956. Birth and development of Parícutin volcano, Mexico. Bulletin, (965D): 355–489; (USGS)

Friedrich, W. L., P. Wagner, and H. Tauber, 1990. Thera and the Ægean World III, Thera Foundation, London, UK

Fries, C.,Jr, and C. Gutiérrez, 1950. Activity of Parícutin volcano from July 1 to December 31, 1949. Transactions American Geophysical Union, 31: 732–740

Gasparini, P., and S. Musella, 1991. Un Viaggio al Vesuvio. Il Vesuvio Visto Attraverso Diari, Lettere e Resoconti di Viaggiatori. Liguori editore, Napoli, pp: 1-307

Genge, M. J., 2018. Electrostatic levitation of volcanic ash into the ionosphere and its abrupt effect on climate, Geology, 46 (10): 835–838; DOI:10.1130/G45092.1

Gilbert, J. S., S. J. Lane, R. S. J. Sparks, and T. Koyaguchi, 1991. Charge measurements on particle fallout from a volcanic plume, Nature, 349: 598-600; DOI:10.1038/349598a0.

Greene, M. T., 2000. Natural Knowledge in Preclassical Antiquity. Johns Hopkins University Press.

Gregori, G. P., 1993. Geo-electromagnetism and geodynamics: "corona discharge" from volcanic and geothermal areas. Physics of the Earth and Planetary Interiors, 77: 39-63; DOI:10 .1016/S0031-9201(02)00211-X

Gregori, G. P., 2000c. Galaxy-Sun-Earth Relations. The Dynamo of the Earth, and the Origin of the Magnetic Field of Stars, Planets, Satellites, and Other Planetary Objects. In The first solar and space weather conference. The solar cycle and terrestrial climate, A. Wilson, (ed.), ESA SP-463, European Space Agency, ESTEC, Noordvijck, The Netherlands, pp: 329-332

Gregori, G. P., 2002. Galaxy – Sun – Earth relations. The Origin of the Magnetic Field and of the Endogenous Energy of the Earth, with Implications for Volcanism, Geodynamics and Climate Control, and Related Items of Concern for Stars, Planets, Satellites, and Other Planetary Objects. A Discussion in a Prologue and Two Parts. Beiträge zur Geschichte der Geophysik und Kosmischen Physik, Band 3, Heft 3: pp. 1-471 [Available at http://ncgtjournal.com/additional-resources.html]

Gregori, G. P., and B. A. Leybourne, 2021. An unprecedented challenge for humankind survival. Energy exploitation from the atmospheric electrical circuit, American Journal of Engineering and Applied Science, 14 (2): 258-291. DOI:10.3844/ajeassp.2021.258.291

Gregori, G. P., and B. A. Leybourne, 2025b. The electrostatic Sun, pending publication on Journal of Engineering and Applied Science

Gregori, G. P., and B. A. Leybourne, 2025d. Measuring the electric field at ground, pending publication on Journal of Engineering and Applied Science

Gregori, G. P., and B. A. Leybourne, 2025e. The physics of electrical discharges – 1. Small-scale phenomena - Fog - atmospheric precipitation – BLs, pending publication on Journal of Engineering and Applied Science

Gregori, G. P., and B. A. Leybourne, 2025f. The physics of electrical discharges – 2. RB & TGFs - Runaway breakdown – terrestrial gamma flashes – GK effect, pending publication on Journal of Engineering and Applied Science

Gregori, G. P., and B. A. Leybourne, 2025g. The physics of electrical discharges – 3. Sparks and lightning - electrostatics of the ionosphere – TLEs - plasma jets collimation – Birkeland currents & sea-urchin spikes - stellar and galactic alignments, pending publication on Journal of Engineering and Applied Science

Gregori, G. P., and M. T. Hovland, 2025. Go for the anomaly – a golden strategy for discovery? Seepology & the origin and crucial role of the biosphere - Earth and planetary objects - Supercritical water and serpentinization, pending publication on Journal of Engineering and Applied Science

Gregori, G. P., B. A. Leybourne, and F. F. Bonavia, 2025v. The origin of lavakas. In press on News Concepts in Global Tectonics

Gregori, G. P., B. A. Leybourne, and G. Paparo†, 2025b. Introduction – Anomalous lesser air-earth phenomena, pending publication on Journal of Engineering and Applied Science

Gregori, G. P., B. A. Leybourne, and J. R. Wright, 2025d. Generalized Cowling theorem and the Cowling dynamo, pending publication on Journal of Engineering and Applied Science

Gregori, G. P., B. A. Leybourne, Dong Wenjie, and Gao Xaoqing, 2025n. Energy release from *ALB*, *CMB* and *ICB* and secular variation. IV – A physical analysis - The Poynting theorem and the estimate of s/σ, separating the roles of terms with different degree n, and a tentative physical explanation concerning the role of the "magpol" *IC* in the *TD* dynamo, New Concepts in Global Tectonics Journal, 13, (3):???

Gregori, G. P., B. A. Leybourne, G. Paparo†, and M. Poscolieri, 2025a. The global Sun-Earth circuit, pending publication on Journal of Engineering and Applied Science

Gregori, G. P., B. A. Leybourne, U. Coppa, and G. Luongo, 2025. Geomagnetic anomalies: lineaments. *American Journal of Engineering and Applied Sciences*, 18, (1): 1-10; DOI: 10.3844/ajeassp.2025.1.10

Gregori, G. P., B. A. Leybourne, U. Coppa, and G. Luongo, 2025r. Geomagnetic anomalies: "double-eye" patterns. In press on News Concepts in Global Tectonics

Gregori, G. P., B. A. Leybourne, W. Soon, and V. Straser, 2025e. The heuristic meaning of variational principles, pending publication on Journal of Engineering and Applied Science

Gregori, G. P., M. T. Hovland, B. A. Leybourne, S. Pellis, V. Straser, B. G. Gregori, G. M. Gregori, and A. R. Simonelli, 2025w. Air-earth currents and a universal "law": filamentary and spiral structures - Repetitiveness, fractality, golden ratio, fine-structure constant, antifragility and "statistics" - The origin of life, News Concepts in Global Tectonics, 3, (1): 106-225

Gregori, G.P., Dong Wen-Jie, F.T. Gizzi, and Xiao-Qing Gao, 1999. The separation of the geomagnetic field originated in the core, in the asthenosphere, and in the crust. Annali di Geofisica, 42 (2): 191-209

Harrison, R. G., K. A. Nicoll, Z. Ulanowski, and T. A. Mather, 2010. Self-charging of the Eyjafjallajökull volcanic ash plume, Environmental Research Letters, 5 (2): 024004 [4 pp.]; DOI:10.1088/1748-9326/5/2/024004

Hatakeyama, H., 1949. Journal of geomagnetism and geoelectricity, 1: 48-

Hatakeyama, H., 1949a. On the disturbance of the atmospheric potential gradient caused by the smoke cloud of the volcano Yake-yama. Journal of the Meteorological Society of Japan, 27: 372-376

Hatakeyama, H., 1958. On the disturbance of the atmospheric electric field caused by the smoke-cloud of volcano Asama-yama, Papers in Meteorology and Geophysics, Tokyo, 8 (4): 302-316

Hatakeyama, H., and K. Uchikawa, 1951. On the disturbance of the atmospheric potential gradient caused by the eruption smoke of the volcano Aso, Papers in Meteorology and Geophysics, Tokyo, 2: 85-89

Hatakeyama, H., and T. Kubo, 1943. On the variation of the atmospheric potential, report; Journal of the Meteorological Society of Japan, 21: 49-52

Hatakeyama, H., and T. Kubo, 1943a. On the variation of the atmospheric potential gradient caused by the cloud of smoke of the volcano Asama. The third report. Journal of the Meteorological Society of Japan. Ser. II, 21 (9): 426-428, (in Japanese)

Hoblitt, R. P., 1994. An experiment to detect and locate lightning associated with eruptions of Redoubt volcano. Journal of Volcanology and Geothermal Research, 62: 499-517

Houghton, I. M. P., K. L. Aplin, and K. A. Nicoll, 2013. Triboelectric charging of volcanic ash from the 2011 Grímsvötn eruption, Physical Review Letters, 111: 118501; DOI:10.1103/PhysRevLett.111.118501

Ichihara, M., P. D. Mininni, S. Ravichandran, C. Cimarelli, and C. Vagasky, 2023. Multiphase turbulent flow explains lightning rings in volcanic plumes, Communications Earth & Environment, 4; DOI:10.1038/s43247-023-01074-z

Ilyinskaya, E., A. Schmidt, T. A. Mather, F. D. Pope, C. Witham, P. Baxter, T. Jóhannsson, M. Pfeffer, S. Barsotti, A. Singh, P. Sanderson, B. Bergsson, B. McCormick Kilbride, A. Donovan, N. Peters, C. Oppenheimer, and M. Edmonds, 2017. Understanding the environmental impacts of large fissure eruptions: Aerosol and gas emissions from the 2014–2015 Holuhraun eruption (Iceland), Earth and Planetary Science Letters, 472: 309–322; DOI:10.1016/j.epsl.2017.05.025

Ishikawa, G., M. Kadena, and M. Misaki, 1951. Journal of geomagnetism and geoelectricity,, 3: 9-

Israël, H., 1951. Instruments and methods for the measurement of atmospheric electricity. In Compendium of Meteorology, T.F. Malone, (ed.), American Meteorological Society, Boston; pp: 144-154

Janackova, A., and L. Urban, 1990. Geomagnetic field: contribution of higher harmonics to the variations of virtual pole positions, Studia Geophysica et. Geodetica, 34: 382-387

Janackova, A., L. Urban, and M. Krs, 1989. Geomagnetic field from the Earth's core: its westward drift rate and some probable global-tectonic implications. Studia Geophysica et. Geodetica, 33: 246-253; DOI:10.1007/BF01633528

Kikuchi, K., and T. Endoh, 1982. Atmospheric electrical properties of volcanic ash particles in the eruption of Mt. Usu volcano, 1977, Journal of the Meteorological Society of Japan, 60 (1): 548-561

Kuniholm, P. I., B. Kromer, S. W. Manning, M. Newton, C. E. Latini, and M. J. Bruce, 1996. Anatolian tree rings and the absolute chronology of the eastern Mediterranean, 2220-718 BC, Nature, 381: 780-783

LaMoreaux, P. E., 1995. Worldwide environmental impacts from the eruption of Thera, Environmental Geology, 26 (3): 172-181; DOI:10.1007/BF00768739

Lane, S. J., and J. S. Gilbert, 1992. Electric potential gradient changes during explosive activity at Sakurajima volcano, Japan, Bulletin of Volcanology, 54 (7): 590-594; DOI:10.1007/BF00569942

Leybourne, B. A., D. W. Johnson, and G. P. Gregori, 2025. Arc-blast as static electricity or interplanetary lightning short circuits in Stellar Transformers. A plausible North American scenario, News Concepts in Global Tectonics, 13, (2): 229-251

Lobley, J. L., 1889. Mount Vesuvius: A Descriptive, Historical, and Geological Account of the Volcano and its Surroundings, Roper and Drowley, London, pp: 1-400

Lowes, F. J., 1974. Spatial power spectrum in the main geomagnetic field, and extrapolation to the core. Geophysical Journal of the Royal Astronomical Society, 36: 717-730

Luce, J. V., 1969. The End of Atlantis: New Light on an Old Legend (New Aspects of Antiquity). London: Thames & Hudson

Luhr, J. F., and T. Simkin, (eds), 1993. Parícutin, the Volcano Born in a Mexican Cornfield. Geoscience, Press Inc., Pheonix Arizona

Mather, T. A., and R. G. Harrison, 2006. Electrification of volcanic plumes, Surveys in Geophysics, 27(4): 387–432; DOI:10.1007/s10712-006-9007-2

McNutt, S. R., and C. M. Davis, 2000. Lightning associated with the 1992 eruptions of Crater Peak, Mount Spurr Volcano, Alaska, Journal of Volcanology and Geothermal Research, 102 (1/2): 45-65; DOI:10.1016/S0377-0273(00)00181-5

Nagata, T., K. Hirao, N. Fukushima, and T. Takashima, 1946. The change in point-discharge current due to the volcanic smoke of Sakura-jima. Bulletin of the Earthquake Research Institute, 24: 221-227

Neal, C. A., R. G. McGimsey, C. A. Gardner, M. L. Harbin, and C. J. Nye, 1995. Tephra-fall deposits from the 1992 eruptions of Crater Peak, Mount Spurr volcano, Alaska: a preliminary report on distribution, stratigraphy, and composition. In The 1992 Eruptions of Crater Peak Vent, Mount Spurr Volcano, Alaska, T.E.C. Keith, (ed.), Bulletin, (2139), USGS, pp: 65-79

Nevanlinna, H., 1987. Notes on global mean-square values of the geomagnetic field and secular variation, Journal of Geomagnetism and Geoelectricity, 39 (3): 165-174

Nye, C. J., and D. L., Turner, 1990. Petrology, geochemistry and age of the Spurr volcanic complex, Eastern Aleutian arc, Bulletin of Volcanology, 52: 205-226

Palmieri, L., 1859. Annali del Reale Osservatorio Meteorologico Vesuviano, I, A. Dekten, Napoli, pp: 1-80

Palmieri, L., 1862a. Sull'origine dell'elettricità atmosferica, Annali del Reale Osservatorio Vesuviano, 2: 1-23

Palmieri, L., 1862b. Intorno all'incendio del Vesuvio cominciato il dì 08/12/1861, Rendiconti dell'Accademia Pontanian, Napol,i Anno X: 1-56

Palmieri, L., 1862c. Intorno all'incendio del Vesuvio cominciato il dì 8 dicembre 1861. Il Nuovo Cimento (1855-1868), 15 (1): 392-419

Palmieri, L., 1891 Le correnti telluriche all'Osservatorio Vesuviano osservate per un anno intero non meno di quattro volte al giorno, Il Nuovo Cimento, Serie 3, 29: 45-53; DOI:10.1007/BF02718601

Parrot, M., 2025. DEMETER observations of the variations of the global electric circuit under various constraints, News Concepts in Global Tectonics, 13, (2): 355-366; ID 530865; DOI:10.1155/2013/530865

Paskievitch, J. F., T. L. Murray, R. P. Hoblitt, and C. A. Neal, 1995. Lightning associated with the August 18, 1992, eruption of Crater Peak Vent, Mount Spurr Volcano, Alaska. In The 1992 Eruptions of Crater Peak Vent, Mount Spurr Volcano, Alaska, T.E.C. Keith, (ed.), Bulletin, (2139), USGS, pp: 179-182

Pinto, L., 1896. Necrologia di Luigi Palmieri, Atti Accademia Pontaniana, Napoli, 26: 14-19

Pulvirenti, F., S. Scollo, C. Ferlito, and F. M. Schwandner, 2023. Dynamics of volcanic vortex rings, Scientifc Reports, 13: 2369; DOI:10.1038/s41598-022-26435-0

Quinn, J. M.,† G. P. Gregori, and B. A. Leybourne, 2025. Satellite monitoring of air-earth currents, pending publication on Journal of Engineering and Applied Science

Renfrew, C., 1996. Kings, tree rings and the Old World. Nature, 381: 733-734

Riehle, J. R., W. I. Rose, T. J. Casadevall, J. S. Langford and D. J. Schneider, 1994. Unmanned aerial sampling of a volcanic ash plume, EOS, Transactions American Geophysical Union, 75 (12): 137-138; DOI:10 .1029/94EO00831

Rose, W. I., A. B. Kostinski, and L. Kelley, 1995. Real-time C-band radar observations of 1992 eruption clouds from Crater Peak, Mount Spurr volcano, Alaska. In The 1992 Eruptions of Crater Peak Vent, Mount Spurr Volcano, Alaska, T.E.C. Keith, (ed.), Bulletin, (2139), USGS, pp: 19-26

Salanave, L. E., 1980. Lightning and its Spectrum. An Atlas of Photographs, The University of Arizona Press, Tucson, Arizona, pp: 1-136

Schneider, D. J., W. I. Rose, L. Kelley, and T. E. C. Keith, 1995. Tracking of 1992 eruption clouds from Crater Peak vent of Mount Spurr Volcano, Alaska, using AVHRR. In The 1992 Eruptions of Crater Peak Vent, Mount Spurr Volcano, Alaska, T.E.C. Keith, (ed.), Bulletin, (2139), USGS, pp: 27-36

Sivertsen, B. J., 2009. The Parting of the Sea: How Volcanoes, Earthquakes, and Plagues Shaped the Story of the Exodus. Princeton University Press

Smith, C. M., A. R. Van Eaton, S. Charbonner, S. R. McNutt, S. A. Behnke, R. J. Thomas, H. E. Edens, and G. Thompson, 2018. Correlating the electrification of volcanic plumes with ashfall textures at Sakurajima volcano, Japan. Earth and Planetary Science Letters, 492: 47–58; DOI:10.1016/j.epsl.2018.03.052

Smith, C. M., D. Gaudin, A. R. Van Eaton, S. A. Behnke, S. Reader, R. J. Thomas, H. Edens, S. R. McNutt, and C. Cimarelli, 2021. Impulsive volcanic plumes generate volcanic lightning and vent discharges: astatistical analysis of Sakurajima volcano in 2015. Geophysical Research Letters, 48; DOI:10. 1029/2020GL092323

Smith, C. M., G. Thompson, S. Reader, S. A. Behnke, R. J., Thomas, and H. E. Edens, 2020. Examining the statistical relationships between volcanic seismic, infrasound, and electrical signals: A case study of Sakurajima volcano, 2015. Journal of Volcanology and Geothermal Research, 402: 106996

St. Fleur, N., 2016. What 50 years of earthquakes and volcanic eruptions look like, *The New York Times*, October 10, 2016

Stefnisson, S., 2010. Eyjafjallajökull volcano lightning's shs_n3_045809, *National Geographic Visions of Earth*

Taylor, A., 2015. *National Geographic Photo Contest*, October 6, 2015

Thomas, R. J., P. R. Krehbiel, W. Rison, H. E. Edens, G. D. Aulich, W. P. Winn, S. R. McNutt, G. Tytgat, and E. Clark, 2007. Volcanic eruptions electrical activity

during the 2006 Mount St. Augustine, Science, 315 (5815): 1097-1097; DOI:10.1126/science.1136091

Thomas, R. J., S. R. McNutt, P. R. Krehbiel, W. Rison, G. Aulich, H. E. Edens, G. Tytgat, and E. Clark, 2010. Lightning and electrical activity during the 2006 eruption of Augustine Volcano. In J. Powers, M. Coombs, and J. Freymueller (eds.), The 2006 eruption of Augustine volcano, Alaska, U.S. Geological Survey. Professional Paper 1769; pp: 579–608; DOI:10. 3133/pp176925

Thorarinsson, S., 1967. The Surtsey eruption and related scientific work, Polar Record, 13 (86): 571-578; DOI:10.1017/S0032247400058113

Thorarinsson, S., 1984. Living on a volcano, Political Geography, 8 (2): 89-112; DOI:10.1080/10889378409377217

Thorarinsson, S., and B. Vonnegut, 1964. Whirlwinds produced by the eruption of Surtsey volcano, Bulletin of the American Meteorological Society, 45: 440-444

Torreson, G. W., 1939. Instruments used in observations of atmospheric electricity. In Terrestrial Magnetism and Electricity, J.A. Fleming (ed.), McGraw-Hill Book Co., New York and London; pp: 231-269

Uman, M. A., 1987. The lightning discharge. Academic Press, Orlando, etc., pp: 1-377

Urban, L., and A. Janackova, 1990. A method for estimating the westward drift velocity and possible correlation with features of global tectonics. Physics of the Earth and Planetary Interiors, 59:342-348; DOI:10.1016/0031-9201(90)90238-S

Vogfjörd, K. S., S. S. Jakobsdóttir, G. B. Gudmundsson, M. J. Roberts, K. Ágústsson, P. Arason, H. Geirsson, S. Karlsdóttir, S. Hjaltadóttir, U. Ólafsdóttir, B. Porbjarnardóttir, P. Skaftadóttir, E. Sturkell, E. B. Jónasdóttir, G. Hafsteinsson, H. Sveinbjörnsson, R. Stefánsson, and V. Jónsson, 2005. Forecasting and monitoring a subglacial eruption in Iceland. EOS, Transactions of the American Geophysical Union, 86: 245–248

Vonnegut, B., 1963. Some facts and speculations concerning the origin and role of thunderstorm electricity, Meteorological Monographs, 5 (27): 224-241

Vossen, C. E. J., C. Cimarelli, A. J. Bennett, A. Geisler, D. Gaudin, D. Miki, M. Iguchi, and D. B. Dingwell, 2021. Long-term observation of electrical discharges during persistent vulcanian activity, Earth and Planetary Science Letters, 570: 11708; DOI:10.1016/j.epsl.2021.117084

Woodhouse, M. J., and S. A. Behnke, 2014. Charge structure in volcanic plumes: a comparison of plume properties predicted by an integral plume model to observations of volcanic lightning during the 2010 eruption of Eyjafjallajökull, Iceland, Bulletin of Volcanology, 76: 828; DOI:10.1007/s00445-014-0828-4

Wulf, T., 1909. Über die in der Atmosphäre vorhandene Strahlung von hoher Durchdringungsfähigkeit, Physikalische Zeitschrift, 10: 152-157

Zhang, M., 2014. Epic photos of the 2010 volcanic eruptions in Iceland, *PetaPixel*, issued May 02, 2014

Acronyms

ADT - Alaska daylight time
AGU – American Geophysical Union
ALB – asthenosphere lithosphere boundary
AVHRR - Advanced Very High Resolution Radiometer
AVO - Alaska Volcano Observatory
CC - cloud-to-cloud, synonymous of IC
CG – cloud-to-ground (discharge or lightning)
CMB – core-mantle boundary
CRF - continual radio frequency
DC – direct current
DEMETER - Detection of Electromagnetic Emissions Transmitted from Earthquake Regions (satellite)
DRE - dense-rock equivalent
ESA – European Space Agency
ESI - electric soldering iron' (mechanism)
IC - inner core
IC - intracloud, synonymous of CC
ICB – inner core boundary
IMT - Icelandic Mean Time
JMA - Japan Meteorological Agency
LDS - Lightning Detection System
LN - Lowes-Nevanlinna's (law or plot)
LT – local time
MAGSAT – Magnetic Satellite
MOR – mid-ocean ridge
NOAA - National Oceanic and Atmospheric Administration
NWS - National Weather Service
OC - outer core
PM - aerosol particle matter
RF - radio frequency
SHE (spherical harmonic expansion)
ss - spherical shells
SV – secular variation
TD - tide-driven (dynamo)
USGS – United States Geological Survey
VAAC - Volcanic Ash Advisory Center (Tokyo)
VHF - very high frequency
WMT – warm-mud tectonics

NCGT Journal
New Concepts in Global Tectonics

New Concepts in Global Tectonics Journal
Volume 13, Number 6, August 2025

ISSN number; ISSN 2202-0039

ABOUT THE NCGT JOURNAL

The NCGT Newsletter, the predecessor of the NCGT Journal, was begun as a result of discussions at the symposium "Alternative Theories to Plate Tectonics" held at the 30th International Geological Congress in Beijing in August 1996. The name is taken from an earlier symposium held in association with the 28th International Geological Congress in Washington, D. C. in 1989. The first issue of the NCGT Newsletter was December 1996. The NCGT Newsletter changed its name in 2013 to the NCGT Journal. Aims of the NCGT Journal include:

1. Providing an international forum for the open exchange of new ideas and approaches in the fields of geology, geophysics, solar and planetary physics, cosmology, climatology, oceanography, electric universe, and other fields that affect or are closely related to physical processes occurring on Earth from its core to the top of its atmosphere.
2. Forming an organizational focus for creative ideas not fitting readily within the scope of dominant tectonic models.
3. Forming the basis for the reproduction and publication of such work, especially where there has been censorship or discrimination.